

DOE/ET-53088-311

IFSR #311

**Some Aspects of Plasma Kinetic Theory:
Energetic Particle Physics;
Renormalization Theory;
Anomalous Electron Transport in Tokamaks**

Yang-Zhong Zhang

Institute for Fusion Studies
The University of Texas at Austin
Austin, Texas 78712

February 1988

**SOME ASPECTS OF PLASMA KINETIC THEORY:
ENERGETIC PARTICLE PHYSICS;
RENORMALIZATION THEORY;
ANOMALOUS ELECTRON TRANSPORT IN TOKAMAKS**

APPROVED BY SUPERVISOR COMMITTEE:

Robert L. Burt

Smadesh M. Mahajan

James W. Van Dam

Richard D. Hazeltine

Edward J. Powers

H. Vernon Wong

Some Aspects of Plasma Kinetic Theory: Energetic Particle Physics; Renormalization Theory; Anomalous Electron Transport in Tokamaks

Yang-zhong Zhang

This dissertation discusses three special topics of collisionless plasma kinetic theory and their applications pertinent to high-temperature magnetic confinement experiments oriented to nuclear fusion research. The first special topic is the energetic particle physics. Appropriate equations are derived from first principles and applied to mirror configurations. A significant contribution is the prediction of a diamagnetic limit due to negative energy precessional waves. Discussion is given on whether experiments exist that violate this stability limit. The major theme of the second special topic is the construction of a set of rigorous formal systematology for nonlinear Vlasov equation with electromagnetic interactions in order to produce a renormalized perturbation theory to arbitrary higher order. This systematology makes it possible to clarify some ambiguities of previous theories as well as to improve a few aspects of calculational techniques. The last topic of the dissertation is the theoretical study of anomalous electron energy transport in tokamak. In combination with phenomenological analysis, a formula for local electron energy transport coefficient is proposed on the theoretical basis for strong microturbulence on the scale of the electromagnetic skin depth. The transport consequences of this formula are found in good agreement with a variety of tokamak experiments. Attempts have also been made to derive such a formula from first principle to clarify the underlying mechanism. Thus far these approaches have not proved to be successful.

TABLE OF CONTENTS

Chapter	Page
I. Introduction	1
I.1 Overview	1
I.2 Organization and Contributions of This Thesis	5
Part A Energetic Particle Physics	
II. Review of Energetic Particle Physics	12
II.1 Overview	12
II.2 Simplified Model	18
III. Variational Form	22
III.1 Drift Kinetic Equation in an Axisymmetric Configuration	24
III.2 Quadratic Form in Cylinder with an Embedded Current	28
III.3 Eigenmode Equation and Current	34
IV. Hot Electron Interchange Mode	
in Disk-like Configuration	40
V. Diamagnetic Limit for a Hot Particle Annulus	55
V.1 Layer Precessional Mode in Ring-like Configuration	56
V.2 Analysis	63
V.3 Discussion.	75

**SOME ASPECTS OF PLASMA KINETIC THEORY:
ENERGETIC PARTICLE PHYSICS;
RENORMALIZATION THEORY;
ANOMALOUS ELECTRON TRANSPORT IN TOKAMAKS**

Publication No.

Yang-zhong Zhang, Ph.D.

The University of Texas at Austin 1988

Supervising Professors: Herbert L. Berk and Swadesh M. Mahajan

This dissertation discusses three special topics of collisionless plasma kinetic theory and their applications pertinent to high-temperature magnetic confinement experiments oriented to nuclear fusion research.

The first special topic is the energetic particle physics. Appropriate equations are derived from first principles and applied to mirror configurations. A significant contribution is the prediction of a diamagnetic limit due to negative energy precessional waves. Discussion is given on whether experiments exist

numerous to mention for their warm friendship and interesting discussions over the last several years.

From administrative staff, I want to acknowledge all of the help of Carolyn Valentine, Dawn East, Saralyn Stewart, Rhandon Hurst, Suzy Crumley, Laura Patterson and Joyce Patton. They have made my stay here an enjoyable one.

I would like to thank Professor T.D.Lee for his initiation of the CASPEA program, that gives me the opportunity to study in the United States. I would also like to thank Professor Kalman, Professor Uritam, Professor Di Bartolo, Professor Goldsmith and Professor Charles Chiu. They have made it easier to get my transfer from Boston College to the University of Texas at Austin.

Finally I would like to express my indebt to The Southwestern Institute of Physics of China for all of the help to my study in the United States.

TABLE OF CONTENTS

Chapter	Page
I. Introduction	1
I.1 Overview	1
I.2 Organization and Contributions of This Thesis	5

Part A Energetic Particle Physics

II. Review of Energetic Particle Physics	12
II.1 Overview	12
II.2 Simplified Model	18
III. Variational Form	22
III.1 Drift Kinetic Equation in an Axisymmetric Configuration	24
III.2 Quadratic Form in Cylinder with an Embedded Current	28
III.3 Eigenmode Equation and Current	34
IV. Hot Electron Interchange Mode	
in Disk-like Configuration	40
V. Diamagnetic Limit for a Hot Particle Annulus	55
V.1 Layer Precessional Mode in Ring-like Configuration	56
V.2 Analysis	63
V.3 Discussion.	75

DEDICATED TO
MY MOTHER
MY WIFE AND MY SON

**SOME ASPECTS OF PLASMA KINETIC THEORY:
ENERGETIC PARTICLE PHYSICS;
RENORMALIZATION THEORY;
ANOMALOUS ELECTRON TRANSPORT IN TOKAMAKS**

by

YANG-ZHONG ZHANG

DISSERTATION

Presented to the Faculty of the Graduate School of
The University of Texas at Austin

in Partial Fulfillment
of the Requirements
for the Degree of

DOCTOR OF PHILOSOPHY

THE UNIVERSITY OF TEXAS AT AUSTIN

(May 1988)

ACKNOWLEDGEMENTS

It has been a great honor and privilege to collaborate with and learn from Professor Herbert L. Berk and Dr. Swadesh M. Mahajan. Without the many productive suggestions they have provided during our numerous discussions, this dissertation would not have been possible. Their guidance, patience, advice and knowledge is deeply appreciated.

I am pleased to also acknowledge contributions to this research made by Dr. Vernon Wong, Dr. James Van Dam, Dr. David Ross and Professor Wendell Horton. Their generosity in sharing of knowledge and personal kindness is greatly appreciated.

I wish to thank the rest of my supervising committee, Professor Richard Hazeltine and Professor Edward Powers for careful reading of my dissertation and their helpful suggestions.

I am also deeply indebted to Professor Marshall Rosenbluth for giving me a chance to discuss with him some fundamental issues in plasma physics during his classroom lectures.

I would like to thank Professor Toshiki Tajima for providing me an opportunity to learn the techniques of particle simulation.

I wish to thank Dr. Joseph Sedlak, Ms. Marcia Engquist and Dr. Daren Stotler for their providing me the basic computer codes.

I am very grateful to Professor Tetsuo Kamimura (Nagoya University in Japan) for collaboration and providing me his simulation results, to Dr. Bill Quon (Applied Microwave Plasma Concepts, Inc.), Dr. Barton Lane and Dr. Xing Chen (Massachusetts Institute of Technology) for sharing of unpublished experimental results and interesting discussions. I am also grateful of Dr. Robert Goldstone (Princeton Plasma Physics Laboratory), Dr. Alan Wootton (Fusion Research Center, University of Texas at Austin), Dr. Nobu Ohyabu (General Atomic Technologies Inc.), Dr. Gerhard Becker (Max-Plank-Institute fur Plasmaphysik in Garching), Dr. Derek Robinson (Culham Laboratory in England), Dr. Tom Stringer (Culham Laboratory in England), Dr. Stanley Kaye (Princeton Plasma Physics Laboratory), Dr. Yuichi Ogawa (Nagoya University in Japan) and Dr. Masao Kasai (Mitsubishi Atomic Power Industries, Inc. in Japan) for either providing detailed informations of their tokamak experiments or verifying and/or correcting my interpretation of their experimental results in published literature.

I greatly appreciate Dr. Shinji Hiroe (Oak Ridge National Laboratory) for using the anomalous electron energy transport coefficient formula proposed in this dissertation to compare with the local experimental values measured in the TFTR tokamak experiments.

I wish to express gratitude to my Chinese colleagues Dr. Zhi-Gang An, Shaobai Zheng, Wenxiao Qu, Jiaqi Dong, Yuanxi Wan, and my fellow graduate students Dr. Xiaoyue Gu, Dr. Jixing Liu, Dr. Chi-Tien Hsu, Dr. Tzihong Chiueh, Changye Chen, Guo-Yong Fu, Wann-Quan Li, and many other too

VI. Trapped Particle Effects on Diamagnetic Limit	77
VI.1 Trail Function Method. Limiting Cases	79
VI.2 Calculation of Trapped Particles	85
VI.3 Numerical Results and Discussion	91

Part B Renormalization Theory

VII. Introduction to Renormalization Theory	101
VIII. Renormalized Perturbation Theory	108
VIII.1 Perturbation Procedure	108
VIII.2 Renormalizability	118
VIII.3 Renormalized Dielectric Function. Weak Turbulence Limit	123
VIII.4 Spectrum Equation. Correlation Broadening	131
IX. Energy Conservation in Electrostatic Drift Waves	137
IX.1 Explicit Illustration up to Fourth Order	140
IX.2 General Proof to Arbitrary Higher Order	142
IX.3 Sheared Slab and Ballooning Representation	152
X. Renormalized Gyrokinetics	155
X.1 Collisionless Plasma with Finite Larmor Radius Effects .	155
X.2 Nonlinear Kinetic η_i Mode	158
X.3 Transport Equation in Gyrokinetic Theory	160

Part C Anomalous Electron Transport in Tokamaks

XI. Experimental Evidence of Anomalous Electron Transport	166
XII. Electromagnetic Turbulence Model for Electron Transport	176
XII.1 Theoretical Model	179
XII.2 Comparison with Tokamak Experiments	183
XIII. η_e -Mode and the Induced Electron Transport	192
XIV. Electromagnetic Fluctuations Induced by η_e -Mode	206
XIV.1 Nonlinear Destablization of A --Mode by η_e -Mode	206
XIV.2 Electromagnetic Fluctuation Forced by η_e - Mode	214
Appendix A	220
Appendix B	222
Appendix C	224
Appendix D	226
Appendix E	227
Appendix F	231
References	235

LIST OF FIGURES

Figure	Page
1. Cylindrical model with an embedded current	30
2. Radial pressure profile in a cylinder	30
3. Marginal stability for hot electron interchange mode	45
4. Marginal stability for hot electron interchange mode	46
5. Marginal stability for interchange modes	47
6. Stable region bound by interchange modes	49
7. Time evolution of numerical simulation	50
8. Growth rate of hot electron interchange mode	54
9. Dispersion curve of surface Alfvén-whistler mode	58
10. Curves of functions $\psi(b)$, $\Phi(b)$, and $Y(b)$	58
11. Radial profile of pressure	62
12. Relativistic effect on the real frequency	62
13. Marginal stability boundaries	69
14. Growth rate versus N^2	70
15. Real frequency versus N^2	71
16. Effect of skewness on growth rate	71
17. Growth rate due to interaction with Alfvén-whistler wave	72
18. ζ dependence of growth rate	72
19. Growth rate versus ζ	74

20. Schematic diagram of broadened pressure profile	74
21. Single mirror cell configuration	78
22. Comparison of marginal stability in different configurations	92
23. Comparison of real frequency in different configurations	92
24. Comparison of growth rate in different configurations	93
25. Comparison of growth rate in different configurations	93
26. Magnetic field modification in NBT	95
27. Comparison of Hall probe and Zeeman beam results in STM	95
28. Examples for forbidden self-energy diagram	120
29. Illustration	139
30. Examples for adjoint diagrams	139
31. Illustration	140
32. Illustration	140
33. Illustration	141
34. Illustration	141
35. Drivative primitive frame diagram	143
36. Illustration	143
37. Illustration	145
38. Illustration	148
39. Illustration	148
40. Illustration	149
41. Illustration	150
42. Illustration	150

43. Illustration	151
44. Power balance of Ohmic discharges in Doublet-III	170
45. $n_e\chi_e$ and $n_i\chi_i$ of Ohmic discharges in Doublet-III	170
46. Transport analysis of XB discharges in Doublet-III	172
47. Transport analysis in PDX	174
48. Normalized electron temperature profile	185
49. Λ versus $T_e(0) _{exp}$	188
50. $\tau_{E_e}(0)$ versus \hat{n}_e	190
51. $T_e(0)$ versus P_{total}	190
52. Minimum marginal stability of η_e -mode	196
53. Marginal stability of η_e -mode	198
54. Marginal stability of η_e -mode	199
55. Marginal stability of η_e -mode	200
56. Comparison of growth rate with sheared slab model	201
57. Phase space plot of η_e -mode	203
58. Maximized transport coefficient due to η_e turbulence	204

I. Introduction

I.1 Overview

There is a general consensus that any magnetic geometry meriting consideration as a fusion reactor must satisfy the equilibrium and stability limits set by ideal MHD (magnetohydrodynamics).¹⁻⁴ If not, violent termination of the plasma on a very short time scale, the Alfvén time τ_A , is often the consequence. There is overwhelming empirical evidence that ideal MHD provides a rather accurate description of a wide variety of macroscopic plasma behavior.⁵⁻⁸

While favorable ideal MHD properties are necessary in a reactor, they may not, even in the restrictive context of low frequency macroscopic behavior, be sufficient. It is sometimes possible for nonideal effects such as electrical resistivity to allow the development of weaker instabilities on a slower time scale, the resistive time τ_R , which, set by resistive MHD, nevertheless may still lead to enhanced transport or even, in certain circumstances, violent termination of the plasma. While the theory of ideal MHD has been refined during the past three decades, a substantial correspondence has been established between resistive MHD predictions and experimentally observed gross instability phenomena.^{9,10}

Sufficient collisionality is required for the MHD description to be valid, especially to limit heat transport along the field line. However, this situation is not generally true even for present-day laboratory plasmas.¹¹ The use of MHD theory may be restricted to the description for those phenomena in which the

equation of state does not play an important role. In open systems, MHD must be modified to include anisotropic pressure effects; nonetheless, it still provides a poor description of plasma behavior along the field line.^{12,13}

In the opposite limit, the high temperature collisionless regime - the regime of fusion reactor interest-, the plasma confinement will most likely be dictated by microinstabilities. These instabilities which can only be derived from a kinetic description of the plasma (as opposed to gross instabilities or macroinstabilities which can be obtained from the MHD descriptions) are generally short wavelength modes with high frequency.

Not every kinetic description must result in microinstability. For instance, a negative energy wave of kinetic nature can be coupled to a gross positive energy wave , giving large spatial scale instability. For example, this kinetic negative energy wave is associated with the precession of a hot component, like α particles in fusion reactor, immersed in background plasma. A new branch of plasma physics, the energetic particle physics, is thus developed and closely related with the study of consequences of the negative energy wave.

In contrast to the macroinstabilities, it is not yet clear how to stabilize microinstabilities. In fact, it is quite likely that not all of them can be stabilized, and the best that one can probably do is to alter the field geometry and other equilibrium parameters of a particular device to minimize their effect. Their high growth rates and short scale lengths mean that most microinstabilities will grow rapidly into the nonlinear regime, whereupon their growth will be saturated. They are thus not expected to be as large scale and chaotic as

macroinstabilities. However they can cause rapid, small scale, but relatively ordered, plasma transport and hence be very detrimental to plasma confinement. In the present generation of devices the energy confinement times are usually much shorter than classical and are thought to be a direct consequence of anomalous transport due to small scale turbulence induced by microinstabilities, although this is not a universally accepted point of view. Other possibilities have been proposed such as losses by impurity radiation, larger scale reconnection of magnetic field lines, or hidden enhancement of neoclassical transport. Certainly, fluctuations at approximately the right frequency and wavelength have been observed in many devices.¹⁴⁻¹⁷ However, the correlation between the intensity of these fluctuations and the diffusion has not yet been demonstrated, for instance, in tokamaks. The identity of the fluctuations in tokamaks is also unclear, this is mainly due to the large number of different instabilities having similar wavelength and frequency, thus making a precise identification very difficult.

While it is generally difficult to establish correspondence between the predictions of kinetic description and experimental observations in high temperature plasmas due to their microscopic feature, the study of energetic particle physics appears interesting in cases where kinetic instability associated with negative energy wave has macroscopic consequences, which can be identified by less sophisticated experimental techniques. On the other hand, as currently conceived, energetic particle physics is a crucial issue for tokamaks in D-T operation that will occur in the near future. In fact, the issue has been investigated

in bumpy tori and in single mirror cells for more than one decade.

There are several types of free energy which are available for driving instabilities. Their sources can be identified by finding the current form in terms of fields or, equivalently, the quadratic form of fields. Among others, there are currents due to curvature drift, polarization drift, drift associated with density and temperature gradients. Since the drift current due to magnetic field gradient is by and large cancelled by its counterpart in the diamagnetic current, it is not a free energy source unless the β -value of the plasma is quite high, so as to leave the pressure gradient alone to be the driving force. Currents responsible for free energy sources can also be induced by velocity space anisotropy; examples of this are the ion distribution of a mirror machine which has an inherent loss cone nature or the distortion of the distribution function due to the plasma current as in a tokamak or the distortion of the distribution function due to the pressure of trapped particles.^{13,18} However, free energy can be either a source or sink. It depends not only on the relative direction of current and wave but also on the relative energy signature of waves. A microinstability with negative energy signature, when coupled to a macroinstability with positive energy signature, may cause new instabilities. The above observations of free energy source provide an insight to the nonlinear saturation mechanism. It is conceivable that the current due to nonlinear effect tends to balance the linear current that drives instability. This estimate is even quantitatively plausible to the order of magnitude in the context of kinetic theory where the linear growth rate is believed to be balanced by the nonlinear damping rate.¹⁸

This dissertation expounds several kinetic aspects of plasma theory, with special attention paid to specific issues. These issues are of fusion interest for near-term as well as long-term machine operations. The phenomena for these issues usually have time scales considerably shorter than collisional scales, which allows the application of the collisionless plasma approximation. Certainly, this does not mean that interaction between particles is neglected, for it is the Coulomb force that also leads to the formation of self-consistent electromagnetic fields in collisionless plasma, with the interaction between particles coming in through wave-particle interaction.

The above discussions justify the application of the kinetic Vlasov equation^{19,20} for ions and electrons and the Maxwell equations for the self-consistent electric field to the theory of waves in a collisionless plasma. This is a closed set of nonlinear integro-differential equations in space and time. Its complexity leaves no hope for a general solution, and therefore certain approximations are used in each particular case to simplify the initial equations and then to find the solution of the simplified set of equations.

I.2 Organization and Contributions of This Thesis

The main achievements of the work reported in this thesis fall into three categories and will now be summarized. Each corresponds to a part (A, B, C), and each part begins with an introduction to its topic [cf. II, VII, XI].

(A) *Energetic Particle Physics*

The main work in this area is devoted to a study of the precessional wave in a hot electron annulus configuration like ELMO Bumpy Torus (EBT) [cf. V,VI]. The remainder of the work in this area is devoted to a study of the high frequency hot electron interchange mode and the interacting background interchange mode in a hot electron disk configuration, such as the proposed axisymmetrical tandem mirror [cf.IV].

* Diamagnetic stability limit in hot electron annulus

We discovered a stability threshold for the precessional wave, which may give the diamagnetic stability limit for the pressure gradient that can be sustained in hot electron experiments. This limit predicts that instability will arise if the self-consistent equilibrium with a diamagnetic well begins to produce a minimum-B field. This conclusion is not consistent with the traditional opinion that a deep enough magnetic well (or drift reversal) had been achieved in EBT-like machines. We point out that indirect measurements based on the Hall probe were probably not accurate enough for verifying if drift reversal existed, since resolution of the radial structure is very difficult to be accurate. Recent direct measurements in the STM experiments at TRW based on the Zeeman effect have found that the current distribution is too broad to form a minimum-B well. Earlier reported achievement of drift reversal in EBT experiments, when reexamined, were found to be inaccurate. No direct experimental measurement has yet found a drift reversal configuration. However, we should be cautious in concluding that there is a universal limit on the diamagnetic limit, since these

particular experiments may have merely encountered a technical limit.

On the other hand, we point out that this study is significant for the understanding of energetic particle physics as well as of the kinetic theory of a collisionless plasma. The prediction of the diamagnetic limit is a direct consequence of destabilization due to wave-particle resonance. The relative simplicity and clarity in both the experiments and the theoretical prediction provide insight into the kinetic theory of plasma physics [cf.V,VI].

* High frequency interchange mode

A layer mode analysis is done for disk-like hot electron pressure profile with inclusion of electromagnetic component. We established the stability window in parameter space. In particular, the density ratio of hot to cold plasma is bounded by the hot electron interchange mode on the upper side, being insensitive to diamagnetic effects, and by the interacting background interchange mode on the lower side, if the diamagnetism is not too high [cf.IV].

(B) *Renormalization Theory*

This part is devoted to an investigation of several generic problems in plasma turbulence:

* Perturbation theory and renormalizability

A systematic perturbation theory to deal with stationary, homogeneous turbulence in a dispersive dissipative system, with focus on a Vlasov-Poisson system, is developed and is shown to be renormalizable by using diagrammatic technique. The theory can be viewed as a generalization of the renormalization

theory developed by Dupree and by Rudakov and Tsytovich , to arbitrary higher order. In particular, the incoherent part of the perturbed distribution function is treated in light of matched perturbation theory, so as to resolve the difficulty of Dupree's theory which fails to reduce to the standard weak turbulence theory [cf.VIII.1,2]. The origin of this difficulty is then clarified by studying the renormalized dielectric function.

* Renormalized dielectric function and spectrum equation

Use is made of the above formalism for calculation of the renormalized dielectric function and for derivation of the renormalized Kadomtsev spectrum equation to lowest non-trivial order. Their asymptotic expressions in weak turbulence limit are found consistent with the known results from DIA. This manifests that the origin of the difficulty of Dupree's theory lies not in the ill-treatment of iteration, as criticized by the DIA approach, but in the use of unmatched perturbation theory [cf.VIII.3,4].

* Energy conservation

The energy conservation for electrostatic drift waves is proved to all orders in perturbation theory. It shows that Dupree's theory and DIAC will violate the energy conservation starting from the next order to the lowest non-trivial order [cf.IX].

* Gyrokinetics

Use is made of the iteration procedure to develop a formalism for renormalization of gyrokinetic equation. In contrast to the known result, this formalism makes manipulation of large Larmor radius effects analytically tractable. Non-

linear transport equations are derived on the eikonal approximation basis. It shows that the energy transport of electrons is usually smaller than that of ions for drift wave turbulence [cf.X].

(C) *Anomalous Electron Transport in Tokamak*

This part is devoted to a study of anomalous electron transport in tokamaks due to turbulence of microinstability. The survey of experimental phenomenology indicates that anomalous electron transport, rather than that of ions is the dominant energy loss channel in typical tokamak discharges [cf. XI]. We are thus motivated to consider fluctuations which have less effect on ions. Electromagnetic turbulence obviously meets this requirement.

* Electron energy transport coefficient

A model electromagnetic microturbulence theory of electron energy transport in tokamaks is proposed for deriving electron energy transport coefficient. The corresponding energy transport equation is solved in a cylindrical plasma. The predicted central electron temperature and the temperature profiles are found to be agreement with various experiments, including the "supershot" in TFTR and the "monster mode" in JET [cf.XII].

* η_e mode

This is an electrostatic wave, to which ions respond adiabatically. The marginal stability of the kinetic η_e mode is solved analytically in a shearless slab model. The analysis of its nonlinear behavior shows that the transport due to η_e -turbulence is more than one order smaller than that of tokamak

experiments [cf. **XIII**].

*** Magnetic fluctuations induced by η_e turbulence**

We have shown that η_e turbulence causes an effective collision frequency which reduces shear damping of the electromagnetic waves. Use is made of the formalism developed in **X.1.** to derive an eigenmode equation for electromagnetic waves under the influence of nonlinear η_e waves. The calculations are carried out on the basis of perturbative expansion for small fluctuating amplitude of the Fourier modes. The solution of the eigenmode equation shows that destabilization due to η_e turbulence is insufficient to balance the shear stabilization to electromagnetic mode, as the perpendicular wavelength of the η_e turbulence is taken to be the order of the electron Larmor radius [cf.**XIV,1**]. We also calculate the annihilation process of two η_e modes into one electromagnetic wave. This may serve as an alternative candidate for the excitation of electromagnetic fluctuations in tokamak. For the two η_e process, the electromagnetic fluctuations are still insufficient to explain the anomalous electron transport in tokamaks. However, we observe that the multi-wave processes such as annihilation due to three, four ... η_e modes give the same order contributions as the two wave annihilation. The above conclusion is limited by the perturbative approach of the present work [cf.**XIV,2**].

PART A

ENERGETIC PARTICLE PHYSICS

II. Review of Energetic Particle Physics

II.1 Overview

The use of hot electrons in several magnetic configurations such as a symmetric tandem mirror or EBT was primarily motivated by the attempt to confine plasma stably in an otherwise unstable MHD trap by forming a diamagnetic well with the hot component plasma. It was hoped that the hot component could anchor the magnetic field lines in much the same way as the quadrupole fields of a minimum-B configuration, but with the advantage of axisymmetry in a tandem mirror and relative simplicity of the magnetic coil geometry in EBT. Therefore, the hot electron diamagnetism must be sufficient to reverse the magnetic drifts of the core plasma²¹ and to do so in the appropriate line average sense for flute-interchange instability.²² However, stability theory has indicated limitations of this method. These limitations include:

(1) a low stability limit for the beta of the background plasma, known as the Lee-Van Dam, Nelson limit^{23,24} that puts a more stringent condition for the background beta value than that obtained by treating the hot electron annulus as a rigid non-interacting current ring²⁵; and

(2) the existence of a negative energy wave at the curvature drift frequency of the hot component that will be destabilized by the excitation of positive energy waves or with the dissipative mechanism of the background plasma and walls.

The mode at the curvature drift frequency is quite analogous to the near rigid precessional mode of Astron,²⁶ where it was found that a "forward" precessing mode is a negative energy mode that is readily destabilized by dissipation or by excitation of positive energy waves of the background system.²⁷

The coupling of the negative energy mode to the background plasma MHD mode yields the hot electron interchange modes [cf. Eq.(5.1)], if the ideal MHD growth rate is not too much less than the curvature drift frequency. Krall²⁸ considered this effect for the hot electron ring configuration and showed that, with a sufficiently large amount of cold plasma, the mode is stable. Berk²⁹ extended Krall's model to describe stability when the electron drift frequency exceeds the ion cyclotron frequency. Dominguez and Berk³⁰ treated the electromagnetic aspects of the problem in a self-consistent fashion and verified the results of Krall²⁸ and of Berk.²⁹ Hence, the hot component energy times the ratio of cold to hot plasma density is required to be sufficiently large for the stability, whereupon the response of the hot component decouples from MHD response of the background plasma.

When the curvature drift frequency is not sufficiently less than the compressional Alfvén frequency, a new magnetic compressional mode is present. As a result, the ratio of cold to hot plasma density is required to be not too high, in order to have a stability window in background beta value, as was pointed out by El Nadi³¹ and Berk *et al.*³² This compressional mode has been numerically studied in great detail by Stotler³³ with inclusion of trapped particles, arbitrary drift reversal, and magnetic component and also has been applied to

tandem mirror by Rosenbluth.³⁴ These comprehensive studies of the compressional mode revealed the origin of a pessimistic prediction from energy principle constructed by Van Dam *et al*³⁵ that is more pessimistic than the conventional kinetic energy principle of Kruskal and Oberman,³⁶ which itself had been unable to indicate stability unless the hot electrons are treated by fiat as rigid and non-interacting with background plasma perturbations.

If the negative energy spectrum of the precessional mode is broadband, there are likely to be modes of excitation to match those of the background plasma such as shear Alfvén waves³⁷⁻³⁹ and whistler-like waves.⁴⁰

A frequency shift that keeps the precession frequency away from the positive energy wave frequency is favorable for stability. An example, pointed out by Tsang and Lee⁴¹, is the radial electric field stabilization in a symmetric tandem mirror, when the $\mathbf{E} \times \mathbf{B}$ precession is opposite to the hot electron curvature drift.

Berk *et al*⁴² have studied how the Lee-Van Dam, Nelson limit is altered in the presence of the coupling of precessional mode to positive energy mode.

More generally, as coupling to positive energy waves is increased by increasing positive energy coupling, the negative energy waves are destabilized. Thus one finds that a small increase of a positive energy source that arises from line bending energy and magnetic compressional finite Larmor radius (FLR) effects is at first destabilizing.^{43,44} However, with enough line bending and FLR effects (this is a stronger stability mechanism than conventional FLR stabilization⁴⁵), all perturbations can be converted to positive energy, and a robust stabil-

ity regime, where all excitations are positive energy, can be found under some conditions.^{38,46,47} The FLR effect on long wavelength layer modes was derived by Hammer and Berk.⁴⁸ Recently, Wong⁴⁹ developed a variational form in the long-thin limit for FLR effect in an arbitrary non-eikonal form.

It was also found that image currents generated in nearby walls could change the sign of the precession and convert the mode to a stable positive energy.^{50,51} Unfortunately, this stabilization mechanism⁵² is not applicable to a hot plasma ring configuration, as in EBT, since the stabilizing wall image current is considerably reduced from that of a disk-shaped pressure profile, as in a tandem mirror configuration.

All radial analyses in the aforementioned publications were restricted either to short radial wavelength modes, which can be examined using WKB methods, or to long radial wavelength modes (referred to as layer modes), for which WKB is invalid. These calculations, though often simplified, are analytically tractable and indicate the important effect of the radial mode structure on stability boundaries and growth rates. In order to allow more realistic mode profiles and to better understand the short and long wavelength limit (as well as intermediate cases), Spong⁵³ developed a shooting code for solving the full radial eigenmode equation in a Z-pinch configuration. In the axial analysis an analytical solution is found only for large drift reversal.^{38,43,52,54} Otherwise, one has to numerically solve the ballooning mode equation, which is an integro-differential equation.

In addition to destabilization due to the coupling of the precessional mode

to positive energy mode, the precessional mode can be destabilized by the interaction with a positive energy dissipative mechanism. Antonson and Lee⁵⁵ in very general geometry of EBT indicated that the precessional mode is always unstable in the drift reversal limit. This instability arises from the positive energy dissipation due to the bounce resonance in background plasma, while dissipation (both the positive and negative energy) on the hot component is assumed to be zero. Berk and Zhang⁴⁰ included the dissipation due to the curvature drift resonances in hot components to find a stability threshold. In the hot electron annulus, as in EBT, the positive energy dissipation arises from hot particle resonances occurring at the inner edge of the annulus, while the negative energy mode is stabilized by negative dissipation arising from the particle resonances located on the outer edge of the annulus. Particle resonances occur from both regions before drift reversal is achieved; generally the effects of the outer resonances are stronger, and the mode is stable. If the drift on the outer edge changes sign, resonances on the outer edge does not occur, while the resonances on the inner edge still arise, thereby causing destabilization of the precessional mode.

The stabilizing effect of hot component still remains on the background perturbations, even if the drift reversal is not achieved. This stabilization mechanism arises from the difference in density between the ions and electrons in background plasma, referred to as "charge uncovering" effect,³² since as plasma ions and electrons are displaced according to $\mathbf{E} \times \mathbf{B}$ motion, the hot component are not, which sets up an electrostatic restoring force proportional

to their charge difference. This results in a frequency shift proportional to the charge difference for the interchange mode, which, in a manner analogous to FLR stabilization,⁴⁵ produces stability. Another stabilizing effect results from the field compressibility coexistent with the presence of hot particles. It is this stabilization mechanism that plays the role to access the second stability of ballooning modes from its first stability in tokamak, as was proposed by Rosenbluth *et al.*⁵⁴

The precessional wave induced by hot components in tokamak is likely to be coupled with positive dissipation inherent to the background plasma, which produces instability. Chen *et al*⁵⁶ explained "fishbone" oscillations, discovered in connection with perpendicular neutral beam injection on PDX,⁵⁷ as a precessional drift resonant destabilization of the $m = n = 1$ internal kink mode.^{56,58,59} An alternative interpretation, proposed earlier by Coppi,⁶⁰ has been described by Porcelli.⁶¹ They contend that the negative energy dissipation arising from the wave-hot ion resonance is sufficient to destabilize a positive energy wave at the ion diamagnetic frequency.

Subsequently, although the energetic particles may have a stabilizing influence on the low frequency MHD branch, a new unstable branch may emerge from the coupling of the precessional mode to the background ballooning mode, in a manner analogous to the hot electron interchange mode.⁶²⁻⁶⁶

Since the hot component beta value is relatively small in tokamak, both the mode coupling and negative as well as positive energy dissipation should be taken into account simultaneously to give a valid threshold for comparison

with experiments.

Both the stabilization and destabilization mechanisms of energetic particles in the research in mirror machine and tokamaks are significant to the study of ignited fusion plasmas with α -particles. In fact, this subject is becoming an extensively active research field.^{59,66,67}

II.2 Simplified Model

Below we illustrate the hot electron physics by studying electrostatic instabilities in a sharp boundary model with hot species.

Let us consider a plasma slab with an artificial gravity model acting on each of the species. The force equation is

$$\frac{d\mathbf{v}_j}{dt} = \mathbf{v}_j \times \mathbf{e}_z \omega_{cj} + \frac{q_j}{m_j} \mathbf{E} - g_j \mathbf{e}_x. \quad (2.1)$$

Let $\mathbf{E} = -\nabla\phi$, $\omega \sim \omega_{ci}$ (ion cyclotron frequency), and suppose $\omega \sim \omega_{ci} \ll \omega_{ce}$ (electron cyclotron frequency),

$$m_e g_e = m_i g_i \frac{T_e}{T_i} \sim m_h g_h \frac{T_e}{T_h}, \quad (2.2)$$

where e, i, h refers to electrons, ions and hot species respectively. For simplicity take the hot species to be electrons. Let us consider an equilibrium where

$$n_j = \begin{cases} n_{j0}, & x > 0; \\ 0, & x < 0, \end{cases} \quad (2.3)$$

and $n_e q_e + n_i q_i + n_h q_h = 0$, where q is the charge. We shall derive the equation for stability.

In equilibrium

$$\mathbf{v}_{j0} = \mathbf{e}_y g_j / \omega_{cj} \equiv v_{dj} \mathbf{e}_y \quad (2.4)$$

and the continuity equation $\nabla \cdot (n\mathbf{v}) = 0$ is satisfied.

The solution of the linearized fluid equations for background ions, where $\delta\mathbf{E} = -ik_y \delta\phi \mathbf{e}_y - \frac{\partial}{\partial x} \delta\phi \mathbf{e}_x$, is

$$\delta\mathbf{v}_i = \frac{q_i}{m_i(\omega^2 - \omega_{ci}^2)} [i(\omega - \omega_{di})\delta\mathbf{E} + \omega_{ci}(\mathbf{e}_z \times \delta\mathbf{E})], \quad (2.5)$$

where $\omega_{di} = k_y g_i / \omega_{ci} \equiv k_y v_{di}$. For the hot and background electrons we use the low frequency drift approximation

$$\delta\mathbf{v} = \frac{c}{B} \delta\mathbf{E} \times \mathbf{b}$$

These velocities need to be substituted into the continuity equation which determines the perturbed density δn_j :

For ions

$$\begin{aligned} -i(\omega - \omega_{di})\delta n_i = & \frac{iq_i}{m_i(\omega^2 - \omega_{ci}^2)} \left\{ (\omega - \omega_{di}) \left[\frac{\partial}{\partial x} n_i \frac{\partial}{\partial x} - k_y^2 n_i \right] \right. \\ & \left. - k_y \omega_{ci} \frac{\partial n_i}{\partial x} \right\} \delta\phi \end{aligned} \quad (2.6)$$

and for electrons

$$-i(\omega - \omega_{de})\delta n_e = i \frac{c}{B} \frac{\partial n_e}{\partial x} k_y \delta\phi, \quad (2.7)$$

and similarly for hot electrons (hereafter, the subscripts 0 for equilibrium quantities are ignored).

Now, substituting for $\delta n_e, \delta n_i$ and δn_h into Poisson's equation yields the eigenmode equation

$$\begin{aligned} \left(\frac{\partial^2}{\partial x^2} - k_y^2\right)\delta\phi = & \frac{\partial}{\partial x} \frac{\omega_{pi}^2(x)}{(\omega^2 - \omega_{ci}^2)} \frac{\partial}{\partial x} \delta\phi - \frac{k_y}{(\omega^2 - \omega_{ci}^2)} \left[k_y \omega_{pi}^2 - \frac{\omega_{ci}}{(\omega - \omega_{di})} \frac{\partial \omega_{pi}^2}{\partial x} \right] \delta\phi \\ & + \frac{k_y}{\omega_{ce}} \left[\frac{\partial \omega_{pe}^2}{\partial x} \frac{1}{(\omega - \omega_{de})} + \frac{\partial \omega_{ph}^2}{\partial x} \frac{1}{(\omega - \omega_{dh})} \right] \delta\phi, \end{aligned} \quad (2.8)$$

where $\omega_{pj}^2 = 4\pi q_j^2 n_j / m_j$.

Notice that the solution of this equation is $\delta\phi = \exp(-|k_y x|)$. If this equation is integrated from $x = 0^-$ to $x = 0^+$, we obtain the contribution from the discontinuity $\partial \omega_{pj}^2 / \partial x$. Assuming $\omega_{di}, \omega_{de} \ll \omega$, and integrating Eq.(2.8) over the discontinuous layer, we obtain

$$\begin{aligned} -\frac{\partial \delta\phi(0^+)}{\partial x} + \frac{\partial \delta\phi(0^-)}{\partial x} + \frac{\omega_{pi}^2}{\omega^2 - \omega_{ci}^2} \cdot \frac{\partial \delta\phi(0^+)}{\partial x} = & \left\{ \frac{k_y \omega_{pi}^2 \omega_{ci} \omega_{di}}{\omega^2 (\omega^2 - \omega_{ci}^2)} \right. \\ & \left. + \frac{\omega \omega_{pi}^2 k_y}{\omega_{ci} (\omega^2 - \omega_{ci}^2)} - \frac{\omega_{de} \omega_{pe}^2 k_y}{\omega_{ce} \omega} - \frac{\omega_{ph}^2 k_y}{\omega_{ce}} \left[\frac{1}{\omega - \omega_{dh}} - \frac{1}{\omega} \right] \right\} \delta\phi(0). \end{aligned} \quad (2.9)$$

Use is made of the following equations

$$\frac{\partial}{\partial x} \delta\phi(x = 0^\pm) = \mp |k_y| \delta\phi(0^\pm), \quad \omega_{pi}^2(0^-) = 0,$$

and $\omega_{ci} \ll \omega_{pi}$, the dispersion relation can be written as

$$\begin{aligned} \omega^2 \left(1 + \text{Sgn}(k_y) \frac{\omega}{\omega_{ci}} - \frac{\gamma_{MHD_e}^2 n_e}{\omega_{ci}^2 n_i} \right) + \gamma_{MHD_i}^2 + \frac{n_e}{n_i} \gamma_{MHD_e}^2 \\ = \frac{\omega(\omega^2 - \omega_{ci}^2)}{\omega - k_y v_{dh}} \frac{\gamma_{MHD_h}^2 n_h}{\omega_{ci}^2 n_i}, \end{aligned} \quad (2.10)$$

where

$$\gamma_{MHD_h}^2 \equiv |k_y| g_h m_e / m_i, \gamma_{MHD_i}^2 = |k_y| g_i, \text{ and } \gamma_{MHD_e}^2 = |k_y| g_e m_e / m_i.$$

For small $\gamma_{MHD_{e,i}}^2$, the hot electron interchange mode results from the high frequency branch of the dispersion relation, Eq.(2.10):

$$\omega^2 - \omega \left(k_y v_{dh} + \text{Sgn}(k_y) \frac{\gamma_{MHD_h}^2 n_h}{\omega_{ci} n_i} \right) + \gamma_{MHD_h}^2 \frac{n_h}{n_i} = 0. \quad (2.11)$$

Noting that $|k_y| v_{dh} = -\gamma_{MHD_h}^2 / \omega_{ci}$, we write the stability criterion as,

$$\frac{n_h}{n_i} < \frac{2\omega_{ci}}{|\omega_{dh}|} \left(1 + \frac{|\omega_{dh}|}{2\omega_{ci}} - \sqrt{1 + \frac{|\omega_{dh}|}{\omega_{ci}}} \right). \quad (2.12)$$

For low frequency limit we have the low frequency interchange branch of Eq. (2.10), with the dispersion relation

$$\omega^2 - \omega \frac{\gamma_{MHD_h}^2 n_h}{k_y v_{dh} n_i} + \gamma_{MHD_i}^2 + \gamma_{MHD_e}^2 \frac{n_e}{n_i} = 0. \quad (2.13)$$

The middle term (proportional to n_h/n_i) is the charge uncovering term, that is stabilizing. The stability condition to the low frequency hot electron interchange mode is

$$\frac{\omega_{ci}^2}{4} \frac{n_h^2}{n_i^2} > \gamma_{MHD_i}^2 + \gamma_{MHD_e}^2 \frac{n_e}{n_i}. \quad (2.14)$$

The electrostatic sharp boundary model, however, does not give a valid description for the diamagnetic stabilizing effect on the background interchange mode.

The analysis including the electromagnetic effects will be discussed in IV.

III. Variational Form

The use of a variational expression to determine the governing equations of a system is a compact way to derive the appropriate normal mode equations and to achieve insight on how to determine approximation solutions.

The energy principle for an anisotropic, guiding center plasma was originally obtained by Kruskal and Oberman.³⁶ Its isotropic form was simultaneously derived by Rosenbluth and Rostoker⁶⁸ using a kinetic approach. This energy principle has subsequently been studied by Taylor and Hastie⁶⁹ and by Grad.⁷⁰ It was then generalized to include electrostatic effects,⁷¹ which were found to be stabilizing.

The derivation presented by Kruskal and Oberman was a thermodynamic argument. That is, they constructed a general macroscopic constant of the motion, namely, the entropy, and varied it so as to remove any variation in the microscopic distribution function.⁷² It has been pointed out,^{73,74} however, that the derivation of this energy principle can be obtained by requiring that both the single particle magnetic moment and the longitudinal action be adiabatically conserved. A key assumption in the derivation of the kinetic energy principle is that instabilities, if they exist, develop on the MHD time scale, or equivalently, that particles and field lines move together. However, this assumption is invalid for a rather energetic plasma component. For this hot species, the normal MHD response is negligible, and the time response is strongly affected by the large precessional magnetic curvature drift, that results in the "charge uncovering"

effect.

Accordingly, a new variational energy principle was derived by Antonsen and Lane,⁷⁵ which yielded certain necessary conditions for stability of short wavelength modes in an isotropic, equal electron and ion temperature plasma.

In a subsequent derivation by Van Dam, Rosenbluth, and Lee,³⁵ the general change in potential energy of an anisotropic plasma due to a zero frequency magnetic perturbation was calculated. This quadratic form gives sufficient conditions for the stability of purely growing magnetic modes.

Antonsen and Lee⁷⁶ developed an elegant form for variational principle which was capable of analyzing the stability of equilibria with electrostatic potentials.

Certain relationships between these formalisms were analyzed by Antonsen *et al*⁴⁴ in a subsequent paper dealing with ballooning perturbations.

A general variational formalism including FLR effects, equilibrium rotation and arbitrary particle bounce effects for both the eikonal and non-eikonal mode was obtained by Berk and Lane,^{77,78} whose derivation in the eikonal limit started from the results of a formalism developed by Wong.⁷⁹

The comparison of the kinetic variational form with those more familiar obtained in MHD is shown in **Appendix A**.

Physical insights usually arise from analysis in a rather simple geometry, as long as the more complicated geometry is not essential to the underlying mechanism for both stabilization and destabilization. It is found that many important features of energetic particle physics can be studied in a rather simple

cylindrical model with embedded current. Since the embedded current, which simulates the equilibrium curvature effects, is not a plasma current, none of the known variational forms is readily reduced to the appropriate one, as derived in III.2., for this configuration. In order to complete the derivation a drift kinetic equation in axisymmetric configuration is rigorously derived in III.1. The new term is found unimportant for long parallel wave length. It is found helpful to invoke a current approach in the derivation of basic equations, namely to construct the perturbed plasma current from the Vlasov equation, as to access further understanding of physical essence in connection with more fundamental considerations. This approach is shown in III.3.

III. 1 Drift Kinetic Equation in an Axisymmetric Configuration

In the nomenclature of plasma physics the drift kinetic equation is the Vlasov equation in the guiding center approximation. It is given directly from the Liouville theorem for guiding center distribution function.

$$\frac{dF}{dt} \equiv \frac{\partial F}{\partial t} + v_{\parallel} \mathbf{b} \cdot \nabla F + \mathbf{v}_d \cdot \nabla F + \dot{H} \left(\frac{\partial F}{\partial H} \right) = 0, \quad (3.1.1)$$

where F is the guiding center distribution function, $v_{\parallel} = p_{\parallel}/m\gamma$, the parallel velocity, with p_{\parallel} being the parallel momentum and $\gamma = H/mc^2$ and

$$\mathbf{v}_d = (1/m\Omega) \mathbf{b} \times [\mu \nabla B + m\gamma^2 v_{\parallel}^2 \kappa] + c(\mathbf{E} \times \mathbf{B})/B, \quad (3.1.2)$$

$$\dot{H} = qE_{\parallel} v_{\parallel} + q\mathbf{E}_{\perp} \cdot \mathbf{v}_d + \frac{\mu}{\gamma} \frac{\partial B}{\partial t}, \quad (3.1.3)$$

with $\Omega = qB/mc\gamma$ the gyrofrequency, $\mu = p_{\perp}^2/2mB$ the magnetic moment, with p_{\perp} being the perpendicular momentum κ the curvature of magnetic field, \mathbf{E} the electric field, B the magnetic field, m the mass, c the speed of light. The polarization drift is ignored in the expression of \mathbf{v}_d for the later convenience, although it is important for ions.

Equilibrium electric field and its perturbed parallel component are assumed zero. The power is then contributed from two terms:

$$\dot{H} \rightarrow \delta\dot{H} = q\delta\mathbf{E}_{\perp} \cdot \mathbf{v}_d + \frac{\mu}{\gamma} \frac{\partial}{\partial t} \delta B, \quad (3.1.4)$$

The coordinate system in the cylindrically axisymmetric configuration is chosen as (ψ, θ, s) , where ψ is the flux variable, θ is the azimuthal angle, and s is the distance along the field line. The equilibrium magnetic field is defined by the Clebsch representation

$$\mathbf{B} = \nabla\psi \times \nabla\theta \quad (3.1.5)$$

The corresponding geometrical properties in this coordinate system are listed below:

$$\nabla\psi = rB\mathbf{e}_{\psi}, \quad \nabla\theta = \mathbf{e}_{\theta}/r, \quad \mathbf{b} \cdot \nabla\psi = 0, \quad \mathbf{b} \cdot \nabla\theta = 0,$$

$$\nabla S = \mathbf{b} - g_{s\psi}\nabla\psi, \quad \mathbf{b} \times \nabla\theta = -\mathbf{e}_{\psi}/r, \quad \mathbf{b} \times \nabla\psi = rB\mathbf{e}_{\theta},$$

where \mathbf{e}_{ψ} , \mathbf{e}_{θ} , and \mathbf{b} are unit vectors in the $\nabla\psi$, $\nabla\theta$, and \mathbf{B} directions, respectively, and $g_{s\psi}$ is a component of the metric tensor of the curvilinear field line coordinates.

The equilibrium version of Eq.(3.1.1) is

$$v_{\parallel} \mathbf{b} \cdot \nabla f_0 + \mathbf{v}_d \cdot \nabla f_0 = 0 \quad (3.1.6)$$

where $f \equiv f_0 + \delta f$ with f_0 the guiding center distribution function in equilibrium. For the axisymmetric configuration $\mathbf{v}_d \sim \nabla \theta$, and $\mathbf{v}_d \cdot \nabla f_0 = 0$. It yields a constraint on f_0 :

$$\partial f_0 / \partial s = 0. \quad (3.1.7)$$

The linearization of Eq.(3.1.1) leads to the equation for δf :

$$\frac{\partial}{\partial t} \delta f + v_{\parallel} \mathbf{b} \cdot \nabla \delta f + \mathbf{v}_d \cdot \nabla \delta f + v_{\parallel} \delta \mathbf{b} \cdot \nabla f_0 + \delta \mathbf{v}_d \cdot \nabla f_0 + \delta \dot{H} \left(\frac{\partial f_0}{\partial H} \right) = 0 \quad (3.1.8)$$

The Fourier transform of Eq.(3.1.8) is

$$[i(\omega - \omega_d) - v_{\parallel} \frac{\partial}{\partial s}] \delta f = v_{\parallel} \delta \mathbf{b} \cdot \nabla f_0 + \delta \mathbf{v}_d \cdot \nabla f_0 + \delta \dot{H} \left(\frac{\partial f_0}{\partial H} \right) \quad (3.1.9)$$

with $\omega_d = l \mathbf{v}_d \cdot \nabla \theta$.

In terms of new variables $\alpha_1 \equiv \delta \psi$ and $\beta_1 \equiv \delta \theta$ for perturbed fields, the displacement of field line ξ , defined by

$$\delta \mathbf{B} = \nabla \times (\xi \times \mathbf{B}), \quad (3.1.10)$$

is expressed as

$$\xi = -(\alpha_1 / r B) \mathbf{e}_{\psi} - r \beta_1 \mathbf{e}_{\theta}, \quad (3.1.11)$$

and

$$\delta B = \delta B_{\parallel} = B \left(\frac{\partial \alpha_1}{\partial \psi} + i l \beta_1 - g_{s\psi} \frac{\partial \alpha_1}{\partial s} \right) \quad (3.1.12)$$

$$\delta \mathbf{b} = \delta \mathbf{B}_{\perp} / B = -(1/r B) \left(\frac{\partial \alpha}{\partial s} \right) \mathbf{e}_{\psi} - r \left(\frac{\partial \beta_1}{\partial s} \right) \mathbf{e}_{\theta} \quad (3.1.13)$$

Now, we have

$$v_{\parallel} \delta \mathbf{b} \cdot \nabla f_0 = -v_{\parallel} \frac{\partial \alpha_1}{\partial s} \frac{\partial f_0}{\partial \psi} \quad (3.1.14)$$

$$\delta \dot{H} \frac{\partial f_0}{\partial H} = \left[\frac{i\omega q}{lc} \omega_d \alpha_1 - i\omega \frac{\mu}{\gamma} \delta B \right] \frac{\partial f_0}{\partial H} \quad (3.1.15)$$

and

$$\begin{aligned} \delta \mathbf{v}_d \cdot \nabla f_0 = & \nabla f_0 \cdot [(1/m\Omega)(\delta \mathbf{b} \times \mu \nabla B + \mathbf{b} \times \mu \nabla \delta B \\ & + \mathbf{b} \times m\gamma^2 v_{\parallel}^2 \delta \kappa) + c(\delta \mathbf{E} \times \mathbf{b}/B)] \end{aligned} \quad (3.1.16)$$

Using the equations $\delta \kappa = (\delta \mathbf{b} \cdot \nabla) \mathbf{b} + (\mathbf{b} \cdot \nabla) \delta \mathbf{b}$, Eq.(3.1.13), $\mathbf{e}_{\theta} \cdot \partial \mathbf{b} / \partial \psi = 0$, $\mathbf{e}_{\theta} \cdot \partial \mathbf{b} / \partial s = 0$, $\mathbf{e}_{\theta} \cdot \partial \mathbf{e}_{\psi} / \partial s = 0$, $\mathbf{e}_{\theta} \cdot \partial \mathbf{e}_{\theta} / \partial s = 0$, and $\mathbf{e}_{\theta} \cdot \partial \mathbf{b} / \partial \theta = \partial r / \partial s$, we obtain

$$\nabla f_0 \cdot \mathbf{b} \times \delta \kappa = -\frac{\partial f_0}{\partial \psi} B \frac{\partial}{\partial s} r^2 \frac{\partial \beta_1}{\partial \theta} \quad (3.1.17)$$

$$\frac{1}{m\Omega} \nabla f_0 \cdot \delta \mathbf{b} \times \mu \nabla B = -\frac{c}{q\gamma} \mu r^2 \frac{\partial \beta_1}{\partial s} \frac{\partial B}{\partial s} \frac{\partial f_0}{\partial \psi} \quad (3.1.18)$$

$$\frac{1}{m\Omega} \nabla f_0 \cdot \mathbf{b} \times \mu \nabla \delta B = -\frac{c}{q\gamma} \frac{\partial f_0}{\partial \psi} \cdot i l \mu \delta B \quad (3.1.19)$$

$$\nabla f_0 \cdot (c/B) \delta \mathbf{E} \times \mathbf{b} = \frac{\partial f_0}{\partial \psi} \cdot i \omega \alpha_1. \quad (3.1.20)$$

Substituting Eqs.(3.1.14) - (3.1.20) into Eq.(3.1.9) yields

$$\begin{aligned} [i(\omega - \omega_d) - v_{\parallel} \frac{\partial}{\partial s}] \delta f = & -v_{\parallel} \frac{\partial \alpha_1}{\partial s} \frac{\partial f_0}{\partial \psi} + i\omega \left(\frac{q}{lc} \omega_d \alpha_1 - \frac{\mu}{\gamma} \delta B \right) \frac{\partial f_0}{\partial H} \\ & + v_{\parallel} \frac{\partial}{\partial s} \left[\frac{m\gamma v_{\parallel} c}{q} \frac{\partial f_0}{\partial \psi} r^2 \frac{\partial \beta_1}{\partial s} \right] \\ & - \frac{c}{q\gamma} \frac{\partial f_0}{\partial \psi} \cdot i l \mu \delta B + \frac{\partial f_0}{\partial \psi} \cdot i \omega \alpha_1. \end{aligned} \quad (3.1.21)$$

Defining

$$\delta f \equiv \delta f_L - \xi \cdot \nabla f_0, \quad (3.1.22)$$

we obtain an equation for δf_L :

$$\begin{aligned} \gamma [i(\omega - \omega_d) - v_{\parallel} \frac{\partial}{\partial s}] \delta f_L = & -i(\omega - \omega^*) \left(\frac{\partial f_0}{\partial H} \right) (\mu Q_L + m\gamma^2 v_{\parallel}^2 \xi \cdot \kappa) \\ & + \gamma v_{\parallel} \frac{\partial}{\partial s} \left[\frac{m\gamma v_{\parallel} c}{q} \frac{\partial f_0}{\partial \psi} r^2 \frac{\partial \beta_1}{\partial s} \right], \end{aligned} \quad (3.1.23)$$

where

$$\omega^* \equiv -\frac{lc}{q} \frac{\frac{\partial f_0}{\partial \psi}}{\frac{\partial f_0}{\partial H}}, \quad (3.1.24)$$

and

$$Q_L \equiv \delta B + \xi \cdot \nabla B. \quad (3.1.25)$$

The last term of Eq.(3.1.23) results from the combination of the perturbed curvature and the perturbed unit vector \mathbf{b} . This term does not appear explicitly in the conventional approach. It is observed⁴⁹ that part of this term will be cancelled when a FLR correction to δf_L ,

$$\frac{1}{\Omega} \langle (\mathbf{v} \times \delta \mathbf{b}) \cdot \nabla f_0 \rangle_{\alpha} = \frac{mc}{q} v_{\parallel} r^2 \frac{\partial \beta_1}{\partial s} \frac{\partial f_0}{\partial \psi}$$

is included, which leaves a higher order term for large bounce frequency, $(\omega - \omega_d)(mc/q)v_{\parallel}r^2(\partial\beta_1/\partial s)(\partial f_0/\partial\psi)$. Since our use of Eq.(3.1.23) will be restricted to the high bounce limit in the later applications of the thesis, this term can be neglected and we will not discuss it further.

III.2 Quadratic Form in Cylinder with an Embedded Current

In an infinitely long cylindrical model with only azimuthal currents the total magnetic field \mathbf{B} is created by the background plasma current \mathbf{J}_{pc} , the hot plasma current \mathbf{J}_{ph} , and an embedded current \mathbf{J}_{ext} . The total plasma current is denoted by $\mathbf{J}_p = \mathbf{J}_{ph} + \mathbf{J}_{pc}$. The currents are in the θ direction; they depend on r but are independent of θ and z . The configuration is shown in Fig.1.

The momentum balance equation for the plasma is

$$\rho_m \left(\frac{\partial \mathbf{v}}{\partial t} + \mathbf{v} \cdot \nabla \mathbf{v} \right) = -\nabla \cdot \mathbf{P} + \mathbf{J}_p \times \mathbf{B}, \quad (3.2.1)$$

where ρ_m is the mass density and \mathbf{v} the fluid velocity. In the guiding center limit the pressure tensor \mathbf{P} has the form

$$\mathbf{P} = P_{\perp}(\mathbf{I} - \mathbf{b}\mathbf{b}) + P_{\parallel}\mathbf{b}\mathbf{b}.$$

Since $\nabla \times \mathbf{B}_{ext} = \mathbf{J}_{ext}$, $\nabla \times \mathbf{b} = \mathbf{J}_p + \nabla \times \mathbf{B}_{ext}$ and since there is no equilibrium flow, Eq.(3.2.1) yields the perpendicular equilibrium condition

$$\frac{\partial}{\partial r} \left(P_{\perp} + \frac{B^2}{2} \right) = B \frac{\partial B_{ext}}{\partial r}. \quad (3.2.2)$$

Note that the role of curvature in maintaining pressure balance is roughly replaced by the external field gradient. Specifically, Eq.(3.2.2) replaces the three-dimensional equilibrium condition

$$\nabla_{\perp}(P_{\perp} + B^2/2) = \sigma B^2 \kappa, \quad (3.2.3)$$

where $\kappa \equiv (\mathbf{b} \cdot \nabla)\mathbf{b}$ and $\sigma \equiv 1 + (P_{\perp} - P_{\parallel})/B^2$. Thus, we see that the quantity $(1/B) \cdot (\partial B_{ext}/\partial r)$ replaces $\sigma \kappa$. Further, our model has the simplifying aspect

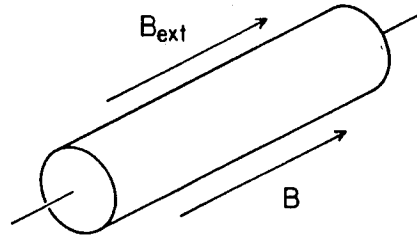


Fig.1 Cylindrical model with an embedded current

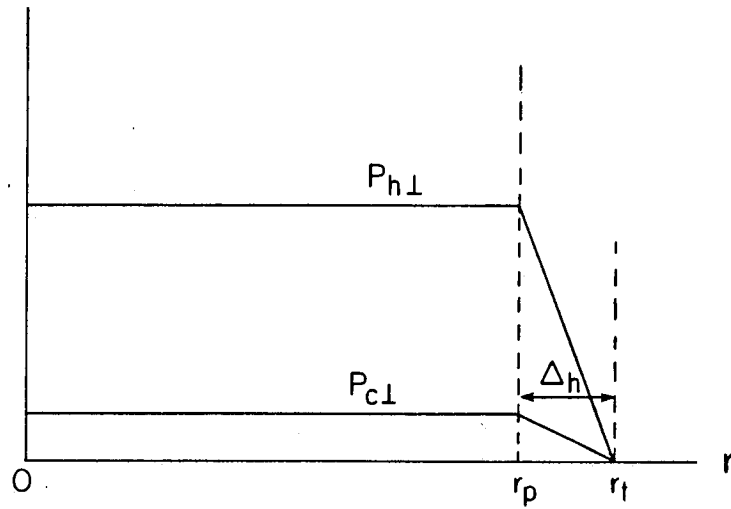


Fig.2 Radial pressure profile for hot electron and background plasma in a cylinder.

" that there is no axial dependence in the equilibrium. A similar model has been used by Ohsawa and Dawson⁸⁰ in numerical simulation of hot particles to produce "curvature" -driven modes.³²

The perturbed electric field (with $E_{\parallel} = 0$) can be written as

$$\delta \mathbf{E} = i\omega(\boldsymbol{\xi} \times \mathbf{B}). \quad (3.2.4)$$

The inertial term in the limit of the cold fluid model is³²

$$i\omega\delta \mathbf{v} = \lambda \boldsymbol{\xi} + i(\omega/\omega_{ci})\lambda(\boldsymbol{\xi} \times \mathbf{b}), \quad (3.2.5)$$

where $\lambda \equiv \omega^2/(1 - \omega^2/\omega_{ci}^2)$, ω_{ci} is the ion cyclotron frequency.

The perturbed pressure is obtained from a perturbed distribution function

δf_j :

$$\begin{aligned} \delta P = & \sum_j \int d\Gamma [\mu B I + (m\gamma^2 v_{\parallel}^2 - \mu B) \mathbf{b} \mathbf{b}] \delta f_j + \delta B_{\parallel} \frac{\partial P}{\partial B} \\ & + \sum_j \int d\Gamma (m\gamma^2 v_{\parallel}^2 - \mu B) (\delta \mathbf{B}_{\perp} \mathbf{b} + \mathbf{b} \delta \mathbf{B}_{\perp}) B^{-1} f_{0j} \end{aligned} \quad (3.2.6)$$

with

$$d\Gamma = \frac{d^3 p}{\gamma} = \frac{2\pi m_h dH d\mu B}{\sqrt{2(H - \mu B)}}, \quad (3.2.7)$$

$$\delta B_{\parallel} = \delta B = -B \nabla \cdot \boldsymbol{\xi} - \boldsymbol{\xi} \cdot \nabla B, \quad (3.2.8)$$

$$\delta \mathbf{B}_{\perp} = \mathbf{B} \cdot \nabla \boldsymbol{\xi}. \quad (3.2.9)$$

In Eq.(3.2.6) f_{0j} is the equilibrium distribution function for species j . We also note that $\delta B_{ext} = 0$.

Therefore the linearization of Eq.(3.2.1) becomes

$$\begin{aligned}
& -\rho_m \lambda \xi - i \frac{\omega}{\omega_{ci}} \rho_m \lambda (\xi \times \mathbf{b}) = \\
& -\nabla \cdot \left(\sum_j \int d\Gamma [\mu B \mathbf{I} + (m\gamma^2 v_{\parallel}^2 - \mu B) \mathbf{b} \mathbf{b}] \delta f_j \right. \\
& + \sum_j \int d\Gamma (m\gamma^2 v_{\parallel}^2 - \mu B) (\delta \mathbf{B}_{\perp} \mathbf{b} + \mathbf{b} \delta \mathbf{B}_{\perp}) B^{-1} f_{0j} + \delta B_{\parallel} \frac{\partial P}{\partial B} \Big) \\
& + (\nabla \times \mathbf{B}_p) \times \delta \mathbf{B} + (\nabla \times \delta \mathbf{B}) \times \mathbf{B},
\end{aligned} \tag{3.2.10}$$

where \mathbf{B}_p is given by $\nabla \times \mathbf{B}_p = \mathbf{J}_p$.

Here we explicitly define the adjoint of ξ in the following forms:

$$\xi_r^{\dagger} \equiv \xi_r(r) \exp(-il\theta - ik_n z)$$

$$\xi_{\theta}^{\dagger} \equiv -\xi_{\theta}(r) \exp(-il\theta - ik_n z)$$

We integrate over the volume of the plasma, and obtain the quadratic form

$$\begin{aligned}
-2\Delta W &= \int dr \left[\rho_m \lambda \xi^{\dagger} \cdot \xi + i \frac{\omega}{\omega_{ci}} \rho_m \lambda \xi^{\dagger} \cdot (\xi \times \mathbf{b}) \right. \\
&\quad \left. - \xi^{\dagger} \cdot \nabla \delta P + \xi^{\dagger} \cdot (\nabla \times \mathbf{B}_p \times \delta \mathbf{B} + \xi^{\dagger} \cdot (\nabla \times \delta \mathbf{B}) \times \mathbf{B}) \right] \\
&= \int dr \left(\rho_m \lambda \xi^{\dagger} \cdot \xi + i \frac{\omega}{\omega_{ci}} \rho_m \lambda \xi^{\dagger} \cdot (\xi \times \mathbf{b}) \right. \\
&\quad \left. + \delta P : \nabla \xi^{\dagger} - \delta \mathbf{B}^{\dagger} \cdot \delta \mathbf{B} + \frac{\delta B}{B} \xi^{\dagger} \cdot \nabla \cdot \mathbf{P} \right) \\
&\quad + \int_{s_i} dA \mathbf{n} \cdot [(\xi^{\dagger} \times \mathbf{B}) \times \delta \mathbf{B} - \xi^{\dagger} \cdot \delta \mathbf{P}] = 0,
\end{aligned} \tag{3.2.11}$$

where we have used $\delta \mathbf{B}^{\dagger} = \nabla \times (\xi^{\dagger} \times \mathbf{B})$ and Eqs.(3.2.8) and (3.3.9), and dA is the incremental area of the bounding surface.

The second equality of Eq.(3.2.11) is obtained by integration by parts, and by using the equilibrium condition. This gives the equation

$$\xi^\dagger \cdot (\nabla \times \mathbf{B}_p) \times \delta \mathbf{B} = \frac{\delta B}{B} \nabla \cdot \mathbf{P} \cdot \xi^\dagger. \quad (3.2.12)$$

The surface term vanishes if the pressure is zero on the boundary and if $(\xi \cdot \mathbf{n}) = 0, (\mathbf{B} \cdot \mathbf{n}) = 0$ (\mathbf{n} is the normal unit vector at the wall). The latter condition is a property of our equilibrium, and $\xi \cdot \mathbf{n} = 0$ is the boundary condition we impose at the wall. After substitution of Eq.(3.2.7), the pressure term in Eq.(3.2.11) becomes

$$\begin{aligned} \int dr \delta P : \nabla \xi^\dagger = & \int dr \left(\nabla \xi^\dagger : \int d\Gamma [\mu B \mathbf{I} + (m\gamma^2 v_\parallel^2 - \mu B) \mathbf{b} \mathbf{b}] \delta f_L \right. \\ & - \nabla \xi^\dagger : (\xi \cdot \hat{\nabla}) \mathbf{P} + \nabla \xi^\dagger : (P_\parallel - P_\perp) \frac{(\delta \mathbf{B}_\perp \mathbf{b} + \mathbf{b} \delta \mathbf{B}_\perp)}{B} \\ & \left. + \delta B \nabla \xi^\dagger : \frac{\partial \mathbf{P}}{\partial B} \right), \end{aligned} \quad (3.2.13)$$

where δf_L is solved from Eq.(3.1.23) in the small v_\parallel limit,

$$\begin{aligned} \delta f_L = & \delta f + \xi \cdot \nabla f_0 \\ = & -\frac{1}{\gamma} \frac{\omega - \omega^*}{\omega - \omega_d} \left(1 + \frac{k_n v_\parallel}{\omega - \omega_d} \right) \mu \delta \hat{B}_L \cdot \frac{\partial f_0}{\partial H} + \frac{k_n v_\parallel}{\omega - \omega_d} \xi_r \frac{\partial f_0}{\partial r}. \end{aligned} \quad (3.2.14)$$

Because there is zero curvature and zero parallel equilibrium current, we have the following equalities for future manipulations:

$$\delta B_L = -B \nabla \cdot \xi,$$

$$\nabla \xi^\dagger : (\xi \cdot \hat{\nabla}) \mathbf{P} = (\nabla \xi^\dagger) (\xi \cdot \hat{\nabla} P_\perp),$$

$$\mathbf{B} \cdot (\delta \mathbf{B}_\perp \cdot \nabla) \xi^\dagger = 0.$$

Then we find

$$\begin{aligned} -2\Delta W = & \int dr \left[(\rho_m \lambda - \sigma k_n^2 B^2) \xi^\dagger \cdot \xi + i \frac{\omega}{\omega_{ci}} \rho_m \lambda \xi^\dagger \cdot (\xi \times \mathbf{b}) \right. \\ & - \tau \delta B_L^\dagger \cdot \delta B_L + \frac{1}{\tau r^2 B^3} (\xi^\dagger \cdot \nabla \psi) (\xi \cdot \nabla \psi) (\hat{\nabla} P_\perp \cdot \nabla B_{ext}) \\ & \left. + \int \frac{d\Gamma}{\gamma} \left(\frac{\omega - \omega^*}{\omega - \omega_d} \right) \left(\frac{\partial f_0}{\partial H} \right) \mu^2 \left(\delta B_L^\dagger + \frac{1}{\tau} \xi^\dagger \cdot \nabla B_{ext} \right) \left(\delta B_L + \frac{1}{\tau} \xi \cdot \nabla B_{ext} \right) \right], \end{aligned} \quad (3.2.15)$$

where

$$\delta B_L \equiv \delta \hat{B}_L - \tau^{-1} \xi \cdot \nabla B_{ext}, \quad \psi \equiv \int^r dr r B.$$

The following equalities were used for the derivation of Eq.(3.2.15):

$$\begin{aligned} -\tau \delta B^\dagger \delta B + \frac{\delta B}{B} \xi^\dagger \cdot \hat{\nabla} P_\perp + \frac{\delta B_L^\dagger}{B} (\xi \cdot \hat{\nabla} P_\perp) \\ = -\tau \delta B_L^\dagger \delta B_L + \frac{1}{\tau B} (\xi^\dagger \cdot \nabla B_{ext}) (\xi \cdot \hat{\nabla}_\perp P_\perp), \end{aligned} \quad (3.2.16)$$

$$\begin{aligned} (\xi^\dagger \cdot \nabla B_{ext}) (\xi \cdot \hat{\nabla} P_\perp) \\ = \frac{1}{r^2 B^2} (\nabla B_{ext} \cdot \hat{\nabla}_\perp P_\perp) (\xi^\dagger \cdot \nabla \psi) (\xi \cdot \nabla \psi). \end{aligned} \quad (3.2.17)$$

The independent variables in the quadratic form Eq.(3.2.15) can be chosen as δB_L and ξ_r . Here ξ_θ is given in terms of δB_L and ξ_r :

$$\xi_\theta = \frac{ir}{l} \left(\frac{\delta B_L}{B} + \frac{\partial \xi_r}{\partial r} - \frac{1}{\tau B^2} \xi_r \frac{\partial P_\perp}{\partial r} \right). \quad (3.2.18)$$

The quadratic form Eq.(3.2.15) is explicitly self-adjoint.

III. 3 Eigenmode Equation and Current

The variation of Eq.(3.2.15) with respect to δB_L^\dagger yields

$$\begin{aligned} & \left(\rho_m \lambda + \frac{l^2}{r^2} B^2 (1 + G_1) - \sigma B^2 k_n^2 \right) \cdot \frac{ir}{l} \left(\frac{\delta B_L}{B} + \frac{d\xi_r}{dr} - \frac{1}{\tau B^2} \xi_r \frac{\partial P_\perp}{\partial r} \right) \\ &= \left(-i \frac{l}{r} B \frac{dB_{ext}}{dr} + \frac{\omega}{\omega_{ci}} \rho_m \lambda - i \frac{l}{r} B^2 (1 + G_1) \frac{1}{r} \frac{d}{dr} r \right) \xi_r, \end{aligned} \quad (3.3.1)$$

where

$$G_1 \equiv \frac{1}{B} \frac{\partial P_\perp}{\partial B} - \frac{1}{B} \int \frac{d\Gamma}{\gamma} \left(\frac{\partial f_0}{\partial H} \right) \frac{\omega - \omega_*}{\omega - \omega_d} \mu^2 B. \quad (3.3.2)$$

Using the equality

$$\frac{1}{\omega - \omega_d} = -\frac{1}{\omega_d} - \frac{\omega}{\omega_d^2} + \frac{\omega^2}{\omega_d^2(\omega - \omega_d)}, \quad (3.3.3)$$

we write

$$1 + G_1 = \left(\frac{dB_{ext}/dr}{dB/dr} \right) - \frac{1}{B} \frac{dB}{dr} \cdot \frac{dP_{\perp c}}{dr} + \beta_{\perp c} - \frac{\omega}{\bar{\omega}_{db}} + K_h(\omega), \quad (3.3.4)$$

where

$$\bar{\omega}_{db} \equiv -\frac{lc}{qB^2 r^2} \left(\frac{dB}{dr} \right)^2 \left[\frac{d}{dr} \left(\frac{n_h}{B} \right) \right]^{-1}, \quad (3.3.5)$$

$$K_h(\omega) \equiv -\frac{\omega^2}{m_h (lc/qB^2 r) (dB/dr)^2} \cdot \int dp_\parallel d\mu \frac{(\partial f_{0h}/\partial r)_{p_\parallel}}{\omega - \omega_d}, \quad (3.3.6)$$

and p_\parallel is the parallel momentum and m_h is the mass of the hot species. In attaining Eq.(3.3.4), use is made of the equality

$$\left(\frac{\partial f_0}{\partial r}\right)_{p_{\parallel}} = \left(\frac{\partial f_0}{\partial r}\right)_H + \left(\frac{\partial f_0}{\partial H}\right)_r \cdot \left(\frac{\partial H}{\partial r}\right)_{p_{\parallel}}.$$

We also note that Eqs.(3.3.4)-(3.3.6) give essentially the same function for $1 + G_1$ that was calculated in Ref.32. Explicitly, we rewrite some important definitions:

$$\omega_d = \frac{\mu l c}{q B r \gamma} \frac{dB}{dr} \quad \text{and} \quad \mu = \frac{p_{\perp}^2}{2mB}, \quad (3.3.7)$$

$$P_{\perp} = 2\pi m B^2 \int dp_{\parallel} d\mu \mu \frac{f_0}{\gamma}, \quad (3.3.8)$$

where

$$\gamma \equiv (1 + 2\mu B/mc^2 + p_{\parallel}^2/m^2 c^2)^{1/2}. \quad (3.3.9)$$

The variation of Eq.(3.2.15) with respect to ξ_r^{\dagger} gives the second equation

$$\begin{aligned} & \left[-i \frac{l}{r} \left(\frac{dB_{ext}}{dr} \right) \left(\frac{dP_{\perp}}{dr} \right) + i \frac{l}{r} B \left(\frac{dB_{ext}}{dr} \right)^2 - i \frac{l}{r} B (\rho_m \lambda - k_n^2 \sigma B^2) \right. \\ & \left. + i \frac{l}{r} B^2 \frac{dB_{ext}}{dr} \frac{1}{r} \frac{d}{dr} r - i \frac{B}{r} \frac{d}{dr} \rho_m \lambda \frac{\omega}{\omega_{ci}} r \right] \xi_r \\ & = \left(\frac{l^2}{r^2} B^2 \frac{dB_{ext}}{dr} - \frac{l}{r} \rho_m \lambda B \frac{\omega}{\omega_{ci}} - \frac{B}{r} \frac{d}{dr} (\rho_m \lambda - k_n^2 \sigma B^2) r \right) \\ & \cdot \frac{ir}{l} \left(\frac{\delta B_L}{B} + \frac{d\xi_r}{dr} - \frac{1}{\tau B^2} \xi_r \frac{\partial P_{\perp}}{\partial r} \right). \end{aligned} \quad (3.3.10)$$

Combining Eq.(3.3.1) and Eq.(3.3.10), we obtain the radial eigenmode equation:

$$\begin{aligned}
& \frac{1}{r} \frac{d}{dr} (\rho_m \lambda - \sigma k_n^2 B^2) \frac{r}{Q} (1 + G_1) \frac{d}{dr} r \xi_r - \xi_r \left\{ \frac{l^2}{r B} \left(\frac{dB_{ext}}{dr} \right) \left(\frac{dP_{\perp}}{dr} \right) \right. \\
& + \frac{d}{dr} \left(\frac{\rho_m \lambda l (\omega / \omega_{ci}) (1 + G_1) - (\rho_m \lambda - \sigma k_n^2 B^2) (r/B) (dB_{ext}/dr)}{Q} \right) \\
& - \rho_m \lambda \frac{\omega}{\omega_{ci}} \frac{2l}{QB} \left(\frac{dB_{ext}}{dr} \right) - \frac{l^2}{Qr} (\rho_m \lambda - \sigma k_n^2 B^2) (1 + G_1) \\
& \left. - \frac{r \rho_m \lambda^2}{Q v_A^2} \left[\left(1 - \frac{\sigma k_n^2 B^2}{\rho \lambda} \right)^2 - \frac{\omega^2}{\omega_{ci}^2} \right] + \frac{l^2}{r} \left(\frac{dB_{ext}}{dr} \right)^2 \cdot \left(\frac{1}{Q} - 1 \right) \right\} = 0,
\end{aligned} \tag{3.3.11}$$

where

$$Q \equiv 1 + G_1 + \sigma k_n^2 r^2 / l^2 - \lambda r^2 / l^2 v_A^2. \tag{3.3.12}$$

Equation (3.3.11) is quite similar to the radial eigenmode equation for the Z-pinch model³² if we note that $(1/B)(dB_{ext}/dr)$ plays the role of curvature. The cylindrical configuration does not produce the G_2, G_3 terms which exist in the Z-pinch model. This is due to the absence of curvature drift. We note that these terms are proportional to the parallel temperature and arise because of bending stresses in the equilibrium. In the present model there are no such bending stresses and G_2 and G_3 do not appear. Even in Ref.32, G_2 and G_3 are of minor importance and can even be ignored if $P_{\parallel}/P_{\perp} \ll 1$. Thus these are not essential terms in the hot particle theory. However we keep perturbed line-bending terms ignored in Ref.32, which dealt with the flute mode. In this way we shall be able to study the interaction between the precessional wave and the whistler-like or shear Alfvén waves in the core plasma.

Eqs.(3.3.1) and (3.3.10) can also be derived from the linearized momentum equation Eq.(3.2.10) by calculating $\mathbf{e}_{\theta} \nabla : \delta \mathbf{P}$, and $\mathbf{e}_r \nabla : \delta \mathbf{P}$ on the basis of the expression of $\delta \mathbf{P}$ given by Eq.(3.2.6). It results in

$$\mathbf{e}_\theta \nabla : \delta \mathbf{P} = -B^2 G_1 \left(\frac{il}{r} \right) \nabla \cdot \xi - \frac{il}{r} \xi_r \frac{dP_\perp}{dr} + k_n^2 B^2 (\sigma - 1) \xi_\theta, \quad (3.3.13)$$

$$\mathbf{e}_r \nabla : \delta \mathbf{P} = -\frac{d}{dr} B^2 G_1 \nabla \cdot \xi - \frac{d}{dr} \left(\xi_r \frac{dP_\perp}{dr} \right) + k_n^2 B^2 (\sigma - 1) \xi_r, \quad (3.3.14)$$

which may be combined as

$$\nabla \cdot \delta \mathbf{P} = \nabla \cdot [\delta B_L B G_1 - \xi \cdot \nabla P_\perp] + k_n^2 B^2 (\sigma - 1) \xi. \quad (3.3.15)$$

Substituting Eq.(3.3.13) into the θ - component of Eq.(3.2.10) yields the first equation, Eq.(3.3.1). The r-component of Eq.(3.2.10), with substitution of Eq.(3.3.14), are then combined with Eq.(3.3.1) to obtain the second equation, Eq.(3.3.10).

It is also interesting to derive the perpendicular perturbed current form in the cylindrical model. This is an alternate approach that leads to eigenmode equation in current literature.⁶⁶

The linearized current in the zero-Larmor radius limit is given by

$$\begin{aligned} \delta \mathbf{J}_\perp = \frac{c}{B} \left\{ -\frac{\delta B}{B} \mathbf{b} \times [\nabla P_\perp + \kappa(P_\parallel - P_\perp)] + \mathbf{b} \times \kappa(\delta P_\parallel - \delta P_\perp) \right. \\ \left. + \delta \mathbf{b} \times [\nabla P_\perp + \kappa(P_\parallel - P_\perp)] \right. \\ \left. + \mathbf{b} \times [\nabla \delta P_\perp + \delta \kappa(P_\parallel - P_\perp)] \right\} + nq\delta \hat{\mathbf{v}}_d, \end{aligned} \quad (3.3.16)$$

of which the last term on the r.h.s., $nq\delta \hat{\mathbf{v}}_d$, is the ion polarization current. For cold ions it is associated with the inertial term given by Eq.(3.2.5). The

remainder of the r.h.s. of Eq.(3.3.16) results from the linearization of CGL (Chew-Goldberger-Low)⁸¹ current to express the perturbed current in terms of the perturbed pressure.

$$\mathbf{J}_\perp = (c/B)\mathbf{b} \times [\nabla P_\perp + \kappa(P_\parallel - P_\perp)]. \quad (3.3.17)$$

Use is made of Eqs.(3.1.22),(3.3.2) and the definition of δP_\perp ,

$$\delta P_\perp \equiv \delta B \frac{\partial P_\perp}{\partial B} + \int d\Gamma \mu B \delta f, \quad (3.3.18)$$

to obtain

$$\delta P_\perp = -B^2 G_1 \nabla \cdot \xi - \xi \cdot \nabla P_\perp. \quad (3.3.19)$$

We note that \mathbf{b}, κ - term does not contribute ($\kappa = 0$ in the cylindrical model), while $\delta \kappa$ contributes a bending term. The perturbed perpendicular current is thus expressed in terms of ξ to be

$$\begin{aligned} \delta \mathbf{J}_\perp = & -\frac{c}{B} \mathbf{b} \times \left[\nabla (B^2 G_1 \nabla \cdot \xi + \xi \cdot \nabla P_\perp) + \left(\frac{1}{B} \xi \cdot \nabla B - \nabla \cdot \xi \right) \nabla P_\perp \right. \\ & \left. + k_n^2 B^2 (1 - \sigma) \xi \right] + \left[\rho_m \lambda \xi + i \frac{\omega}{\omega_{ci}} \rho_m \lambda (\xi \times \mathbf{b}) \right] \times \mathbf{b}. \end{aligned} \quad (3.3.20)$$

Substituting Eq.(3.3.20) into Ampere's Law yields the same equations as Eqs. (3.3.1) and (3.3.10). The physics contained in the parallel perturbed current is retained in the formalism through current conservation $\nabla \cdot \delta \mathbf{J} = 0$, although δJ_\parallel does not appear explicitly.

IV. Hot Electron Interchange Mode in Disk-like Configuration

The hot electron interchange mode has been studied for both WKB - type modes^{28,29,32} (low and high frequency) and for the layer - type of mode⁴² (low frequency only in ring - like configuration). This interchange mode is believed important since it sets an upper limit on the ratio of hot to cold plasma density for the stability. For sufficiently high density of hot electrons the MHD growth rate is likely to approach the curvature frequency of hot electrons, which results in coupling between positive energy MHD mode and negative precessional mode.

For the theory presented below the hot electron interchange mode of layer type is analyzed in a disk configuration with steep boundary layer (Fig.2) in connection with interacting background interchange mode. Comparison is also given with numerical simulation⁸² in the electrostatic limit [cf. II].

In the theoretical analysis, use is made of the eigenmode equation in the cylindrical model with embedded current, Eq.(3.3.11) with the following approximations:

- (1) $k_{\parallel} = 0$ (flute - type).
- (2) For low background plasma density and steep boundary layer, the 4th and 6th terms of Eq.(3.3.11) are negligible and we may take

$$\frac{\lambda r^2}{lv_A^2} \ll 1 + G_1. \quad (4.1)$$

- (3) The exponential hot electron distribution is replaced by a δ - function.

Then Eq.(3.3.1) reduces to an eigenmode equation

$$\begin{aligned} \frac{d}{dr} \rho \lambda r \frac{d}{dr} \phi - \phi \left\{ \kappa \frac{l^2}{r} \left(\frac{dP_{h\perp}}{dr} \right) \frac{\hat{\omega} + \tilde{\beta}_{c\perp}}{\hat{\omega} - (1 - \tilde{\beta}_{c\perp})} + \kappa \frac{l^2}{r} \left(\frac{dP_{c\perp}}{dr} \right) \right. \\ \left. + \frac{d}{dr} \rho \lambda \left[l \frac{\omega}{\omega_{ci}} - \kappa r \frac{\hat{\omega} - (1 - \tilde{\beta}_{c\perp} - \zeta)}{\hat{\omega} - (1 - \tilde{\beta}_{c\perp})} \right] + \frac{l^2}{r} \rho \lambda \right\} = 0, \end{aligned} \quad (4.2)$$

where $\hat{\omega} \equiv \omega/\bar{\omega}_\kappa$, with $\bar{\omega}_\kappa \equiv (T_h c l / e B r) \kappa$, the curvature frequency, $\kappa \equiv (1/B)(dB_{ext}/dr)$, the effective curvature, $\zeta \equiv (1/\kappa B^2)(dP_{h\perp}/dr)$, $\phi \equiv r \xi_r$, and $\tilde{\beta}_{c\perp} \equiv (1/\kappa B^2)(dP_{c\perp}/dr)$.

For a steep boundary layer we expand

$$\phi = \phi_0 + \epsilon \phi_1, \quad \epsilon \sim l \Delta / r,$$

with Δ the boundary layer width.

The lowest order equation is

$$\frac{d}{dr} \rho \lambda r \frac{d\phi_0}{dr} = 0. \quad (4.3)$$

We only take the layer - type solution, a slowly varying solution within the layer: $\phi_0 = \text{const.}$

The integration over r to r_1 (Fig.2) yields the first order solution:

$$\begin{aligned} \frac{d\phi_1(r)}{dr} = \frac{\kappa}{\rho \lambda} \left(\frac{l}{r} \right)^2 \left[\left(\frac{dP_{h\perp}}{dr} \right) \frac{\hat{\omega} + \tilde{\beta}_{c\perp}}{\hat{\omega} - (1 - \tilde{\beta}_{c\perp})} + \left(\frac{dP_c}{dr} \right) \right] \phi_0(r - r_1) \\ + \left(\frac{l}{r} \right) \frac{\omega}{\omega_{ci}} \phi_0 + \frac{1}{2} \left(\frac{l}{r} \right)^2 (r_1 - r) \phi_0 - \kappa \frac{\hat{\omega} - (1 - \tilde{\beta}_{c\perp} - \zeta)}{\hat{\omega} - (1 - \tilde{\beta}_{c\perp})} \phi_0. \end{aligned} \quad (4.4)$$

The dispersion relation is obtained by integrating of Eq.(4.2) over the steep boundary layer, substituting Eq.(4.4), and matching the solution in the homogeneous plasma regions:

$$\frac{1}{\phi(r_p)} \frac{d\phi(r_p)}{dr} = \frac{|l|}{r_p}, \quad (4.5)$$

where r_p is the boundary position in Fig.2. The dispersion relation is

$$\frac{\omega^2}{1 + Sgn(l)\frac{\omega}{\omega_{ci}}} + \gamma_{MHD}^2 \frac{\omega + \tilde{\beta}_{c\perp}\tilde{\omega}_\kappa}{\omega - (1 - \tilde{\beta}_{c\perp})\tilde{\omega}_\kappa} + \gamma_{MHD_c}^2 = 0 \quad (4.6)$$

with

$$\gamma_{MHD}^2 \equiv |\tilde{\omega}_\kappa|\omega_{ci}(n_h/n_i), \quad (4.7)$$

$$\gamma_{MHD_c}^2 \equiv (\tilde{\beta}_{c\perp}/\zeta)\gamma_{MHD}^2, \quad (4.8)$$

and n_h the hot electron density, n_i the ion density.

A similar dispersion relation is derived from the sharp boundary gravity model in the electrostatic limit⁸³

$$\frac{\omega^2}{1 + Sgn(k_y)\frac{\omega}{\omega_{ci}}} + \gamma_{MHD}^2 \frac{\omega}{\omega - \tilde{\omega}_\kappa} + \gamma_{MHD_c}^2 + \gamma_{MHD_i}^2 \frac{\omega^2}{\omega_{ci}^2 - \omega^2} = 0, \quad (4.9)$$

where $k_y \rightarrow l/r$, and $\gamma_{MHD_c}^2 = \gamma_{MHD_i}^2 + (n_e/n_i)\gamma_{MHD_e}^2$, with n_e the background electron density, $\gamma_{MHD_i}^2 \equiv |k_y|g_i$, $\gamma_{MHD_e}^2 \equiv |k_y|(m_e/m_i)g_e$, with $g_i \equiv |\kappa|v_{th,j}^2 > 0$, j the species and $v_{th,j}$ the thermal velocity of j species. For later convenience, we also introduce $\gamma_{MHD_h}^2 \equiv |k_y|(m_e/m_i)g_h$, and have $\gamma_{MHD}^2 = \gamma_{MHD_h}^2(n_h/n_i)$. We note that Eq.(4.9) is an alternative form of Eq.(2.10) [by transforming $k_y \rightarrow -k_y$, $v_d \rightarrow -v_d$ and identifying $\tilde{\omega}_\kappa$ with $k_y v_d$].

When comparing Eq.(4.9) with Eq.(4.6), we find that the $\tilde{\beta}_{c\perp}$ term is negligible in the electrostatic gravity model; however, the finite ion temperature for finite ω_{ci} is neglected in the cylindrical model since the ω_{ci} effect is merely taken into account in the inertial term of the quadratic form, Eq.(3.2.15). Hence, the dispersion relation, Eq.(4.6), is valid only for low ion temperature, $T_i \rightarrow 0$, if the γ_{MHD_i} term is important when $\omega \geq \omega_{ci}$.

Eq.(4.6) is a cubic equation in ω . For low frequency limit we ignore the cubic ω^3 terms. The stability criterion is found to be

$$\frac{n_h}{n_i} \geq 4 \frac{|\tilde{\omega}_\kappa|}{\omega_{ci}} \cdot \tilde{\beta}_{c\perp} (1 - \tilde{\beta}_{c\perp}) \left(1 + \frac{\tilde{\beta}_{c\perp}}{\zeta}\right)^2 \cdot \left(\frac{1 - \tilde{\beta}_{c\perp}}{\zeta} - 1\right). \quad (4.10)$$

If $\zeta > 1 - \tilde{\beta}_{c\perp}$, the diamagnetic well effect plays the role of stabilization and there is no restriction on n_h/n_i for the interacting background interchange mode. However, this mechanism does not exist in the electrostatic limit. Instead, the stability criterion then becomes [cf.Eq.(2.13)]

$$\frac{n_h}{n_i} > \frac{4(|\tilde{\omega}_\kappa|/\omega_{ci})(P_c/P_h)}{(1 + P_c/P_h)^2} \quad (4.11)$$

When the diamagnetic well vanishes, charge uncovering effects enter for stabilization and set a lower limit on n_h/n_i .

The hot electron interchange mode is the solution of Eq.(4.6) with neglect of γ_{MHDc}^2 term. The stability criterion is

$$\frac{[(1 + \tilde{\beta}_{c\perp}/\zeta)(n_h/n_i) - (1 - \tilde{\beta}_{c\perp})]^2}{1 + \frac{|\tilde{\omega}_\kappa|}{\omega_{ci}} \tilde{\beta}_{c\perp} + \frac{\tilde{\beta}_{c\perp}}{\zeta} \left[1 - \frac{|\tilde{\omega}_\kappa|}{\omega_{ci}} (1 - \tilde{\beta}_{c\perp})\right]} \geq \frac{n_h}{n_i} \cdot \frac{\omega_{ci}}{|\tilde{\omega}_\kappa|}. \quad (4.12)$$

For small $\tilde{\beta}_{c\perp}/\zeta$ Eq.(4.12) can be reduced to either

$$\frac{n_h}{n_i} \leq 1 + 2 \frac{\omega_{ci}}{|\tilde{\omega}_\kappa|} + \tilde{\beta}_{c\perp} - 2 \frac{\omega_{ci}}{|\tilde{\omega}_\kappa|} \sqrt{\left(1 + \frac{|\tilde{\omega}_\kappa|}{\omega_{ci}}\right) \left(1 + \tilde{\beta}_{c\perp} \frac{|\tilde{\omega}_\kappa|}{\omega_{ci}}\right)}, \quad (4.13)$$

or

$$\tilde{\beta}_{c\perp} \leq 1 + \frac{n_h}{n_i} - \sqrt{4 \left(\frac{n_h}{n_i}\right) \left(1 + \frac{\omega_{ci}}{|\tilde{\omega}_\kappa|}\right)}. \quad (4.14)$$

In the limit of $\tilde{\beta}_{c\perp} \rightarrow 0$ this criterion just reduces to that from an electrostatic model⁸² [cf. Eq.(2.11)].

The solution for marginal stability of Eq.(4.6) is given by Fig.3 and Fig.4. In Fig.3 we also give the marginal stability determined by Eq.(4.13) for comparison. In Fig.5 we show the results for fixed n_h/n_i and $|\omega_\kappa|/\omega_{ci}$, including the results given by Eq.(4.14), which is valid for small $\tilde{\beta}_{c\perp}/\zeta$. Note that Eq.(4.6) is more pessimistic than Eq.(4.13). Results only agree for $\beta_{c\perp} \ll \zeta$.

When ζ is below unity, the behavior of hot electron interchange mode undergoes a change. Its turning point occurs at the place where the r.h.s. of Eq.(4.14) equals zero. For example, when n_h/n_i is just a bit higher than the critical value (for $|\tilde{\omega}_\kappa|/\omega_{ci} = 3.0$, this critical value is $n_h/n_i = 1/3.0$), the marginal stability of hot electron interchange mode does not have a large ζ limit (curve h4 in Fig.5).

Because the hot electron interchange mode sets an upper limit of n_h/n_i , while the low frequency mode sets up a lower limit of n_h/n_i , when $\zeta < 1 - \tilde{\beta}_{c\perp}$, we expect there is a situation for which no stable region can exist. Using Eqs.(4.11) and (4.12) and assuming $(1 + \tilde{\beta}_{c\perp}/\zeta)(n_h/n_i) \ll 1 - \tilde{\beta}_{c\perp}$, we find that there is no stable region unless the following inequality holds:

$$\frac{1 - \tilde{\beta}_{c\perp}}{1 + \frac{|\omega_\kappa|}{\omega_{ci}}\tilde{\beta}_{c\perp} + \frac{\tilde{\beta}_{c\perp}}{\zeta} \left[1 - \frac{|\tilde{\omega}_\kappa|}{\omega_{ci}}(1 - \tilde{\beta}_{c\perp}) \right]} > \frac{16\tilde{\beta}_{c\perp}}{\left(1 + \frac{\tilde{\beta}_{c\perp}}{\zeta}\right)^2} \left(\frac{1 - \tilde{\beta}_{c\perp}}{\zeta} - 1 \right). \quad (4.15)$$

Since smaller $|\tilde{\omega}_\kappa|/\omega_{ci}$ favors the existence of stable region, Eq.(4.15) can be simplified to be

$$(1 - \tilde{\beta}_{c\perp})(1 + \tilde{\beta}_{c\perp}/\zeta) > 16\tilde{\beta}_{c\perp} [(1 - \tilde{\beta}_{c\perp})/\zeta - 1] \quad (4.16)$$

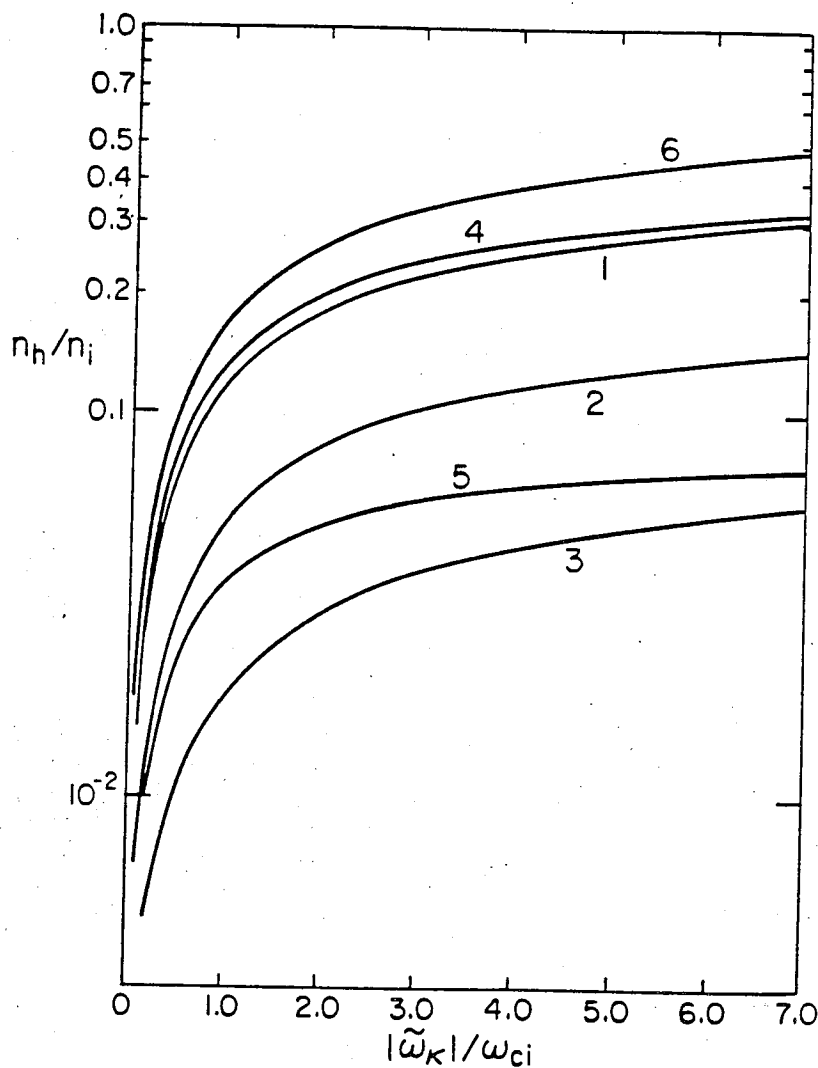


Fig.3 Marginal stability for hot electron interchange mode. Curve 1, 2, and 3 are numerical solutions of Eq.(4.6) with $\zeta = 5.0$, $\tilde{\beta}_{c\perp} = 0.1, 0.3$, and 0.5 respectively. Curve 4 and 5 are approximate analytical results from Eq.(4.13) for $\zeta = 5.0$, $\tilde{\beta}_{c\perp} = 0.1, 0.5$ respectively. Curve 6 is the exact analytical result of Eq.(4.13) with $\tilde{\beta}_{c\perp} = 0.0$. The stable regions are below the corresponding curves.

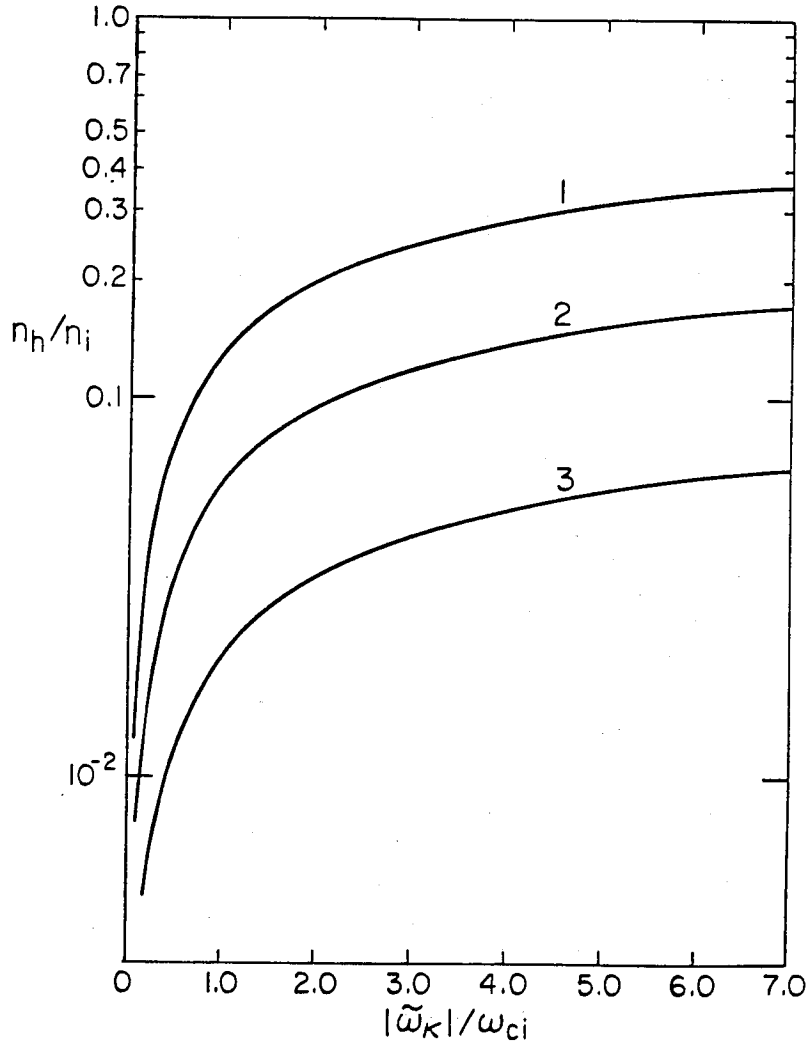


Fig.4 Marginal stability for hot electron interchange mode. Curve 1, 2 and 3 are numerical solutions of Eq.(4.6) with $\zeta = 1.0$, $\tilde{\beta}_{c\perp} = 0.1, 0.3$ and 0.5 respectively. The stable regions are below the corresponding curves.

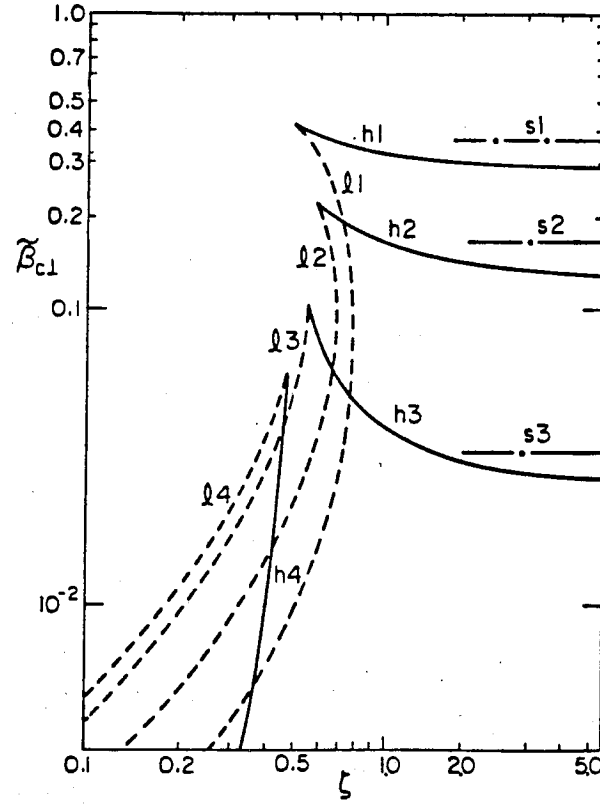


Fig.5 Marginal stability for hot electron interchange mode and low frequency mode. The solid lines are hot electron interchange branch (curve $h1, h2, h3$, and $h4$ with $|\bar{\omega}_\kappa|/\omega_{ci} = 3.0, n_h/n_i = 0.1, 0.2, 0.3$, and 0.335 respectively); the dashed lines are low frequency mode branch ($l1, l2, l3$, and $l4$ for the same respective parameters $|\bar{\omega}_\kappa|/\omega_{ci} = 3.0, n_h/n_i = 0.1, 0.2, 0.3$, and 0.335). The marginal stability curves given by the approximate analytic expression as $\zeta \rightarrow \infty$ are shown by the dash-dot straight lines on the right part of the plot ($s1, s2$, and $s3$ with $|\bar{\omega}_\kappa|/\omega_{ci} = 3.0, n_h/n_i = 0.1, 0.2$ and 0.3 , respectively). The stability region corresponds to the area enclosed by the h_j, l_j curves.

or

$$\zeta > 15\tilde{\beta}_{c\perp}(1 - \tilde{\beta}_{c\perp})/(1 + 15\tilde{\beta}_{c\perp}) \quad (4.17)$$

We illustrate two examples for small stable regions in Fig.6. Higher values of $\tilde{\beta}_{c\perp}$ decrease the stable region.

In Fig.5 we find a transition between low frequency branch to high frequency branch or vice versa occurring at cusp points for various n_h/n_i with $|\tilde{\omega}_\kappa|/\omega_{ci} = 3.0$. This phenomenon is indeed valid as the solution of our dispersion relation, Eq.(4.6), but we should be careful in evaluating its significance, as our theory is subject to a restriction that the diamagnetic drift frequency of the background plasma is less than curvature drift frequency of the hot particles. Therefore, there exists a constraint on parameters:

$$\frac{T_c}{E_h} \equiv \frac{n_h}{n_i} \frac{\tilde{\beta}_{c\perp}}{\zeta} \ll \Delta_h \kappa \quad (4.18)$$

where T_c is the background plasma temperature and E_h , the hot particle energy. Thus, typically, $\kappa\Delta_h \geq 0.1$ is the restriction that needs to be satisfied near the cusp points.

Comparisons are given between the analytical theory for the electrostatic gravity model, Eq.(4.9)⁸³, and numerical simulation done by T.Kamimura⁸². The time evolution of the hot electron interchange instability is illustrated in Fig.7. It shows that the growth rate is smaller for lower hot to cold density ratio. In Fig.8 the theoretical curve of growth rate is compared with the simulation points for the following parameters: $g_e = 6.25 \times 10^{-5}$, $g_h = 2.5 \times 10^{-2}$, $g_i \sim 0$, $|\tilde{\omega}_\kappa|/\omega_{ci} = 3.927$. We find that the agreement between the two is fairly good, considering how simple the theoretical model is.

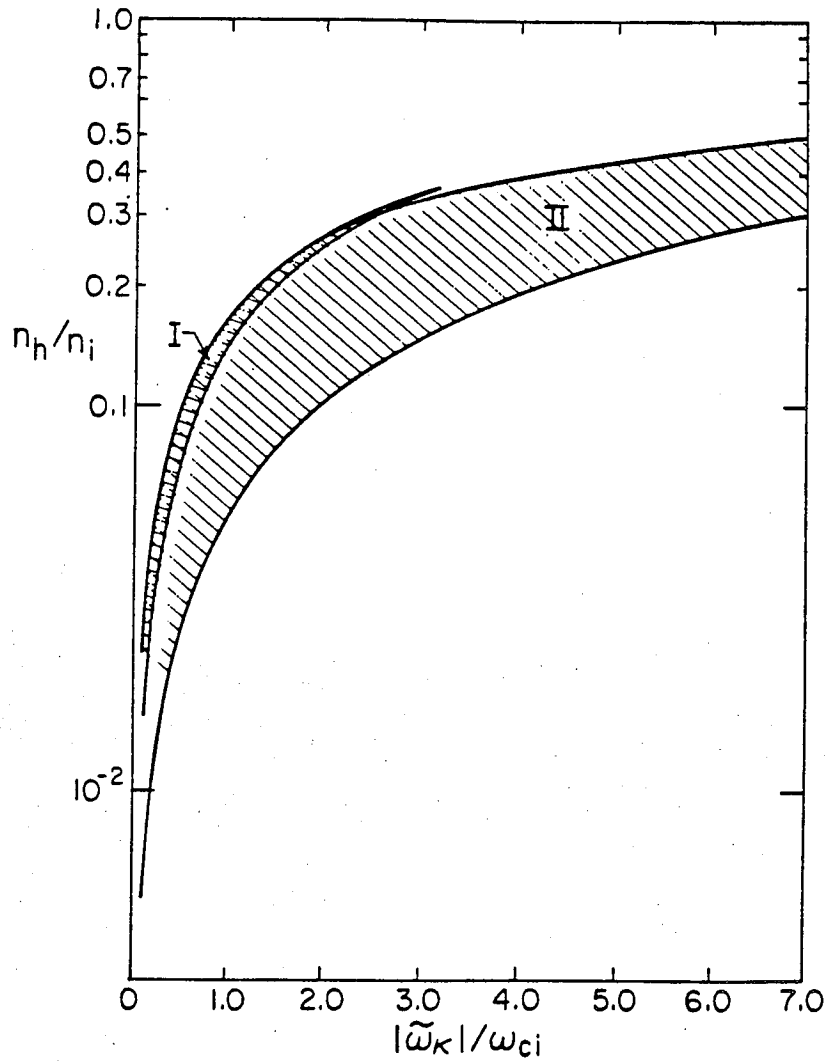


Fig.6 Stable region bound by hot electron interchange mode (upper bound) and low frequency mode (lower bound) when $\zeta < 1 - \tilde{\beta}_{c\perp}$. Stable regions are labeled by shaded area. Region I is for $\zeta = 0.4, \tilde{\beta}_{c\perp} = 0.04$; Region II is for $\zeta = 0.4, \tilde{\beta}_{c\perp} = 0.01$.

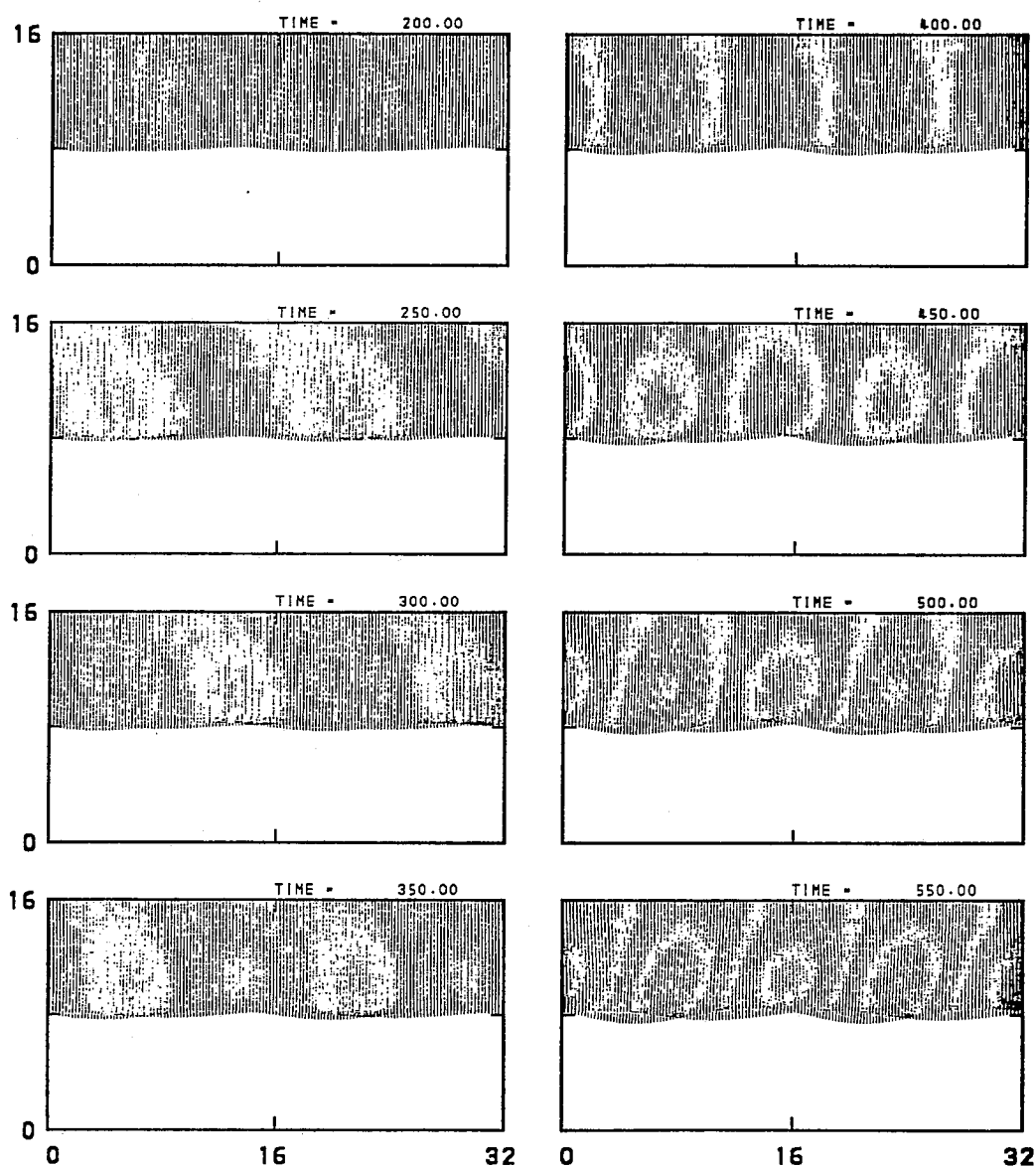
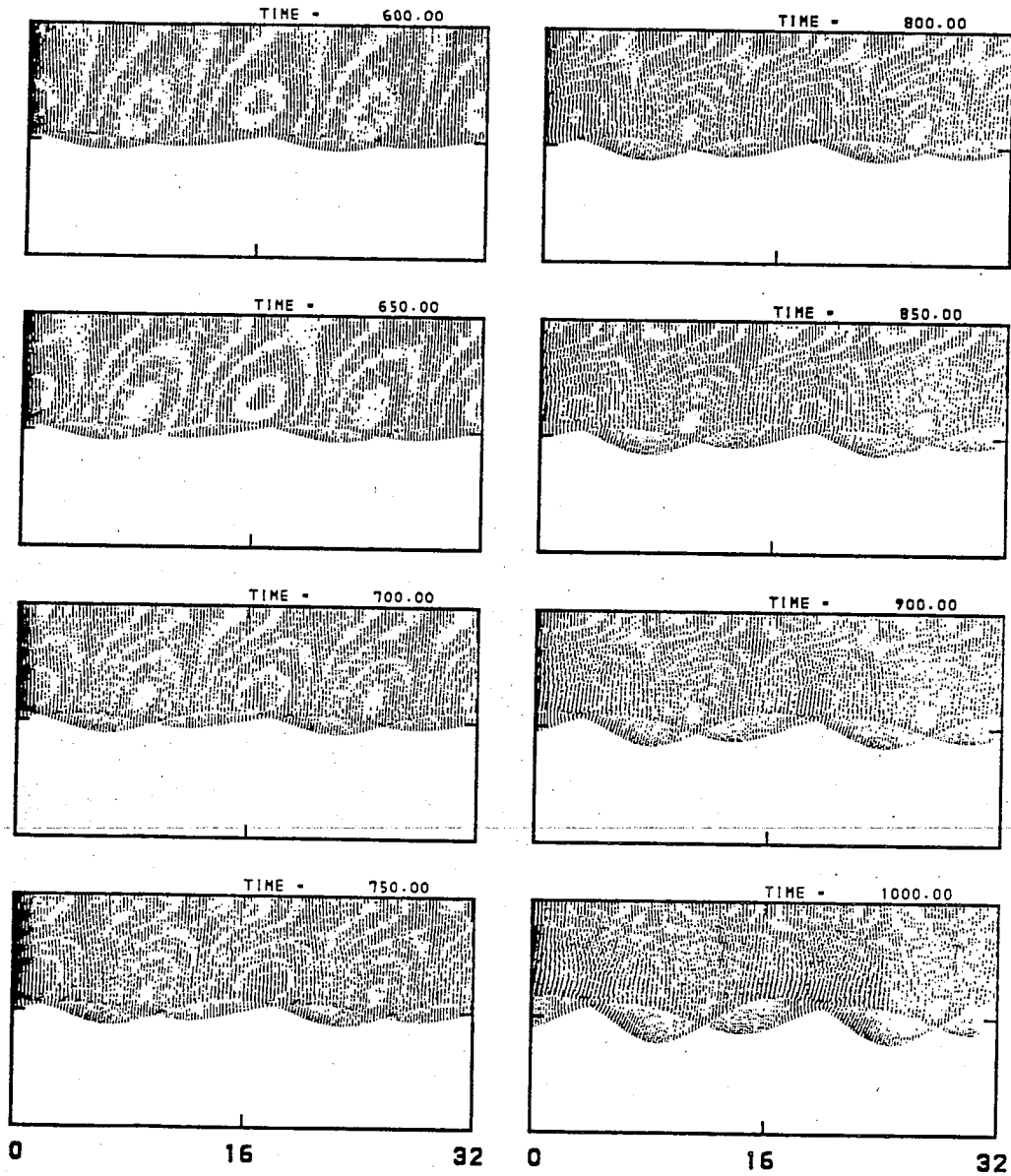


Fig.7 Time evolution of numerical simulation in a sharp boundary gravity model⁸² for $|\tilde{\omega}_\kappa|/\omega_{ci} = 3.927$.

Fig.7 (a) $n_h/n_i = 0.5$.



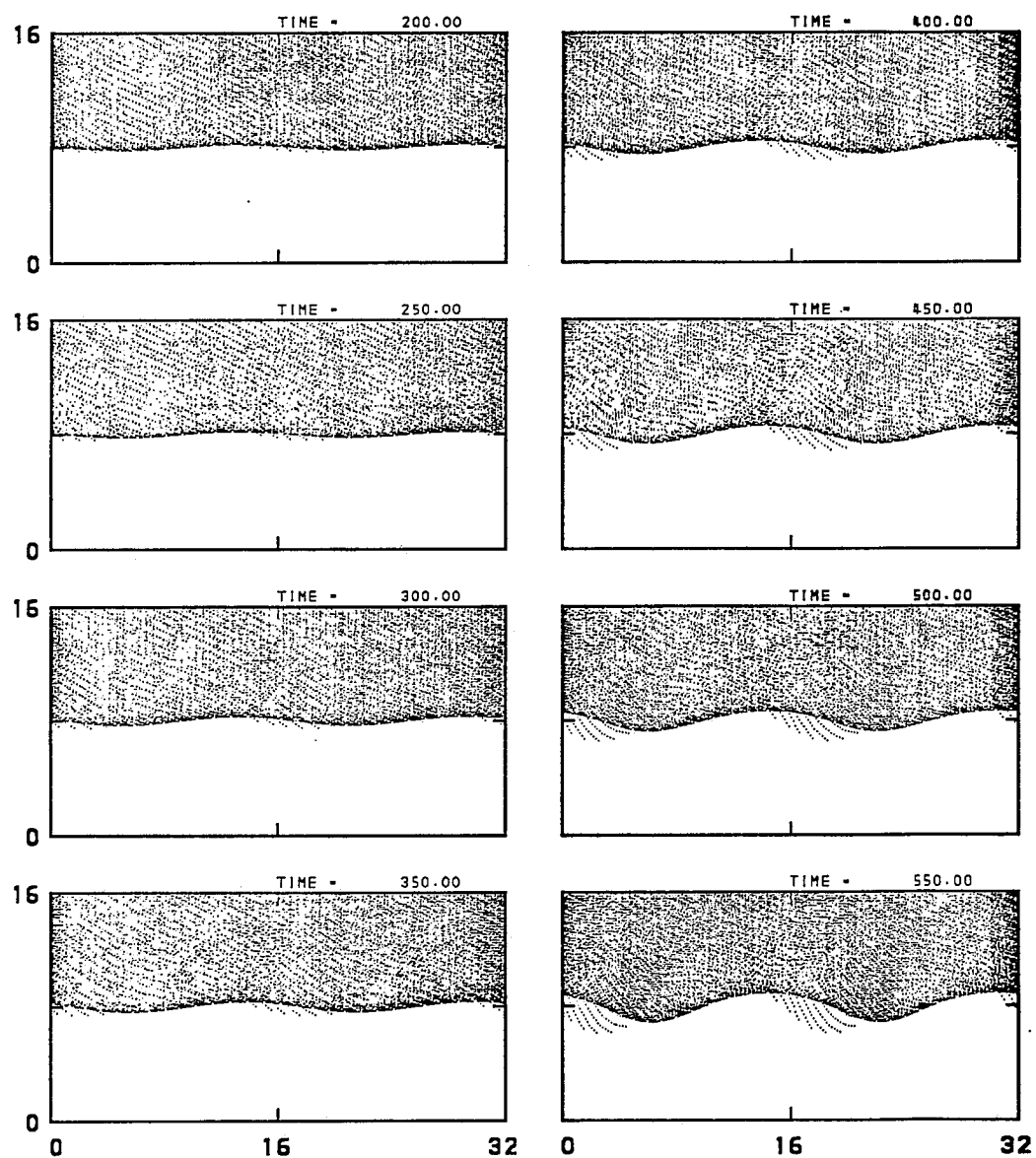
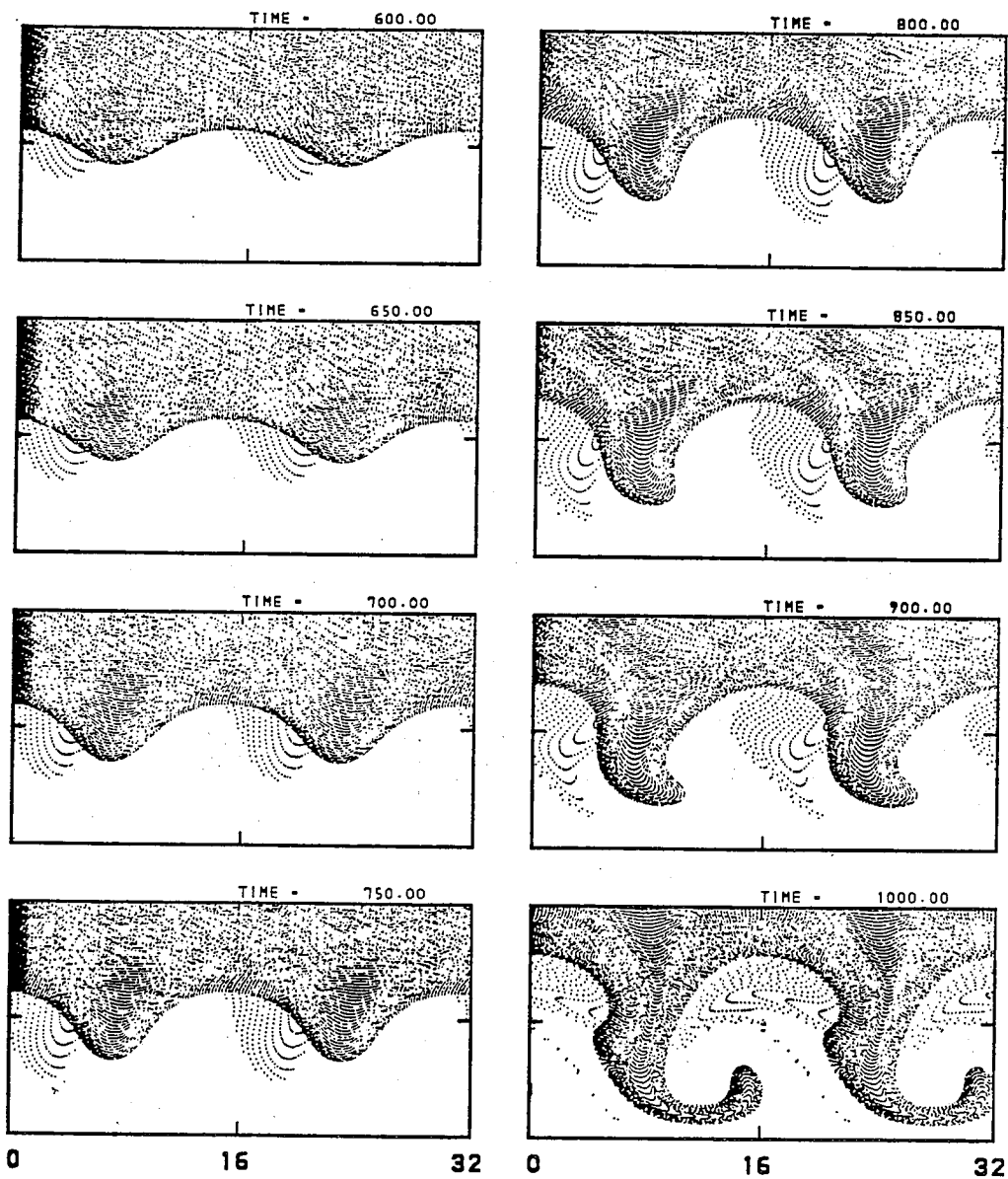


Fig.7 (b) $n_h/n_i = 0.9$.



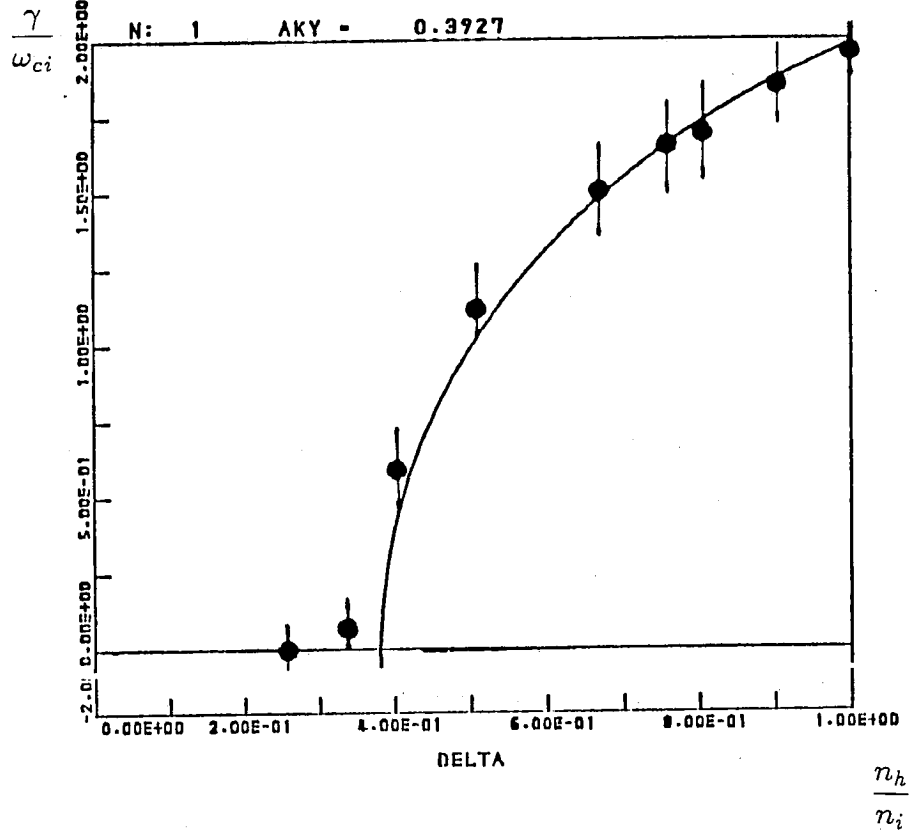


Fig.8 The growth rate of hot electron interchange (electrostatic) mode in the sharp boundary gravity model. The solid line on the upper half plane is the solution of Eq.(2.11), that is equivalent to eq.(4.6) with $\bar{\beta}_{c\perp} = 0, \gamma_{MHD_c}^2 = 0$. The dots with error bar are the results from numerical simulation⁸²

V. Diamagnetic Limit for a Hot Particle Annulus

The dispersion relation, Eq.(4.6) reduces to a simple form in the limits of $\tilde{\beta}_{c\perp}, \gamma_{MHDc}^2$ and $\omega/\omega_{ci} \rightarrow 0$:

$$\tilde{\omega}(\tilde{\omega} - 1) = -\frac{\gamma_{MHD}^2}{\tilde{\omega}_\kappa^2}. \quad (5.1)$$

The quantity $(1/N^2)$, with $N^2 \equiv \tilde{\omega}_\kappa^2/\gamma_{MHD}^2$, is known as the “ coupling constant ”. It is a measure of the coupling strength between the background interchange mode, $\omega \sim i\gamma_{MHD}$, and the precessional mode $\omega \sim \tilde{\omega}_\kappa$. The decoupling condition is thus found to be $N^2 > 4$. However, when this decoupling condition is satisfied, the precessional mode still can be destabilized by positive energy dissipation. Previous papers investigated the limit of large drift reversal, in which limit there is no negative-energy dissipation mechanism to counterbalance positive-energy dissipation mechanisms. Hence, the negative-energy precessional mode is predicted to be unstable.^{26,37,39} As will be discussed below, in systems with smaller pressure gradients, where drift reversal has not been reached, strong negative-energy dissipation mechanism do exist to stabilize the negative-energy precessional mode. It is thus important to investigate the threshold for such an instability as a function of the reversal parameter, ζ on the outer edge of the hot electron annulus. The study will be confined to hot electrons in a thin annulus of thickness Δ , and long wavelength waves are analyzed where $l\Delta/r_0 < 1$. We shall also assume $P_\perp/B^2, P_\parallel/B^2 \ll 1$, and $\sigma = 1$.

V.1 Layer Precessional Mode in Ring-like Configuration

In the thin layer approximation the lowest order term of Eq.(3.3.11) is the first term and we take the layer solution, $\phi_0 \equiv (r\xi_r)_0 = \text{const}$ (taken as 1 hereafter for convenience). In weak coupling approximation ($1/N^2 \ll 1$), the first order term of Eq.(3.3.11) is the third term. Thus, the first order layer solution of Eq.(3.3.11) is

$$\frac{d\phi_1}{dr} = \left(\frac{l}{r} \frac{\omega}{\omega_{ci}} \cdot \frac{1}{1 - k_n^2 v_A^2 / \lambda} - \frac{\kappa}{1 + G_1} \right), \quad (5.1.1)$$

where $\phi \equiv r\xi_r = 1 + \phi_1$ with $\phi_1 \sim O(l\Delta/r)$ and $\kappa = (1/B)(dB_{ext}/dr)$ is the effective curvature.

Integrating Eq.(3.3.11) across the layer and substituting the approximate solution for ϕ , we find

$$\begin{aligned} & \int_{r_-}^{r_+} dr \left[\rho_m \lambda \left(\frac{l}{r} \right) \left(1 - \frac{k_n^2 v_A^2}{\lambda} - \frac{(\omega/\omega_{ci})^2}{1 - k_n^2 v_A^2 / \lambda} \right) \right. \\ & \quad \left. + \left(\frac{dB_{ext}}{dr} \right)^2 \left(\frac{l}{r} \right) \left(\frac{1}{1 + G_1} - [1 - \zeta'(r) - \tilde{\beta}_c] \right) \right] \\ & = \left[\rho_m \lambda \left(1 - \frac{k_n^2 v_A^2}{\lambda} \right) \frac{r}{Ql} (1 + G_1) \frac{1}{\phi} \frac{d\phi}{dr} \right. \\ & \quad \left. - \frac{\rho_m \lambda (\omega/\omega_{ci}) (1 + G_1)}{Q} + \rho_m \lambda \left(1 - \frac{k_n^2 v_A^2}{\lambda} \right) \frac{\kappa r}{rQ} \right]_{r_-}^{r_+} \equiv S, \end{aligned} \quad (5.1.2)$$

where r_- and r_+ are to the inside and outside of the layer, respectively, and $\kappa \equiv (1/B)(dB_{ext}/dr)$ is the effective curvature and $\zeta'(r)$ is the local reversal parameter.

We also note that from the equilibrium condition, we can write

$$\frac{1}{B} \frac{dB}{dr} = \frac{1}{B} \frac{dB_{ext}}{dr} (1 - \tilde{\beta}_c - \zeta'). \quad (5.1.3)$$

The r.h.s. of Eq.(5.1.2) is then matched with the core plasma at r_- , where $G_1 \rightarrow \beta_{c\perp}$ and

$$Q \rightarrow Q_c \equiv -[\lambda/v_A^2 - k_n^2 - (1 + \beta_{c\perp})(l/r)^2]/(l/r)^2; \quad (5.1.4)$$

and with the vacuum at r_+ , where $G_1 \rightarrow 0$ and $Q \rightarrow 1$. Then the r.h.s. of Eq.(5.1.2) becomes

$$S = B^2 \frac{1 + \beta_{c\perp}}{(l^2/r^2)(1 + \beta_{c\perp}) - (\lambda/v_A^2 - k_n^2)} \left(\frac{l}{r} \right) \cdot \left[\left(\frac{\lambda}{v_A^2} - k_n^2 \right) \frac{1}{\phi} \frac{d\phi}{dr} - \left(\frac{l}{r} \right) \frac{\lambda}{v_A^2} \frac{\omega}{\omega_{ci}} \right]_{r_-}^{r_+}, \quad (5.1.5)$$

where we neglect the κ term. The boundary conditions are

$$\left(\frac{1}{\phi} \frac{d\phi}{dr} \right)_{r_-} = \frac{|l|}{r} \quad \text{and} \quad \left(\frac{1}{\phi} \frac{d\phi}{dr} \right)_{r_+} = -\frac{l}{r} \Lambda_{|l|}, \quad (5.1.6)$$

with

$$\Lambda_{|l|} \equiv \frac{(r_w/r_p)^{2|l|} + 1}{(r_w/r_p)^{2|l|} - 1}. \quad (5.1.7)$$

After the substitution of Eqs.(5.1.6) and (5.1.7) into Eq.(5.1.5) we find

$$S = Sgn(l) \frac{B^2}{v_A^2} \left(k_n^2 v_A^2 (1 + \Lambda_{|l|}) - \frac{\omega^2}{1 + Sng(l)\omega/\omega_{ci}} \right), \quad (5.1.8)$$

where we have assumed that $\beta_{c\perp} \ll 1$.

In the case when there are no hot electrons, the dispersion relation is determined by Eq.(5.1.8) being set zero with an error of $O(l\Delta/r)$. Its solution is given in Fig.9 for $k_n^2 v_A^2 / \omega_{ci}^2 \ll 1$. The wave is a surface shear Alfvén wave with a dispersion relation $\omega \sim \pm(1 + \Lambda_{|l|})^{1/2} k_n v_A$.⁸⁴ For $k_n^2 v_A^2 / \omega_{ci}^2 \gg 1$ there is

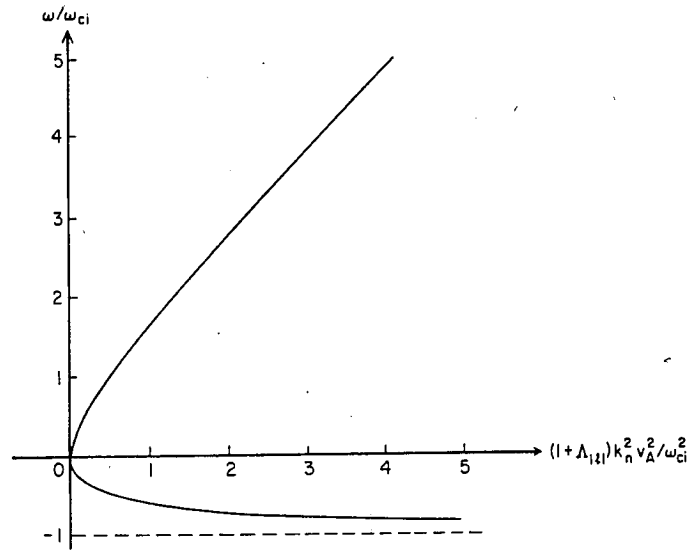


Fig.9 The dispersion curve of surface shear Alfvén-whistler mode.

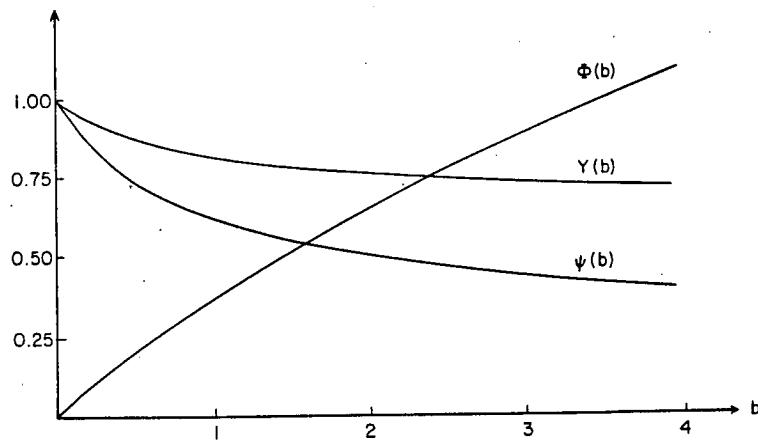


Fig.10 Curves of functions $\psi(b)$, $\Phi(b)$, and $Y(b)$.

a branch where $\omega \rightarrow -Sgn(l)\omega_{ci}$ and a branch that is a surface whistler wave with $\omega = Sgn(l)(k_n^2 v_A^2 / \omega_{ci})$. This branch crosses the cyclotron frequency when $k_n^2 v_A^2 / \omega_{ci}^2 = (1/2)(1 + \Lambda_{|l|})$. If $|\omega / \omega_{ci}| < 1$ one can show that the surface shear Alfvén wave is damped for a diffuse density profile.³⁹ This damping is related to the vanishing of $\lambda / v_A^2 - k_n^2$, which leads to resonant dissipation. However, for $|\omega / \omega_{ci}| > 1$, which corresponds to the surface whistler wave, $\lambda / v_A^2 - k_n^2$ cannot equal zero, and there is no resonant dissipation present.

The first term on the l.h.s. of Eq.(5.1.2) is small, by the factor $(l\Delta/r)$, compared to the r.h.s. In further calculations of $1 + G_1$, we take $f_{0h} = m_h n(r) \delta(p_{||}) h(\mu B(r)/\eta) (2\pi)^{-1}$ with the normalization $\int_0^\infty d\mu B h(\mu B)/\eta = 1$. Note that η is a parameter that measures the thermal energy. Then

$$K_h(\omega) = - \frac{\omega^2}{(lc/qB^2r)(dB/dr)^2} \frac{d}{dr} \left(\frac{n_h}{B} \right) \cdot \int_0^\infty d\mu B \frac{h(\mu B/\eta)}{\omega - \omega_d}. \quad (5.1.9)$$

In the limit of $P_{h\perp}/B^2 \ll 1$ we can assume $(1/n_h)(dn_h/dr) \gg (1/B)(dB/dr)$, and for simplicity we take $(dP_{h\perp}/dr)/(dn_h/dr)$ independent of space. For dB/dr we use Eq.(5.1.3). We define global "curvature" drift frequency (i.e., the mean drift frequency in the external magnetic field including the embedded currents) as

$$\tilde{\omega}_\kappa \equiv \frac{lc}{qB^2r} \left(\frac{dB_{ext}}{dr} \right) \left(\frac{P_{h\perp}}{n_h} \right) = \frac{lc\eta}{qB^2r} \left(\frac{dB_{ext}}{dr} \right) \psi(b) \quad (5.1.10)$$

and

$$\psi(b) \equiv \int_0^\infty dx \frac{xh(x)}{(1+bx)^{1/2}} \rightarrow \begin{cases} 1, & b \ll 1, \\ (\pi/2)^{1/2}/2, & b \gg 1, \end{cases}$$

with $b \equiv 2\eta/m_h c^2$. We write ω_d as

$$\omega_d = \tilde{\omega}_\kappa [B\mu/\psi(b)\eta(1+bB\mu/\eta)^{1/2}](1 - \tilde{\beta}_c - \zeta') \quad (5.1.11)$$

Then we find for $1 + G_1$,

$$1 + G_1 = \frac{1 - \tilde{\beta}_c + \zeta' F\left(\frac{\hat{\omega}}{1 - \tilde{\beta}_c - \zeta'}\right)}{1 - \tilde{\beta}_c - \zeta'}, \quad (5.1.12)$$

where

$$F(\bar{\omega}) \equiv \bar{\omega}[1 - \bar{\omega}\Gamma(\bar{\omega})] \quad (5.1.13)$$

with $\bar{\omega} \equiv \hat{\omega}/(1 - \tilde{\beta}_c - \zeta')$, $\hat{\omega} \equiv \omega/\tilde{\omega}_\kappa$,

$$\Gamma(\bar{\omega}) \equiv \eta \int_0^\infty dx \frac{h(x)}{\bar{\omega} - x/[\psi(b)(1 + bx)^{1/2}]}. \quad (5.1.14)$$

For $h(\mu B/\eta)$ we shall use an exponential distribution function,

$$h(\mu B/\eta) = (1/\eta) \exp[-\mu B(r)/\eta], \quad (5.1.15)$$

so that Eq.(5.1.14) becomes

$$\Gamma(\bar{\omega}) = \int_0^\infty dx \frac{\exp(-x)}{\bar{\omega} - x/[\psi(b)(1 + bx)^{1/2}]}. \quad (5.1.16)$$

In further analysis we need to relate b and $\psi(b)$ to the mean kinetic energy T_h .

If we define $\Phi(b) \equiv T_h/m_h c^2$, we have

$$\begin{aligned} \Phi(b) &= \int_0^\infty dx [(1 + bx)^{1/2} - 1] \exp(-x) \\ &\rightarrow \begin{cases} b/2, & b \ll 1, \\ (\pi b)^{1/2}/2, & b \gg 1. \end{cases} \end{aligned}$$

The equation of state of our relativistic component can be written as

$$Y(b) \equiv \frac{P_{h\perp}}{n_h T_h} = \frac{b\psi(b)}{2\Phi(b)} \rightarrow \begin{cases} 1, & b \ll 1, \\ 1/2, & b \gg 1. \end{cases}$$

The curve $\psi(b)$, $\Phi(b)$, and $Y(b)$ vs b are shown in Fig.10.

We simplify the layer dispersion by substituting our relation into Eq.(5.1.2), and we find

$$\begin{aligned} \int_{r_-}^{r_+} dr \left(\frac{dB_{ext}}{dr} \right)^2 \left(\frac{|l|}{r} \right) \left(\frac{1}{1+G_1} - (1 - \zeta' - \tilde{\beta}_c) \right) \\ = \frac{B^2}{v_A^2} \left(k_n^2 v_A^2 (1 + \Lambda_{|l|}) - \frac{\omega^2}{1 + Sgn(l)\omega/\omega_{ci}} \right). \end{aligned} \quad (5.1.17)$$

Then assuming

$$\begin{aligned} \frac{dP_{h\perp}}{dr} &= \frac{P_{h\perp}}{\Delta_{in}} (r_0 - r_-), \quad r_- < r < r_- + \Delta_{in}, \\ \frac{dP_{h\perp}}{dr} &= \frac{P_{h\perp}}{\Delta_{out}} (r_- + \Delta_{out} + \Delta_{in} - r), \\ r_- + \Delta_{in} < r < r_- + \Delta_{in} + \Delta_{out} &\equiv r_+, \end{aligned} \quad (5.1.18)$$

with the pressure gradients locally constant but with opposite sign in the inner and outer edge of the hot electron layer, respectively, and $dP_{c\perp}/dr = 0$ in the inner edge (see Fig.11), we obtain the final form of the dispersion relation:

$$\begin{aligned} \frac{1+a\zeta}{a\zeta} \left(\frac{(1+a\zeta)^2}{(1+a\zeta)^2 - \hat{\omega}a\zeta[1+a\zeta - \hat{\omega}\Gamma(\frac{\hat{\omega}}{1+a\zeta})]} - 1 \right) \\ + \frac{1-\tilde{\beta}_c-\zeta}{\zeta} \left(\frac{(1-\tilde{\beta}_c-\zeta)^2}{(1-\tilde{\beta}_c)(1-\tilde{\beta}_c-\zeta)^2 + \hat{\omega}\zeta[1+\tilde{\beta}_c-\zeta - \hat{\omega}\Gamma(\frac{\hat{\omega}}{1-\tilde{\beta}_c-\zeta})]} - 1 \right) \\ = N^2 \left(\Omega_A^2 (1 + \Lambda_{|l|}) - \frac{\hat{\omega}^2}{1 + \hat{\omega}/\hat{\omega}_{ci}} \right), \end{aligned} \quad (5.1.19)$$

where $\hat{\omega}_{ci} \equiv Sgn(l)(\omega_{ci}/\tilde{\omega}_\kappa)$, $\zeta \equiv -P_h/\Delta_{out}B^2\kappa > 0$, $\Omega_A \equiv k_n v_A/\tilde{\omega}_\kappa$, $a \equiv \Delta_{out}/\Delta_{in}$, Δ_{out} , Δ_{in} are the thickness of the outer and inner edge of the layer,

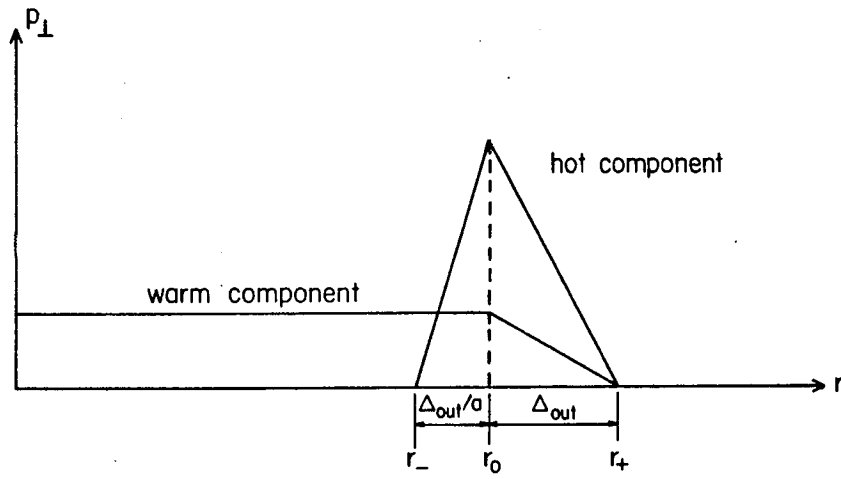


Fig.11 Radial profile of pressure.

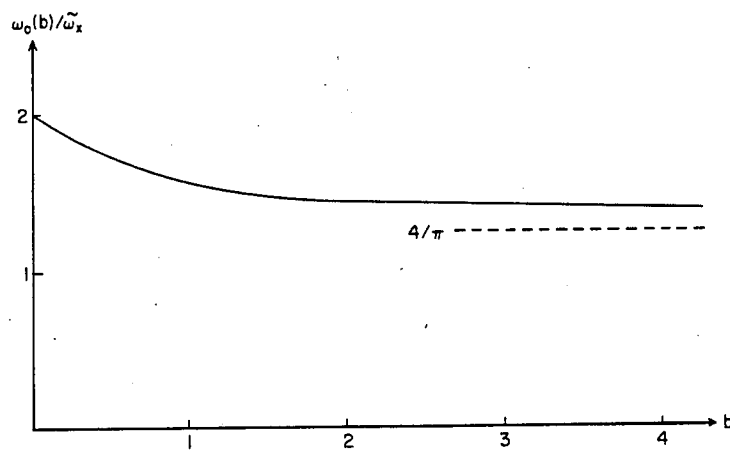


Fig.12 The relativistic effect on the real frequency $\omega/\tilde{\omega}_\kappa$ at marginal stability in the limit of large N^2 .

respectively. We also note that $\hat{\omega}_{ci} > 0$ if the hot species are electrons. The $\Gamma(\bar{\omega})$ is a function defined by Eq.(5.1.14) and has been expressed by Eq.(5.1.16) for the exponential distribution functions.

V.2 Analysis

We now analyze Eq.(5.1.19) for marginal stability and growth rates. In the limit of $N^2 \gg 1$, one can show that the dispersion relation predicts instability when

$$1 > \bar{\beta}_c > 1 - \zeta. \quad (5.2.1)$$

Since the r.h.s. of Eq.(5.1.19) is large in this limit, a mode can only arise if one of the denominator of the l.h.s. of Eq.(5.1.19) nearly vanishes. The two denominators are:

$$Q_{in}(\hat{\omega}) = (1 + a\zeta)^2 - \hat{\omega}a\zeta[1 + a\zeta - \hat{\omega}\Gamma(\hat{\omega}/(1 + a\zeta))] \quad (5.2.2)$$

$$Q_{out}(\hat{\omega}) = (1 - \bar{\beta}_c)(1 - \bar{\beta}_c - \zeta)^2 + \hat{\omega}\zeta[1 - \bar{\beta}_c - \zeta\hat{\omega}\Gamma(\hat{\omega}/(1 - \bar{\beta}_c - \zeta))] \quad (5.2.3)$$

with the imaginary parts, for $\hat{\omega}$ real, given by

$$\text{Im}Q_{in}(\hat{\omega}) =$$

$$\begin{cases} \pi Sgn(l) \left| \frac{\partial X[x(\bar{\omega}_{in})]}{\partial x} \right|^{-1} \hat{\omega}^2 a\zeta \cdot \exp[-X(\bar{\omega}_{in})], & \text{if } \bar{\omega}_{in} > 0, \\ 0, & \text{if } \bar{\omega}_{in} < 0, \end{cases}$$

$$\text{Im}Q_{out}(\hat{\omega}) =$$

$$\begin{cases} \pi Sgn(l) \left| \frac{\partial X[x(\bar{\omega}_{out})]}{\partial x} \right|^{-1} \hat{\omega}^2 \zeta \cdot \exp[-X(\bar{\omega}_{out})], & \text{if } \bar{\omega}_{out} > 0, \\ 0, & \text{if } \bar{\omega}_{out} < 0, \end{cases}$$

where

$$\begin{aligned} \bar{\omega}_{in} &= \frac{\bar{\omega}}{1 + a\zeta}, \bar{\omega}_{out} = \frac{\hat{\omega}}{1 - \tilde{\beta}_c - \zeta}, \\ X(x) &= \frac{x}{\psi(b)(1 + bx)^{1/2}}, \frac{dX}{dx} = \frac{1 + bx/2}{\psi(b)(1 + bx)^{3/2}}, \\ x(\bar{\omega}) &= b\psi^2(b)\bar{\omega}^2/2 + \sqrt{b^2\psi^4(b)\bar{\omega}^4/4 + \psi^2(b)\bar{\omega}^2} \end{aligned}$$

We note that $Sgn(l)\text{Im}Q_{in}(\hat{\omega}) \leq 0$, while $Sgn(l)\text{Im}Q_{out} \geq 0$. One can show that $\text{Im}Q_{in}(\hat{\omega})$ contributes to damping of cold plasma waves (or more generally, positive energy waves), while $\text{Im}Q_{out}(\hat{\omega})$ contributes to the growth of positive energy waves. On the other hand, for negative energy waves one finds $\text{Im}Q_{in}(\hat{\omega})$ contributes to destabilization while $\text{Im}Q_{out}(\hat{\omega})$ contributes a stabilizing term.

In order to balance the r.h.s. of Eq.(5.1.19), we look for a root $\hat{\omega}$ near $\hat{\omega}_0$, which satisfies

$$\text{Re}Q_{out}(\hat{\omega}_0) = 0. \quad (5.2.4)$$

Then, defining $\delta\hat{\omega} \equiv \hat{\omega} - \hat{\omega}_0$, we have

$$Q_{out}(\hat{\omega}) = \delta\hat{\omega} \frac{\partial}{\partial \hat{\omega}} \text{Re}Q_{out}(\hat{\omega}_0) + i\text{Im}Q_{out}(\hat{\omega}_0 + \delta\hat{\omega})$$

Now, substituting this relation into Eq.(5.1.19) solving for $\delta\hat{\omega}$, and assuming

we can set $\hat{\omega} = \hat{\omega}_0$ in the other terms, we find

$$\begin{aligned}
& \delta\hat{\omega} \left(\frac{\partial}{\partial\omega} \text{Re}Q_{out}(\hat{\omega}_0) \right) \frac{\zeta}{(1 - \bar{\beta}_c - \zeta)^3} \\
&= -i \frac{\zeta}{(1 - \bar{\beta}_c - \zeta)^3} \text{Im}Q_{out}(\hat{\omega}_0 + \delta\hat{\omega}) \\
& \left[N^2 \left(\Omega_A^2 (1 + \Lambda_{|l|}) - \frac{\hat{\omega}_0}{1 + \hat{\omega}/\hat{\omega}_{ci}} \right) + \frac{1 - \bar{\beta}_c}{\zeta} \right. \\
& \left. + \frac{1}{a\zeta} - \frac{(1 + a\zeta)^3 [\text{Re}Q_{in}(\hat{\omega}_0) - i\text{Im}Q_{in}(\hat{\omega}_0)]}{a\zeta |Q_{in}(\hat{\omega}_0)|^2} \right]^{-1}.
\end{aligned} \tag{5.2.5}$$

Now if N^2 is large, and $\hat{\omega}_0$ is primarily real, so that we need only retain the leading imaginary contribution of Eq.(5.2.5), we find

$$\delta\hat{\omega} \left(\frac{\partial}{\partial\hat{\omega}} \text{Re}Q_{out}(\hat{\omega}_0) \right) \frac{\zeta}{(1 - \bar{\beta}_c - \zeta)^3} = A + iB, \tag{5.2.6}$$

with

$$A \equiv \frac{i}{N^2 [\Omega_A^2 (1 + \Lambda_{|l|}) - \hat{\omega}_0 / (1 + \hat{\omega}_0 / \hat{\omega}_{ci})]} + O\left(\frac{1}{N^4}\right), \tag{5.2.7}$$

$$\begin{aligned}
B \equiv & - \frac{(1 + a\zeta)^3 \text{Im}Q_{in}}{a\zeta |Q_{in}|^2 N^4 [\Omega_A^2 (1 + \Lambda_{|l|}) - \hat{\omega}_0 / (1 + \hat{\omega}_0 / \hat{\omega}_{ci})]^2} \\
& - \frac{\zeta}{(1 - \bar{\beta}_c - \zeta)^3} \text{Im}Q_{out}(\hat{\omega}_0 + \delta\hat{\omega}).
\end{aligned} \tag{5.2.8}$$

Since $\text{Sgn}(l)\text{Im}Q_{in} < 0$ if $\hat{\omega}_0$ is real and positive, and $\text{Im}Q_{out} = 0$ if $\zeta > 1 - \bar{\beta}_c$, instability (which requires $\bar{\omega}_\kappa \text{Im}(\delta\hat{\omega}) > 0$) requires

$$\left(\frac{\partial}{\partial\hat{\omega}} \text{Re}Q_{out}(\hat{\omega}_0) \right) (1 - \bar{\beta}_c - \zeta)^{-3} > 0 \quad \text{for} \quad \zeta > 1 - \bar{\beta}_c. \tag{5.2.9}$$

We can explicitly show that this condition is achieved when $|1 - \bar{\beta}_c - \zeta| \ll 1$ or $\zeta \gg 1$. We shall also assume $\bar{\beta}_c < 1$ in this discussion so that we

need not discuss the MHD instabilities associated with the Lee-VanDam,Nelson threshold.^{23,24} We first construct $\partial \text{Re}Q_{out}(\hat{\omega}_0)/\partial \hat{\omega}$ and find

$$\begin{aligned} \frac{\partial}{\partial \hat{\omega}} \text{Re}Q_{out}(\hat{\omega}_0) &= \zeta(1 - \tilde{\beta}_c - \zeta) \left(1 - \bar{\omega}_{out} P \int_0^\infty dx \frac{\exp(-x)}{\bar{\omega}_{out} - X} \right) \\ &\quad + \zeta \hat{\omega} P \int_0^\infty dx \frac{X \exp(-x)}{(\bar{\omega}_{out} - X)^2}. \end{aligned} \quad (5.2.10)$$

Thus using $\text{Re}Q_{out}(\hat{\omega}_0) = 0$, we find

$$\begin{aligned} \frac{\partial}{\partial \omega} \text{Re}Q_{out}(\hat{\omega}_0) &= -\frac{(1 - \tilde{\beta}_c - \zeta)}{\bar{\omega}_{out}} (1 - \tilde{\beta}_c) + \hat{\omega} \zeta P \int_0^\infty dx \frac{X \exp(-x)}{(\bar{\omega}_{out} - X)^2} \\ &\rightarrow \begin{cases} -\frac{(1 - \tilde{\beta}_c)(1 - \tilde{\beta}_c - \zeta)^2}{\hat{\omega}_0}, & \text{if } \zeta \gg 1, \\ \frac{2(1 - \tilde{\beta}_c - \zeta)^3 \zeta}{\hat{\omega}_0^2 \psi^2(b)} \int_0^\infty dx \frac{x^2 \exp(-x)}{1 + bx}, & \text{if } \bar{\omega} \gg 1. \end{cases} \end{aligned}$$

For $\zeta \gg 1$, we have the approximation solution from Eq.(5.2.4) and Eq.(5.2.2),

$$\hat{\omega}_0 = (1 - \tilde{\beta}_c) + O(1/\zeta),$$

and therefore

$$\left(\frac{\partial}{\partial \hat{\omega}} \text{Re}Q_{out} \right) (1 - \tilde{\beta}_c - \zeta)^{-3} = \zeta^{-1} > 0. \quad (5.2.11)$$

Thus instability is guaranteed for $\zeta \gg 1$ if $\tilde{\beta}_c < 1$.

For $|1 - \tilde{\beta}_c - \zeta| \ll 1$, we can solve the dispersion relation by taking $\bar{\omega}_{out} \gg X$.

Then by using

$$\frac{1}{\bar{\omega}_{out} - X} = \frac{1}{\bar{\omega}_{out}} \left(1 + \frac{X}{\bar{\omega}_{out}} + \frac{X^2}{\bar{\omega}_{out}^2} + \frac{X^3}{\bar{\omega}_{out}^3} + \dots \right),$$

the solution to $\text{Re}Q_{out}(\hat{\omega}_0) = 0$ is found to be

$$\begin{aligned} \hat{\omega}_0 &= \frac{\zeta}{\psi^2(b)} \int_0^\infty dx \frac{x^2 \exp(-x)}{1 + bx} + \frac{(1 - \tilde{\beta}_c - \zeta)\zeta}{\hat{\omega}_0 \psi^3(b)} \int_0^\infty dx \frac{x^3 \exp(-x)}{(1 + bx)^{3/2}} \\ &\quad + O[(1 - \tilde{\beta}_c - \zeta)^2]. \end{aligned} \quad (5.2.12)$$

To the lowest order in $(1 - \bar{\beta}_c - \zeta)$

$$\hat{\omega}_0 \rightarrow \begin{cases} 2\zeta & \text{for } b \ll 1 \\ 4\zeta/\pi & \text{for } b \gg 1. \end{cases}$$

A plot of $\hat{\omega}_0$ as a function of b when $\zeta = 1 - \bar{\beta}_c$ is shown in Fig.12. Substituting Eq.(5.2.12) into Eq.(5.2.10) then gives

$$\left(\frac{\partial}{\partial \hat{\omega}} \text{Re} Q_{out}(\hat{\omega}_0) \right) (1 - \bar{\beta}_c - \zeta)^{-3} = \frac{2\psi^2(b)}{\int_0^\infty dx \frac{x^2 \exp(-x)}{1 + bx}} + O(1 - \bar{\beta}_c - \zeta), \quad (5.2.13)$$

which guarantees instability if $\zeta > 1 - \bar{\beta}_c$, so that $\text{Im} Q_{out} = 0$.

We find $\delta\omega$ from Eq.(5.2.6)

$$\begin{aligned} \delta\omega = & [2\zeta\psi^2(b)]^{-1} \cdot \int_0^\infty dx \frac{x^2 \exp(-x)}{1 + bx} \\ & \times \left\{ \frac{1}{N^2[\Omega_A^2(1 + \Lambda_{||}) - \hat{\omega}_0^2/(1 + \hat{\omega}_0/\hat{\omega}_{ci})]} \right. \\ & - i \frac{(1 + a\zeta)^3 \text{Im} Q_{in}}{a\zeta|Q_{in}|^2 N^4[\Omega_A^2(1 + \Lambda_{||}) - \hat{\omega}_0/(1 + \hat{\omega}_0/\hat{\omega}_{ci})]} \\ & \left. - i \frac{\zeta \text{Im} Q_{out}(\hat{\omega}_0 + \delta\omega)}{(1 - \bar{\beta}_c - \zeta)^3} \right\}. \end{aligned} \quad (5.2.14)$$

Thus if $\zeta < 1 - \bar{\beta}_c$, $\text{Sgn}(l)\text{Im} Q_{out} > 0$ and stabilizing. However, we see that $\text{Im} Q_{out}$ is exponentially small for small $|1 - \bar{\beta}_c - \zeta|$, and thus, the $\text{Im} Q_{in}$ term will be larger, and destabilizing for $1 - \bar{\beta}_c - \zeta$ sufficiently small. For $\zeta > 1 - \bar{\beta}_c$, $\text{Im} Q_{out} = 0$, and Eq.(5.2.14) is always unstable.

The above analytic analysis indicates that relativistic dynamics do not alter the stability conclusion in any essential manner. The numerical work we have performed has primarily been for the nonrelativistic case ($b = 0$) since it is easier and faster to compute. In this case we neglect the relativistic nature

of the hot electrons, but assume that Newtonian dynamics can be used for electrons at 0.5 Mev. When $b = 0$ is chosen, the other parameters are chosen self-consistently with a Newtonian dynamics model. As a check our assertion, we will also show some numerical results for $b = 3.5$ ($T_h = 0.5$ Mev). In Fig.13, the marginal nonrelativistic stability boundary of ζ vs. N^2 for a standard parameters set ($\tilde{\beta}_c = 0, \Omega_A = 0, a = 1, \hat{\omega}_{ci} = 1.3$) is shown by the solid curve. (The sensitivity to Ω_A is shown in Fig.17.) The dashed curve is the prediction of marginal stability obtained by our analytic method, which shows excellent agreement for $N^2 > 2$. Recall that the analytic results showed the relativistic and nonrelativistic marginal plots in close agreement. In Fig.14, we plot growth rates as a function of N^2 for the standard parameters set and with $\zeta = 1.1$ and 1.5 for $b = 0$. We observe the rapid fall-off as N^{-4} . The isolated points are the results from the $b = 3.5$ relativistic calculation which show nearly the same dependence as the nonrelativistic case. In Fig.15, we plot the real frequency as a function N^2 for the same parameters. Observe that the real frequency is $\hat{\omega}_0 \sim 1 - 2$, which is characteristic of the precessional mode. In Fig.16, we examine the effect of skewness where we compare the growth rate at $\zeta = 1.1$ for $a = 1$ and $a = 2$. We see that there is little sensitivity to the parameter a . In Fig.17, we vary Ω_A^2 for $\zeta = 1.1$ and 1.5 to show how resonance with the surface wistler wave can enhance the growth rate. We choose $N^2 = 12.6$ and $\hat{\omega}_{ci} = 1.3$. In Fig.18, we plot the dependence of the growth rate on ζ for $N^2 = 12.6, \hat{\omega}_{ci} = 1.3, a = 1$ and $\tilde{\beta}_c = 0.1$. We see a maximum in the growth rate at moderate ζ . In Figs.16-18, $b = 0$ is chosen.

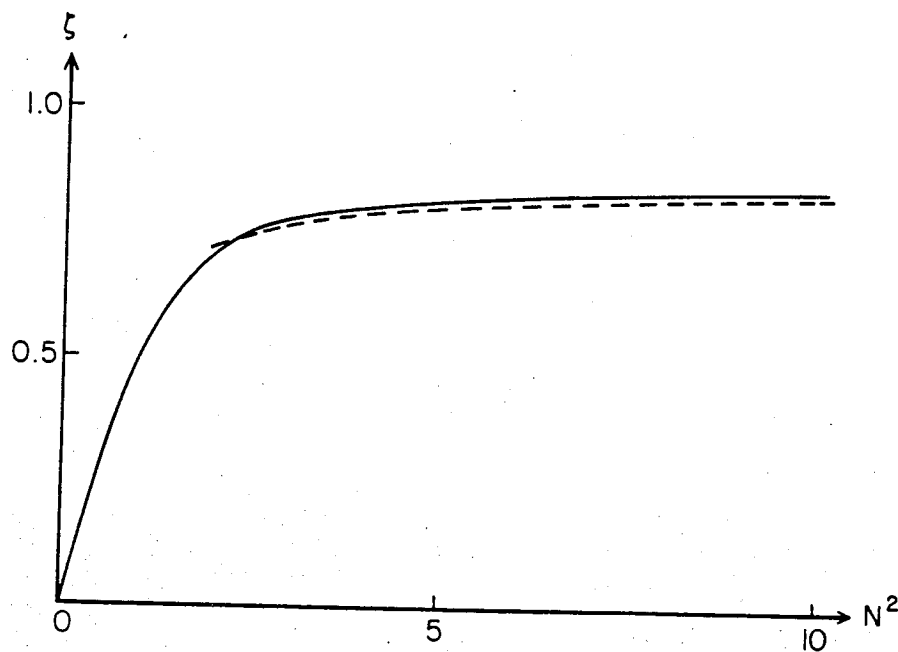


Fig.13 The marginal stability boundaries. The solid curve represents the numerical result and dashed curve is the analytical result ($\tilde{\beta}_c = 0, \Omega_A = 0, a = 1, \hat{\omega}_{ci} = 1.3$).

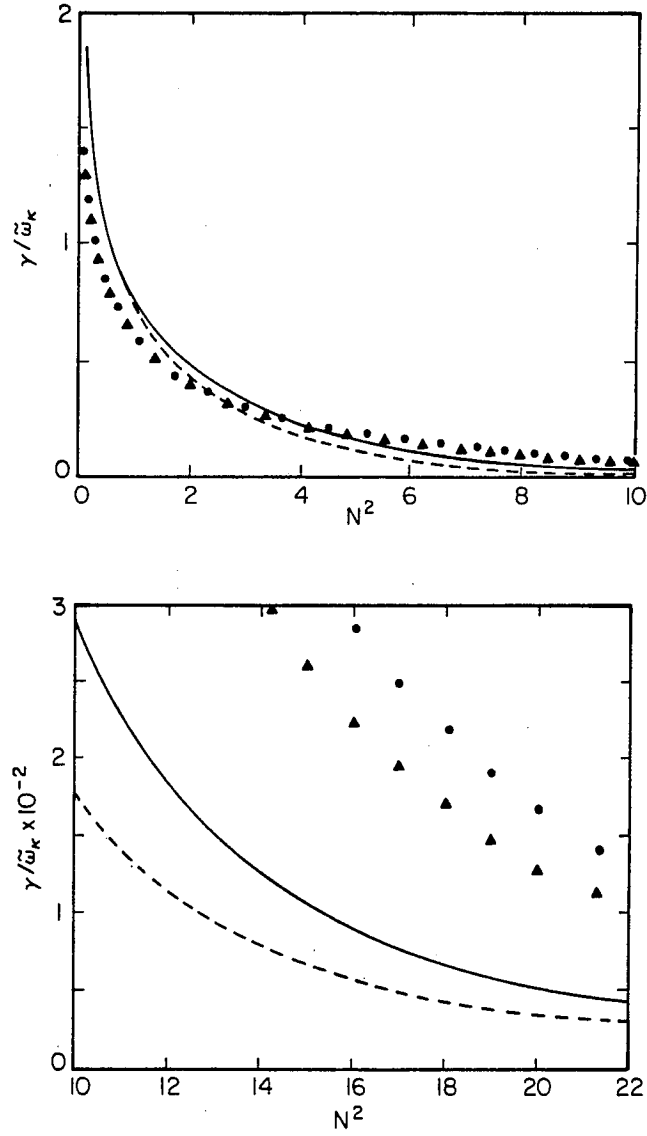


Fig.14 The growth rate versus N^2 at $\tilde{\beta}_c = 0, \Omega_A = 0, a = 1, \hat{\omega}_{ci} = 1.3$. The solid curve (for $\zeta = 1.5$) and dashed curve (for $\zeta = 1.1$) are the numerical results in the nonrelativistic case. Dots (for $\zeta = 1.5$) and triangles (for $\zeta = 1.1$) are the numerical results in the relativistic case ($b = 3.5$).

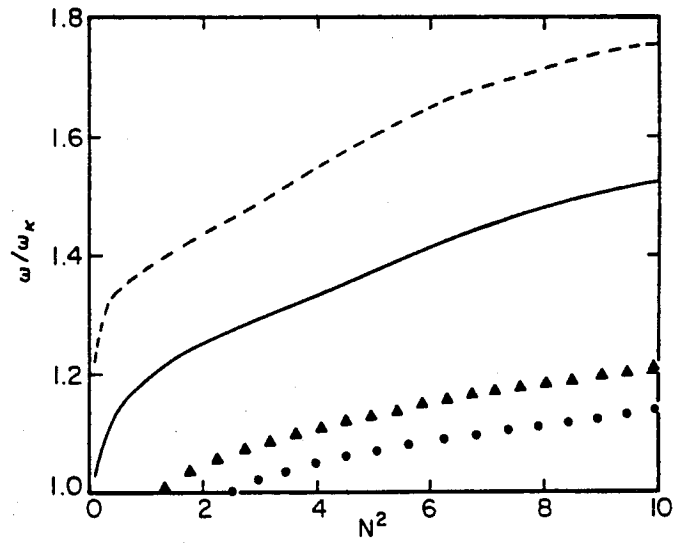


Fig.15 The real frequency versus N^2 for mthe same parameters as Fig.14.

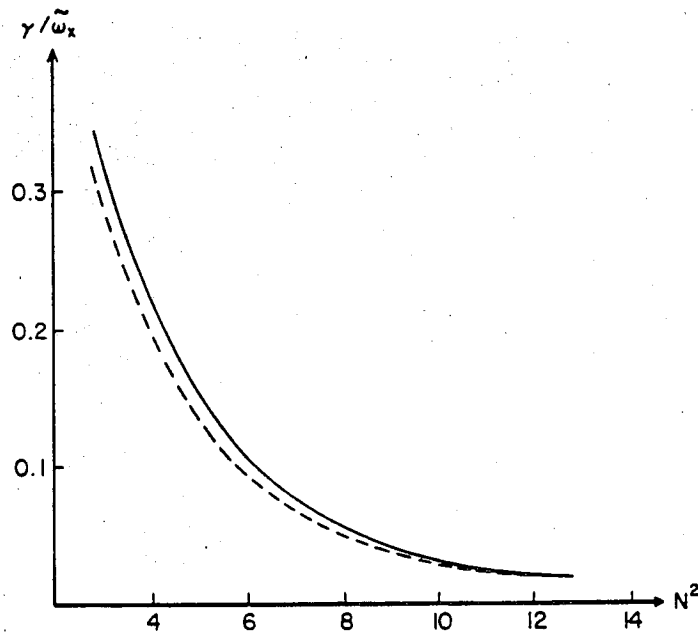


Fig.16 The effect of skewness on growth rate at $\zeta = 1.1, \tilde{\beta}_c = 0, \Omega_A = 0, \hat{\omega}_{ci} = 1.3$. The solid curve represents $a = 1$ and the dashed curve represents $a = 2$.

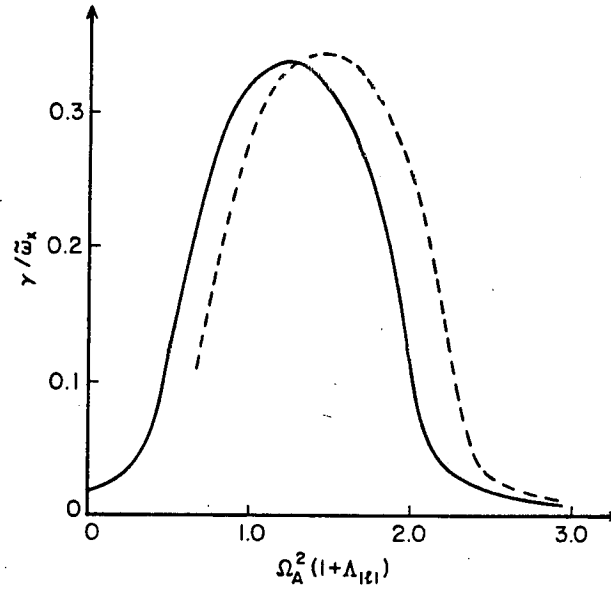


Fig.17 The growth rate due to interaction with surface shear Alfvén-whistler wave at $N^2 = 12.6$, $\hat{\omega}_{ci} = 1.3$, $\tilde{\beta}_c = 0$, $a = 1$. The solid curve represents $\zeta = 1.5$ and the dashed curve represents $\zeta = 1.1$.

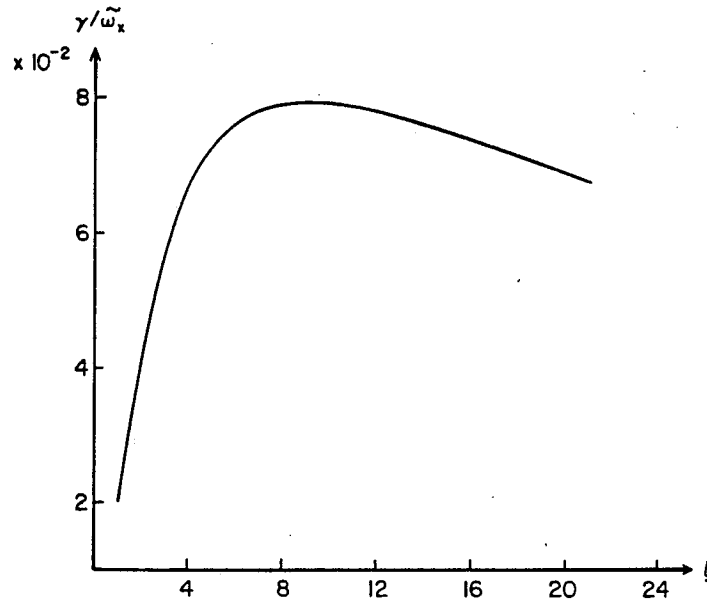


Fig.18 The ζ dependence of the growth rate at $N^2 = 12.6$, $\hat{\omega}_{ci} = 1.3$, $a = 1$, $\tilde{\beta}_c = 0.1$, $\Omega_A = 0$.

In these calculations we can observe that the threshold for instability is associated with the disappearance of negative energy dissipation source, which then allows for the destabilization of the negative energy precessional wave due to the remaining positive energy dissipation source that arises from the particle resonances on the inner edge of the layer. To avoid the destabilization it is necessary to have a negative energy dissipation mechanism which our model has discarded. One possible mechanism comes from considering a smooth radial pressure profile rather than the tent-like profile we considered in the text. Then, even in large ζ cases, there is always sources for some negative dissipation. These arise because on the outer side of the layer the pressure gradient is small near the peak and at the wings of the radial pressure profile. In these regions hot particles can still resonate and give a negative dissipation contribution. Accordingly, we have solved Eq.(5.1.17) for a pressure profile of the form

$$P_{h\perp} = P_{0\perp} \exp[-(r - r_p)^2 / \Delta_0^2]$$

The results for how the growth rate changes as a function of ζ_0 ($\zeta_0 \equiv \beta_{0\perp} / 2\kappa\Delta_0$, $\beta_{0\perp} \equiv 8\pi P_{0\perp} / B^2$), for $N^2 = 10$ with the assumption that the curvature is nearly constant over the layer thickness, is shown in Fig.19. Two profiles are compared, the tent-like pressure profile used previously and the smooth pressure profile written above. The local value of $\zeta'(r)$ becomes $\zeta'(r) = 2\zeta_0 y \exp(-y^2)$, with $y = (r - r_p) / \Delta_0$, for the smooth pressure profile. Observe that the growth rate is somewhat lower than that of the tent-like profile, and the threshold for ζ_0 somewhat higher. However, even for the marginal condition

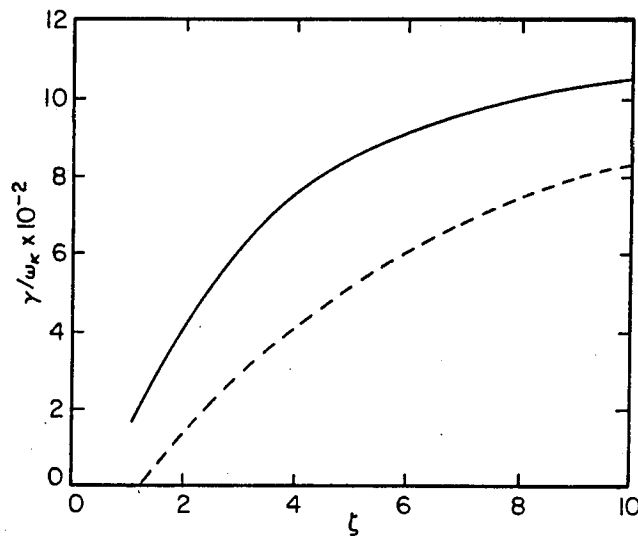


Fig.19 Growth rate versus ζ at $N^2 = 10, \bar{\omega}_{ci} = 1.3, a = 1, \bar{\beta}_c = 0, \Omega_A = 0$. The solid curve represents the result from a tent-like pressure profile. The dashed curve represents the result from a Gaussian-type profile. Both are nonrelativistic cases.

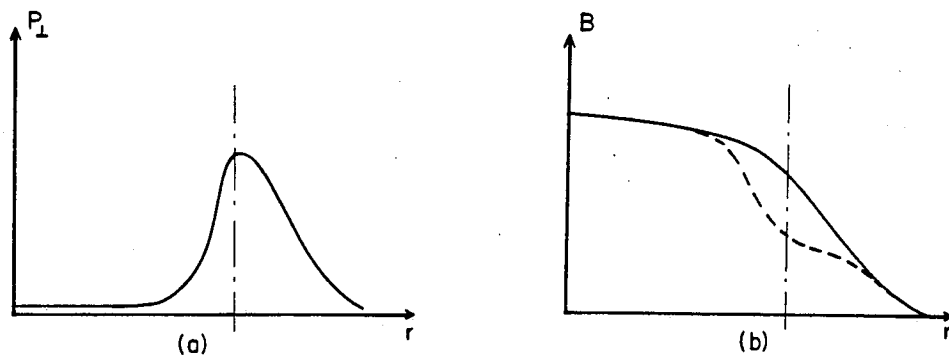


Fig.20 Schematic diagram of broadened pressure profile in (a). The solid curve in (b) represents the vacuum field. The dashed curve in (b) represents the magnetic field due to a plasma with substantial stored energy but without drift reversal.

$\zeta_0 \sim 1.2$, drift reversal is not quite achieved at the maximum of ζ (at $y = 1/\sqrt{2}$). Hence, the conclusion of instability arises as drift reversal is reached still remains for the smooth pressure profile case.

V.3 Discussion

We have demonstrated that for the model studied here, the approximate threshold of instability of a hot plasma ring arises when the pressure gradient is large enough to reverse the gradient of the magnetic field in the hot plasma region. For our model this instability is intrinsic to a hot plasma annulus.

The reason for this is that there is a negative energy wave that is excited at a frequency comparable to the mean curvature drift frequency. The mode is damped by negative dissipation and amplified by positive dissipation. However, the dominant mechanism for negative dissipation disappears with achievement of drift reversal, as the particles on the outer edge of the annulus can no longer resonate with the precessional mode frequency (which is approximately at the curvature drift frequency), as the grad-B drift of these particles is now of opposite sign to the curvature drift frequency. The negative energy wave is then destabilized by the positive energy dissipation, which arises from the resonance of particles, in the inner edge of the annulus, whose grad-B drift frequency matches the wave frequency. Since grad-B and curvature are of the same sign in the inner edge of the layer, such a resonance can always be found for a distribution function that is continuous in energy. The sign of the dissipation

is proportional to the radial pressure gradient, which on the inner edge is increasing (opposite in sign to the pressure gradient on the outer edge) and leads to positive dissipation. Thus, when drift reversal is achieved on the outer edge, conditions are established for the dissipative destabilization of a negative energy wave which oscillates at the curvature drift frequency (precessional frequency).

A crucial question is what are the consequences of this instability. One pessimistic speculation is that a hot electron layer is broadened radially to produce a profile close to a marginally stable profile. Then when a large amount of stored energy is present, the radial pressure and magnetic field profiles would resemble the profile shown in Fig.20. Then, even though there can be a large amount of stored energy present, grad-B drift reversal is not achieved. One may also note that reversal factor is proportional to the stored energy divided by the square of the thickness. Therefore, the thickness of a layer, which is difficult to measure, is a crucial element in the experimental determination of whether drift reversal is attained.

The question of whether any experiment has actually achieved drift reversal is crucially important to the validity of our speculation. If the experimental claims of strong grad-B reversal being achieved are correct, a major reassessment of our theory is needed to find a crucial aspect that is missing. Our theory may be deficient in being too simplified, and a more realistic axial geometry model may alter our conclusions.

VI. Trapped Particle Effects on Diamagnetic Limit

The previous analysis in cylindrical model with embedded current shows that instability of the negative energy precessional mode arises just below the formation of a magnetic well by hot electron ring. However, in a mirror configuration the entire disappearance of the negative energy dissipation in the outer edge is governed by the drift reversal condition for the hot particles with largest pitch angle. Therefore, it is possible for formation a magnetic well near the mirror midplane because of this mechanism.

The flute-type global dispersion relation is constructed by a quadratic form with the assumption of a radial trial function [cf.VI.1] and a trapped particle distribution function [cf.VI.2]. The numerical solution [cf. VI.3] of the dispersion relation shows that the drift reversal parameter at the midplane $\zeta_0 \sim 1.5$ can be reached for typical parameters in experiments, but that the mean bounce averaged drift reversal parameter is not reversed.

The notation used in the following is the same as that in III.1 for a simple mirror configuration (Fig.21). The equilibrium equation is

$$\nabla_{\perp} P_{\perp} + B \nabla_{\perp} B = \sigma \kappa B^2$$

with

$$\sigma = 1 + (P_{\perp} - P_{\parallel})/B^2$$

and

$$P_{\perp} = \sum \frac{2\pi B}{m^2} \int \frac{d\mu dE}{|v_{\parallel}|} \mu B f_0$$

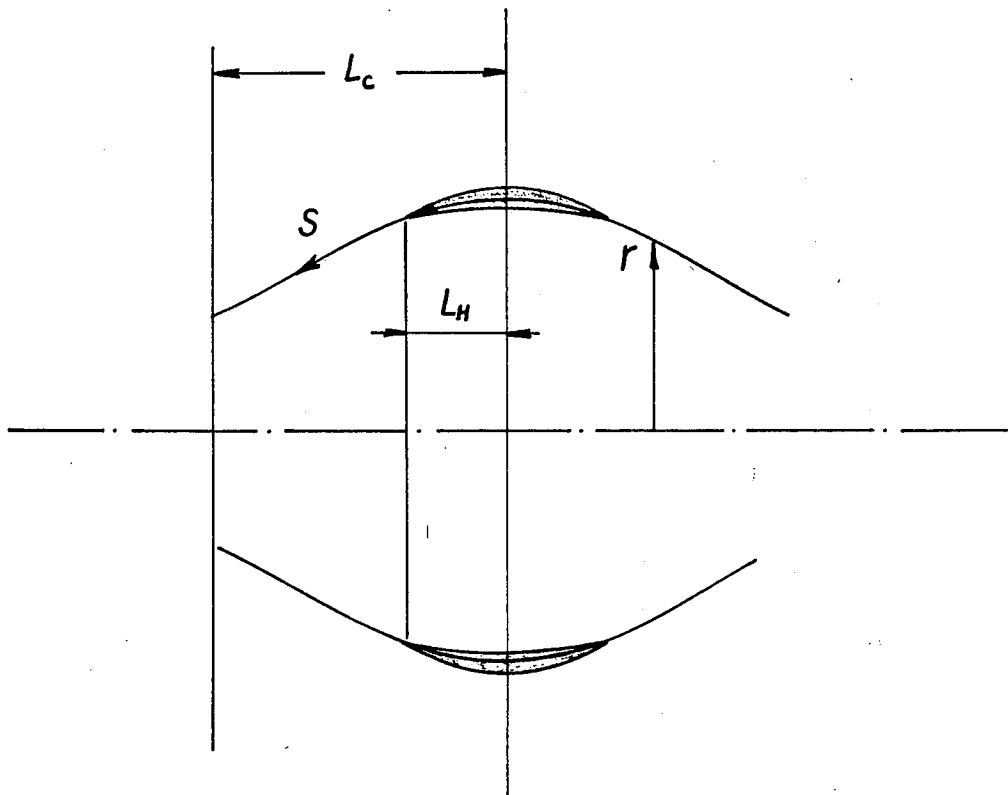


Fig.21 The single mirror cell configuration. The dark area denotes hot electron ring.

$$P_{\parallel} = \sum \frac{2\pi B}{m^2} \int \frac{d\mu dE}{|v_{\parallel}|} m v_{\parallel}^2 f_0$$

The summation is over all species, as well as positive and negative parallel velocities.

VI.1 Trial Function Method. Limiting Cases.

The eigenmode equations are derived from the following quadratic variational form⁷⁶ with finite ion gyrofrequency included in the inertial term:

$$W = \int \frac{d\psi ds d\theta}{B} \left\{ -\rho\lambda [\xi^{\dagger} \cdot \xi + \frac{i\omega}{\omega_{ci}} (\xi^{\dagger} \times \xi) \cdot \mathbf{b}] + \sigma \mathbf{Q}_{\perp}^{\dagger} \cdot \mathbf{Q}_{\perp} + \tau Q_L^{\dagger} Q_L \right. \\ \left. - \xi \cdot \kappa \left(\frac{\sigma}{\tau} \xi \cdot \hat{\nabla} P_{\perp} + \xi \cdot \hat{\nabla} P_{\parallel} \right) - \int d\Gamma \left(\frac{\partial f_0}{\partial H} \right) \frac{\omega - \omega^*}{\omega - \bar{\omega}_d} \bar{K}^{\dagger} \bar{K} \right\} = 0, \quad (6.1.1)$$

where

$$\xi = \frac{1}{B} [\alpha_1 \mathbf{b} \times \nabla \theta - \frac{1}{il} \left(\frac{Q_L}{B} - \hat{\chi}_1 \alpha_1 \right) \mathbf{b} \times \nabla \psi], \quad (6.1.2)$$

$$\delta \mathbf{B} \equiv \nabla \alpha_1 \times \nabla \theta + \nabla \psi \times \nabla \beta_1, \quad (6.1.3)$$

$$Q_L \equiv B(\hat{\chi}_1 \alpha_1 + il\beta_1), \quad (6.1.4)$$

$$\hat{\chi}_1 \alpha_1 \equiv B \frac{\partial}{\partial \psi} \left(\frac{\alpha_1}{B} \right) - B g_{s\psi} \frac{\partial}{\partial s} \alpha_1 \partial B + \frac{\kappa \sigma}{r B \tau} \alpha_1, \quad (6.1.5)$$

$$\mathbf{Q}_{\perp} \equiv \frac{\partial \alpha_1}{\partial s} \mathbf{b} \times \nabla \theta - r^2 B \frac{\partial \beta_1}{\partial s} \nabla \theta, \quad (6.1.6)$$

$$K \equiv \mu Q_L + \xi \cdot \kappa \left(\mu \frac{B\sigma}{\tau} + m v_{\parallel}^2 \right), \quad (6.1.7)$$

$$\bar{A} \equiv \frac{\oint \frac{ds}{|v_{\parallel}|} A}{\oint \frac{ds}{|v_{\parallel}|}}. \quad (6.1.8)$$

The eigenmode equations in the fluid and vacuum part obtained from stationary variation with respect to Q_L^\dagger and α^\dagger are

$$\begin{aligned} & [l^2 - \frac{1}{B} \left(\frac{\lambda r^2 B}{v_A^2} + \frac{\partial}{\partial s} r^2 B \frac{\partial}{\partial s} \right)] Q_L \\ & + \left(\frac{\lambda r^2 B}{v_A^2} + \frac{\partial}{\partial s} r^2 B \frac{\partial}{\partial s} \right) \hat{\chi}_1 \alpha_1 - \frac{\lambda \omega}{v_A^2 \omega_{ci}} l \alpha_1 = 0 \end{aligned} \quad (6.1.9)$$

and

$$\begin{aligned} & -l^2 \left(\frac{\lambda}{v_A^2 r^2 B} + \frac{\partial}{\partial s} \frac{1}{r^2 B} \frac{\partial}{\partial s} \right) \alpha_1 - l \hat{\chi}_2 \frac{\lambda \omega}{v_A^2 \omega_{ci}} \alpha_1 \\ & - \left\{ l \frac{\lambda \omega}{v_A^2 \omega_{ci}} + \hat{\chi}_2 \left[\frac{\lambda r^2 B}{v_A^2} + \frac{\partial}{\partial s} r^2 B \frac{\partial}{\partial s} \right] \right\} \left(\frac{Q_L}{B} - \hat{\chi}_1 \alpha_1 \right) = 0 \end{aligned} \quad (6.1.11)$$

where

$$\hat{\chi}_2 \alpha_1 \equiv \frac{1}{B} \frac{\partial}{\partial \psi} B \alpha_1 - \frac{1}{B} \frac{\partial}{\partial s} g_{s\psi} B \alpha_1 - \frac{\kappa \sigma}{r \tau B} \alpha_1 \sim \frac{1}{B} \frac{\partial}{\partial \psi} B \alpha_1, \quad (6.1.11)$$

In a long thin approximation and in the assumption

$$l^2 \gg \frac{\lambda r^2}{v_A^2} + \frac{\partial}{\partial s} r^2 B \frac{\partial}{\partial s} \quad (6.1.12)$$

Eq.(6.1.8) gives

$$Q_L = -\frac{1}{l^2} \left(\frac{\lambda r^2 B}{v_A^2} + \frac{\partial}{\partial s} r^2 B \frac{\partial}{\partial s} \right) \frac{\partial \alpha_1}{\partial \psi} + \frac{\lambda \omega}{l v_A^2 \omega_{ci}} \alpha_1. \quad (6.1.13)$$

Substituting Eq.(6.1.13) into Eq.(6.1.10) in the assumption that for surface wave in cold plasma

$$F - \frac{S^2}{F} \ll 1 \quad (6.1.14)$$

with

$$F \equiv \frac{1}{r^2 B} \left(\frac{\lambda r^2 B}{v_A^2} + \frac{\partial}{\partial s} r^2 B \frac{\partial}{\partial s} \right), \quad S \equiv \frac{\lambda \omega}{v_A^2 \omega_{ci}}, \quad (6.1.15)$$

we obtain an eigenmode equation for cold plasma waves

$$\frac{\partial}{\partial \psi} \left(\frac{\lambda r^2 B}{v_A^2} + \frac{\partial}{\partial \psi} r^2 B \frac{\partial}{\partial s} \right) \frac{\partial \alpha_1}{\partial \psi} - \frac{l^2}{r^4 B^2} \left(\frac{\lambda r^2 B}{v_A^2} + \frac{\partial}{\partial s} r^2 B \frac{\partial}{\partial s} \right) \alpha_1 = 0 \quad (6.1.16)$$

Eq.(6.1.16) has a solution with appropriate boundary conditions

$$\alpha_1 = f(s) \times \begin{cases} (\psi/\psi_-)^{|l|/2} & \text{for } (\psi < \psi_-) \\ \Lambda_{|l|} & \text{for } (\psi_w > \psi > \psi_+), \end{cases}$$

where $\Lambda_{|l|}$ is defined by Eq.(3.1.7), with r replaced by ψ . For the thin layer we approximate $\alpha_1 \sim f(s)$ within the layer as the lowest order of the layer mode.

The essential assumption in the layer is the use of a trial function

$$Q_L(\psi, s) \sim C(\psi) \frac{1}{\tau B} \frac{\partial P_{h\perp}}{\partial \psi}. \quad (6.1.17)$$

This trial function rather than $Q_L(\psi, s) \sim C(\psi)(\partial B/\partial \psi)$ guarantees the valid low frequency limit (see the discussion at the end of this section). Then the quadratic form after the above assumptions is written as

$$\begin{aligned} W = & \int_{\text{layer}} \frac{d\psi ds}{B} \left\{ \tau \left(\frac{1}{\tau B} \frac{\partial P_{h\perp}}{\partial \psi} \right)^2 C^2(\psi) - \frac{\kappa}{\tau B} \left(\frac{\sigma}{\tau} \frac{\partial P_{h\perp}}{\partial \psi} + \frac{\partial P_{\parallel}}{\partial \psi} \right) f^2(s) \right. \\ & - \int d\Gamma \left(\frac{\partial f_0}{\partial H} \right) \frac{\omega - \omega^*}{\omega - \bar{\omega}_d} \left[\mu \left\langle \frac{1}{\tau B} \frac{\partial P_{h\perp}}{\partial \psi} \right\rangle C(\psi) - \left\langle f \frac{\kappa}{\tau B} \left(\mu \frac{\sigma B}{\tau} + m v_{\parallel}^2 \right) \right\rangle \right]^2 \Big\} \\ & + \frac{1}{|l|} \int_{\text{fluid}+\text{vac.}} ds \left\{ - \frac{\omega^2}{v_A^2 \left(1 + \text{Sgn}(l) \frac{\omega}{\omega_{ci}} \right)} f^2(s) + (1 + \Lambda_{|l|}) \left(\frac{\partial f}{\partial s} \right)^2 \right\} = 0, \end{aligned} \quad (6.1.18)$$

where

$$\langle A \rangle \equiv \bar{A}$$

In the derivation of Eq.(6.1.18) we neglect those terms in the layer which have the similar form in the core plasma (fluid + vac. part). Also we note that the contribution from β_1 -term in the layer is small and neglected.

The variation of the quadratic form Eq.(6.1.18) with respect to $C(\psi)$ yields an equation for $C(\psi)$. Its solution gives

$$C(\psi) = \frac{\int \frac{ds}{B} \int d\Gamma \left(\frac{\partial f_0}{\partial H} \right) \frac{\omega - \omega^*}{\omega - \bar{\omega}_d} \mu \left\langle \frac{1}{\tau B} \frac{\hat{\partial} P_{h\perp}}{\partial \psi} \right\rangle \cdot \left\langle \frac{\kappa}{rB} \left(\mu \frac{\sigma B}{\tau} + m v_{\parallel}^2 \right) f \right\rangle}{\int \frac{ds}{B} \left[\int d\Gamma \left(\frac{\partial f_0}{\partial H} \right) \frac{\omega - \omega^*}{\omega - \bar{\omega}_d} \mu^2 \left\langle \frac{1}{\tau B} \frac{\hat{\partial} P_{h\perp}}{\partial \psi} \right\rangle^2 - \frac{1}{\tau B} \left(\frac{\hat{\partial} P_{h\perp}}{\partial \psi} \right)^2 \right]} \quad (6.1.19)$$

In a tent-like pressure profile [Fig.11], $C(\psi)$ becomes piecewise constant on the inner and outer edges respectively. Substituting the expression for $C(\psi)$, Eq.(6.1.19) into the quadratic form Eq.(6.1.18) and assuming $f(s)$ approximately constant in the layer, we obtain the global dispersion relation

$$\begin{aligned} \sum_{i=\pm} \left\{ \frac{A_i^2}{D_i} - H_i + \int_i \frac{d\psi ds}{B} \left[\frac{\sigma \kappa}{\tau} \frac{\partial B}{\partial \psi} - \frac{\kappa}{rB} \frac{\hat{\partial} P_{\parallel}}{\partial \psi} \right] \right\} \\ = |l| \int ds \left\{ \frac{\omega^2}{v_A^2 \left(1 + \text{Sgn}(l) \frac{\omega}{\omega_{ci}} \right)} - k_{\parallel}^2 (1 + \Lambda_{|l|}) \right\}, \end{aligned} \quad (6.1.20)$$

where

$$D_i \equiv \int_i \frac{ds}{B} \left[\int d\Gamma \left(\frac{\partial f_0}{\partial H} \right) \frac{\omega - \omega^*}{\omega - \bar{\omega}_d} \mu^2 \left\langle \frac{1}{\tau B} \frac{\hat{\partial} P_{h\perp}}{\partial \psi} \right\rangle^2 - \frac{1}{\tau B^2} \left(\frac{\hat{\partial} P_{h\perp}}{\partial \psi} \right)^2 \right], \quad (6.1.21)$$

$$A_i \equiv \int_i \frac{ds}{B} \int d\Gamma \left(\frac{\partial f_0}{\partial \psi} \right) \frac{\omega - \omega^*}{\omega - \bar{\omega}_d} \mu \left\langle \frac{1}{\tau B} \frac{\hat{\partial} P_{h\perp}}{\partial \psi} \right\rangle \cdot \left\langle \frac{\kappa}{rB} \left(\mu \frac{\sigma B}{\tau} + m v_{\parallel}^2 \right) \right\rangle, \quad (6.1.22)$$

$$H_i \equiv \int_i \frac{ds}{B} \left[\int d\Gamma \left(\frac{\partial f_0}{\partial \psi} \right) \frac{\omega - \omega^*}{\omega - \bar{\omega}_d} \left\langle \frac{\kappa}{rB} \left(\mu \frac{\sigma B}{\tau} + m v_{\parallel}^2 \right) \right\rangle^2 + \tau \left(\frac{\sigma \kappa}{r\tau} \right)^2 \right], \quad (6.1.23)$$

and k_{\parallel}^2 is a small quantity, measuring $(\partial f / \partial s)^2$ in the whole bumpy cylinder region. Here, $i = \pm$ stands for outer and inner layer respectively.

In the derivation of the global dispersion relation, Eq.(3.1.20), as well as the calculation of trapped particles we find that the contribution from parallel motion is not important for small mirror ratio. For the present purpose, all parallel contributions will be neglected.

In cylindrical limit the quantities become constant along the field lines. Assuming v_{\parallel} is small we find that

$$D_i \rightarrow - \int_i \frac{d\psi ds}{B} \left(\frac{1}{\tau B} \frac{\partial P_{h\perp}}{\partial \psi} \right)^2 (\tau + \tilde{G}_1^i), \quad (6.1.24)$$

$$A_i \rightarrow - \int_i \frac{d\psi ds}{B} \left(\frac{1}{\tau B} \frac{\partial P_{h\perp}}{\partial \psi} \right) \left(\frac{\kappa \sigma}{r \tau} \right) \tilde{G}_1^i, \quad (6.1.25)$$

$$H_i \rightarrow \int_i \frac{d\psi ds}{B} \left(\frac{\sigma \kappa}{r \tau} \right)^2 (\tau - \tilde{G}_1^i), \quad (6.1.26)$$

where

$$\tilde{G}_1^i \equiv \int_i d\Gamma \left(\frac{\partial f_0}{\partial H} \right) \frac{\omega - \omega^*}{\omega - \omega_d} \mu^2, \quad (6.1.27)$$

and

$$\tau + \tilde{G}_1^i \rightarrow 1 + G_1. \quad (6.1.28)$$

Substituting Eqs.(6.1.24)-(6.1.26) into Eq.(6.1.20) yields the dispersion relation in cylindrical limit, that is the same as Eq.(5.1.19), obtained in the cylindrical model with embedded current. This agreement indicates that the radial dependence of the trial function is reasonable.

It is also important to check low frequency limit of the global dispersion relation, Eq.(6.1.20). With the assumption that $\omega \rightarrow 0$ in the layer and the contributions from $\tilde{\beta}_c$ and parallel motion are ignorable, we find

$$D_i \rightarrow \int_i \frac{d\psi ds}{B} \left[\int d\Gamma \left(\frac{\partial f_0}{\partial H} \right) \frac{\omega^*}{\bar{\omega}_d} \mu^2 \frac{1}{\tau B} \left\langle \frac{\hat{\partial} P_{h\perp}}{\partial \psi} \right\rangle^2 - \tau \left(\frac{1}{\tau B} \frac{\hat{\partial} P_{h\perp}}{\partial \psi} \right)^2 \right], \quad (6.1.29)$$

$$A_i \rightarrow \int_i \frac{d\psi ds}{B} \left(\frac{\partial f_0}{\partial \psi} \right) \frac{\omega^*}{\bar{\omega}_d} \mu^2 \left\langle \frac{1}{\tau B} \frac{\hat{\partial} P_{h\perp}}{\partial \psi} \right\rangle \left\langle \frac{\kappa \sigma}{r \tau} \right\rangle, \quad (6.1.30)$$

$$H_i \rightarrow \int_i \frac{d\psi ds}{B} \left[\int d\Gamma \left(\frac{\partial f_0}{\partial H} \right) \frac{\omega^*}{\bar{\omega}_d} \mu^2 \left\langle \frac{\kappa \sigma}{r \tau} \right\rangle^2 + \tau \left(\frac{\sigma \kappa}{r \tau} \right)^2 \right], \quad (6.1.31)$$

with

$$\omega_d \rightarrow \frac{l_c}{q} \mu \frac{\partial B}{\partial \psi}, \quad (6.1.32)$$

and

$$\frac{1}{\tau B} \frac{\hat{\partial} P_{h\perp}}{\partial \psi} \rightarrow \frac{\kappa \sigma}{r \tau} - \frac{\partial B}{\partial \psi}. \quad (6.1.33)$$

Using Eqs.(6.1.32),(6.1.33), we find, after some algebra

$$\frac{A_i^2}{D_i} - H_i = - \int_i \frac{d\psi ds}{B} \frac{\sigma \kappa}{r} \frac{\partial B}{\partial \psi}. \quad (6.1.34)$$

When the driving forces to the interchange mode, such as $\hat{\partial}/\partial \psi$ and $\tilde{\beta}_c$, are dropped, we arrived merely at the surface Alfven wave:

$$\frac{\omega^2}{v_A^2 \left(1 + \text{Sgn}(l) \frac{\omega}{\omega_{ci}} \right)} - k_{\parallel}^2 (1 + \Lambda_{|l|}) = 0. \quad (6.1.35)$$

We stress that the exact Eq.(6.1.35) can not be obtained if the trial function for Q_L is chosen to be $C(\psi)(\partial B/\partial \psi)$. This choice leads to unphysical instabilities for the surface Alfven wave.

VI.2 Calculation of Trapped Particles

A trapped particle distribution function of the following form is chosen for the calculation of macroscopic quantities of hot electrons:

$$f_0(H, \mu) = \hat{a} \cdot \sqrt{\mu B_c - H} \cdot \exp(-H/T), \quad (6.2.1)$$

where \hat{a} is the normalization and B_c is the maximum magnetic field. The magnetic field in the hot electron region is approximated by

$$B(s) = B_0(1 + s^2/L_0^2). \quad (6.2.2)$$

Then we obtain

$$n_h(s) = n_{h0} \sqrt{\frac{B_0}{B}} \cdot \frac{B_c - B}{B_c - B_0}, \quad (6.2.3)$$

$$P_{h\perp}(s) = P_{\perp 0} \sqrt{\frac{B_0}{B}} \cdot \frac{B_c - B}{B_c - B_0} \left(\frac{3}{4} + \frac{B}{4B_c} \right), \quad (6.2.4)$$

$$P_{h\parallel}(s) = 2P_{h\perp}(s) \left(\frac{B_c - B}{3B_c + B} \right), \quad (6.2.5)$$

with

$$n_{h0} \equiv n_h(0), \quad P_{\perp 0} \equiv P_{h\perp}(0).$$

The energy integral shows that $T_h = 2T$, where T_h is the hot electron temperature.

In the long thin approximation, assuming that the flux $\psi \sim \frac{1}{2}Br^2$ and the curvature $\kappa \sim \frac{\partial^2 r}{\partial s^2}$, we have

$$\frac{\kappa}{rB} = \frac{3}{4B^3} \left(\frac{\partial B}{\partial s} \right)^2 - \frac{1}{2B} \frac{\partial^2 B}{\partial s^2} = -\frac{1}{B_0 L_0^2} \cdot \frac{1 - \frac{2s^2}{L_0^2}}{\left(1 + \frac{s^2}{L_0^2} \right)^3}. \quad (6.2.6)$$

Then,

$$\begin{aligned} \left\langle \frac{\kappa}{rB} m v_{\parallel}^2 \right\rangle &= \frac{\oint \frac{ds}{\sqrt{H - \mu B}} \frac{\kappa}{rB} m v_{\parallel}^2}{\oint \frac{ds}{\sqrt{H - \mu B}}} \\ &= -\frac{\mu}{4L_0^2} \left[\sqrt{\frac{H}{\mu B_0}} + 2\sqrt{\frac{\mu B_0}{H}} - 3 \left(\frac{\mu B_0}{H} \right)^{3/2} \right], \end{aligned} \quad (6.2.7)$$

and

$$\begin{aligned} \left\langle \frac{\partial B}{\partial \psi} \right\rangle &= \frac{\oint \frac{ds}{\sqrt{H - \mu B}} \frac{\partial B}{\partial \psi}}{\oint \frac{ds}{\sqrt{H - \mu B}}} \\ &= \left(\frac{\sigma \kappa}{r} \right)_0 \left\{ 1 - \zeta_0 \left[1 - \frac{B_0}{2(B_c - B_0)} \cdot \frac{H - \mu B_0}{\mu B_0} \right] - \tilde{\beta}_c \right\}, \end{aligned} \quad (6.2.8)$$

where hereafter quantities with a nought subscript indicate the value at the midplane.

For $(B_c - B_0)/B_0 \ll 1$, which implies small $(H - \mu B_0)/\mu B_0$, we ignore the parallel motion contribution to $\bar{\omega}_d$ and assume that $(\sigma \kappa/r\tau)$ and $(1/\tau B)(\partial P_{c\perp}/\partial \psi)$ are slowly varying functions along the magnetic field line.

Then the quantities contained in the dispersion relation Eq.(6.1.20), D_i , A_i , H_i are written as

$$D_i = \int_i \frac{d\psi ds}{B} \left\{ \left(\frac{\sigma\kappa}{r} \right)^2 (1 - \tilde{\beta}_c)^2 K_0 - 2 \left(\frac{\sigma\kappa}{r} \right) (1 - \tilde{\beta}_c) K_1 + K_2 \right\}, \quad (6.2.9)$$

$$A_i = \int_i \frac{d\psi ds}{B} \left\{ \left(\frac{\sigma\kappa}{r} \right)^2 (1 - \tilde{\beta}_c) K_0 - \left(\frac{\sigma\kappa}{r} \right) K_1 \right\}, \quad (6.2.10)$$

$$H_i = \int_i \frac{d\psi ds}{B} \left(\frac{\sigma\kappa}{r} \right)^2 (1 + K_0), \quad (6.2.11)$$

where

$$K_0 \equiv \int d\Gamma \left(\frac{\partial f_0}{\partial H} \right) \frac{\omega - \omega^*}{\omega - \bar{\omega}_d} \mu^2, \quad (6.2.12)$$

$$K_1 \equiv \int d\Gamma \frac{\partial f_0}{\partial H} \frac{\omega - \omega^*}{\omega - \bar{\omega}_d} \left\langle \frac{\partial B}{\partial \psi} \right\rangle \mu^2, \quad (6.2.13)$$

$$K_2 \equiv \int d\Gamma \left(\frac{\partial f_0}{\partial H} \right) \frac{\omega - \omega^*}{\omega - \bar{\omega}_d} \left\langle \frac{\partial B}{\partial \psi} \right\rangle^2 \mu^2 - \frac{1}{\tau B^2} \left(\frac{\hat{\partial} P_{h\perp}}{\partial \psi} \right)^2, \quad (6.2.14)$$

with

$$\bar{\omega}_d \sim \frac{lc}{q} \mu \left(\frac{\sigma\kappa}{r} \right) \left(1 - \tilde{\beta}_c - \zeta_0 + \frac{\zeta_0}{2} \frac{B_0}{B_c - B_0} \cdot \frac{H - \mu B_0}{\mu B_0} \right). \quad (6.2.15)$$

Making use of standard results

$$\int d\Gamma \left(\frac{\partial f_0}{\partial \psi} \right) \mu = \frac{1}{B} \frac{\hat{\partial} P_{h\perp}}{\partial \psi}, \quad (6.2.16)$$

$$\int d\Gamma \left(\frac{\partial f_0}{\partial \psi} + \mu \frac{\partial f_0}{\partial H} \frac{\partial B}{\partial \psi} \right) = B \frac{\partial}{\partial \psi} \left(\frac{n_h}{B} \right), \quad (6.2.17)$$

we may write

$$\int_i \frac{d\psi}{B} K_0 = \int_i \frac{d\psi}{B} \int d\Gamma \frac{\omega \left(\frac{\partial f_0}{\partial H} \right) + \frac{lc}{q} \left(\frac{\partial f_0}{\partial \psi} \right)}{\omega - \bar{\omega}_d} \mu^2, \quad (6.2.18)$$

$$\int_i \frac{d\psi}{B} K_1 = \int_i \frac{d\psi}{B} \left\{ -\frac{1}{B} \frac{\partial P_{h\perp}}{\partial \psi} + \omega \int d\Gamma \frac{\frac{\partial f_0}{\partial \psi} + \mu \frac{\partial f_0}{\partial H} \frac{\partial B}{\partial \psi}}{\omega - \bar{\omega}_d} \mu \right\}, \quad (6.2.19)$$

$$\begin{aligned} \int_i \frac{d\psi ds}{B} K_2 = \int_i \frac{d\psi ds}{B} \left\{ -\left(\frac{\sigma \kappa}{r \tau} \right) (1 - \tilde{\beta}_c) \frac{1}{b} \frac{\partial P_{h\perp}}{\partial \psi} - \frac{\omega}{\left(\frac{lc}{q} \right)} B \frac{\partial}{\partial \psi} \left(\frac{n_h}{B} \right) \right. \\ \left. + \frac{\omega^2}{\left(\frac{lc}{q} \right)} \int d\Gamma \frac{\frac{\partial f_0}{\partial \psi} + \mu \frac{\partial f_0}{\partial H} \frac{\partial B}{\partial \psi}}{\omega - \bar{\omega}_d} \right\}. \end{aligned} \quad (6.2.20)$$

In the integration of the phase space (H, μ) we introduce a new variable $\hat{\tau}$ by $\hat{\tau} = [(H - \mu B)/\mu(B_c - B)]^{1/2}$, and approximate the exponential argument in the distribution function by

$$-\frac{H}{T} = -\frac{B\mu}{T} - \frac{\mu(B_c - B)}{T} \hat{\tau}^2 \sim -\frac{B\mu}{T}. \quad (6.2.21)$$

This allows us to perform the $\hat{\tau}$ -integration analytically. Then we obtain

$$\int d\Gamma \frac{\frac{\partial f_0}{\partial \psi} + \mu \frac{\partial f_0}{\partial H} \frac{\partial B}{\partial \psi}}{\omega - \bar{\omega}_d} = 4 \left(\frac{\partial n_{h0}}{\partial \psi} \right) \frac{1}{\bar{\omega}_{\kappa 0} \zeta_0} [1 - \Gamma_0(\hat{s}, \zeta_0)], \quad (6.2.22)$$

$$\int d\Gamma \frac{\frac{\partial f_0}{\partial \psi} + \mu \frac{\partial f_0}{\partial H} \frac{\partial B}{\partial \psi}}{\omega - \bar{\omega}_d} \mu = 4 \left(\frac{\partial n_{h0}}{\partial \psi} \right) \frac{1}{\bar{\omega}_{\kappa 0} \zeta_0} \left(\frac{T}{B_0} \right) [1 - \Gamma_1(\hat{s}, \zeta_0)], \quad (6.2.23)$$

$$\int d\Gamma \frac{\omega \left(\frac{\partial f_0}{\partial H} \right) + \frac{lc}{q} \left(\frac{\partial f_0}{\partial \psi} \right)}{\omega - \bar{\omega}_d} \mu^2 = 4 \left(\frac{\partial n_{h0}}{\partial \psi} \right) \frac{1}{\bar{\omega}_{\kappa 0} \zeta_0} \left(\frac{1}{B_0} \right) [2 - \Gamma_2(\hat{s}, \zeta_0)], \quad (6.2.24)$$

where

$$\bar{\omega}_{\kappa 0} \equiv \left(\frac{lc}{q} \right) \left(\frac{T\kappa}{B_0 r} \right), \quad (6.2.25)$$

and

$$\Gamma_n(\hat{s}, \zeta_0) \equiv \int_0^\infty dx x^n \cdot \exp(-x) \sqrt{\frac{\bar{\omega} - x(1 - \bar{\beta}_c - \zeta_0/2)}{\bar{\omega} - x(1 - \bar{\beta}_c - \zeta_0 + \zeta_0 \hat{s}^2/2)}}, \quad (6.2.26)$$

with $\hat{s} \equiv s/s_c$ and $B(s_c) \equiv B_c$. In the Eqs.(6.2.22),(6.2.23) we have assumed $\omega \ll \omega^*, \beta_h \ll 1, B_c - B_0 \ll B_0$.

The integrand of Eq.(6.2.26) reveals the stabilizing effect of trapped particle. In the cylindrical model we recall that the negative energy dissipation originates from the Landau damping in outer edge, where ζ_0 is positive. Therefore, once $1 - \bar{\beta}_c - \zeta_0 < 0$, the Landau damping no longer exists, so that the negative energy dissipation mechanism vanishes. In lieu of $1 - \bar{\beta}_c - \zeta_0$, we find a line-dependent quantity $1 - \bar{\beta}_c - \zeta_0 + \zeta_0 \hat{s}^2/2$, which determines the existence of Landau damping. In the midplane, where $\hat{s} = 0$, the critical condition for the vanish of Landau damping is unaltered. However, at the farthest end of the hot layer, where $\hat{s} = 1$, the critical condition becomes $1 - \bar{\beta}_c - \zeta_0/2 \geq 0$.

This implies that even the negative energy dissipation mechanism vanishes in the midplane when $\zeta_0 > 1$, the same mechanism still persists at the places off the midplane. Averagely, we expect the critical ζ_0 lying between $1 - \tilde{\beta}_c$ and $2(1 - \tilde{\beta}_c)$.

In the integrals containing $K_j (j = 0, 1, 2)$ the integration over field line (\hat{s}) can further be performed analytically, so that D_i, A_i, H_i can be calculated explicitly.

Defining the line average function $\bar{\Gamma}_n(\zeta_0) \equiv \langle \Gamma_n(\hat{s}, \zeta_0) \rangle$,

$$\bar{\Gamma}_n(\zeta_0) \equiv \int_0^\infty dx x^n e^{-x} \sqrt{\frac{\hat{\omega} - (1 - \tilde{\beta}_c - \zeta_0/2)x}{\zeta_0 x/2}} \text{Arcsin} \sqrt{\frac{\zeta_0 x/2}{\hat{\omega} - (1 - \tilde{\beta}_c - \zeta_0)x}}, \quad (6.2.27)$$

we obtain the final form of the dispersion relation, Eq.(6.1.20)

$$\begin{aligned} & \frac{1}{a\zeta} \cdot \left\{ \frac{[4 - 2\bar{\Gamma}_2(-a\zeta) - \frac{2a}{3}\zeta - 2\hat{\omega}(1 - \bar{\Gamma}_1(-a\zeta))]^2}{-\frac{2a}{3}\zeta + 4 - \bar{\Gamma}_2(-a\zeta) + \frac{a\zeta}{3}\hat{\omega} + 2\hat{\omega}^2(1 - \bar{\Gamma}_0(-a\zeta)) - 4\hat{\omega}(1 - \bar{\Gamma}_1(-a\zeta))} \right. \\ & \quad \left. + 2\bar{\Gamma}_2(-a\zeta) - 4 + \frac{2a}{3}\zeta \right\} + \frac{1}{\zeta} \cdot \left\{ \frac{[(1 - \tilde{\beta}_c)(4 - 2\bar{\Gamma}_2(\zeta)) + \frac{2}{3}\zeta - 2\hat{\omega}(1 - \bar{\Gamma}_1(\zeta))]^2}{(1 - \tilde{\beta}_c)[\frac{2\zeta}{3} - 4\hat{\omega}(1 - \bar{\Gamma}_1(\zeta))] + (1 - \tilde{\beta}_c)^2(4 - 2\bar{\Gamma}_2(\zeta)) - \frac{\hat{\omega}\zeta}{3} + 2\hat{\omega}^2(1 - \bar{\Gamma}_0(\zeta))} \right. \\ & \quad \left. + 2\bar{\Gamma}_2(\zeta) - 4 - \frac{2}{3}\zeta - \tilde{\beta}_c \right\} = N^2 \left(\frac{L_c}{L_H} \right) \left[\Omega_A^2 (1 + \Lambda_{|l|}) - \frac{\hat{\omega}^2}{1 + \text{Sgn}(l) \frac{\hat{\omega}}{\hat{\omega}_{ci}}} \right], \quad (6.2.28) \end{aligned}$$

where $\hat{\omega} \equiv \omega/\tilde{\omega}_{\kappa 0} = 2(\omega/\tilde{\omega}_{\kappa})$, $\hat{\omega}_{ci} \equiv \omega_{ci}/\tilde{\omega}_{\kappa 0}$, $a = \Delta_{out}/\Delta_{in}$, $\Omega_A \equiv k_n v_A/\tilde{\omega}_{\kappa 0}$, $N^2 \equiv \tilde{\omega}_{\kappa 0}^2/\gamma_{MHD}^2$, L_c - the length of the field line, L_H - the length of the hot electron region [cf.Fig.21]. More precisely, it is

$$\frac{L_c}{L_H} = \frac{n_{ho} \int \frac{ds}{B} n_c}{n_{c0} \int \frac{ds}{B} n_h}$$

VI.3 Numerical Results and Discussion.

The dispersion relation, Eq.(6.2.28), is numerically solved for the precessional mode which is characterized by the real frequency around the curvature frequency $\tilde{\omega}_{\kappa}$. For simplicity, we assume $a = 1$, $\tilde{\beta}_c = 0$, $\Omega_A^2 = 0$, $\hat{\omega}_{ci} = 1$. The results are given in Fig.22 through Fig.25 in contrast with those in the cylindrical model (Fig.13-15,18). For convenience we introduce the parameter $N_{eff}^2 = N^2(L_c/L_H)$, to indicate an incomplete coupling between cold plasma and hot electron. This indicates that the coupling constant is less than that we have considered in the cylindrical model by a factor of L_c/L_H . It introduces a stabilizing effect. Fig.22 illustrates the marginal stability. For the moderate N^2 (or N_{eff}^2) the stability threshold is almost the twice of that for the cylindrical model ($\zeta_0 \sim 1.5$) so that a shallow magnetic well can be formed around the midplane without destabilizing the precessional mode. The resemblance of the real frequency behavior between the cylindrical model and axially dependent geometry shown in Fig.23 indicates that they belong to the same kind of mode. In Fig.24 we have shown the mode growth rate versus ζ for different N_{eff}^2 .

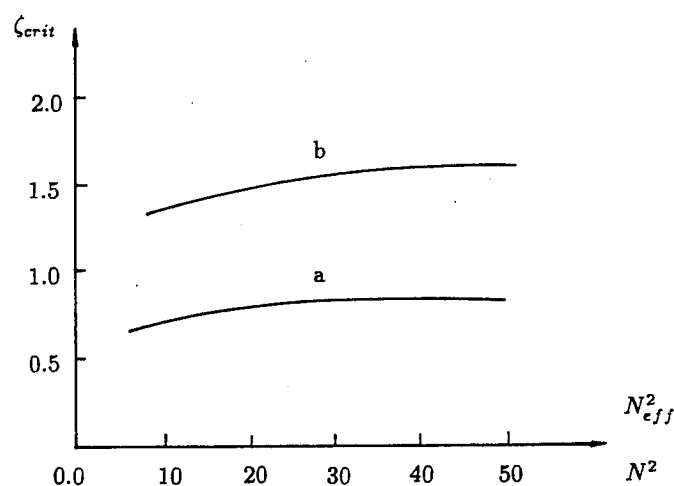


Fig.22 Marginal stability in cylindrical model (curve a) and in a single mirror cell (curve b). Stable region are below the corresponding curves.

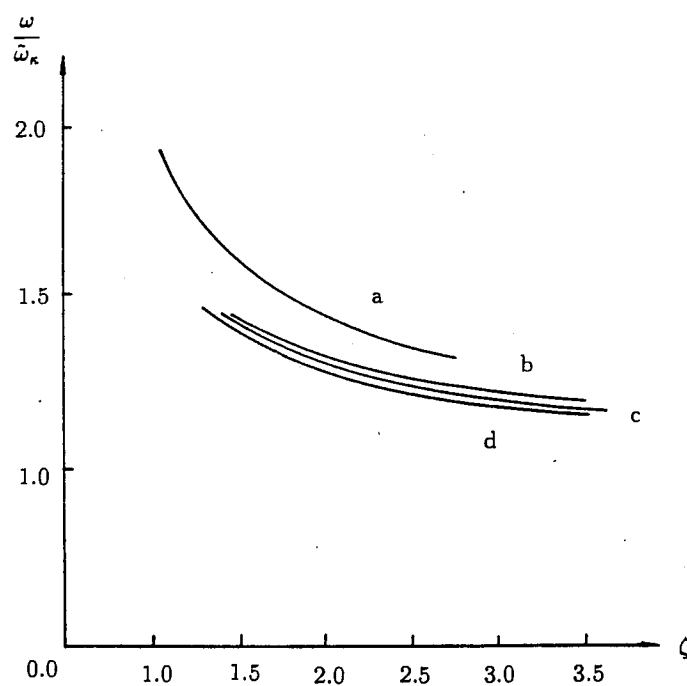


Fig.23 Real frequency of precessional mode in cylindrical model (curve a with $N^2 = 10.0$) and in single mirror cell (curve b, c, d with $N_{eff}^2 = 50.0, 20.0$ and 10.0 respectively).

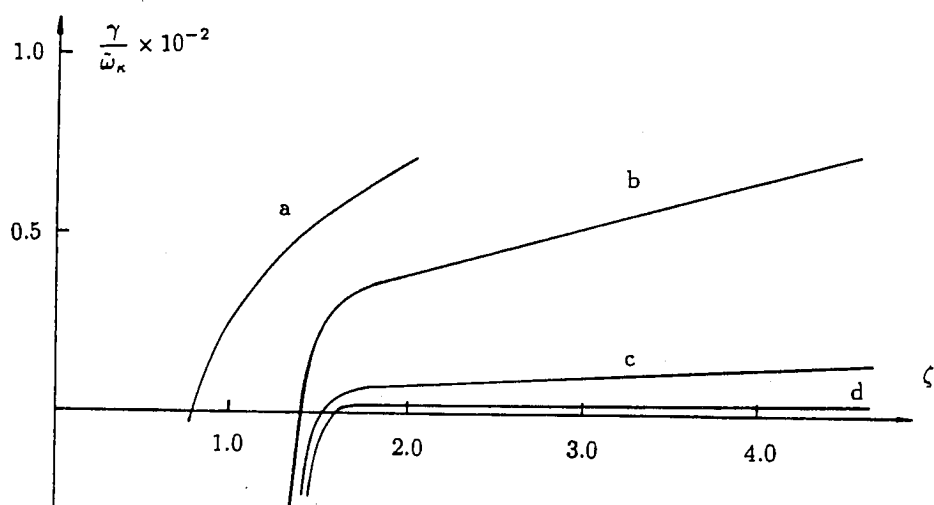


Fig.24 Growth rate of precessional mode in cylindrical model (curve *a* with $N^2 = 10.0$) and in single mirror cell (curve *b, c, d* with $N_{eff}^2 = 10.0, 20.0$ and 50.0 respectively).

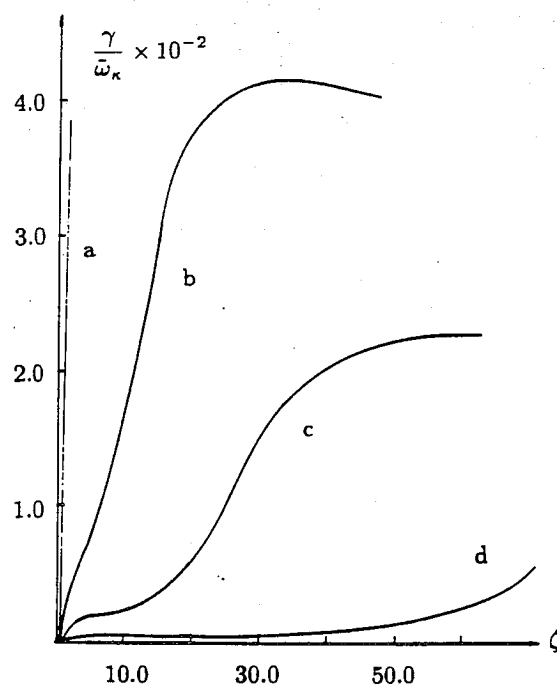


Fig.25 Growth rate of precessional mode for same parameters as Fig.24.

Compared to the growth rate in the cylindrical model it is almost suppressed one order of magnitude for the same N^2 (N_{eff}^2). Therefore, we can not rule out the possibility that a rather deep magnetic well can be formed if N_{eff}^2 is large enough. The growth rate versus ζ in a larger scale is shown in Fig.25. Though the growth rate is depressed in large ζ limit, the mode is always unstable.

Now we discuss whether experiments exist that violate our prediction for the diamagnetic limit.

In bumpy tori as EBT-S⁸⁵ and NBT(Fig.26)⁸⁶ the drift reversal parameter ζ is now thought to be considerably less than unity so that the instability described here should not arise. In bumpy tori the radial component of the toroidal drift may make it difficult to achieve thin layers. Thin layer are more likely to be achieved in simple mirror machines where there is no radial component to the grad-B and curvature drifts.

In fact, in simple mirrors very high stored energy has been obtained, and analysis of the data in the SM experiment ^{87,88} indicates that mid-plane ζ values of order 6 has been obtained with no detrimental containment or obvious instabilities at the precessional drift frequency being observed. The determination of such a large ζ -value is based on a reconstruction of the hot particle diamagnetic currents that are needed to match Hall probe measurements of the magnetic field. The analysis performed in Refs.87 and 88 concludes that it is highly improbable that radially broad-pressure profiles could produce the magnetic field measured by Hall probes. Nonetheless, one must be cautious with the complete acceptance of such a conclusion as it is well known that a

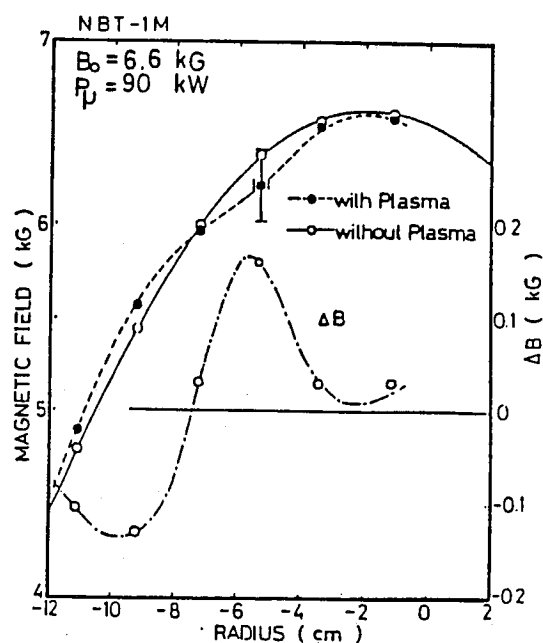


Fig.26 Magnetic field modification by hot electron ring generated with 90 kw (28 GHz, 50 ms) microwave power in NBT⁸⁶.

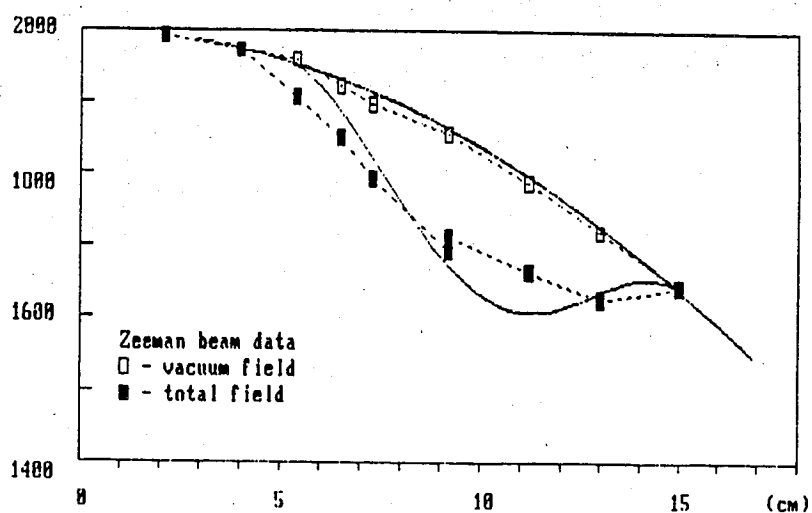


Fig.27 A comparison of Hall probe results (solid curve) with Zeeman beam data (dashed curve) in STM⁸⁹.

given magnetic field configuration in a fixed region of space can be produced by a continuum of different current configurations. For example, a separability assumption in the axial and radial dependences of the pressure profile is made. The actual experiment may not have this separability. As a result, a fit close to the true experimental conditions may have been filtered away. The assumption on separability is more likely to affect fits on broader profiles than narrower profiles as more structure is possible in smooth broad profiles than in smooth narrow profiles. It appears that auxiliary and/or alternative measurements are needed to determine whether drift-reversal configurations have indeed been produced.

A direct measurement, using the Zeeman principle, of the magnetic field structure has been developed and employed in hot-electron experiments in STM.⁸⁹ To date, the observed radial pressure profiles have been too broad and the stored energy too low to produce grad-B reversal (Fig.27). There are several technical factors that makes plasma conditions in STM experiment different than in the SM experiment. Thus, it is not clear whether the failure to obtain grad-B reversal in experiments that can measure grad-B directly, was due to a technical failure to obtain the optimal experimental conditions such as were achieved in the SM experiment (or even in ELMO) or is due to an intrinsic stability limitation.

To our best knowledge, the only unmentioned set of experiments that claims achieving of the drift reversal is that carried out in Constance B,⁹⁰ where a hollow hot electron plasma is found stable. Since the baseball config-

uration of the Contance B is an intrinsical three dimensional one and the axial length comparable to radial length, it might be too simplified to account for the experimental results by using a two dimensional axisymmetric model with the long thin approximation. The motivation behind searching for the correlation between our axial dependence calculation and the results in Constance B is merely to show whether or not the prediction of the diamagnetic limit can be severely altered in any circumstance where the negative energy dissipation vanishes (at least partly), while the positive energy dissipation presents.

It is observed in the Contance B that a local maximum $\beta_{h\perp} \sim 0.3 - 0.45$ has been achieved with a typical hot electron density thickness $\Delta_{in} \sim 6\text{cm}$ and $\kappa^{-1} > 30\text{cm}$ (Note that the effect of inner and outer edge on the precessional instability is interchanged for the good curvature baseball configuration). Although, the pressure gradient of the inner edge (measured only for $\beta_{h\perp} \sim 0.3$) has not been determined precisely, it is believed very close to the measured density gradient, while their difference at the outer edge looks quite large. Two independent measurement methods (visible light imaging and X-ray imaging) are adopted for the determination of the density profile, giving results in good agreement. The pressure gradient is determined by the magnetic measurement similar to that performed in SM experiment, particularly, the separability is assumed in thier pressure model. Making use of the pressure gradient given above, we find the typical local maximum drift reversal parameter $\zeta \sim 1.1$ for $\beta_{h\perp} \sim 0.3$ (the local curvature radius at the largest drift reversal is $\kappa^{-1} \sim 55\text{cm}$). There are some complexities in the determination of N_{eff}^2 . For example,

we do not know exactly what is the least mode number l and how to identify the ratio L_c/L_H . If the least mode number l is assumed to be 4 from symmetry consideration and L_c/L_H is simply taken to be 1, the N_{eff}^2 is then typically about 5. Our axial dependence calculation predicts the local maximum $\zeta \sim 1.3$ (Fig.22), obviously above the experimental observations in Constance B. It seems to be very intriguing then to increase the store energy in Constance B further, to see if substantial augment of ζ can be obtained.

Although the experimental results in EBT-S, NBT, STM and Constance B (in the latter case the extreme good geometry severely complicates interpretation) are not inconsistent with our theory, it is still worthwhile to examine if in the SM experimental circumstances exist some potential stabilizing mechanisms that may cause substantial augment of the ζ -value beyond our theoretical prediction.

An additional stabilizing source for negative energy dissipation is available through hot particle bounce harmonic resonances. However, since the bounce frequency is typically much larger than the precessional frequency, only hot electrons that are barely trapped contribute to this dissipation mechanism, and we doubt that there are enough such hot electrons present to alter our stability predictions.

The possibility that a smooth radial profile can lead to a qualitatively different stability results seems to be ruled out from the results of Fig.19, which also shows that the instability threshold is near the grad-B reversal condition. In this case instability arises even though there is always some source of negative

dissipation, which is not enough to produce stabilization.

The results that we have obtained from the axial geometry calculation are based on a tent-like radial pressure profile, in the long thin limit. In an actual geometry, the long thin limit is often a marginally accurate assumption and radial pressure profiles are smooth. There are further complications in the lack of separability in axial and radial dependences. Thus, it is possible that our improved calculations are still too idealized to properly describe the stability mechanisms that are present in an actual experimental configuration.

Finite Larmor radius effects might be another aspect that can be invoked as a limitation of our stability calculation. Previous work analyzing the type of layer modes described here⁴⁸ indicate that finite Larmor radius effects do not strongly influence this theory if the Larmor radius is less than the layer width. FLR corrections are nondissipative and of order $(l\rho_h/r_0)^2$, where ρ_h is the hot particle Larmor radius, l is the mode number, and r_0 the plasma radius. However, it should be noted that in the SM experiment, where $B_{vacuum} \sim 1600G$, the Larmor radius of 400 Kev hot electrons is ~ 1.5 cm, while the claimed half-width is 3cm. Thus the analytic theory is on the edge of validity if the layer widths are indeed as narrow as claimed, and perhaps finite Larmor corrections may be strong enough to bring in dissipative approximations.

Another possibility is that the instability saturates at a sufficiently low level to lead to benign consequences. Direct measurements of the fluctuation spectrum are needed to support this viewpoint.

PART B

RENORMALIZATION THEORY

VII. Introduction to Renormalization Theory

There are two different popular approaches to deal with strong turbulence in a Vlasov-Poisson system; the perturbative and the non-perturbative (functional approach). The former was initiated by Dupree's pioneering work,⁹¹ commonly known as the "resonance broadening theory", in which the bare propagator $(\omega - \mathbf{k} \cdot \mathbf{v})^{-1}$ in the Vlasov equation is intuitively replaced by a renormalized propagator $(\omega - \mathbf{k} \cdot \mathbf{v} + i\Gamma_k)^{-1}$, where $i\Gamma_k$ stands for the stochastic diffusion arising from the turbulent fields acting on the particles. Further progress in perturbation theories consists mainly of the following two developments:

(1) The "single renormalization theory" (named by Horton and Choi⁹²) is replaced by the "fully renormalized theory", in which $i\Gamma_k$ is related to the spectrum and is no longer determined through the bare propagator alone.⁹²⁻⁹⁴

(2) Dupree and Tetrault⁹⁵ added the famous β -term to the nonlinear coherent dielectric function (the terminology of coherent dielectric function will be explained in VIII.3) in order to conserve energy in electrostatic drift waves. This property of the exact system was violated in earlier versions of the perturbation theory.

The incorporation of these developments has led to the new widely used modern perturbation theories.⁹⁵⁻⁹⁸ These theories are limited to second order (of coherent part) in expansion, although the concept of "order" is not unambiguous. An important shortcoming of these conventional perturbation theories

consists in their failure to reduce in the corresponding limit, to the commonly accepted weak turbulence theory, e.g., the well-known Kadomtsev spectrum equation [Eq.(11.50) in Ref.99] does not follow from the weak turbulence limit of Dupree's equations.¹⁰⁰

The non-perturbative approach¹⁰⁰ for a Vlasov-Poisson system can be constructed on the basis of the rigorous MSR (Martin - Siggia - Rose) systematology.¹⁰¹ It is basically a generating functional method for constructing the Green function. However, the system of equations in the MSR systematology contains a functional differential equation for the renormalized vertex Γ . Its rigorous solution seems illusive with present mathematical techniques. In practice, progress is achieved by introducing a rather ad-hoc closure technique of replacing the renormalized vertex Γ by its lowest order approximation - the bare vertex γ , which is a known quantity. This is the Direct Interaction Approximation (DIA).^{100,102-104} The DIA, although an approximate theory, has the advantage of keeping the form of the exact equations in the MSR systematology.

A very important success of the DIA (which is not solvable in the general form) lies in its ability to reproduce the weak turbulence equations. In addition, the dielectric function derived from the DIA equations for the Vlasov-Poisson system corresponds precisely to the definition of the dielectric function in statistical mechanics.

This success of the DIA is to be contrasted with the already mentioned failure of the perturbation theories. We should also mention that the coherent dielectric function used by Dupree is indeed different from the rigorously defined

dielectric function in statistical mechanics.

The failure of the perturbation theories to yield the correct weak turbulence limit has been attributed to their lack of proper, self-consistent treatment of the Vlasov-Poisson system.¹⁰⁰ The difference between, for example, Dupree's approach and the DIA emerges when we examine the renormalized propagator used in these two approaches. The propagator used in Dupree's approach contains only the diffusion part (which is related to the self-energy effects), while the propagator used in the MSR systematology and hence the DIA includes a polarization part also; this part is related to the polarization cloud around a test particle and to the statistical fluctuations in the dielectric response. We shall see in VIII.3 that the effects like $\delta f_k(\phi^{(e)})/\delta\phi_{k'}^{(e)}|_{\phi^{(e)}=0}$ for $k \neq k'$ are intrinsically related to the incoherent waves, or more precisely, to the correlation between the background waves and the induced (by the external source) waves. It is precisely the exclusion of the incoherent wave effects which renders the standard perturbation theories incapable of yielding the correct form for the limiting cases. In fact, the coherent approximation to DIA (DIAC: introduced and analysed by Krommes¹⁰⁵) with diffusive part alone in the propagator suffers from the same problems and is equivalent to the theory of Dupree and Tetrault.

To make further progress one must either deal with the DIA in its entirety, or find a way to improve the perturbation theory so that its glaring failures can be overcome. Unfortunately, the theories based on the DIA, when applied to problems of strong turbulence, have gone little beyond the perturbative re-

sults. For example, the renormalized versions of Kadomtsev's equation and the dielectric function have still not been derived from this approach.

Thus we seek an alternative perturbation theory which is internally consistent and which includes all the effects contained in DIA. We must remark that the effects like the " polarization " do not have to appear in the propagator as they do in DIA. In fact, the secularities appearing in higher order terms of the weak turbulence perturbation series can be wholly eliminated by just the self-energy renormalization of the propagator (akin to the mass renormalization of the Dirac propagator). The physical effects represented by the polarization part etc. can be readily displayed by the correct manipulation of the incoherent part in a properly matched renormalized perturbation theory.

The perturbation theory presented in VIII.1 fulfills the above mentioned requirements. The renormalizability is demonstrated by generalizing the procedure of Rudakov-Tsyтович to arbitrary higher orders. Renormalizability, here, means that the counter (or compensating) term $i\Gamma_k$ (corresponding to frequency broadening and shift in the propagator) formally added to equations, has to be eliminated in each perturbative order [cf. VIII.2]. The proof of renormalizability thus leads to a self-consistent determination of $i\Gamma_k$, and in addition, provides a unique definition of " order " (counted by the numbers of vertices in the diagram) putting the theory on a firm formal footing.

The proof of renormalizability, however, is not enough to guarantee that the perturbative approach is, at least, equivalent to the DIA. To do this we must demonstrate that this approach can match the most important success of the

DIA in the weak turbulence limit, i.e., the calculation of the dielectric function and the derivation of Kadomtsev's spectrum equation. Therefore, we present in VIII.3 a detailed derivation of the renormalized dielectric function (starting from its statistical mechanics definition¹⁰⁶), and then obtain its explicit form to second order and show that it reduces to the correct weak turbulence limit. The renormalized version of Kadomtsev spectrum equation is derived in VIII.4. The correct weak turbulence limit is readily verified.

Proper treatment of the incoherent terms distinguishes the present perturbation theory from the earlier ones. Although both the DIA and our theory reproduce the standard weak turbulence results, our theory is not equivalent to DIA. In fact, the propagator in our theory has contribution from the self-energy effects only while the propagator in DIA includes the effects of polarization as well.

We must, however, mention that Dupree did include contributions from the incoherent part in the framework of a two-point theory.¹⁰⁷⁻¹¹⁰ We do not discuss these complicated theories here, because this thesis is devoted to the proper development of a one-point perturbation theory.

It is to be noted that the lowest order of the incoherent part corresponds to the terms associated with the three wave interaction in the weak turbulence limit. This process gives substantial contribution only if the phase space for the three wave resonance is sufficiently large. In many cases of interest to the " physics of fusion ", the phase space is so small that the effect of the three wave interaction is believed to be unimportant. However, the conditions

for the three wave resonance (in a linear sense) are somewhat relaxed in a renormalized perturbation theory. For a given \mathbf{k} , the frequency ω is no longer solely determined by the linear dispersion, $\omega(\mathbf{k})$. Instead, the spectrum is spread in ω ; it is centered at $\omega(\mathbf{k})$ and has a width $\Delta\omega$, (known as the correlation broadening).¹¹¹ The broadening is caused by the three wave interaction in the allowable phase space. This phenomenon becomes very important in the processes involving the annihilation of two high frequency waves to produce a low frequency wave. In fact, the three wave resonance condition is always satisfied if the correlation broadening of the high frequency waves is equal to or greater than the frequency of the low frequency wave. This effect is studied in VIII.4.

In IX we deal with the problem of proving energy conservation for the electrostatic drift waves to all orders in the perturbation theory. This is a crucial test for the validity of several theories. The perturbation approach passed this test to second order only after Dupree and Tetrault introduced their β -term. We show that for orders greater than two the incoherent part starts to contribute to the energy, and thus the theories with no incoherent part (like the DIAC etc.) are not expected to conserve energy for these orders.

Use is made of the perturbative procedure to study the nonlinear gyrokinetic equation in X. Since finite Larmor radius effects are considered quite important in plasma microturbulence we choose a low- β gyrokinetic system as our object of study. We first show that the perturbative procedure is ideally suited to develop an analytical " finite Larmor radius " renormalized theory [cf.

X.1], then apply it to illustrate the nonlinear behavior of the kinetic η_i mode; i.e., we derive the coupled nonlinear wave equations. The transport equation is derived in X.3 so that the turbulent transport coefficients are readily identified. The general properties of the energy transport coefficients are discussed with particular emphasis on the finite Larmor radius effects.

The formalism constructed for the Vlasov-Poisson system can be readily generalized¹¹² to a variety of models used to describe the nonlinear behavior of physical phenomena in different areas of physics and engineering. The renormalizability can be proved for all the nonlinear systems with Yukawa-type interaction, i.e., for systems like the Korteweg-de Vries equation,¹¹³ Boussinesq equation,¹¹⁴ Navier- Stokes equation.¹¹⁵ However, the equations with Fermi-type interaction, like the nonlinear Schrodinger equation¹¹⁶ do not fall within the scope of the present renormalization procedure.

The work presented in the following is essentially of a formal nature. No self-consistent solutions (i.e., a rigorous simultaneous determination of $i\Gamma_k$ and the spectrum) are presented; they remain a challenging task for the future.

VIII. Renormalized Perturbation Theory

Diagrammatic techniques are used for the development of the renormalized perturbation theory. We believe that these techniques are particularly suitable for proving renormalizability and demonstrating energy conservation to arbitrary high orders. Out of this analysis an unambiguous definition of “order” automatically emerges. Details about the rules guiding diagrammatic manipulation are given in **Appendix B**.

In VIII.1 the perturbation procedure is described primarily for a stationary homogeneous plasma without magnetic field. However, it is straightforward to generalize the formalism to an inhomogeneous magnetized plasma to deal with the cases for which the turbulence scale length is much shorter than the macroscopic scale lengths.

VIII.1 Perturbation Procedure

For simplicity we study the Vlasov equation without external magnetic and electric fields.

$$\left[\partial_t + \mathbf{v} \cdot \nabla + (q/m) \mathbf{E} \cdot \partial \right] f(\mathbf{r}, \mathbf{v}; t) = 0. \quad (8.1.1)$$

Ensemble averaging on Eq.(8.1.1) yields

$$(\partial_t + \mathbf{v} \cdot \nabla) f_0 + (q/m) \langle \mathbf{E} \cdot \partial f' \rangle = 0, \quad (8.1.2)$$

where $f_0 \equiv \langle f \rangle$, $f' \equiv f - f_0$, $\langle \dots \rangle$ means the ensemble average.

The equation for the fluctuating distribution function is

$$(\partial_t + \mathbf{v} \cdot \nabla)f' = -(q/m)\mathbf{E} \cdot \partial f_0 - (q/m)(\mathbf{E} \cdot \partial f')', \quad (8.1.3)$$

where

$$(\mathbf{E} \cdot \partial f')' \equiv (\mathbf{E} \cdot \partial f') - \langle \mathbf{E} \cdot \partial f' \rangle$$

is the fluctuating part of $(\mathbf{E} \cdot \partial f')$.

Taking the Fourier transformation of Eq.(8.1.3) and substituting $\mathbf{E} = -\nabla\phi$ into Eq.(8.1.3), yields

$$(\omega - \mathbf{k} \cdot \mathbf{v})\delta f_k = -\frac{q}{m}(\mathbf{k} \cdot \partial)f_0\delta\phi_k + \frac{q}{m} \sum_{k_1 \neq k} (\mathbf{k}_1 \cdot \partial)\delta\phi_{k_1}\delta f_{k-k_1}, \quad (8.1.4)$$

where δf_k and $\delta\phi_k$ are fluctuating quantities. Using the notation

$$\hat{L}(k) \equiv -(q/m)(\mathbf{k} \cdot \partial),$$

Eq.(8.1.4) becomes

$$(\omega - \mathbf{k} \cdot \mathbf{v})\delta f_k = \hat{L}(k)f_0\delta\phi_k + \sum_{k_1 \neq k} \hat{L}(k_1)\delta f_{k-k_1}\delta\phi_{k_1}. \quad (8.1.5)$$

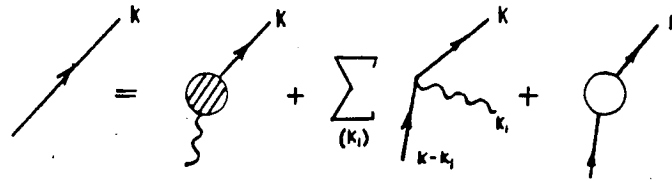
Adding $i\Gamma_k f_k$ on both sides of Eq.(8.1.5) (Γ_k is the frequency broadening operator) and defining

$$G_k \equiv (\omega - \mathbf{k} \cdot \mathbf{v} + i\Gamma_k)^{-1}, \quad (8.1.6)$$

we have

$$\delta f_k = G_k \hat{L}(k) f_0 \delta \phi_k + \sum_{k_1 \neq k} G_k \hat{L}(k_1) \delta f_{k-k_1} \delta \phi_{k_1} + G_k i\Gamma_k \delta f_k. \quad (8.1.7)$$

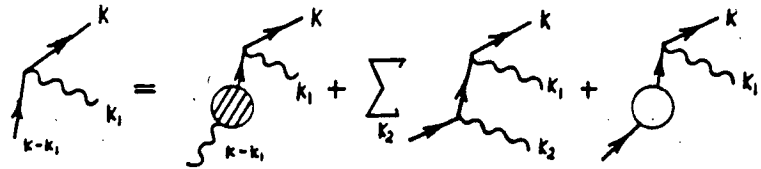
It can be drawn diagrammatically as



$$= \text{[diagram: line with } k \text{ and a shaded circle with a wavy line]} + \sum_{(k_1)} \text{[diagram: line with } k \text{ and a wavy line } k_1 \text{ and a line with } k-k_1] + \text{[diagram: line with } k \text{ and an open circle]} \quad (8.1.8)$$

The precise definitions of various terms, and further discussion of these diagrams are given in **Appendix B**.

The first term on the r.h.s. of Eq.(8.1.8) is the lowest order coherent term and the third term containing $i\Gamma_k$ on the r.h.s. of Eq.(8.1.8) is the frequency broadening term. We cease further iterating on these two terms. The iteration of the second term on the r.h.s. of Eq.(8.1.8) gives



$$= \text{[diagram: line with } k \text{ and a shaded circle with a wavy line } k_1] + \sum_{k_2} \text{[diagram: line with } k \text{ and a wavy line } k_1 \text{ and a line with } k-k_1 \text{ and a wavy line } k_2] + \text{[diagram: line with } k \text{ and an open circle with a wavy line } k_1] \quad (8.1.9)$$


For a given $\delta \phi_k (k \neq 0)$ which is characteristic of the coherent wave, the waves $\delta \phi_{k_1}$ and $\delta \phi_{k_2}$ in the first term on the r.h.s. of Eq.(8.1.9) must not be $\delta \phi_k$. We call this term the intrinsically incoherent term. The last term of Eq.(8.1.9) is the term containing $i\Gamma_k$ which is not iterated any further. The important step

at this point is to note that before we make a further iteration on the second term on the r.h.s. of Eq.(8.1.9) we need to separate the self-energy structure. The self-energy terms are just the objects that are needed to cancel the $i\Gamma_k$ terms.

Correlation expansion of $\delta\phi_{k_1}\delta\phi_{k_2}$ given in **Appendix C** constitutes the required separation:

$$\delta\phi_{k_1}\delta\phi_{k_2} = (\delta\phi_{k_1})(\delta\phi_{k_2}) + \langle\langle\delta\phi_{k_1}\delta\phi_{k_2}\rangle\rangle. \quad (8.1.10)$$

Notice that, by assumption, the nonzero contribution of the correlation function $\langle\langle\delta\phi_{k_1}\delta\phi_{k_2}\rangle\rangle$ stems only from the case $k_1 + k_2 = 0$. Hence, the correlation function can be represented by the closed wiggly lines diagrammatically. The separation of the second term on the r.h.s. of Eq.(8.1.10) is thus drawn as



$$(8.1.11)$$

The waves denoted by (k') (with parenthesis) are uncorrelated with each other, while the closed structure (the first term on the r.h.s. of Eq.(8.1.11)) represents the correlated part.

Eqs.(8.1.8),(8.1.9) and (8.1.11) form the renormalized perturbation theory to the second order (counting order by the number of wave - particle interaction vertices excluding the shaded bubble $\textcircled{\bullet}$) when we ask for the cancellation between $-i\Gamma_k$ and the self-energy structure,

$$\text{Diagram 1} + \text{Diagram 2} = 0 \quad (8.1.12)$$

This is more or less the same theory as given by Rudakov-Tsyтович⁹⁴ and Choi-Horton.⁹² A crucial point at this step is that we cannot ignore the contribution of the last term in Eq.(8.1.11) to this lowest order in the renormalized theory. This inclusion is the essential difference between the theory of Dupree-Tetrault⁹⁵ and previous theories. Since the last term of Eq.(8.1.11) implicitly contains contribution to the same order, the first term of Eq.(8.1.13) shown below is formally as important as the frequency broadening terms; its omission can lead to serious errors, e.g. in a related drift-wave problem it leads to a violation of energy conservation.

The next step goes along similar lines with only some additional observations.

The iterations of the last set of terms of Eq.(8.1.11) gives

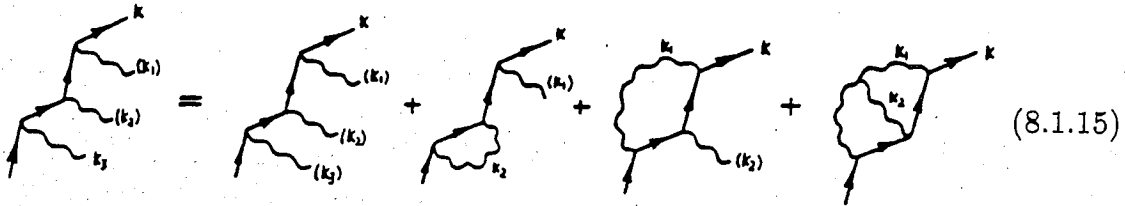
$$\text{Diagram 1} = \text{Diagram 2} + \text{Diagram 3} + \text{Diagram 4} \quad (8.1.13)$$

Both the first and the third terms on the r.h.s. of Eq.(8.1.13) cease iterating. Further decomposition is needed for the second term before iter-

ating it. This decomposition is the same as the correlation expansion for $(\delta\phi_{k_1})(\delta\phi_{k_2})\delta\phi_{k_3}$, [cf. Eq.(C.7)],

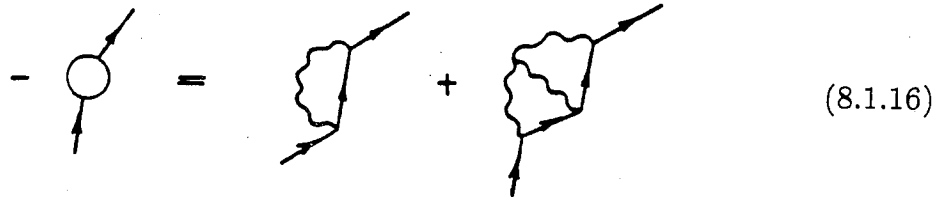
$$\begin{aligned} (\delta\phi_{k_1})(\delta\phi_{k_2})\delta\phi_{k_3} &= (\delta\phi_{k_1})(\delta\phi_{k_2})(\delta\phi_{k_3}) + \langle\langle\delta\phi_{k_1}\delta\phi_{k_3}\rangle\rangle(\delta\phi_{k_2}) \\ &\quad + \langle\langle\delta\phi_{k_2}\delta\phi_{k_3}\rangle\rangle(\delta\phi_{k_1}) + \langle\langle\delta\phi_{k_1}\delta\phi_{k_2}\delta\phi_{k_3}\rangle\rangle. \end{aligned} \quad (8.1.14)$$

The nonzero contribution from $\langle\langle\delta\phi_{k_1}\delta\phi_{k_2}\delta\phi_{k_3}\rangle\rangle$ exists only if $k_1+k_2+k_3=0$, as we had argued for $\langle\langle\delta\phi_{k_1}\delta\phi_{k_2}\rangle\rangle$. The decomposition corresponding to Eq.(8.1.14) is thus drawn as



$$(8.1.15)$$

We note that the second term on the r.h.s. of Eq.(8.1.15) cancels the last term on the r.h.s. of Eq.(8.1.9), if one uses the lowest order (second order) expression for the frequency broadening term. However, we must now add an additional term to the frequency broadening to third order, the frequency broadening term is given by



$$(8.1.16)$$

Continuing the iteration, we have

$$\begin{aligned}
 & \text{Diagram 1} = \text{Diagram 2} + \sum_{K_4} \text{Diagram 3} + \text{Diagram 4} \quad (8.1.17)
 \end{aligned}$$

[illegible]

The second term on the r.h.s. of Eq.(8.17) and (8.18) needs separating.

It yields

(8.1.19)

$$\text{Diagram 1} = \text{Diagram 2} + \text{Diagram 3} \quad (8.1.20)$$

The correction to the fourth order for the frequency broadening is thus determined by the eighth term on the r.h.s. of Eq.(8.1.19) and the last term of Eq.(8.1.20). The second term on the r.h.s. of Eq.(8.1.19) will cancel the last term of Eq.(8.1.13) to this order. To the appropriate order the fifth term on the r.h.s. of Eq.(8.1.19) is the necessary correction for the cancellation between the last term of Eq.(8.1.19) and the second term on the r.h.s. of Eq.(8.1.15).

Except those self-energy terms all other terms in Eqs.(8.1.19) and (8.1.20) should be iterated to produce the next order.

The general rules for the perturbative expansion are summarized as follows:

(a) The terms containing the shaded bubble, the self-energy terms and the frequency broadening terms (which contain a hollow bubble) will be kept without further manipulation except that a cancellation between the last two sorts of terms is required.

(b) A term, not belonging to the above mentioned categories, contains an external wiggly line without parenthesis, it needs separating according to the correlation expansion.

(c) After the separation those terms, which do not contain a self-energy structure, need iterating to produce the next order. We shall prove that there will be an exact cancellation between the terms containing self-energy structures and the terms containing frequency broadening. The final result for δf_k is illustrated diagrammatically (to the fifth order) in **Appendix D**.

Now we manipulate the perturbative expression of δf_k further since the wiggly line pertaining to the shaded bubble may be still correlated with other

open wiggly lines in the diagram.

It is easily seen that the first terms on the r.h.s. of Eqs.(8.1.8) and (8.1.9) retain their form. The first term on the r.h.s. of Eq.(8.1.13) becomes

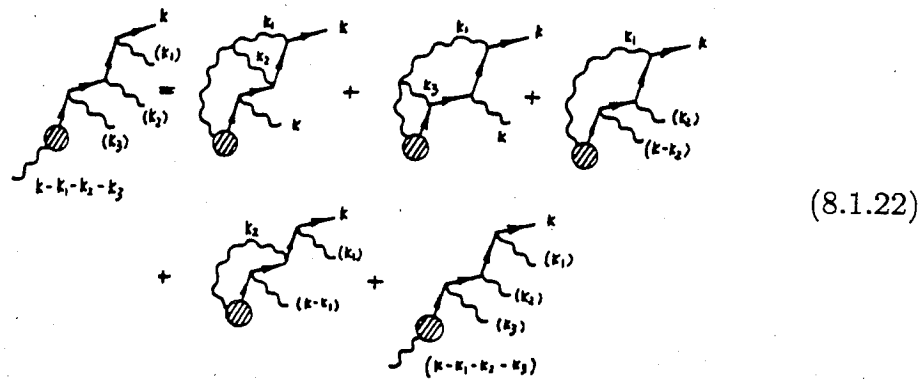
$$(8.1.21)$$

The diagram obtained by connecting the wiggly line of $\delta\phi_{k_2}$ with the wiggly line $\delta\phi_{k-k_1-k_2}$ in the last term of Eq.(8.1.21) is not present. It requires the propagator corresponding to solid line between $\delta\phi_{k_1}$ and $\delta\phi_{k_2}$ to have zero momentum, which cannot be produced in the iteration procedure. The first term on the r.h.s. of Eq.(8.1.21) is the coherent term to second order of the perturbation theory, because all parts of this term except $\delta\phi_k$ belong to the non-fluctuating effect. The last term of Eq.(8.1.21) is thus the intrinsically incoherent term to second order, i.e., any wiggly line in this term cannot be assigned a momentum k , for such an assignment will result in an excluded diagram. For example, if we assign a momentum k to the wiggly line under the shaded bubble, it will force $k_1 = -k_2$, which is an excluded choice for the last diagram in Eq.(8.1.21) owing to the separation of the self-energy term in Eq.(8.1.11). Thus, we conclude that in a diagram in which all the wiggly lines are uncorrelated, none of them can have a momentum k .

For a consistent renormalized lowest order (second) theory, all of the second order terms must be retained. As can be easily seen, the first term on

the r.h.s. of Eq.(8.1.21) is a second order term, and is just the β -term proposed by Dupree and Terault⁹⁵ to maintain energy conservation in the drift-wave problem.

In third order, (after the renormalization cancellation in Eq.(8.1.17)) the following terms contribute to δf_k .



(8.1.22)

The first two terms on the r.h.s. of Eq.(8.1.22) are coherent terms, while the last three terms on the r.h.s. of Eq.(8.1.22) are intrinsically incoherent terms.

The first term for δf_k in Eq.(8.1.18) is an intrinsically incoherent term, since the setting of $k_1 - k_2 = k$ or $k_2 = k$ gives zero contribution to this diagram.

Whithin the framework of the preceding discussion, it is convenient to devide fluctuating function into a coherent, and an intrinsicslly incoherent part:

$$\delta f_k = \delta f_k^{(c)} + \delta \tilde{f}_k, \quad (8.1.23)$$

where $\delta f_k^{(c)}$ represents all the coherent terms, and $\delta \tilde{f}_k$ represents all the incoherent terms. To third order of perturbation they are expressed diagrammatically as:

$$\delta f_k^{(c)} = \text{diagram 1} + \text{diagram 2} + \text{diagram 3} + \text{diagram 4} + \dots \quad (8.1.24)$$

$$\delta \tilde{f}_k = \text{diagram 1} + \text{diagram 2} + \text{diagram 3} + \text{diagram 4} + \dots \quad (8.1.25)$$

A perturbative expressions for δf_k up to fifth order, and other general rules for diagram constructions are given in **Appendix E**.

VIII.2 Renormalizability

The statement in VIII.1 implies that all terms containing self-energy structure cancel with all the terms containing frequency broadening so that none of these terms explicitly appear in the final expression of δf_k . By virtue of this cancellation, we will show that $i\Gamma_k$ is determined as the sum of all possible irreducible self-energy structures taken once and only once. We note that the definition of renormalizability means that $i\Gamma_k$ can be expressed as the sum of all self-energy terms, and that all diagrams, containing self-energy and frequency

broadening sub-structure, will cancel each other.

We first discuss in detail several properties that manifest themselves as results of our iteration procedures.

Observation I. In a given order all possible self-energy structure must appear except those (and never those) that contain self-energy sub-structures. (Henceforth, the allowable self-energy structure will be called a completely overlapping diagram in which no self-energy sub-structure can be isolated.)

Proof. According to the iteration rule indicated in VIII.1, when a simple self-energy diagram once appears, further iteration of the diagram ceases. This means that any term in higher order does not contain the self-energy structure of lower order. In other words the allowable self-energy structure can only be formed by connecting the lowest wiggly line (we refer it as the active line) with the upper lines (we refer to them as the passive lines). Because no self-energy structure can appear above the active line, the connection can only produce the completely overlapping diagram.

In order to show that all types of completely overlapping patterns are possible, we need only note that all types of vertex structures are possible in the terms of lower order since the operation $k_i \rightarrow (k_i)$ makes each active line connect with every possible combination of passive lines. Therefore, all types of self-energy structure should be taken into account except those containing the lower order self-energy structure as a sub-diagram.

According to Observation I the following diagrams are examples of struc-

tures that should be excluded from the proper self-energy diagrams :



Fig.28

Observation II. A given diagram can only appear once. There is no repeated diagram.

Proof. All terms appearing in the theory can be produced in two ways only. One is the iteration, the other is the separation (i.e., the operation $k_i \rightarrow (k_i)$). The iteration obviously cannot produce a repeated diagram. In the operation $k_i \rightarrow (k_i)$, only the lower wiggly line is active (the word “ active ” meaning that the lower line can correlate with any other passive lines). In contrast, the passive lines, for which the momenta have been denoted by (k_i) cannot be correlated with any but the active wiggly line . Hence, new diagrams can only be formed from the active part, i.e., by connecting only to the lowest line. This kind of diagram certainly does not appear in the previous order.

Observation III. For non-self-energy diagrams containing self-energy substructure all types of self-energy structure produced in the lower perturbative order are reproduced totally in the higher perturbative order.

Proof. All diagrams containing self-energy structures form a subset of diagrams produced by the operation $k_i \rightarrow (k_i)$ on the lowest wiggly line. Clearly all $(n+1)$ th order diagrams contain the n th order diagrams in their entirety. As

a result all the self-energy structures in the lower order diagram are faithfully reproduced in the higher order diagrams.

Observation IV. In the higher order diagrams there exists no new type of self-energy sub-structures with the same number of contracted vertices (order of the sub-structure) as the self-energy structures that appeared in a lower order diagram.

Proof. According to the Observation I, the completely overlapping structures exhaust (to a given order) the set of allowed diagrams, so no new type of sub-structure which has the same order as a sub-structure in the lower order diagram can appear in higher orders.

With the help of these four observations, it is now straightforward to prove the renormalizability of the theory, and to obtain the general form of the renormalized propagator to any specified order.

Observation I suggests that $-i\Gamma_k$ be the sum of all types of possible self-energy structures. The combination of Observation II, III and IV would then imply that there will be a complete cancellation diagrams that have any structure plus $i\Gamma_k$ with the diagrams with that very structure plus all self-energy structures. Thus a unique expression for $i\Gamma_k$ results, and the expression for δf_k will contain no terms including $i\Gamma_k$ or self-energy structures.

The explicit diagrammatical expression $i\Gamma_k$ to the sixth order is given as follows; the iterative order of each diagram is readily recognized by counting the number of vertices.

$$\begin{aligned}
 -i\Gamma_k = & \text{Diagram 1} + \text{Diagram 2} + \text{Diagram 3} + \text{Diagram 4} \\
 & + \text{Diagram 5} + \text{Diagram 6} + \text{Diagram 7} + \text{Diagram 8} \\
 & + \text{Diagram 9} + \text{Diagram 10} + \text{Diagram 11} + \text{Diagram 12} \\
 & + \text{Diagram 13} + \text{Diagram 14} + \text{Diagram 15} + \text{Diagram 16} \\
 & + \text{Diagram 17} + \text{Diagram 18} + \text{Diagram 19} + \text{Diagram 20} \\
 & + \text{Diagram 21} + \text{Diagram 22} + \text{Diagram 23} + \text{Diagram 24} \\
 & + \text{Diagram 25} + \text{Diagram 26} + \dots
 \end{aligned}$$

(8.2.1)

VIII.3 Renormalized Dielectric Function. Weak Turbulence Limit

We now use the methodology developed in VIII.1 to calculate the renormalized dielectric function for the Vlasov-Poisson system. We use the standard statistical physics definition of the inverse dielectric function (ϵ_k^{-1}) pertaining to the electrostatic waves. Defined through the Poisson equation,¹⁰⁶ ϵ_k^{-1} is given as the functional derivative

$$\epsilon_k^{-1} = \frac{k^2}{4\pi} \cdot \frac{\delta \langle \phi_k(\phi^{(e)}) \rangle}{\delta \rho_k^{(e)}}, \quad (8.3.1)$$

where ϕ_k is the potential induced in the plasma in response to the disturbance $\phi^{(e)}$ generated by an infinitesimal external (unrandom) source $\rho^{(e)}$. Note that the bare source quantities $\phi_k^{(e)}$ and $\rho_k^{(e)}$ are related through

$$\phi_k^{(e)} = \frac{4\pi}{k^2} \rho_k^{(e)}, \quad (8.3.2)$$

and the potential ϕ_k is determined by the Poisson equation

$$\phi_k = \phi_k^{(e)} - \frac{4\pi q}{k^2} \int d\mathbf{v} f_k(\phi^{(e)}) \equiv \phi_k^{(e)} + \Phi_k f_k(\phi^{(e)}), \quad (8.3.3)$$

where f is the plasma distribution function which obeys the Vlasov equation

$$[\partial_t + \mathbf{v} \cdot \nabla - (q/m) \nabla \phi(\phi^{(e)}) \cdot \partial] f(\phi^{(e)}) = 0. \quad (8.3.4)$$

Making use of Eqs.(8.3.2) and (8.3.3), Eq.(8.3.1) takes the form

$$\epsilon_k^{-1} = 1 + \Phi_k \left\langle \frac{\delta f_k(\phi^{(e)})}{\delta \phi_k^{(e)}} \right\rangle_{\phi^{(e)}=0}. \quad (8.3.5)$$

Thus to calculate ϵ_k^{-1} , we must solve f_k in terms of $\phi_k^{(e)}$, and obtain the required functional derivative. The problem is, in fact, not forbiddingly difficult, since we need to calculate the response only linearly in the infinitesimal source $\phi^{(e)}$. Before manipulating the Vlasov equation, we notice from Eq.(8.3.3) that the variation in the induced potential due to an infinitesimal source $\phi^{(e)}$ is

$$\delta\phi_k = \phi_k(\phi^{(e)}) - \phi_k(0) = \left[\delta_{k,k'} + \Phi_k \frac{\delta f_k(\phi^{(e)})}{\delta\phi_{k'}^{(e)}} \right] \phi_{k'}^{(e)}, \quad (8.3.6)$$

where

$$\phi_k(0) = \Phi_k f_k(\phi^{(e)})|_{\phi^{(e)}=0},$$

and $\delta\phi_k$ is linear in $\phi_{k'}^{(e)}$.

With the definitions $\langle f(\phi^{(e)} = 0) \rangle = f_0$, and $f(\phi^{(e)}) = f_0 + \delta f(\phi^{(e)})$, the Fourier transformed Vlasov equation becomes

$$\begin{aligned} \delta f_k(\phi^{(e)}) = & \text{diagram with wavy line} = \text{diagram with wavy and dashed lines} + \text{diagram with dashed and wavy lines} + \sum_{(k_i)} \text{diagram with wavy and dashed lines} \\ & + \sum_{(k_i)} \text{diagram with dashed and wavy lines} + \text{diagram with dashed line and circle} \end{aligned} \quad (8.3.7)$$

where the wiggly lines represent $\phi_k(0)$, the dashed lines represent $\delta\phi_k$. The iteration procedure for $f_k(\delta\phi^{(e)})$ should be modified to include the dashed lines. Since the external source $\delta\phi^{(e)}$ makes sense only in its linear form, all diagrams containing more than one dashed line are automatically dropped; their contribution to the dielectric ϵ_k^{-1} is zero. The manipulation of the stochastic field ϕ is

done exactly in the manner described earlier. Clearly, in the relevant diagrams, the dashed line will always be an external line. This realization allows us to write

$$f_k(\delta\phi^{(e)}) = f_k(0) + f_k|_{\text{open}\phi_k \rightarrow \delta\phi_k}, \quad (8.3.8)$$

where the first term, $f_k(0)$, is just the solution obtained in VIII.1 (i.e., without the external source), while the last term of Eq.(8.3.8) stands for terms that have the same structure as $f_k(0)$, with each open wiggly line replaced once and only once by a dashed line. Using Eqs.(8.1.23) and (8.3.8), we obtain

$$(1 - \Phi_k A_k) \Phi_k \frac{\delta f_k}{\delta \phi_k^{(e)}} = \Phi_k A_k \delta_{k,k'} + \Phi_k \bar{f}_k|_{\text{open}\phi_{k_i} \rightarrow \delta_{k_i,k'} + \Phi_{k_i} \frac{\delta f_{k_i}}{\delta \phi_{k_i}^{(c)}}}, \quad (8.3.9)$$

where we have defined (the superscript (c) means coherent)

$$A_k \equiv \frac{\delta f_k^{(c)}}{\delta \phi_k},$$

and the last term of Eq.(8.3.9) stands for terms that have the same structure as $\delta \bar{f}_k$ [the incoherent terms without the external source as shown in Eq.(8.1.25)], with each open wiggly line $\delta\phi_{k_i}$ replaced once and only once by $\delta_{k_i,k'} + \Phi_{k_i} \frac{\delta f_{k_i}}{\delta \phi_{k_i}^{(c)}}$.

The formal expression for the inverse dielectric function ϵ_k^{-1} is thus found to be

$$\begin{aligned} \epsilon_k^{-1} &= 1 + \Phi_k \left\langle \frac{\delta f_k}{\delta \phi_k^{(e)}} \right\rangle_{\phi^{(e)}=0} \\ &= \langle Q_{k,k}^{-1} \rangle \Phi_k A_k + \sum_{k_i} \left\langle Q_{k,k_i}^{-1} \Phi_{k_i} \bar{f}_{k_i} |_{\phi_{k_j} \rightarrow \delta_{k_j,k}} \right\rangle, \end{aligned} \quad (8.3.10)$$

where Q_{k_i,k_j}^{-1} is the inverse matrix of Q_{k_i,k_j} with

$$Q_{k_i,k_j} \equiv (1 - \Phi_{k_i} A_{k_i}) \delta_{k_i,k_j} - P_{k_i,k_j}, \quad (8.3.11)$$

and P_{k_i, k_j} is defined by

$$\sum_{k_j} P_{k_i, k_j} \Phi_{k_j} \frac{\delta f_{k_j}}{\delta \phi_{k'}^{(e)}} \equiv \Phi_{k_i} \tilde{f}_{k_i} \Big|_{\phi_j \rightarrow \Phi_{k_j} \frac{\delta f_{k_j}}{\delta \phi_{k'}^{(e)}}} \quad (8.3.12)$$

To second order, P_{k_i, k_j} is shown below

$$P_{k_i, k_j} = \Phi_{k_i} \left\{ \begin{array}{l} \text{Diagram 1: } \text{Shaded circle with } k_i \text{ (solid), } k_j \text{ (solid), } k_i - k_j \text{ (dotted)} \\ \text{Diagram 2: } \text{Shaded circle with } k_i \text{ (solid), } k_i - k_j \text{ (dotted), } k_j \text{ (solid)} \\ \text{Diagram 3: } \text{Shaded circle with } k \text{ (solid), } k_j \text{ (dotted), } k_i \text{ (solid), } k_i - k_j \text{ (solid)} \\ \text{Diagram 4: } \text{Shaded circle with } k_i \text{ (solid), } k_i \text{ (solid), } k_j \text{ (dotted), } k_i - k_j \text{ (solid)} \\ \text{Diagram 5: } \text{Shaded circle with } k_i \text{ (solid), } k_i - k_j \text{ (solid), } k_j \text{ (dotted)} \end{array} \right\} \quad (8.3.13)$$

By following our general perturbative technique, we now calculate an expression for the renormalized dielectric function ϵ_k correct to second order.

Setting $k' = k$ in Eq.(8.3.9), we have (to second order)

$$\Phi_k \frac{\delta f_k}{\delta \phi_k^{(e)}} = (\epsilon_k^{(c)-1} - 1) + \epsilon_k^{(c)-1} \Phi_k \left\{ \begin{array}{l} \text{Diagram 1: } \text{Shaded circle with } k \text{ (solid), } k_i \text{ (solid), } k - k_i \text{ (dotted)} \\ \text{Diagram 2: } \text{Shaded circle with } k \text{ (solid), } k_i \text{ (solid), } k - k_i \text{ (dotted)} \end{array} \right\} \Phi_{k-k_i} \frac{\delta f_{k-k_i}}{\delta \phi_k^{(e)}} + \begin{array}{l} \text{Diagram 3: } \text{Shaded circle with } k \text{ (solid), } k_i \text{ (solid), } k - k_i \text{ (dotted)} \\ \text{Diagram 4: } \text{Shaded circle with } k \text{ (solid), } k_i \text{ (solid), } k - k_i \text{ (dotted)} \end{array} \Phi_{k_1} \frac{\delta f_{k_1}}{\delta \phi_k^{(e)}} \Bigg\}, \quad (8.3.14)$$

where

$$\epsilon_k^{(c)} \equiv 1 - \Phi_k A_k \longrightarrow 1 - \Phi_k \left\{ \begin{array}{c} \text{diagram 1} \\ + \text{diagram 2} \end{array} \right\}$$

$$= 1 + \frac{4\pi q}{k^2} \int d\nu G_k \left[\hat{L}(k) + \sum_{k_1} \hat{L}(k_1) G_{k-k_1} \hat{L}(k) G_{-k_1} \hat{L}(-k_1) I_{k_1} \right] f_0, \quad (8.3.15)$$

with $I_{k_1} \equiv \langle \phi_{k_1} \phi_{k_1}^* \rangle$.

Those terms like

$$\epsilon_k^{(c)-1} \Phi_k \begin{array}{c} \text{diagram} \\ \text{with } k-k_1-k_2 \end{array} \Phi_{k-k_1-k_2} \frac{\delta f_{k-k_1-k_2}}{\delta \phi_k^{(e)}}$$

do not contribute to the second order because ϕ_{k_1} and ϕ_{k_2} are uncorrelated. An iteration of the $\delta f_{k_1}/\delta \phi_k^{(e)}$, and $\delta f_{k-k_1}/\delta \phi_k^{(e)}$ [Eq.(8.3.14)] to the second order gives

$$\Phi_{k_1} \frac{\delta f_{k_1}}{\delta \phi_k^{(e)}} = \epsilon_{k_1}^{(c)-1} \Phi_{k_1} \left\{ \begin{array}{c} \text{Diagram: A shaded circle with an incoming dashed line from the bottom left labeled } k, \text{ an outgoing solid line to the top right labeled } k_1, \text{ and an outgoing wavy line to the right labeled } k_1 - k. \end{array} \right. \epsilon_k^{(c)-1} \quad (8.3.16)$$

$$+ \left\{ \begin{array}{c} \text{Diagram: A shaded circle with an incoming dashed line from the bottom left labeled } k, \text{ an outgoing solid line to the top right labeled } k_1, \text{ and an incoming wavy line from the bottom left labeled } k_1 - k. \end{array} \right. \epsilon_k^{(c)-1} \Bigg\}$$

$$\Phi_{k-k_1} \frac{\delta f_{k-k_1}}{\delta \phi_k^{(e)}} = \epsilon_{k-k_1}^{(c)-1} \Phi_{k-k_1} \left\{ \begin{array}{c} \text{Diagram: A shaded circle with an incoming dashed line from the bottom left labeled } k, \text{ an outgoing solid line to the top right labeled } k-k_1, \text{ and an outgoing wavy line to the right labeled } -k_1. \end{array} \right. \epsilon_k^{(c)-1} \quad (8.3.17)$$

$$+ \left\{ \begin{array}{c} \text{Diagram: A shaded circle with an incoming dashed line from the bottom left labeled } k, \text{ an outgoing solid line to the top right labeled } k-k_1, \text{ and an incoming wavy line from the bottom left labeled } -k_1. \end{array} \right. \epsilon_k^{(c)-1} \Bigg\}.$$

Then we obtain

$$\epsilon_k^{-1} = 1 + \Phi_k \left\langle \frac{\delta f_k}{\delta \phi_k^{(e)}} \right\rangle_{\phi^{(e)}=0} \quad (8.3.18)$$

$$= \epsilon_k^{(c)-1} + 4 \epsilon_k^{(c)-1} \tilde{\epsilon}_{k_1, k-k_1}^{(2)} \epsilon_{k-k_1}^{(c)-1} \tilde{\epsilon}_{-k_1, k}^{(2)} \epsilon_k^{(c)-1} I_{k_1},$$

where

$$\bar{\epsilon}_{k_1, k_2}^{(2)} \equiv \frac{1}{2} \Phi_{k_1 + k_2} \left[\begin{array}{c} \text{diagram 1} + \text{diagram 2} \end{array} \right]$$

$$= \frac{-2\pi q}{|\mathbf{k}_1 + \mathbf{k}_2|^2} \int d\nu G_{k_1 + k_2} [\hat{L}(k_1) G_{k_2} \hat{L}(k_2) + \hat{L}(k_2) G_{k_1} \hat{L}(k_1)] f_0. \quad (8.3.19)$$

Substituting Eq.(8.3.15) into Eq.(8.3.18), we obtain the renormalized dielectric function to second order

$$\epsilon_k = \epsilon_k^{(c)} - 4 \sum_{k_1} \bar{\epsilon}_{k_1, k-k_1}^{(2)} \epsilon_{k-k_1}^{(0)} {}^{-1} \bar{\epsilon}_{k, k-k_1}^{(2)} I_{k_1}, \quad (8.3.20)$$

with

$$\epsilon_k^{(0)} \equiv 1 - \Phi_k \left[\begin{array}{c} \text{diagram} \end{array} \right] = 1 - \Phi_k G_k \hat{L}(k) f_0. \quad (8.3.21)$$

In the limit of weak turbulence, the renormalized propagator must be expanded to second order yielding

$$\begin{aligned}
\epsilon_k^{(c)} \longrightarrow \epsilon_{k(\text{weak})} &= 1 - \Phi_k \left[\begin{array}{c} \text{diagram: a shaded circle with an incoming dashed line from below labeled } k \text{ and an outgoing solid line to the top right labeled } k \end{array} \right] \\
&- \Phi_k \left\{ \begin{array}{c} \text{diagram 1: a shaded circle with an incoming dashed line from below, a wavy line to the right labeled } k_1, \text{ and an outgoing solid line to the top right labeled } k \\ \text{diagram 2: a shaded circle with an incoming dashed line from below, a wavy line to the right labeled } k_1, \text{ and an outgoing dashed line to the right labeled } k \end{array} \right\} \quad (8.3.22)
\end{aligned}$$

$$= \epsilon_k^{(l)} + 2 \sum_{k_1} \epsilon_{k_1, -k_1, k}^{(3)} J_{k_1}$$

with

$$\epsilon_{k_1, k_2, k_3}^{(3)} \equiv -\frac{1}{2} \Phi_k \left\{ \begin{array}{c} \text{diagram: a shaded circle with an incoming dashed line from below labeled } k_2, \text{ a wavy line to the right labeled } k_1, \text{ and an outgoing solid line to the top right labeled } k \end{array} \right\}$$

$$= \frac{2\pi q}{|\mathbf{k}_1 + \mathbf{k}_2 + \mathbf{k}_3|^2} \int d\mathbf{v} G_{\mathbf{k}_1 + \mathbf{k}_2 + \mathbf{k}_3}^{(0)} \hat{L}(k_1) G_{\mathbf{k}_2 + \mathbf{k}_3}^{(0)}$$

$$\left[\hat{L}(k_2) G_{k_3}^{(0)} \hat{L}(k_3) + \hat{L}(k_3) G_{k_2}^{(0)} \hat{L}(k_2) \right] f_0,$$

(8.3.23)

where $G_k^{(0)}$ is the bare propagator. Finally, Eq.(8.3.20) becomes

$$\epsilon_{k(\text{weak})} = \epsilon_k^{(l)} + 2 \sum_{k_1} \epsilon_{k_1, -k_1, k}^{(3)} I_{k_1} - 4 \sum_{k_1} \frac{\epsilon_{k_1, k-k_1}^{(2)} \epsilon_{k, k_1}^{(2)}}{\epsilon_{k-k_1}^{(l)}} I_{k_1}, \quad (8.3.24)$$

where $\epsilon_{k_1, k_2}^{(2)}$ and $\epsilon_k^{(l)}$ are just $\bar{\epsilon}_{k_1, k_2}^{(2)}$ and $\epsilon_k^{(0)}$, respectively, with G_k replaced by $G_k^{(0)}$.

Equation (8.3.24) with Eq.(8.3.22) is just the dielectric function (in the weak turbulence limit) obtained by Krommes and Kleva using DIA.¹¹⁷ Thus the perturbation theory developed in VIII.1 has the correct weak turbulence limit for the dielectric function.

VIII.4 Spectrum Equation. Correlation Broadening

Since the concept of " order " is clearly delineated in our perturbation theory, it is obvious that the contribution of the lowest order incoherent source term (to the equation describing the fluctuation spectrum) should be more important than the higher order corrections due to the renormalization of the propagator. When the phase-space available for the three wave interaction becomes significant, the incoherent source is expected to play a crucial role in the determination of the saturated level of the turbulence. For electrostatic turbulence (Vlasov-Poisson system), a closed set of spectrum equations can be constructed from the renormalized perturbation theory, provided $e\phi/T$ [the ratio of the potential to the kinetic energy] is small enough to be a perturbation parameter.

From the formalism presented in Sec. II, it is straightforward to derive the nonlinear Poisson equation (to second order),

$$\epsilon_k^{(c)} \delta\phi_k = \sum_{k_1+k_2=k} \tilde{\epsilon}_{k_1,k_2}^{(2)} \delta\phi_{k_1} \delta\phi_{k_2} + \sum_{k_1+k_2+k_3=k} \tilde{\epsilon}_{k_1,k_2,k_3}^{(3)} \delta\phi_{k_1} \delta\phi_{k_2} \delta\phi_{k_3}, \quad (8.4.1)$$

where the coherent dielectric function $\epsilon_k^{(c)}$ is given by Eq.(8.3.15), $\tilde{\epsilon}_{k_1,k_2}^{(2)}$ is given by Eq.(8.3.19), and

$$\tilde{\epsilon}_{k_1,k_2,k_3}^{(3)} \equiv -\frac{4\pi q}{|\mathbf{k}_1 + \mathbf{k}_2 + \mathbf{k}_3|^2} \int d\nu G_{k_1+k_2+k_3} \hat{L}(k_1) G_{k_2+k_3} \hat{L}(k_2) G_{k_3} \hat{L}(k_3) f_0. \quad (8.4.2)$$

Multiplying both sides of Eq.(8.4.2) by $\delta\phi_k^*$ and ensemble averaging yields
[$I_k = \langle \delta\phi_k \delta\phi_k^* \rangle$]

$$\epsilon_k^{(c)} I_k = \sum_{k_1+k_2=k} \tilde{\epsilon}_{k_1,k_2}^{(2)} \langle \delta\phi_{k_1} \delta\phi_{k_2} \delta\phi_k^* \rangle + \sum_{k_1+k_2+k_3=k} \tilde{\epsilon}_{k_1,k_2,k_3}^{(3)} \langle \delta\phi_{k_1} \delta\phi_{k_2} \delta\phi_{k_3} \delta\phi_k^* \rangle. \quad (8.4.3)$$

Notice that the last term of Eq.(8.4.3) does not contribute to the lowest order (quadratic in I_k). When the triplet is evaluated by the quasi-Gaussian process

$$\langle \delta\phi_{k_1} \delta\phi_{k_2} \delta\phi_k^* \rangle = 2 \frac{\tilde{\epsilon}_{k_1,k_2}^{(2)*}}{\epsilon_k^{(c)*}} I_{k_1} I_{k_2} + 2 \frac{\tilde{\epsilon}_{-k_1,k}^{(2)}}{\epsilon_{k_2}^{(c)}} I_{k_1} I_k + 2 \frac{\tilde{\epsilon}_{-k_2,k}^{(2)}}{\epsilon_{k_1}^{(c)}} I_{k_2} I_k, \quad (8.4.4)$$

converting Eq.(8.4.3) to

$$\left[\epsilon_k^{(c)} - 4 \sum_{k_1} \frac{\tilde{\epsilon}_{k_1,k-k_1}^{(2)} \epsilon_{-k_1,k}^{(2)}}{\epsilon_{k-k_1}^{(c)}} I_{k_1} \right] I_k = 2 \sum_{k_1+k_2=k} \frac{|\tilde{\epsilon}_{k_1,k_2}^{(2)}|^2}{\epsilon_k^{(c)*}} I_{k_1} I_{k_2}, \quad (8.4.5)$$

which alongwith the other independent equation (correct to second order)

$$-i\Gamma_k = G_k^{(0)-1} - G_k^{-1} = \sum_{k_1} \hat{L}(k_1) G_{k-k_1} \hat{L}(-k_1) I_{k_1}, \quad (8.4.6)$$

where $G_k^{(0)-1} = G_k^{-1} - i\Gamma_k$ is the inverse bare propagator, provides a closed set of equation for I_k and G_k (all $\bar{\epsilon}_k$'s are functionals of G_k). Eqs. (8.4.5) and (8.4.6) are quite similar to the equations proposed by Biskamp¹¹⁸ (using diagrammatical technique), and by Orzag and Kraichnan.¹⁰³

If the turbulent level is so small that the renormalized propagator G_k^{-1} can be replaced by the bare propagator $G_k^{(0)-1}$ [making Eq.(8.4.6) trivial], Eq.(8.4.5) with $\epsilon_k^{(c)}$ given by Eq.(8.3.22) reduces to the standard spectrum equation in weak turbulence theory [cf.Appendix of Ref.116]. In a sense the set of Eqs.(8.4.5),(8.4.6) is the renormalized version of the weak turbulence theory, in which the resonance broadening (and shift), the three wave interaction and the nonlinear scattering are all included in a consistent way.

For small, but finite I_k Eq.(8.4.6) is approximated by the single renormalization

$$G_k^{-1} \sim G_k^{(0)-1} - \sum_{k_1} \hat{L}(k_1) G_{k-k_1}^{(0)} \hat{L}(-k_1) I_{k_1}. \quad (8.4.7)$$

Substituting Eq.(8.4.7) into Eq.(8.4.5) yields a spectrum equation for I_k only. The back-reaction of particle on waves still exists through the spectrum equation.

By doing explicit calculation to second order (for the construction of the spectrum equation as well as the calculation of the dielectric function), we have demonstrated that our perturbation approach is, indeed, naturally reducible to

the weak turbulence theory in the appropriate limit; this constitutes a definite advantage over the conventional perturbation approaches⁹⁰⁻⁹⁸ which do not.

Generally, the spectrum equation [Eq.(8.4.5)], a highly nonlinear integral equation, is very difficult to solve. Nonetheless, much useful information can be gleaned by simple arguments. As an example, the correlation broadening of the frequency spectrum will be briefly discussed.¹¹¹

Since I_k is positive, we may neglect the second term on the l.h.s. of Eq.(8.4.5) as a first approximation to estimate the correlation broadening, i.e.

$$I_k = \frac{\sum_{k_1+k_2=k} |\tilde{\epsilon}_{k_1,k_2}^{(2)}|^2 I_{k_1} I_{k_2}}{|\epsilon_k^{(c)}|^2}. \quad (8.4.8)$$

In the weak turbulence limit, the r.h.s. of Eq.(8.4.8) becomes

$$I_k = \frac{\int dk_1 dk_2 |\epsilon_{k_1,k_2}^{(2)}|^2 \delta(k - k_1 - k_2) I_{k_1} I_{k_2}}{|\epsilon_k^{(l)} + 2 \sum_{k_1} \epsilon_{k_1,-k_1,k}^{(3)} I_{k_1}|^2}, \quad (8.4.9)$$

where $\epsilon_k^{(l)}$ is the linear dielectric function [the first two terms on the r.h.s. of Eq.(8.3.22)], $\epsilon_{k_1,k_2}^{(2)}$ is defined by (8.3.19) with replacement of the renormalized propagator G_k by the bare one, $G_k^{(0)}$, and $\epsilon_{k_1,k_2,k_3}^{(3)}$ is defined by (8.3.23) and is essentially characteristic of the Compton scattering in the weak turbulence theory.

Expanding the denominator of Eq.(8.4.9) at the linear frequency ω_k^l yields

$$I_k = \frac{\alpha_k}{(\omega - \omega_k^N)^2 + (\gamma_k^N)^2}, \quad (8.4.10)$$

with

$$\omega_k^N \equiv \omega_k^l - \frac{2Re \sum_{k_1} \epsilon_{k_1, -k_1, k}^{(3)} I_{k_1}}{\left. \frac{\partial \epsilon_k^{(l)}}{\partial \omega} \right|_{\omega=\omega_k^l}}, \quad (8.4.11)$$

where the second term of the r.h.s. is the nonlinear frequency shift due to the Compton scattering, and

$$\gamma_k^N \equiv \gamma_k^{(l)} - \frac{2Im \sum_{k_1} \epsilon_{k_1, -k_1, k}^{(3)} I_{k_1}}{\left. \frac{\partial \epsilon_k^{(l)}}{\partial \omega} \right|_{\omega=\omega_k^l}}, \quad (8.4.12)$$

where the second term of the r.h.s is the nonlinear growth rate due to Compton scattering,

$$\alpha_k \equiv \frac{\int dk_1 dk_2 |\epsilon_{k_1, k_2}^{(2)}|^2 \delta(k - k_1 - k_2) I_{k_1} I_{k_2}}{\left(\left. \frac{\partial}{\partial \omega} Re \epsilon_k^{(l)} \right|_{\omega=\omega_k^{(l)}} \right)^2}. \quad (8.4.13)$$

Since α_k is a rather weak function of ω and \mathbf{k} , when $\omega \rightarrow \omega_k^N$, Eq.(8.4.10) implies that the correlation broadening in a turbulent plasma is approximated by the nonlinear growth rate γ_k^N in the above weak turbulence limit. For a plasma turbulence with the correlation broadening smaller than its linear growth rate, Eq.(8.4.12) indicates that the Compton scattering is more important for the nonlinear saturation of the linear instability than the three wave interaction. Otherwise, the three wave interaction plays a role either in the saturation mechanism or in the introduction of the correlation broadening.

The correlation broadening is significant for the relaxation of the strict linear conditions for three wave resonance. For the process involving the annihilation of two high-frequency waves to yield a rather low frequency wave,

the limitations on the three wave resonance condition disappear completely, when the low frequency is of the order of the correlation broadening of the high frequency waves.

IX. Energy Conservation in Electrostatic Drift Waves

It is well known that energy conservation is an essential test for the validity of a nonlinear wave-particle interaction theory. For the electrostatic drift waves the perturbed power term $\langle \delta \mathbf{j}_\perp \cdot \delta \mathbf{E}_\perp \rangle$ is rigorously equal to zero. This property should remain valid for any approximate theory with the implication that any plausible and acceptable perturbation theory must conserve energy in each order of perturbation.

We now show that the perturbation theory developed in VIII does meet the required demands of energy conservation. In particular, we prove the energy conservation in the perturbation order higher than the second to which most earlier analyses (including DIAC with diffusion approximation) were limited.^{95,96,105} For simplicity, we begin with the shearless slab model, then generalize the proof to a sheared slab model and to the ballooning representation.

The starting point here is the Fourier transformed drift kinetic equation [Vlasov equation for the guiding center in a uniformly magnetic plasma],

$$\delta f_k = G_k \hat{L}_0(k) f_0 \delta \phi_k + G_k \sum_{k_1} \hat{L}(k, k_1) \delta \phi_{k_1} \delta f_{k-k_1} + G_k i \Gamma_k \delta f_k, \quad (9.1)$$

where

$$\hat{L}_0(k) \equiv -(e/T_e)(k_\parallel v_\parallel - \omega_{en}^*)$$

$$\hat{L}(k, k_1) \equiv (e/m) k_{1,\parallel} \partial_\parallel - i(c/B)(\mathbf{k} \times \mathbf{k}_1) \cdot \mathbf{b} \equiv \hat{L}_1(k, k_1) + \hat{L}_2(k, k_1)$$

$$G_k \equiv (\omega - k_\parallel v_\parallel + i \Gamma_k)^{-1}, \quad \partial_\parallel \equiv \partial / \partial v_\parallel$$

with the ambient magnetic field $\mathbf{B} = B\mathbf{b}$, the electron diamagnetic drift frequency $\omega_{en}^* = (cT_e/eB)|d\ln n/dr|$ and $v_{\parallel} = \mathbf{v} \cdot \mathbf{b}$. The rate of work done by the drift current is expressed as

$$\langle \delta \mathbf{j}_{\perp} \cdot \delta \mathbf{E}_{\perp} \rangle = ie \int dv_{\parallel} dk G_k^{(0)-1} \langle \delta f_k \delta \phi_k^* \rangle, \quad (9.2)$$

where

$$G_k^{(0)-1} \equiv \omega - k_{\parallel} v_{\parallel}.$$

Notice that Eq.(9.1) is formally equivalent to Eq.(8.1.7).

Substituting $\delta f_k = A\delta\phi_k + \delta\tilde{f}_k$ and $G_k^{(0)-1} \equiv G_k^{-1} - i\Gamma_k$ into Eq.(9.2), we have

$$\begin{aligned} \langle \delta \mathbf{j}_{\perp} \cdot \delta \mathbf{E}_{\perp} \rangle = ie \int dv_{\parallel} dk \Big\{ & \langle \delta \phi_k^* G_k^{-1} A \delta \phi_k \rangle + \langle \delta \phi_k^* (-i\Gamma_k) A \delta \phi_k \rangle \\ & + \langle \delta \phi_k^* G_k^{-1} \delta \tilde{f}_k \rangle + \langle \delta \phi_k^* (-i\Gamma_k) \delta \tilde{f}_k \rangle \Big\}. \end{aligned} \quad (9.3)$$

All four terms on the r.h.s. of Eq.(9.3) can be expressed by connected diagrams. Energy conservation holds if we can show that sum of the four terms is zero in every order. For convenience, we first prove the following two useful lemmata.

Lemma I

In a given diagram if two wiggly lines k and k_1 , connected to the highest vertex, intersect at a multi-wave vertex, the contribution of this diagram to Eq.(9.3) vanishes [Fig.29].

Proof :

The part relevant to k and k_1 in the diagram can be written as

$$\hat{L}(k, k_1) P(k - k_1) \delta \phi_{k_1} \delta \phi_k^*,$$

where $P(k - k_1)$ is some functional of $k - k_1$. Notice that $\hat{L}(k, k_1)$ has two parts. For the highest vertex, the contribution from the part with the explicit velocity derivative, i.e., $\hat{L}_1(k, k_1) \equiv (e/m)k_{1,\parallel} \partial_{\parallel}$, becomes zero after integration over v_{\parallel} . The contribution from the second part also vanishes, because

$$\hat{L}_2(k, k_1) \equiv -i(c/B)(\mathbf{k} \times \mathbf{k}_1) \cdot \mathbf{b}$$

is odd under the transformation $(k \leftrightarrow -k_1)$ while the rest of the term are even.

Let us define that two diagrams are adjoint to each other, if they have the same highest vertex $\hat{L}(k, k_1)$ where the two wiggly lines k and k_1 meet, and if their remaining parts transform into each other through the operation $(k \leftrightarrow -k_1)$. An example is illustrated in Fig.30 [also cf. Figs.32, 33 and 34].

This leads us to the second lemma.

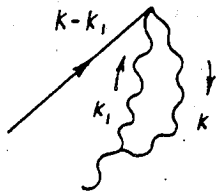
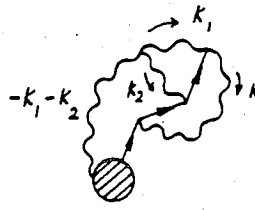
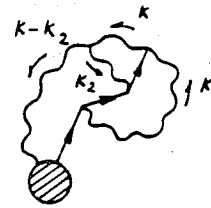


Fig.29



(a)



(b)

Fig.30

Lemma II

The sum of the contributions of two adjoint diagrams to the integral of Eq.(9.3) is zero.

Proof:

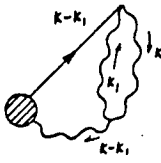
For the highest vertex the contribution from \hat{L}_1 is trivially zero, as each term individually integrated to zero. The sum of the contribution from $\hat{L}_2(k, k_1)$ terms vanishes because $\hat{L}_2(k, k_1)$ is odd under $(k \leftrightarrow -k_1)$.

IX.1 Explicit Illustration up to Fourth Order

We shall show the energy conservaton in the first few orders explicitly by using the above two lemmata.

To zero order only the linear term $\hat{L}_0 f_0$ from $\langle \delta\phi_k^* G_k^{-1} A \delta\phi_k \rangle$ contributes which changes sign under k - inversion and thus the summation over k yields zero.

To first order only the incoherent source $\langle \delta\phi_k^* G_k^{-1} \delta\tilde{f}_k \rangle$ contributes a term [Fig.31(a)]. It gives no contribution because of Lemma I.

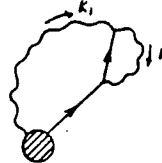


(a)

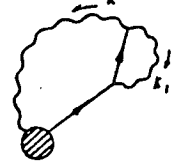


(b)

Fig.31



(a)



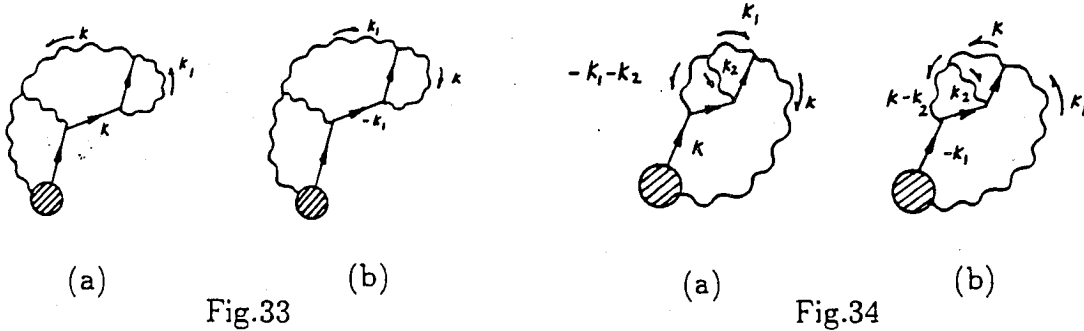
(b)

Fig.32

In the second order, we have three nontrivial terms making up the energy: the term from the incoherent term $\langle \delta\phi_k^* G_k^{-1} \delta\tilde{f}_k \rangle$ [Fig.31(b)], the term from $\langle \delta\phi_k^* G_k^{-1} A \delta\phi_k \rangle$ [Fig.32(a)], and the term from $\langle \delta\phi_k^* (i\Gamma_k) A \delta\phi_k \rangle$ [Fig.32(b)]. It is obvious that energy conservation is valid in this order because the contribution from the diagram of Fig.31(b) is zero by Lemma I and the sum of diagram of Fig.32(a) and Fig.32(b) is zero by Lemma II. Notice that violation of energy conservation would occur if we had kept only the term proportional to the resonance broadening $i\Gamma_k$ [$\langle \delta\phi_k^* G_k^{-1} A \delta\phi_k \rangle$] and neglected the second order contribution from the term $\langle \delta\phi_k^* G_k^{-1} A \delta\phi_k \rangle$ which represents the renormalized

average distribution function. This latter is just the β -term introduced by Dupree and Teraut to insure energy conservation to this order.

The energy conservation in second order is essentially a consequence of the cancellation of the two coherent contributions because the incoherent contribution was indentially zero due to Lemma I. Thus up to second order, a theory would pass the energy conservation test even if the incoherent part were neglected altogether. The situation changes entirely in the third and higher orders where incoherent terms are not individually (and hence trivially) equal to zero. Thus the proof of energy conservation in third (and higher) order becomes a crucial test to any progress beyond Dupree and Teraut. In third order, $\langle \delta\phi_k^* (-i\Gamma_k) \delta\tilde{f}_k \rangle$ gives a term [Fig.33(a)], cancelled by its adjoint [Fig.33(b)], contributed by $\langle \delta\phi_k^* G_k^{-1} A \delta\phi_k \rangle$, which also gives a term [Fig.30(a)] cancelling its own adjoint [Fig.30(b)], originating from $\langle \delta\phi_k^* G_k^{-1} \delta\tilde{f}_k \rangle$. The non-Gaussian frequency broadening term [Fig.34(a)] added to its adjoint coming from $\langle \delta\phi_k^* G_k^{-1} \delta\tilde{f}_k \rangle$ [Fig.34(b)], also gives zero contribution to the integral of Eq.(9.3); the conservation of energy in third order, thereby, is proved.



At this point we would like to stress that the energy conservation in third order resulted from exact cancellation between the non-Gaussian contribution

from the coherent part, and similar contributions from the intrinsically incoherent source. Clearly a theory like DIAC (without diffusive approximation) will violate energy conservation in this order because it neglects the incoherent part altogether. To the best of our knowledge, energy conservation has not yet been proved for DIAC.

The energy conservation to the fourth order is shown explicitly in **Appendix F**.

IX.2 General Proof to Arbitrary Higher Order

We organize the general proof by a sequence of definitions and lemmata. The proof will be completed with a summary at the end of the sequence.

Definition I Power Term:

The four terms that appear in the expression for the work done by the drift current in the r.h.s. of Eq.(9.3):

$$\langle \delta\phi_k^* G_k^{-1} A \delta\phi_k \rangle, \quad \langle \delta\phi_k^* (-i\Gamma_k) A \delta\phi_k \rangle, \quad \langle \delta\phi_k^* G_k^{-1} \delta\bar{\phi}_k \rangle, \quad \langle \delta\phi_k^* (-i\Gamma_k) \delta\bar{f}_k \rangle.$$

Each power term corresponds to a set of connected diagrams according to the diagrammatical rule in **Appendix B**.

Lemma III

The highest vertices in the diagram corresponding to the power terms are all the same.

Proof :

In the construction of diagrams we assumed that k is the momentum of the highest propagator. The other momentum pertaining to the highest vertex is k_1 . Hence, the expression of the highest vertex is $\hat{L}(k, k_1)$.

Definition II Derivative Primitive Frame Diagram:

A diagram that is derived from the primitive frame diagram [defined in Appendix E] by replacing the highest propagator G_k by $\delta\phi_k^*$ [Fig.35].

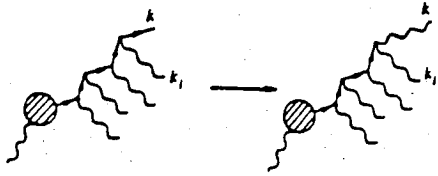


Fig.35

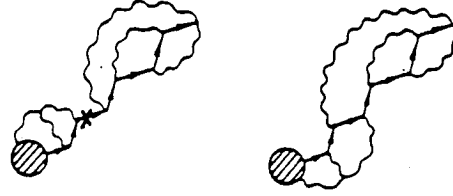


Fig.36

Lemma IV

For a given perturbation order any topologic structure of the power term is a type of closed structure by connecting all open wiggly lines of the derivative primitive frame diagram of the same order.

Proof :

For $\langle \delta\phi_k^* G_k^{-1} A\delta\phi_k \rangle$ and $\langle \delta\phi_k^* G_k^{-1} \delta\tilde{f}_k \rangle$, in which $A\delta\phi_k$ and $\delta\tilde{f}_k$ are formed by primitive frame diagram, the operation acting $\delta\phi_k^*$ on a primitive frame diagram is merely a replacement of the primitive frame diagram by the derivative frame diagram. In $\langle \delta\phi_k^* (-i\Gamma_k) A\delta\phi_k \rangle$ and $\langle \delta\phi_k^* (-i\Gamma) \delta\tilde{f}_k \rangle$ the parts $(-i\Gamma_k) A\delta\phi_k$, and $(-i\Gamma_k) \delta\tilde{f}_k$ are connected diagrams satisfying the conservation law at the vertex that connects $-i\Gamma_k$ to the lower parts, because the highest solid line of $A\delta\phi_k$ and $\delta\tilde{f}_k$ is G_k . Putting $\delta\phi_k^*$ on the highest vertex of $-i\Gamma_k$ and ensemble averaging

the terms yield closure of all open wiggly lines in the diagrams.

Definition III Non-Zero Power Term:

For a given power term if k and k_1 intersect at a multi-wave vertex, it is named as zero power term (due to Lemma I); if k and k_1 intersect at other wave-particle vertex than the highest, it is named as the non-zero power term.

Lemma V

For any non-zero power term there exists at most one self-energy structure in the diagram. If any, it must be located at the upmost part of the diagram with the following property that if one of $\delta\phi_k^$ and $\delta\phi_{k_1}$ is a wiggly line in the self-energy structure, the other must be connected to the part outside the self-energy structure in an overlapping manner.*

Proof :

In $\langle \delta\phi_k^* G_k^{-1} A \delta\phi_k \rangle$ and $\langle \delta\phi_k^* G_k^{-1} \delta\tilde{f}_k \rangle$ the self-energy structure, if any, can only be formed by connecting $\delta\phi_k^*$, that is bound to the highest vertex, to the lower part, because there is no self-energy structure in $A\delta\phi_k$ and $\delta\tilde{f}_k$, in which the open lines are all uncorrelated with each other. The self-energy structure can appear only at the upmost part of the diagram. On the other hand, a self-energy structure has been already contained in the terms

$$\langle \delta\phi_k^* (-i\Gamma_k) A \delta\phi_k \rangle \quad \text{and} \quad \langle \delta\phi_k^* (-i\Gamma_k) \delta\tilde{f}_k \rangle$$

due to the term $-i\Gamma_k$. New self-energy structure besides this can not be constructed, since any non-overlapping connection of $\delta\phi_k^*$ must cause a zero momentum propagator just beneath the new self-energy structure [Fig.36].

Lemma VI

For all non-zero power term no self-energy structure can be isolated from the diagram by cutting solid lines alone.

Proof :

Owing to the Lemma V the self-energy structure must be connected to $\delta\phi_k^*$ or $\delta\phi_{k_1}$, which is connected to the other parts of the diagram outside the self-energy structure in an overlapping manner.

Definition IV Quasi-Self-Energy Diagram:

The diagram of a non-zero power term is a quasi-self-energy diagram if a self-energy structure can be isolated by cutting a solid line and a $\delta\phi_k$ [Fig.37].

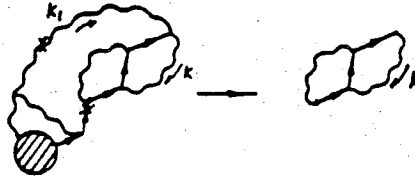


Fig.37

Definition V Self-Energy Free Diagram:

The diagram for a non-zero power term that contains no self-energy structure.

Lemma VII

The quasi-self-energy diagram can only appear in the terms of

$$\langle \delta\phi_k^* G_k^{-1} A \delta\phi_k \rangle \quad \text{and} \quad \langle \delta\phi_k^* G_k^{-1} \delta\phi_k \rangle.$$

Proof :

The Lemma V demands that the self-energy structure only appear at the upmost part of a diagram, whereupon the $\delta\phi_k^*$ and $\delta\phi_{k_1}$ are connected. However, $\delta\phi_k^*$ is not a part of the self-energy structure in $\langle\delta\phi_k^*(-i\Gamma_k)A\delta\phi_k\rangle$ and $\langle\phi_k^*(-i\Gamma_k)\delta\tilde{f}_k\rangle$, and $\delta\phi_{k_1}$ must be a part of self-energy structure. Thus, there is no quasi-self-energy diagram in $\langle\delta\phi_k^*(-i\Gamma_k)A\delta\phi_k\rangle$ and $\langle\delta\phi_k^*(-i\Gamma_k)\delta\tilde{f}_k\rangle$.

Lemma VIII

All non-zero power term are different. There is no repeated non-zero power term.

Proof :

It is obvious that no repeated term may exist in the four power terms individually, since there is no repeated terms in $A\delta\phi_k + \delta f_k$ and $-i\Gamma_k$. Furthermore, $\langle\delta\phi_k^*G_k^{-1}A\delta\phi_k\rangle$ can not be repeated with $\langle\delta\phi_k^*(-i\Gamma_k)\delta\tilde{f}_k\rangle$. If the former term does not contain a self-energy structure, they have the different topological structure; the possibly existed self-energy structure in the former term must be associated with $\delta\phi_k$, while $\delta\phi_k$ must be outside the self-energy structure of the latter term, $\langle\delta\phi_k^*(-i\Gamma_k)\delta\tilde{f}_k\rangle$. For the same reason $\langle\phi_k^*G_k^{-1}\delta\tilde{f}_k\rangle$ can not be repeated with $\langle\delta\phi_k^*(-i\Gamma_k)A\delta\phi_k\rangle$. Finally, $\langle\delta\phi_k^*G_k^{-1}A\delta\phi_k\rangle$ can not be repeated with $\langle\delta\phi_k^*(-i\Gamma_k)A\delta\phi_k\rangle$, and $\langle\delta\phi_k^*G_k^{-1}\delta\tilde{f}_k\rangle$ can not be repeated with $\langle\delta\phi_k^*(-i\Gamma_k)\delta\tilde{f}_k\rangle$, because there is no self-energy sub-structure in $A\delta\phi_k$ and $\delta\tilde{f}_k$.

Lemma IX

For a given quasi-self-energy diagram there must exist a unique adjoint diagram in $\langle\delta\phi_k^(-i\Gamma_k)A\delta\phi_k\rangle$ or in $\langle\delta\phi_k^*(-i\Gamma_k)\delta\tilde{f}_k\rangle$.*

Proof :

According to Lemma VII the quasi-self-energy diagram exists only in

$$\langle \delta\phi_k^* G_k^{-1} A \delta\phi_k \rangle \quad \text{and} \quad \langle \delta\phi_k^* G - k^{-1} \delta\tilde{f}_k \rangle,$$

where k is leaving the vertex, while k_1 is entering the vertex. After the transform ($k \leftrightarrow -k_1$) this property is unchanged. The isolation of a self-energy structure in the quasi-self-energy diagram (after the transform $k \leftrightarrow -k_1$) results from cutting $\delta\phi_k$ and a solid line, i.e., an isolation of $\delta\phi_k^*(-i\Gamma_k)$. If $\delta\phi_k^*$ connects to a wave-particle vertex, the remaining diagram must belong to $A\delta\phi_k$. If $\delta\phi_k^*$ connects to a multi-wave vertex, the remaining diagram must belong to $\delta\tilde{f}_k$. It is because the remaining structure is formed by the primitive frame diagram without any self-energy sub-structure in it. Use is made of Lemma III yields the conclusion that they are adjoint diagrams.

Definition VI $\hat{\xi}$ -Operation:

For a given non-zero power term this operation is the cutting-up the internal line associated with $\delta\phi_k$ or disclosing the multi-wave vertex connected to $\delta\phi_k^$, then replacing the $\delta\phi_k^*$ by G_k .*

Lemma X

For any non-zero power term in $\langle \delta\phi_k^(-i\Gamma_k) A \delta\phi_k \rangle$ and $\langle \delta\phi_k^*(-i\Gamma_k) \delta\tilde{f}_k \rangle$ with $\delta\phi_{k_1}$ being an internal line in it, there always exists a unique adjoint diagram in $\langle \delta\phi_k^* G_k^{-1} A \delta\phi_k \rangle$.*

Proof :

After the transform ($k \leftrightarrow -k_1$) of the term in

$$\langle \delta\phi_k^*(-i\Gamma_k) A \delta\phi_k \rangle \quad \text{and} \quad \langle \delta\phi_k^*(-i\Gamma_k) \delta\tilde{f}_k \rangle$$

and the $\hat{\xi}$ -operation, the resultant diagram must belong to $A\delta\phi_k$, because there is no self-energy structure in the diagram any longer [Fig.38].

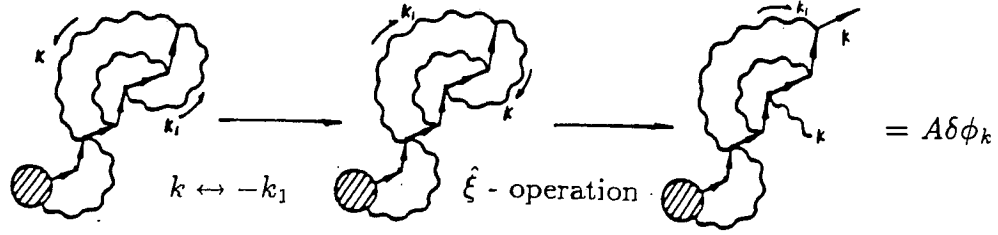


Fig.38

Lemma XI

For any non-zero power term in $\langle \delta\phi_k^*(-i\Gamma_k)A\delta\phi_k \rangle$ and $\langle \delta\phi_k^*(-i\Gamma_k)\delta\tilde{f}_k \rangle$ if $\delta\phi_{k_1}$ connects to a multi-wave vertex, there always exists a unique adjoint diagram in $\langle \delta\phi_k^*G_k^{-1}\delta\tilde{f}_k \rangle$.

Proof :

After the transform $k \leftrightarrow -k_1$ of the term in

$$\langle \delta\phi_k^*(-i\Gamma_k)A\delta\phi_k \rangle \quad \text{and} \quad \langle \delta\phi_k^*(-i\Gamma_k)\delta\tilde{f}_k \rangle$$

and the $\hat{\xi}$ -operation, the resultant diagram must belong to $\delta\tilde{f}_k$ [Fig.39].

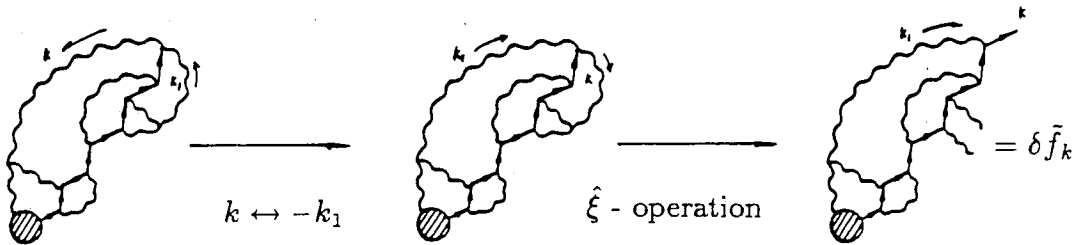


Fig.39

The combination of Lemmata IX through XI implies that all the quasi-self-energy diagrams in $\langle \delta\phi_k^*G_k^{-1}A\delta\phi_k \rangle$ and $\langle \delta\phi_k^*G_k^{-1}\delta\tilde{f}_k \rangle$ cancel all terms of $\langle \delta\phi_k^*(-i\Gamma_k)A\delta\phi_k \rangle, \langle \delta\phi_k^*(-i\Gamma_k)\delta\tilde{f}_k \rangle$ completely.

Lemma XII

If $\delta\phi_k^*$ is an internal line in a self-energy free diagram the corresponding diagram exists only in $\langle\delta\phi_k^* G_k^{-1} A\delta\phi_k\rangle$.

Proof :

Because none of open wiggly line in $\delta\tilde{f}_k$ is $\delta\phi_k$.

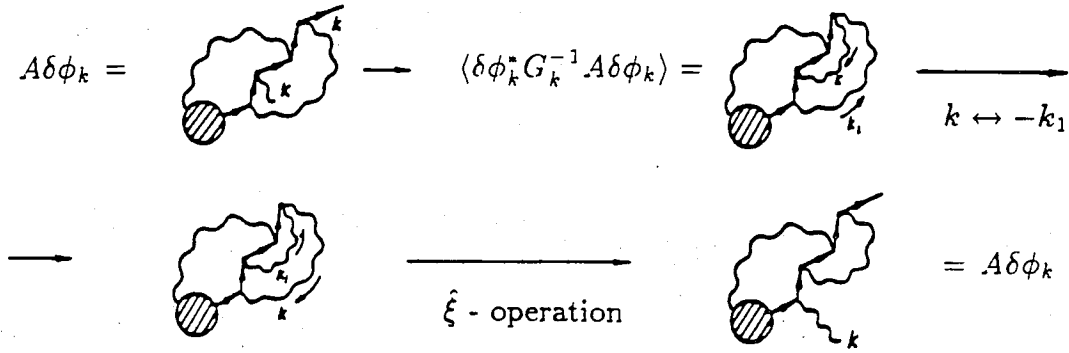


Fig.40

Lemma XIII

For a self-energy free diagram if both $\delta\phi_k$ and $\delta\phi_{k_1}$ are internal lines, this type of diagram must appear pairwise in $\langle\delta\phi_k^* G_k^{-1} A\delta\phi_k\rangle$ and the pair is composed of the adjoint diagrams.

Proof :

If there is such a diagram, it must belong to $\langle\delta\phi_k^* G_k^{-1} A\delta\phi_k\rangle$ according to Lemma XII. Making a transform $k \leftrightarrow -k_1$ to the former type of diagram we have an adjoint diagram that belongs to another term in $\langle\delta\phi_k^* G_k^{-1} A\delta\phi_k\rangle$, because it becomes one diagram of $A\delta\phi_k$ after the $\hat{\xi}$ -operation [Fig.40].

Lemma XIV

If $\delta\phi_k$ is an internal line in a self-energy free term of $\langle\delta\phi_k G_k^{-1} A\delta\phi_k\rangle$, while

$\delta\phi_{k_1}$ connects to a multi-wave vertex, there must exist a unique adjoint diagram in $\langle\delta\phi_k^* G_k^{-1} \delta\tilde{f}_k\rangle$, in which $\delta\phi_{k_1}$ is an internal line and $\delta\phi_k^*$ connects to a multi-wave vertex.

Proof :

When a transform $k \leftrightarrow -k_1$ is applied to the given diagram in the Lemma, the $\delta\phi_k$ in the resultant diagram will connect to a multi-wave vertex. Making the $\hat{\xi}$ -operation, we obtain a diagram belonging to $\delta\tilde{f}_k$ [Fig.41].

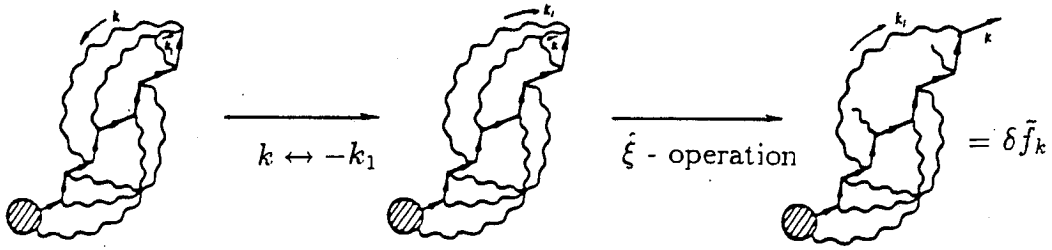


Fig.41

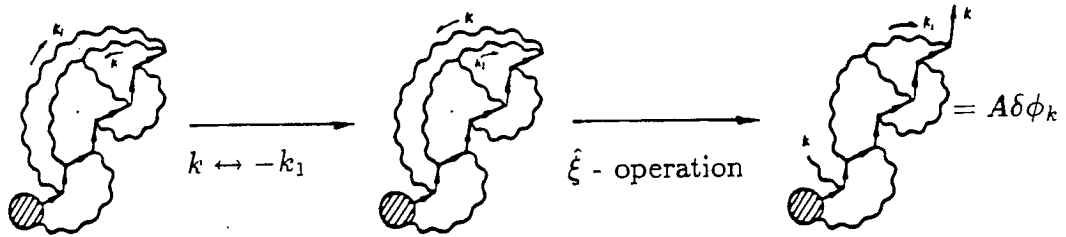


Fig.42

Lemma XV

If $\delta\phi_{k_1}$ is an internal line in a self-energy free diagram of $\langle\delta\phi_k^* G_k^{-1} \delta\tilde{f}_k\rangle$, there must exist a unique adjoint diagram in $\langle\delta\phi_k^* G_k^{-1} A\delta\phi_k\rangle$.

Proof :

The $\delta\phi_k^*$ can not be an internal line in $\langle\delta\phi_k^* G_k^{-1} \delta\tilde{f}_k\rangle$. After the transform $k \leftrightarrow -k_1$, it becomes a diagram, in which $\delta\phi_k$ becomes an internal line (between two wave-particle vertecies). The $\hat{\xi}$ -operation then results in $A\delta\phi_k$ [Fig.42].

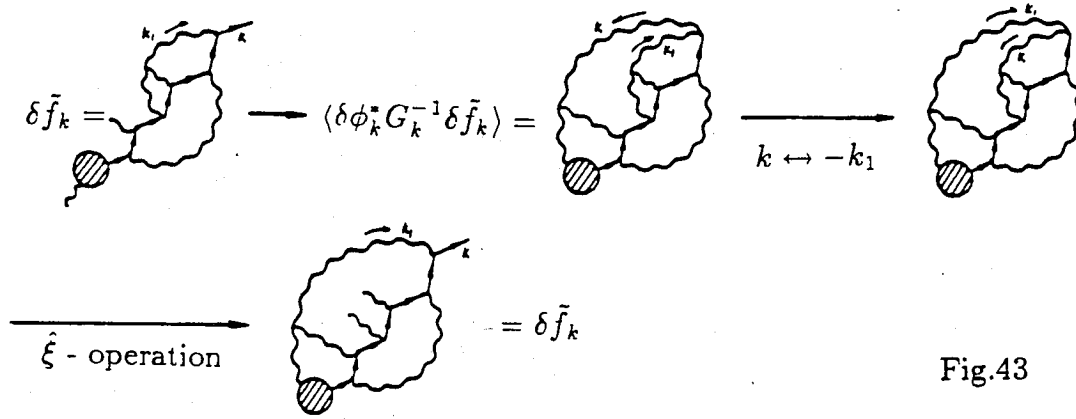


Fig.43

Lemma XIV and Lemma XV imply that the self-energy free diagrams with one of $\delta\phi_k$ and $\delta\phi_{k_1}$ being an internal line and the other connecting to a multi-wave vertex will cancell with each other between $\langle\delta\phi_k^* G_k^{-1} A\delta\phi_k\rangle$ and $\langle\delta\phi_k^* G_k^{-1} \delta\tilde{f}_k\rangle$.

Lemma XVI

If both $\delta\phi_k^*$ and $\delta\phi_{k_1}$ in a self-energy free diagram of $\langle\delta\phi_k^* G_k^{-1} \delta\tilde{f}_k\rangle$ connect to the different multi-wave vertex, this type of diagrams must appear pairwise and they are adjoint diagrams.

Proof :

When the transform $k \leftrightarrow -k_1$ and the $\hat{\xi}$ -operation are applied to such a diagram, the resultant diagram must belong to $\delta\tilde{f}_k$, since there are more than one open wiggly line [Fig.43].

It becomes apparent now that the Lemmata IX through XI have demonstrated the cancellation of all terms containing self-energy structure. The self-energy free terms are divided into three categories: (1) Both $\delta\phi_k^*, \delta\phi_{k_1}$ are internal lines, their contribution equals zero by Lemma XIII; (2) One of $\delta\phi_k^*, \delta\phi_{k_1}$ is an internal line, while the other is connected to a multi-wave vertex, their contribution equals to zero by Lemmata XIV and XV; (3) Both $\delta\phi_k^*, \delta\phi_{k_1}$ are connected to different multi-wave vertex, their contribution is zero due to Lemma XVI. Therefore, we have shown the full cancellation of all non-zero power term by the diagrammatical technique. This completes the proof of the energy conservation for the electrostatic drift wave to arbitrary higher order.

IX.3 Sheared Slab and Ballooning Representation

In a sheared slab model the only change in the nonlinear equation Eq.(9.1) lies in the wave-particle interaction vertex, $\hat{L}(k, k_1)$. It becomes

$$\hat{L}(k, k_1) \longrightarrow (e/m)k_{1,\parallel} \partial - \frac{c}{B} (k_{1,y} \frac{\partial}{\partial x} - k_y \frac{\partial}{\partial x}), \quad (9.3.1)$$

where k stands for ω, k_y and k_z , $\partial/\partial x$ acts on all quantities behind it, while $\dot{\partial}/\partial x$ only acts on the wave pertaining to the vertex. The ensemble average is taken as the integral over x-space, merely for rapid variations.

The relevant quantity in the proof of Lemma I becomes

$$\langle \delta\phi_k^* \hat{L}(k, k_1) \delta\phi_{k_1} P(k - k_1) \rangle = \left\langle \delta\phi_k^* \left[k_{1,y} \frac{\partial}{\partial x} \delta\phi_{k_1} - k_y \left(\frac{\partial \delta\phi_{k_1}}{\partial x} \right) \right] P(k - k_1) \right\rangle,$$

An integration by parts, and the transformation $k \leftrightarrow -k_1$ makes the equation change sign. The Lemma I is thus verified for the sheared slab model.

Since the pair of adjoint diagrams are defined in the sheared model by

$$\langle \delta\phi_k^* \hat{L}(k, k_1) \delta\phi_{k_1}^* P(k, k_1) \rangle, \quad \text{and} \quad \langle \delta\phi_k^* \hat{L}(k, k_1) \delta\phi_{k_1}^* P(-k_1, -k) \rangle,$$

we find that one of the adjoint diagrams becomes the other with a minus sign after integration by parts in x -space and the transform $k \leftrightarrow -k_1$. So the Lemma II is also generalized to the sheared model. Based on these two lemmata, in addition to the other fourteen lemmata that are only consequence of the diagram topology and independent of the geometry, we then complete the proof of the energy conservation in the sheared slab model.

For a cylindrical configuration we replace k_y by m/r and x by r , $\partial/\partial x$ by $\partial/\partial r$, dx by rdr . Obviously, the consequence of integration by parts over r is just the same as that for x , since there is only one vertex, the highest vertex, involved.

We wish to emphasize that the energy conservation in electrostatic drift waves is a consequence of the antisymmetry (change of sign for $k \leftrightarrow k_1$) of the wave-particle interaction vertex. Explicit antisymmetry must be maintained in any treatment, otherwise energy conservation will be violated. To illustrate our point, we make a small digression to show that there exist examples in published literature¹¹⁸ (using ballooning representation) where antisymmetry and hence energy conservation is not preserved.

Manipulation of the gyrokinetic equation in the ballooning representation (in the electrostatic, and small gyro-radius approximation) yields the explicitly

antisymmetric nonlinear term

$$\begin{aligned} \pi(c/B)\tilde{F} \sum_{n_1+n_2=n} n_1 n_2 \sum_l [\exp(-2\pi i \bar{q} n_1 l) \delta \hat{\phi}_{n_1}(\psi, \theta + 2\pi l) \delta \hat{h}_{n_2}(\psi, \theta) \\ - \exp(-2\pi i \bar{q} n_2 l) \delta \hat{\phi}_{n_2}(\psi, \theta) \delta \hat{h}_{n_1}(\psi, \theta + 2\pi l)], \end{aligned} \quad (9.3.2)$$

where $\delta \hat{h}_n(\psi, \theta)$ is the non-adiabatic part of ballooning amplitude $\delta \hat{\phi}_n$ defined by

$$\delta \phi(\psi, \theta, \zeta) = \sum_n \exp \left[i n \left(\zeta - \int^\theta d\theta' q(\psi, \theta') \right) \right] \sum_l \delta \hat{\phi}_n(\psi, \theta + 2\pi l) \exp(-2\pi i n \bar{q} l), \quad (9.3.3)$$

with

$$\bar{q} = \oint d\theta' q(\psi, \theta'), \quad \tilde{F} = \nabla \left(\zeta - \int^\theta d\theta' q(\psi, \theta') \right) \times \nabla q \cdot \mathbf{b}.$$

It is obvious that it is only the combination of the two terms on the r.h.s. of Eq.(9.3.2) that guarantees the antisymmetry which makes Eq.(9.3.2) correspond to the slab model nonlinear term

$$(c/B)(\nabla \delta \phi \times \mathbf{b}) \cdot \nabla \delta \phi = 0.$$

Unfortunately, the second term in Eq.(9.3.2) is missing in the aforementioned treatment, and in that treatment there is no way to assure energy conservation in each order of the perturbation theory.

X. Renormalized Gyro-Kinetics

The methodology developed in VIII can be readily generalized to deal with more complicated and realistic problems in plasma physics.

X.1 Collisionless Plasma with Finite Larmor Radius Effects

An obvious extension of the renormalized perturbation theory in VII is to develop a renormalized theory of collisionless plasmas including finite Larmor radius effects. Clearly one must begin with the nonlinear gyro-kinetic version of the Vlasov equation. To make the problem more realistic and interesting, we allow the equilibrium to have temperature and density gradients also.

Notice that in a gyro-kinetic theory, the perpendicular (to the magnetic field) thermal motion of the particles comes into its own implying that self-energy term, etc. will become function of the perpendicular velocity v_{\perp} . Thus the evaluation of all the renormalized (linear as well as nonlinear) terms will involve cumbersome v_{\perp} integrations.¹¹⁷ It turns out, however, that in slab model and to second order in perturbations, the v_{\perp} -dependent self-energy terms can be replaced by the v_{\perp} -averaged terms (independent of v_{\perp}) provided the drift frequencies are ignored. As a result, only the familiar v_{\parallel} integration (just like the drift-kinetic treatment) will be necessary to derive the nonlinear wave equation.

In a slab model, the non-adiabatic part of the perturbed distribution function obeys (in Fourier space with $\delta A_{\perp} = 0$)

$$\begin{aligned}
(\omega - k_{\parallel} v_{\parallel}) \delta h_k &= \hat{L}_0(k) J_0(v_{\perp} k_{\perp} / \Omega) F_0 \delta \psi_k \\
&+ \sum_{k_1 + k_2 = k} \hat{L}_1(k_1, k_2) J_0(v_{\perp} k_{1,\perp} / \Omega) \delta \psi_{k_1} \delta h_{k_2},
\end{aligned} \tag{10.1.1}$$

with the definitions

$$\hat{L}_0(\mathbf{k}) \equiv (q/T) \{ \omega - \omega_n^* [1 + \eta(H/T - 3/2)] \} \tag{10.1.2}$$

$$\hat{L}_1(k_1, k_2) \equiv i(c/B)(\mathbf{k}_1 \times \mathbf{k}_2) \cdot \mathbf{b} \tag{10.1.3}$$

and

$$\delta \psi_k = \delta \phi_k - (v_{\parallel}/c) \delta A_k, \tag{10.1.4}$$

where $\omega_n^* = (cT/eB)(k_y/L_n)$ is the density gradient induced diagramatic frequency, L_n is the density scale length, $\eta = L_n/L_T$, L_T is the temperature scale length, $H = (m/2)(v_{\parallel}^2 + v_{\perp}^2)$ is the particle energy, Ω is the gyrofrequency, B is the ambient magnetic field and J_0 representing finite gyroradius effects, is the Bessel function of order zero. Direct renormalization of Eq.(10.1.1) would yield the \mathbf{v}_{\perp} -dependent self-energy term

$$-i\Gamma_k = \sum_{k_1} (c/B)^2 [\mathbf{k}_1 \times \mathbf{k} \cdot \mathbf{b}]^2 J_0^2(v_{\perp} k_{1,\perp} / \Omega) G_{k-k_1} |\delta \psi_{k_1}|^2, \tag{10.1.5}$$

and an appropriate expression for the distribution function $\delta h_k(\mathbf{v})$. As pointed out earlier, it is much more convenient to deal with the \mathbf{v}_{\perp} -averaged distribution function

$$\delta \bar{h}_k(v_{\parallel}) \equiv I_{v_{\perp}} \delta h_k(\mathbf{v}) \equiv \int_0^{\infty} v_{\perp} dv_{\perp} J_0(v_{\perp} k_{\perp} / \Omega) \delta h_k(\mathbf{v}), \tag{10.1.6}$$

whose equation of motion is obtained by applying the operator, I_{v_\perp} , to both sides of Eq.(10.1.1). Standard manipulation of the resulting equation along with the reasonable assumption $F_0(\mathbf{v}) = F_0(v_\parallel^2) \cdot F_0(v_\perp^2)$ yields the renormalized second order expression,

$$\begin{aligned} \delta \bar{h}_k(v_\parallel) = & G_k \hat{L}_0^{(0)}(k) F_0(v_\parallel^2) \delta \psi_k \\ & + \sum_{k_1+k_2=k} G_k \hat{L}(k_1, k_2) G_{k_2} \hat{L}_0^{(1)}(k_1, k_2) F_0(v_\parallel^2) \delta \psi_{k_1} \delta \psi_{k_2} \\ & + \sum_{\substack{k_1+k_2+k_3=k \\ k_3 \neq k}} G_k \hat{L}(k_1, k-k_1) G_{k-k_1} \hat{L}(k_2, k_3) G_{k_3} \\ & \cdot \hat{L}_0^{(2)}(k_1, k_2, k_3) F_0(v_\parallel^2) \delta \psi_{k_1} \delta \psi_{k_2} \delta \psi_{k_3}, \end{aligned} \quad (10.1.7)$$

with

$$\hat{L}_0^{(0)}(k) \equiv (q/T) \{ (\omega - \omega_n^* [1 + \eta(v_\parallel^2/v_0^2 - 1/2 - b)]) \Gamma_0(b) - \omega_n^* \eta b \Gamma_1(b) \}, \quad (10.1.8)$$

$$\begin{aligned} \hat{L}_0^{(1)}(k_1, k_2) \equiv & \int_0^\infty v_\perp dv_\perp J_0(v_\perp |\mathbf{k}_{1,\perp} + \mathbf{k}_{2,\perp}|/\Omega) \cdot \\ & J_0(v_\perp k_{1,\perp}/\Omega) J_0(v_\perp k_{2,\perp}/\Omega) \hat{L}_0(k_2) F_0(v_\perp^2), \end{aligned} \quad (10.1.9)$$

$$\begin{aligned} \hat{L}_0^{(2)}(k_1, k_2, k_3) \equiv & \int_0^\infty v_\perp dv_\perp J_0(v_\perp |\mathbf{k}_{1,\perp} + \mathbf{k}_{2,\perp} + \mathbf{k}_{3,\perp}|/\Omega) \cdot \\ & J_0(v_\perp k_{1,\perp}/\Omega) J_0(v_\perp k_{2,\perp}) J_0(v_\perp k_{3,\perp}) \hat{L}_0(k_3) F_0(v_\perp^2), \end{aligned} \quad (10.1.10)$$

$$G_k \equiv (\omega - k_\parallel v_\parallel + i\Gamma_k)^{-1}, \quad (10.1.11)$$

and

$$-i\Gamma_k = \sum_{k_1} J(k_\perp, k_{1,\perp}) \hat{L}(k_1, k) G_{k-k_1} \hat{L}(-k_1, k-k_1) |\delta \psi_{k_1}|^2, \quad (10.1.12)$$

with

$$J(k_{\perp}, k_{1,\perp}) \equiv \frac{\int_0^{\infty} v_{\perp} dv_{\perp} J_0^2(v_{\perp} k_{\perp} / \Omega) J_0^2(v_{\perp} k_{1,\perp} / \Omega) \hat{L}_0(k) F_0(v_{\perp}^2)}{\int_0^{\infty} v_{\perp} dv_{\perp} J_0^2(v_{\perp} k_{\perp} / \Omega) \hat{L}_0(k) F_0(v_{\perp}^2)}. \quad (10.1.13)$$

Substituting $\delta \bar{h}_k(v_{\parallel})$ into Poisson equation and Ampere's law will yield the set of nonlinear coupled equations in $\delta \phi_k$ and δA_k .

X. 2 Nonlinear Kinetic η_i Mode

The renormalized gyrokinetic formalism presented in X.1 can be used to delineate some general features of the behavior of the η_i mode which is thought to be a possible candidate responsible for anomalous particle transport in Tokamaks.¹¹⁹ Since the η_i mode is essentially electrostatic, the basic dynamics is contained in the equation of quasi-neutrality. Perturbed density can be readily calculated from Eq.(10.1.7). We begin with the first term on the r.h.s. which leads to the renormalized linear ion response (G_k is the renormalized propagator)

$$\delta n_k^{(r,l)} = -(en/T_i) \delta \psi_k [1 - (1 - \omega_{in}^*/\omega) \Gamma_0(b_i) - (\omega_{iT}^*/\omega) b_i [\Gamma_i(b_i) - \Gamma_0(b_i)] - \bar{\sigma}(k)], \quad (10.2.1)$$

where

$$\bar{\sigma}(k) \equiv \left(\frac{\omega_{in}^*}{\omega} - 1 \right) \Gamma_0(b_i) W_1(\zeta) + \frac{\omega_{iT}^*}{\omega} \{ W_2(\zeta) \bar{\zeta} \Gamma_0(b_i) + [1 + \bar{\zeta} Z(\zeta)] \bar{\Gamma}(b_i) \}, \quad (10.2.2)$$

where $W_1 \equiv 1 + \zeta Z(\zeta)$, $W_2(\zeta) \equiv \zeta W_1(\zeta) - Z(\zeta)/2$, Z is the plasma dispersion function, $\bar{\Gamma}(b) \equiv b[\Gamma_1(b) - \Gamma_0(b)]$, $\Gamma_n(b) = \exp(-b) \cdot I_n(b)$, $I_n(b)$ is the

modified Bessel function, and $b_i = k_{\perp}^2 \rho_i^2 / 2$. Notice that the argument of the Z -function $\zeta = (\omega + i\Gamma_k) / k_{\parallel} v_i = \tilde{\zeta} + i\Gamma_k / k_{\parallel} v_i$ contains the effects of renormalization (frequency broadening and shift). Since the electron response for the η_i mode is adiabatic, a nonlinear dispersion relation is obtained by equating $\delta n_k^{(i)} = e\phi_k / T_e$. The solution (of the nonlinear dispersion relation) at marginal stability yields the saturation level for the spectrum allowing us to determine the saturation frequency broadening which can be associated with the transport coefficients. At this level, the result has no contribution from the incoherent part, particularly, the three wave interaction. Since longer perpendicular wavelength modes cause a larger transport, while the shorter wavelength ($k_{\perp} \rho_i \sim 1$) modes are more easily destabilized (due to finite ion Larmor radius effects), it is important to examine the three wave interaction processes which can carry energy from the shorter to the longer wavelength part of the spectrum.

Let $k_{1,\perp}$ and $k_{2,\perp}$ be the two short wavelength modes which produce a long wave length (small k) beat wave k_{\perp} . This process will be mediated by the term $\hat{L}_0(k_1, k_2)$ given by Eq.(10.1.9). Straightforward algebra leads to the nonlinear perturbed density (the density characterized by k_{\perp} driven by the interaction of waves $k_{1,\perp}$ and $k_{2,\perp}$) corresponding to the second term on the r.h.s. of Eq.(10.1.5),

$$\begin{aligned} \delta n_k^{(n,l)'} = i(c/Bv_i)(en/T_i) \sum_{k_1+k_2=k} (k_1 \times k_2) \cdot b \left\{ [\hat{\Omega}(2)\{sgn(k_{\parallel})Z(\zeta) \right. \\ - sgn(k_{2,\parallel})Z(\zeta_2)\} - \omega_{iT}^*(2)\Gamma_0(b_i)\{sgn(k_{\parallel})\hat{W}(\zeta) - sgn(k_{2,\parallel})\hat{W}(\zeta_2)\}] \\ \left. [k_{2,\parallel}(\omega + i\Gamma_{k_2}) - k_{\parallel}(\omega_2 + i\Gamma_{k_2})]^{-1} - (1 \leftrightarrow 2) \right\} \delta\phi_{k_1} \delta\phi_{k_2}, \end{aligned} \quad (10.2.3)$$

where

$$\hat{\Omega}(2) \equiv [\omega_2 - \omega_{in}^*(2)]\Gamma_0(b_i) + \omega_{iT}^*(2)b_i[\Gamma_0(b_i) - \Gamma_1(b_i)], \quad (10.2.4)$$

$$\hat{W}(\zeta) \equiv \zeta[1 + \zeta Z(\zeta)] - Z(\zeta)/2, \quad (10.2.5)$$

which, incidentally, is just the term $\sum_{k_1+k_2=k} \tilde{\epsilon}^{(2)}(k_1, k_2) \delta\phi_{k_1} \delta\phi_{k_2}$ in the nonlinear wave equation Eq.(8.4.1). In a similar manner, we can evaluate $\delta n_k^{(n,l)''}$ which corresponds to the third term on the r.h.s. of Eq.(10.1.7), and is naturally divided into the coherent and the incoherent part. As expected these terms are nothing but the appropriate explicit expressions for the terms in the nonlinear wave Eq.(8.4.1); the coherent part is determined by $\epsilon^{(3)}(k_1, k, -k_1)$, and the incoherent part by $\epsilon^{(3)}(k_1, k_2, k_3)$. The finite ion Larmor radius effect is thus explicitly expressed in terms of the Γ functions, and the rest of the manipulation is the same as that for the zero Larmor radius case.

X. 3. Transport Equations in Gyrokinetic Theory

Several of the recent candidates believed to be responsible for causing turbulent transport in Tokamaks are modes which depend on finite Larmor radius effects. Now we derive the transport theory relevant for these modes. We begin with the (for simplicity, the drift frequency ω_d has been neglected) collisionless gyro-kinetic equation¹²⁰

$$\left[\frac{\partial}{\partial t} + v_{\parallel} \mathbf{b} \cdot \hat{\nabla} - \Omega \frac{\partial}{\partial \alpha} \right] f = -q(\delta R f) \quad (10.3.1)$$

with

$$\delta R \equiv -\nabla \delta \psi \cdot \left[\mathbf{v} \frac{\partial}{\partial H} + \frac{\mathbf{v}_\perp}{B} \frac{\partial}{\partial \mu} - \frac{\mathbf{v} \times \mathbf{b}}{mv_\perp^2} \frac{\partial}{\partial \alpha} \right] - \frac{1}{m\Omega} \nabla \delta \psi \times \mathbf{b} \cdot \hat{\nabla}, \quad (10.3.2)$$

and where $\hat{\nabla}$ acts on the guiding center motion, and α is the gyro-angle. Ensemble averaging Eq.(10.3.1), we obtain

$$\left[\frac{\partial}{\partial t} + v_\parallel \mathbf{b} \cdot \nabla - \Omega \frac{\partial}{\partial \alpha} \right] F = q \left\langle \nabla \psi \cdot \left[\mathbf{v} \frac{\partial}{\partial H} + \frac{\mathbf{v}_\perp}{B} \frac{\partial}{\partial \mu} - \frac{\mathbf{v} \times \mathbf{b}}{mv_\perp^2} \frac{\partial}{\partial \alpha} + \frac{1}{m\Omega} \mathbf{b} \times \hat{\nabla} \right] \delta f \right\rangle, \quad (10.3.3)$$

where $F = \langle f \rangle$ is the ensemble averaged distribution function; $\delta f [\langle \delta f \rangle = 0]$ is the perturbed or the fluctuating part. From the point of view of transport, the quantity of basic physical interest is the gyro-averaged distribution function $\langle F \rangle_\alpha = \langle \langle f \rangle \rangle_\alpha$ which obeys

$$\left(\frac{\partial}{\partial t} + v_\parallel \mathbf{b} \cdot \nabla \right) \langle F \rangle_\alpha = q \left\langle v_\parallel \mathbf{b} \cdot \nabla \langle \delta \psi \rangle_\alpha \frac{\partial}{\partial H} \delta f_0 \right\rangle + \frac{q}{m\Omega} \left\langle \langle \nabla \delta \psi \rangle_\alpha \cdot \mathbf{b} \times \hat{\nabla} \delta h_0 \right\rangle, \quad (10.3.4)$$

obtained by gyro-averaging Eq.(10.3.3), and where δh_0 satisfies the nonlinear equation

$$\left(\frac{\partial}{\partial t} + v_\parallel \mathbf{b} \cdot \nabla \right) \delta h_0 = q \left[\frac{\partial F_0}{\partial H} i\omega + \frac{1}{m\Omega} \mathbf{b} \times \hat{\nabla} F_0 \cdot \hat{\nabla} \right] \cdot \delta \psi + (c/B) \mathbf{b} \times \hat{\nabla} \delta h_0 \cdot \hat{\nabla} \langle \delta \psi \rangle_\alpha. \quad (10.3.5)$$

Notice that we have not yet specified the nature of ensemble averaging; a convenient ensemble will be defined later. We shall also show that the second term on the r.h.s. of Eq.(10.3.4) is the diffusion term (the first term is clearly

the power term). The analysis becomes much more perspicuous in the Fourier representation in which the aforementioned term takes the form

$$\begin{aligned} \langle \nabla \delta \psi \rangle_\alpha \cdot \mathbf{b} \times \hat{\nabla} \delta h_0 &= \hat{\nabla} \cdot [\langle \nabla \delta \psi \rangle_\alpha \times \mathbf{b} \delta h_0] \\ &= \hat{\nabla} \cdot \sum_{\mathbf{k}_1, \mathbf{k}_2} i(\mathbf{k}_1 \times \mathbf{b}) \delta \psi_{\mathbf{k}_1} J_0(k_{1,\perp} v_\perp / \Omega) \delta h_{\mathbf{k}_2} \end{aligned} \quad (10.3.6)$$

The ensemble is now so chosen that the ensemble averaging implies $\mathbf{k}_1 + \mathbf{k}_2 = 0$, i.e., one chooses only those modes which have equal and opposite four momenta. The operator $\hat{\nabla}$ outside the summation over Fourier component acts only on the macroscopic quantities contained in the summation (these quantities are slowly varying and hence are not Fourier transformed). Equation (10.3.6) becomes

$$\left\langle \langle \nabla \delta \psi \rangle_\alpha \cdot \mathbf{b} \times \hat{\nabla} \delta h_0 \right\rangle = \hat{\nabla} \cdot \sum_{\mathbf{k}_1 + \mathbf{k}_2 = 0} i(\mathbf{k}_1 \times \mathbf{b}) \delta \psi_{\mathbf{k}_1} J_0(k_{1,\perp} v_\perp / \Omega) \delta h_{\mathbf{k}_2}. \quad (10.3.7)$$

At this stage, we go back and apply the standard renormalizing procedure to Eq.(10.3.5) and obtain the linear response

$$\delta h_{\mathbf{k}} = -G_{\mathbf{k}q} \left(\frac{\partial F_0}{\partial H} \omega + \frac{1}{m\Omega} \mathbf{b} \times \hat{\nabla} F_0 \cdot \mathbf{k}_1 \right) J_0(k_\perp v_\perp / \Omega) \delta \psi_{\mathbf{k}}, \quad (10.3.8)$$

where $G_{\mathbf{k}}$ is the renormalized propagator [Eq.(10.1.11)]. The nonlinear power term (the first term on the r.h.s of Eq.(10.3.5)) is associated with transport in velocity space and will not be investigated here. Substituting Eqs.(10.3.7), (10.3.8) into Eq.(10.3.5), and integrating over \mathbf{v}_\perp , we obtain

$$\begin{aligned} \left(\frac{\partial}{\partial t} + v_\parallel \mathbf{b} \cdot \hat{\nabla} \right) F_0(v_\parallel) &= \hat{\nabla} \cdot (c/B)^2 \text{Im} \sum_{\mathbf{k}_1 + \mathbf{k}_2 = 0} (\mathbf{k}_1 \times \mathbf{b}) G_{\mathbf{k}_2} (\mathbf{k}_2 \times \mathbf{b}) \\ &\quad \cdot \hat{\nabla} F_0(v_\parallel) \Gamma_0(\rho^2 k_{1,\perp}^2 / 2) \langle \delta \psi_{\mathbf{k}_1} \delta \psi_{\mathbf{k}_1}^* \rangle + \dots \end{aligned} \quad (10.3.9)$$

The set of transport equations can be built up by taking various v_{\parallel} moments of Eq.(10.3.9); the associated transport coefficient can also be readily identified. In particular, the energy transport coefficient is associated with the term (from the second moment)

$$\hat{\nabla} \cdot \frac{c^2}{B} \text{Im} \sum_k (\mathbf{k} \times \mathbf{b}) \Gamma_0(b) (\mathbf{k} \times \mathbf{b}) \cdot \mathbf{m} \int dv_{\parallel} v_{\parallel}^2 G_k \hat{\nabla} F_0(v_{\parallel}) \langle \delta \psi_k \delta \psi_k^* \rangle, \quad (10.3.10)$$

where $F_0(v_{\parallel}) \equiv (\sqrt{\pi} v_0)^{-1} \exp(-v_{\parallel}^2/v_0^2)$ is the one dimensional Maxwellian, and $b \equiv k_{\perp}^2 \rho_{\perp}^2/2$. From Eq.(10.3.9) we see that the turbulent transport coefficient can be written in the familiar form $D_{\perp}^{(T)} \sim (\delta v_{\perp})^2 \tau_c$, where δv_{\perp} is some perturbed perpendicular velocity induced by the fluctuations, and τ_c is the shortest correlation time. Several general properties of the diffusion coefficient are easily gleaned from Eq.(10.3.9):

(1) Larmor radius effects cause the diffusion coefficient to be suppressed by the factor $\Gamma_0(b) = I_0(b) \exp(-b) \sim (1/\sqrt{b})$ ($b \rightarrow \infty$),

(2) In the expression for the diffusion coefficient there are two competing times scales (provided ω is small so that $\omega^{-1} \gg \tau_c$) $(k_{\parallel} v_{\parallel})^{-1}$ and $\Gamma_k^{-1} = (k_{\perp}^2 D_{\perp})^{-1}$; their origin is in the renormalized propagator $G_k \sim (\omega - k_{\parallel} v_{\parallel} + i\Gamma_k)^{-1}$. Thus τ_c will equal the shorter of these times, $(k_{\parallel} v_0)^{-1}$ if $k_{\parallel} v_0 > k_{\perp}^2 D_{\perp}$, or $(k_{\perp}^2 D_{\perp})^{-1}$ if $k_{\perp}^2 D_{\perp} > k_{\parallel} v_{\parallel}$,

(3) It is possible to obtain the ratio of electron to ion turbulent transport coefficient, $R = \Gamma_k^{(e)}/\Gamma_k^{(i)}$ although neither of these can be individually evaluated without knowing the saturation fluctuation level which, of course, requires the complete solution of the nonlinear problem. As an example, we work out the

ratio R for the energy transport caused by kinetic electrostatic drift waves which are characterized by the inequality $k_{\parallel} v_i < \omega < k_{\parallel} v_e$. For the regime $k_{\parallel} v_e > \Gamma_k^{(e)}$, $k_{\parallel} v_i < \Gamma_k^{(i)}$, it is straightforward to evaluate $\tau_c^{(e)} \sim (\sqrt{\pi}/k_{\parallel} v_e)(\omega/k_{\parallel} v_e)^2$, and $\tau_c^{(i)} = \Gamma_0^{-1} \Gamma_k^{(i)} / (\omega^2 + (\Gamma_k^{(i)})^2)$ leading to the ratio between the transport coefficients

$$R = \chi_e / \chi_i = \tau_c^{(e)} / \tau_c^{(i)} = \frac{\sqrt{\pi}}{\Gamma_0(b)} \left(\frac{\omega}{k_{\parallel} v_e} \right)^3 \frac{\omega}{\Gamma_k^{(i)}}. \quad (10.3.11)$$

Notice that for drift waves ($k_{\perp} \rho_s \sim 1$ and $\omega < k_{\parallel} v_e$) $R < 1$. The conclusion $R < 1$ does not change even if the other limit ($k_{\parallel} v_{\parallel} < \Gamma_k^{(e)}$) were examined. This conclusion seems to be in direct conflict with the tokamak experiments where $R = \chi_e / \chi_i > 1$. It is thus difficult to believe that the electrostatic drift wave could be responsible for the observed anomalous electron transport in tokamaks.

PART C

ANOMALOUS ELECTRON TRANSPORT

IN TOKAMAKS

XI. Experimental Evidence of Anomalous Electron Transport

Because of its importance to the scientific feasibility of magnetically confined fusion, the energy confinement and, in particular, the anomalous thermal transport of electrons is one of the major physics problem posed by tokamaks. The most frequently used measure of tokamak performance is the global confinement time, $\tau_E = W_{tot}/P_{in}$ where W_{tot} is the total energy stored in the plasma,

$$W_{tot} = \int dv \frac{3}{2} n (T_e + T_i)$$

and P_{in} is the rate at which energy is being supplied to the plasma, which may be from Ohmic heating, neutral beam injection or some form of radio frequency (RF) heating. The measured global energy confinement time, when compared to the confinement time calculated with all classical losses included, indicates whether or not anomalous losses present.

Clear evidence for anomalous electron transport losses came from ohmically heated tokamaks operating in a low density regime. For ohmically heated tokamaks, the total input power is simply the Ohmic power that goes directly into the electrons. If one assumes that there is no significant anomalous energy transfer from electrons to ions , the rate of Ohmic heating of the electrons is much faster than the rate of classical energy transfer from the electrons to the ions for sufficiently low plasma densities. This allows the energy transport of ions and electrons to be studied separately, and a large uncertainty in the ion losses causes only a small uncertainty in the total loss. Many tokamaks

operating in this regime, including Ormak,^{121,122} TFR,^{123,124} Alcator A,¹²⁵ PLT,^{126,127} and ISX-A,¹²⁸ clearly showed that the electron losses were anomalous, i.e., the observed energy confinement time was much shorter, typically by a factor of 10-100, than that expected on the basis of the known neoclassical processes.

To understand the processes governing the energy confinement, it is essential to determine first the dominant energy loss channels in the plasma, i.e., if the energy loss through the electron channel exceeds the losses from other channels, especially, the energy loss from the ion channel. The following is mainly concentrated on the analysis of experiments in comparison of these two types of losses. This comparison is also important to identify the nature of the anomalous energy losses.

For present generation of tokamaks operating in a rather high density regime, it is generally a much more complicated matter to determine the magnitude of the anomalous electron losses. However, the power balance can be investigated from the knowledge of electron density and temperature profiles and the reasonable assumption on the ion temperature profile. Of course, the contributions to the power losses due to impurity radiation and charge exchange have to be determined.

A well-known example is the comparison of energy confinement times at similar densities between pellet and gas fuelled discharges in Alcator C.^{129,130} In the gas fuelled discharges only if the ion conduction of four times the Hinton-Hazeltine neoclassical value¹³¹ is consistent with the temperature data and

implies the well-known Alcator scaling,¹³² the linear dependence of τ_{E_e} on \bar{n} , where $\tau_{E_e} = W_e/P_e$ (W_e , the electron stored energy and P_e , the net power to electron), the electron energy confinement time, and, \bar{n} , the line averaged density. In this analysis the ion temperature profile is inferred from the ion power balance equation using the assumed model for the ion thermal conduction, χ_i . It is also found that the anomaly factor four on χ_i seems to be independent of current over the range $250 < I_p < 720$ kA.¹²⁹ Another feature in the gas puffing discharges is the density profile much broader than that in other high density plasma, such as Alcator A and FT, discharges.^{132,133}

The assumed anomalous ion conduction is verified by the pellet fuelled discharges in Alcator C. Because of the transient nature of pellet fuelled plasmas, the study of energy confinement properties is somewhat complicated with respect to steady state discharges with gas puffing only. A 1D transport code was used to solve the following time dependent equations: magnetic diffusion, electron energy balance, ion energy balance, particle balance, and neutral transport. The outputs of this code are energy and particle confinement times, thermal and particle diffusivities and neutron rates, and β and inductance values which can be compared with the measured values. Alternatively, confinement can be calculated by using the standard procedure from measured profiles and including the inductive correction to the loop voltage. These two methods give similar results when the temperature before pellet injection has recovered and a quasi-steady state has been reached, 30 to 50 ms after pellet injection. The pellet fuelled discharges show a clear improvement in confinement and the apparent

saturation of τ_E as a function of density can now be explained by the Chang-Hinton neoclassical ion conduction.¹³⁴ Thus, for pellet fuelled discharges, the energy confinement in Alcator C behaves like that observed in Alcator A and FT tokamak,¹³⁵ and the production of very peaked density profiles removes the anomalous ion transport, which had to be invoked to explain the gas fuelled Alcator C results. The typical value of χ_e at the half-radius after pellet injection is about $0.1 - 0.25 \text{ m}^2 \cdot \text{s}^{-1}$ (the calculation is subject to uncertainties in the radiated power term), while the χ_i at the half-radius is less than $0.1 \text{ m}^2 \cdot \text{s}^{-1}$ after pellet injection, a decrease from $0.5 \text{ m}^2 \cdot \text{s}^{-1}$ before pellet injection.

Details of the energy transport processes has also been investigated in the ohmically heated Doublet III plasma¹³⁶ with the aid of transport code ONETWO.¹³⁷ The experimental profiles of T_e, n_e and P_{rad} are inputs to the code together with the global parameters I, V, B_T , etc. The calculation of the ion power balance includes power lost by conduction, convection and charge exchange and power gained by ionization. Since the observed gross electron confinement time ($\tau_{E_e}^G \equiv W_e/P_{oh}$) can not be explained by setting the ion thermal conduction equal to the neoclassical value, χ_i^{NC} by Hinton-Hazeltine¹³¹ (for the calculation of χ_i^{NC} oxygen is assumed to be the sole impurity), the procedure used is to vary the magnitude χ_i/χ_i^{NC} until the code value of T_i agrees with the experimental value. An example of the transport analysis is the H_2 discharges with $\bar{n}_e \sim 2.9 \times 10^{13} \text{ cm}^{-3}$, $B_T = 20 \text{ kG}$, $I = 464 \text{ kA}$, $T_e(0) = 0.8 \text{ keV}$. Agreement between measured and calculated T_i is obtained for $2 < \chi_i/\chi_i^{NC} < 7$. The typical electron conduction is about the twice of the ion conduction (Fig. 44

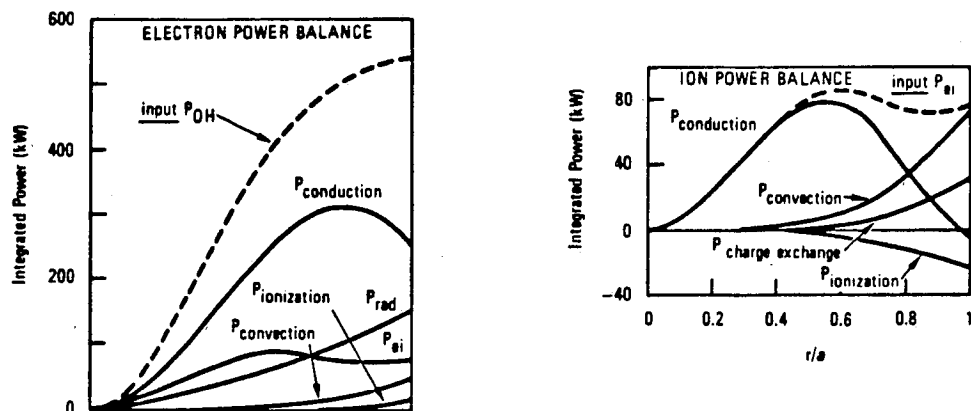


Fig.44 Power balance from transport code analysis of H_2 Ohmic discharges in Doublet-III¹³⁶ with $\bar{n}_e = 2.9 \times 10^{13} \text{ cm}^{-3}$, $a = 44 \text{ cm}$, $I = 464 \text{ kA}$ and $B_T = 20 \text{ kG}$.

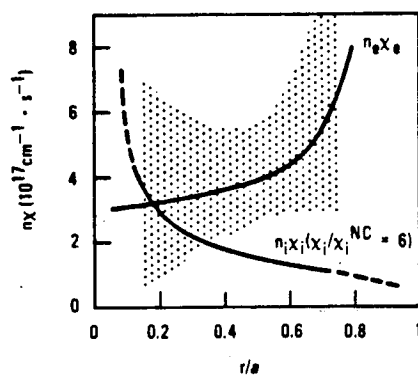


Fig.45 $n_e X_e$ and $n_i X_i$ as results from transport code analysis of H_2 Ohmic discharges in Doublet-III¹³⁶ for same parameters as Fig.44.

and Fig. 45¹³⁶). For higher densities the energy confinement times saturate and decrease with \bar{n} implying that neoclassical ion thermal conductivity is expected to dominate the energy transport. The constant anomalous factor of ion conduction, χ_i/χ_i^{NC} is also reported in ISX-A¹²⁸ (1 - 2), in TFR-600¹³⁸ (~ 5). Good agreement was reported between measured T_i and those calculated by neoclassical theories for TFR¹³⁹ and PLT,¹⁴⁰ but it is not T_i but $T_e - T_i$ that determines the power balance and the latter is difficult to measure accurately.

The energy balance is studied for XB discharges in beam injected Doublet III.¹⁴¹ Neutral beam particle deposition is calculated by using a modified version of the NFREYA code.¹⁴² Fast ion slowing down is modelled by using the method of Callen et al.¹⁴³ The code is used to solve the current diffusion and ion energy balance equations. The ion energy balance includes energy exchange with electrons and neutral beam produced fast ions as well as conduction, convection and charge exchange losses. The code adjusts Z_{eff} to match the loop voltage. Assuming that Z_{eff} is due to oxygen, the code adjusts the χ_i/χ_i^{NC} to match the measured neutron rate. Ion heat transport is consistent with four times the Chang-Hinton neoclassical heat transport¹³⁴ for $B_T = 22$ kG, $I_p = 520$ kA, $\bar{n}_e = 5.8 \times 10^{-13} \text{ cm}^{-3}$, $P_{tot} = 2.8$ MW, minorradius = 40 cm, $\kappa = 1.6$. The heat conduction of electron and ion is almost the same at $r = a/2$ (Fig. 46 (a)¹⁴¹), however, the electron heat conduction is higher near the edge and lower at the center than the ion heat conduction and, in terms of the volume integrated power the loss through electron channel is dominate (Fig. 46 (b)¹⁴¹).

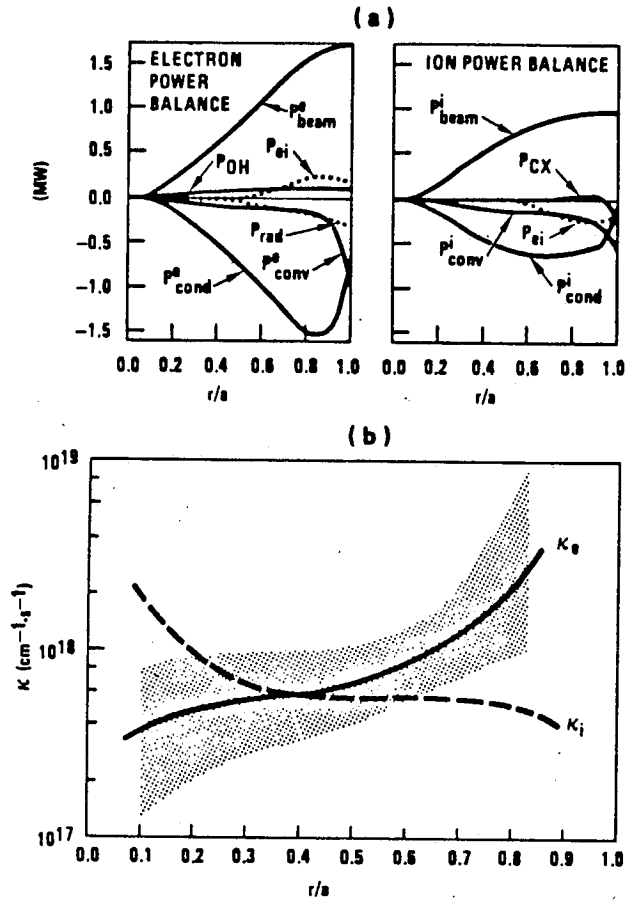


Fig.46 Transport analysis output for a typical XB discharge in Doublet-III¹⁴¹,
 $B_T = 22$ kG, $I_p = 520$ kA, $\bar{n}_e = 5.8 \times 10^{13} \text{ cm}^{-3}$, $a = 40$ cm, $\kappa = 1.6$,
 $P_{total} = 2.8$ MW.

The energy balance analysis in PDX discharges is carried out¹⁴⁴ by the kinetic transport code TRANSP.^{145,146} The data inputs to the code include electron density and temperature profiles, line averaged electron density, radiated power, central ion temperatures, plasma current and position, surface voltage, Z_{eff} , neutral beam power, injection voltage, and beam geometry. The calculations in the code are divided into five major sections: magnetic diffusion, thermal neutral penetration, beam heating, particle balance, energy balance. Ion conduction is assumed to be some multiple of the neoclassical value, in order to match the fit to the thermal charge exchange spectrum and the magnetically measured $\langle\beta_T\rangle$. The fully stripped oxygen is assumed the sole impurity. A typical example of the volume integrated ion and electron power balance profiles is shown in Fig. 47(a),(b)¹⁴⁴ for a three beam discharge with 1.5 T and 300 kA. For this case, $T_e(0) = 1.25$ keV, $T_i = 1.90$ keV and $\bar{n}_e = 3.8 \times 10^{13} \text{ cm}^{-3}$. A neoclassical multiplier of two, using Chang-Hinton¹³⁴ value, was needed to bring the fits to the measured and calculated thermal charge exchange spectra into agreement. Beyond the radius of 10-15 cm, the coupling of the ions to the electrons becomes the dominant loss term for the ions. The dominant loss term for the electrons is clearly the anomalous transport loss, which is attributed to thermal conduction. In contrast to the analysis of Doublet III, the electron conduction very substantially exceeds the ion transport loss across the plasma.

In summary, the electron energy transport is apparently anomalous in all tokamak discharges. The ion thermal transport is found to scale as the neoclassical heat conduction with a constant factor from 2 to 5 for most tokamak

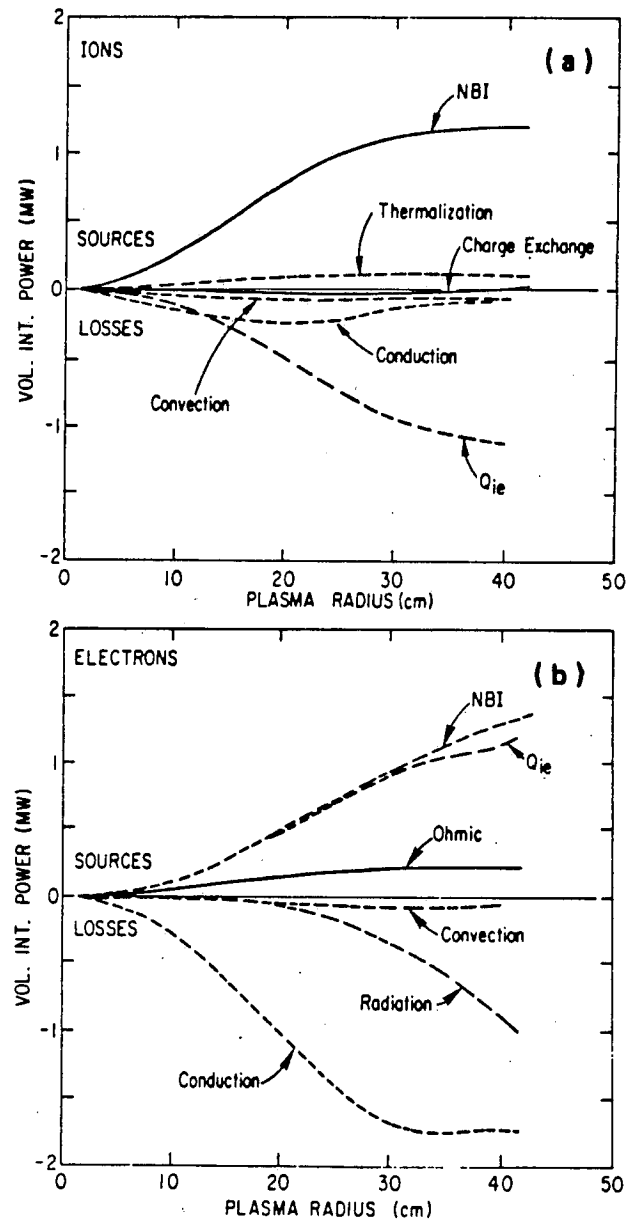


Fig.47 Transport code analysis in PDX¹⁴⁴ for three beam discharges with $B_T = 15$ kG and $I_p = 300$ kA.

discharges. It is not yet conclusive whether or not the ion energy transport must be anomalous whenever $\chi_i/\chi_i^{NC} > 1$. The important thing, however, is that the electron energy transport is the dominant energy loss channel for a variety of important discharge condition, no matter if the ion energy loss is considered as anomalous or not. The energy loss from electron channel can be estimated about two to three times of the energy loss from ion channel in the typical discharges of present day tokamaks.

XII. Electromagnetic Turbulence Model for Electron Transport

The subject of anomalous electron transport in tokamaks has been intensively investigated¹⁴⁷⁻¹⁵⁸ with a view to obtaining scaling laws for energy confinement and electron temperature. A very important feature of the recent tokamak experiments, namely the universal deterioration of energy confinement in the presence of auxiliary heating (irrespective of the heating scheme) has prompted several authors to propose mechanisms for anomalous transport that are expected to operate for Ohmic as well as auxiliary heating.¹⁵⁶⁻¹⁵⁹ Most of these mechanisms result in transport coefficients of the Ohkawa¹⁴⁷ type. These interesting phenomena indicate that there must exist a strong common feature to all these turbulence theories.

The analysis of the experimental evidence in XI shows that the energy loss of a tokamak is mainly through the electron channel rather than the ion channel. The candidate fluctuations responsible for the anomalous transport must be such that their effect on ions is minimized. The electromagnetic fluctuations obviously meet this requirement. The density dependence of the energy confinement time is another reason that favors electromagnetic fluctuations to be a candidate responsible for the anomalous transport, since the pure electrostatic fluctuations can not lead to the observed density dependence of transport in collisionless plasmas.

At this stage, it must be clearly stated that the anomalous transport may be a result of a variety of processes. A model based on a limited number of

processes is bound to have limitations. However, if a particular process has the potential for explaining some salient features of the experimental observations, it must be taken seriously. It is precisely in this spirit that we are arguing for the usefulness of a model based on the electromagnetic fluctuations.

We begin by making a comment on the linear stability of the electromagnetic fluctuation in collisionless tokamak plasmas. It is found that the electromagnetic fluctuations are strongly damped by the effects of magnetic shear. The shear damping is usually measured by $k_{\parallel} v_e$, where k_{\parallel} is the shear-induced parallel wavenumber, and v_e is the electron thermal speed. Obviously electromagnetic fluctuations can grow to significant levels only if $k_{\parallel} v_e$ were to become sufficiently small. At this stage, we have no clear cut mechanism for driving the electromagnetic mode unstable, although several possibilities are being pursued. Thus, we shall simply assume that an appropriate unstable mode (due to the shear damping suppression by some nonlinear effect, or a forced mode driven by some other fluctuations) exists and proceed and explore its consequences. This exploration has to be of a " generic " or a general nature because the details of the instability are not available.

A general analysis of turbulent diffusion [cf. Eq.(10.3.9)] shows that the known anomalous electron transport scalings due to electromagnetic micro-turbulence are characterized by one or more of the inverse time scales in the renormalized propagator: the mode frequency ω , $k_{\parallel} v_e$ (k_{\parallel} is the parallel wave number, v_e is the electron thermal velocity), and $\Gamma_k = k_{\perp}^2 D_{\perp}^{(T)}$ the turbulent collision frequency associated with the turbulent diffusion coefficient $D_{\perp}^{(T)}$.

Three distinct types of scaling emerge

- (1). Rechester-Rosenbluth type:¹⁴⁸ $k_{\parallel} v_e \sim \omega > \Gamma_k$ (weak turbulence scaling),

$$D_{\perp}^{(T)} = \frac{v_e}{k_{\parallel}} \left(\frac{\delta B}{B} \right)^2; \quad (12.1)$$

- (2). Ohkawa type¹⁴⁷ (strong turbulence scaling): $k_{\parallel} v_e \sim \Gamma_k > \omega$,

$$D_{\perp}^{(T)} = \frac{v_e k_{\parallel}}{k_{\perp}^2}, \quad \text{with} \quad \frac{\delta B}{B} \sim \frac{k_{\parallel}}{k_{\perp}}; \quad (12.2)$$

- (3). A new type (strong turbulence scaling, which we develop here): $\omega \sim \Gamma_k > k_{\parallel} v_e$,

$$D_{\perp}^{(T)} = \frac{\omega}{k_{\perp}^2}, \quad \text{with} \quad \frac{\delta B}{B} \sim \frac{\omega}{k_{\perp} v_e}. \quad (12.3)$$

For electromagnetic turbulence $k_{\perp} \sim \omega_{pe}/c$, and $k_{\parallel} \sim \hat{s}/qR$ in Eqs.(12.1) and (12.2).

It is interesting to observe that the saturation level $\delta B/B$ in the new type scaling [Eq.(12.3)] is an expression of the condition that the electron drift speed in the fluctuating fields ($v_e \delta B/B$) equals the perpendicular phase velocity of the wave. This balance is fundamentally different from the conventional balance where the nonlinear damping rate is balanced by the linear growth rate to yield $D_{\perp} \sim \gamma/k_{\perp}^2$.¹⁸ Clearly the saturation mechanism leading to the new type scaling has no dependence on γ , and results from a balance of the linear current with the nonlinear current induced by the fluctuations. Since the

underlying microturbulence is considered to be due to the expansion free energy, $\omega \sim \omega^*$, where ω^* is the diamagnetic drift frequency, is an obvious choice. The above argument then leads to a new formula for the anomalous electron energy transport:

$$D_{\perp}^{(T)} \sim \left(\frac{c}{\omega_{pe}} \right)^2 \omega^*. \quad (12.4)$$

Notice that k_{\parallel} plays a fundamental role in both the Rechester - Rosenbluth type weak turbulence as well as the Ohkawa type strong turbulence scaling. The basic point for seeking a new type scaling is that the inequality $k_{\parallel} v_e > \omega$ (which is needed to obtain these two scalings) is precisely the wrong limit for the electromagnetic modes to grow in a collisionless plasma. In fact, unless the effective k_{\parallel} is suppressed by some mechanism, it will be inconsistent to assume that the dominant transport process stems from essentially magnetic fluctuations.

Scaling implied by Eq.(12.4) can be rigorously derived from a theory of collisionless electromagnetic turbulence based on the Vlasov equation and the Ampere's law, in which the shear damping suppression is modelled by setting $k_{\parallel} = 0$. One must, of course, stipulate that somehow the required modes have grown to suprathermal levels.

XII.1 Theoretical Model

We now derive the nonlinear wave equation and show how it suggests the aforementioned [Eq.(12.4)] scaling for the diffusion coefficient. The diffusion

equation is then solved and its predictions are compared with a variety of tokamak experiments.

Our starting point for a low- β tokamak plasma is the system of two-dimensional electron drift kinetic equation ($k_{\parallel} = \nabla_{\parallel} = 0$) and the parallel component of Ampere's law:

$$\left\{ \partial_t + \left(\frac{v_{\parallel}}{B} \right) (\nabla \delta A_{\parallel} \times \mathbf{b}) \cdot \nabla + (e/mc) (\partial_t \delta A_{\parallel}) \partial_{\parallel} \right\} f = 0 \quad (12.1.1)$$

$$\nabla_{\perp}^2 \delta A_{\parallel} = \frac{4\pi e}{c} \int dv_{\parallel} v_{\parallel} \delta f, \quad (12.1.2)$$

where $f = f_0 + \delta f$ with $f_0 \equiv \langle f \rangle$ satisfying $\partial_t f_0 = 0$, and $\langle \dots \rangle$ denoting ensemble average.

A straightforward iteration procedure in which we retain terms up to $(\delta A)^3$ (in this simple model, the propagator of the drift kinetic equation is simply ω^{-1}) leads to our basic nonlinear wave equation

$$(\omega - \omega_{\mathbf{k}}) \delta A_{\mathbf{k}} = \sum_{\mathbf{k}_1 + \mathbf{k}_2 + \mathbf{k}_3 = \mathbf{k}} \epsilon^{(3)}(\mathbf{k}_1, \mathbf{k}_2, \mathbf{k}_3) \delta A_{\mathbf{k}_1} \delta A_{\mathbf{k}_2} \delta A_{\mathbf{k}_3} \quad (12.1.3)$$

with $\omega_{\mathbf{k}} = \omega^* (1 + \mathbf{k}^2 c^2 / \omega_{pe}^2)^{-1}$ where $\omega^* = (cT_e / eB) k_y L_T^{-1}$ is the diamagnetic drift frequency, $L_T^{-1} = T_e^{-1} (dT_e / dx)$ is the temperature gradient scale length, $\mathbf{k} = (\omega, \mathbf{k})$ and $\mathbf{k} = \mathbf{k}_{\perp}$ is the perpendicular wave number, $\omega_{pe} = (4\pi n e^2 / m)^{1/2}$ is the plasma frequency, and

$$\begin{aligned} \text{Re} \epsilon^{(3)}(\mathbf{k}_1, \mathbf{k}_2, \mathbf{k}_3) \equiv & \frac{3}{4} \left(\frac{\omega_{pe} v_e}{cB} \right)^2 \frac{(\mathbf{k}_1 \times \mathbf{k}) \cdot \mathbf{b} (\mathbf{k}_2 \times \mathbf{k}_3) \cdot \mathbf{b}}{(\omega_2 + \omega_3)(\mathbf{k}^2 + \omega_{pe}^2 / c^2)} \\ & \left(\frac{\omega_2 - \omega^*(k_2)}{\omega_2} - \frac{\omega_3 - \omega^*(k_3)}{\omega_3} \right), \end{aligned} \quad (12.1.4)$$

$$\text{Im}\epsilon^{(3)}(k_1, k_2, k_3) \equiv - \frac{\omega_{ce}}{B^2(\omega_2 + \omega_3)(\mathbf{k}^2 + \omega_{pe}^2/c^2)} \left[(\omega_2 \mathbf{k}_3^2 + \omega_3 \mathbf{k}_2^2) \cdot (\mathbf{k}_1 \times \mathbf{k}) \cdot \mathbf{b} + \frac{1}{2} \omega_1 (\mathbf{k}_2 \times \mathbf{k}_3) \cdot \mathbf{b} (\mathbf{k}_3^2 - \mathbf{k}_2^2) \right]. \quad (12.1.5)$$

Notice that Eq.(12.1.3) does not contain a linear growth rate term. In fact, our model is quite independent of the linear instability responsible for turbulence as long as it is assumed that some instability with a characteristic frequency ω^* exists. Consequently, the turbulent spectrum cannot be derived by the conventional balancing of the linear growth rate with nonlinear damping. Instead, we derive our spectrum by the condition that the nonlinear dispersion arising from the mode-coupling term balances the linear terms.

We now follow the standard methodology of renormalized strong turbulence theories; we divide the nonlinear $[(\delta A)^3]$ term into coherent and intrinsically incoherent parts, group the nonlinear coherent term with the linear term (renormalization of the wave propagator), and finally obtain the spectrum equation by multiplying both sides of the renormalized equation by their complex conjugates and using quasi-Gaussian approximation to evaluate the correlations

$$I_k = \frac{2 \sum_{k_1+k_2+k_3=k} \epsilon(k_1, k_2, k_3) \hat{\epsilon}^{(3)*}(k_1, k_2, k_3) I_{k_1} I_{k_2} I_{k_3}}{\left(\omega - \omega_k - 2 \sum_{k_1} \text{Re}\epsilon^{(3)}(k_1, k, -k_1) I_{k_1} \right)^2 + \left(2 \sum_{k_1} \text{Im}\epsilon^{(3)}(k_1, k, -k_1) I_{k_1} \right)^2} \quad (12.1.6)$$

where $I_k \equiv \langle \delta A_k \delta A_k^* \rangle$, and

$$\hat{\epsilon}^{(3)}(k_1, k_2, k_3) \equiv \epsilon^{(3)}(k_1, k_2, k_3) + \epsilon^{(3)}(k_2, k_3, k_1) + \epsilon^{(3)}(k_3, k_1, k_2).$$

Since $\text{Im}\epsilon^{(3)}$ is much smaller than $\text{Re}\epsilon^{(3)}$ and can be neglected, Eq.(12.1.6) becomes a simple numerical integral equation in the dimensionless quantities $\hat{\omega}, \hat{I}_k, \hat{k}_\perp$ which have the following normalizations:

$$\mathbf{k}_\perp = \hat{\mathbf{k}}_\perp (\omega_{pe}/c) \quad (12.1.7)$$

$$I_k = \hat{I}_k (c/\omega_{pe})^4 (B\omega_0^*/v_e)^2 \quad (12.1.8)$$

$$\omega = \hat{\omega}\omega_0^* \quad (12.1.9)$$

with $\omega_0^* \equiv (dT_e/dr)(\omega_{pe}/eB)$, i.e., the value of ω_* for $k_y = \omega_{pe}/c$. Remembering that $I_k = \langle \delta A_k \delta A_k^* \rangle = k_\perp^{-2} \langle \delta B \rangle^2$, we readily deduce from Eq.(12.1.8) that the perturbed magnetic field must follow the scaling

$$\frac{\langle \delta B \rangle}{B} \sim \frac{\omega^*}{k_\perp v_e} \equiv \frac{\omega^* c}{v_e \omega_{pe}} \quad (12.1.10)$$

which is just the scaling obtained by Drake *et al.* in a similar model. ¹⁴⁹ Eq. (12.1.10) allows a very simple physical interpretation; the saturation is achieved when the electron drift velocity in the fluctuating field ($\delta v_d \sim v_\parallel \delta B/B \sim v_e \delta B/B$) resonates with the perpendicular phase velocity of the wave. This scaling is crucially dependent on the assumption of a small k_\parallel electromagnetic turbulence, therefore, it is not surprising to find its consistency with diffusion of the "strong turbulence" type, where k_\parallel is small.

Whithin the framework of the renormalized strong turbulence theories, it is known that the electron turbulent diffusion coefficient in a fluctuating magnetic field δB obeys

$$D_\perp^{(T)} \sim \frac{v_e}{k_\perp} \delta B/B \quad (12.1.11)$$

which, when combined with Eq.(12.1.10), yields

$$D_{\perp}^{(T)} \sim \frac{\omega^*}{k_{\perp}^2}$$

or explicitly,

$$D_{\perp}^{(T)} = \xi(1 + \alpha/\eta_e) \frac{dT_e}{dr} \frac{c^2}{eB\omega_{pe}}, \quad (12.1.13)$$

where $\alpha \sim 1$, $\eta_e \equiv d \ln T_e / d \ln n$, and ξ is a number to be determined.

XII.2 Comparison with Tokamak Experiments

Substitution of Eq.(12.1.13) into the energy transport equation (in a cylindrical model)

$$\frac{1}{r} \frac{d}{dr} r D_{\perp}^{(T)} \frac{d}{dr} n T_e = P_e(r) \quad (12.2.1)$$

leads to the dimensionless system (where, for simplicity $\eta_e > 1$ has been assumed)

$$\frac{1}{x} \frac{d}{dx} \frac{x}{\sqrt{\tilde{n}(x)}} \frac{d\tilde{T}_e}{dx} \frac{d}{dx} \tilde{n}(x) \tilde{T}_e(x) = \kappa \tilde{P}_e(x) \quad (12.2.2)$$

$$\kappa \equiv \frac{\Lambda^2}{2\xi T_*^2} \equiv eB\omega_{pe}(0) \bar{P}_e / 2\xi c^2 n(0) T_*^2, \quad (12.2.3)$$

where $x = r/a$ is the normalized radial variable, $\tilde{n}(x) = n(r)/n(0)$, $n(0)$ is the central electron density, $\tilde{T}_e(x) = T_e(r)/T_*$, T_* is some arbitrary normalizing temperature, and $\tilde{P}_e(x) = P_e(r)/\bar{P}_e$, where \bar{P}_e is scaled to the average net electron power density in the tokamak. The structure of Eq.(12.2.2) leads us to conclude that the central electron temperature must be of the form

$$T_e(0) = T_* \tilde{T}_e(0) = T_* F\left(\frac{\Lambda^2}{2\xi T_*^2}, b, p\right) = \left[\frac{eB\omega_{pe}(0) a^3 \bar{P}_e}{c^2 n(0)}\right]^{1/2} \frac{\tilde{F}(b, p)}{\sqrt{2\xi}}, \quad (12.2.4)$$

where $\tilde{F}(b, p)$ is a form factor depending on the parameter b and p which are respectively the characteristics of the electron power, and number density profiles. Notice that the last step in Eq.(12.2.4) is merely a statement of the fact that the central temperature must not depend on our normalization choice.

Numerical solutions of Eq.(12.2.2) confirm Eq.(12.2.4), and in addition, reveal the following interesting properties:

(1). The normalized temperature profile $\tilde{T}_e(x)$ remains essentially unaltered for physically reasonable density profiles. This is in agreement with the experimental observation commonly referred to as the decoupling between energy transport and particle transport.¹⁶⁰

(2). For a large variety of power density profiles $\tilde{P}_e(x)$, the variation in $\tilde{T}_e(x)$ is comparatively small. Even for the " edge heating " case, a small amount of ohmic heating power in the central region is sufficient to provide a reasonable $\tilde{T}_e(x)$ profile, thus supporting the so-called " principle of profile consistency ".¹⁶⁰ The curve 1 and 2 in Fig. 48 compare the results of the experiments in edge heating¹⁶¹ in TFTR, and of the results in normal heating. There are exceptions, however: (i) if $\tilde{P}_e(x)$ vanishes completely in the central region (like some stellarator experiments¹⁶²), the temperature profile develops a " flat top " in the central region; (ii) if the net electron power density is very small or negative in the edge region, or it is highly concentrated in the central region, a substantial deviation of $\tilde{T}_e(x)$ from its normal shape may and does occur (Curve 3 in Fig. 48).

(3). The form factor $\tilde{F}(b, p)$ is generally an insensitive function of b and

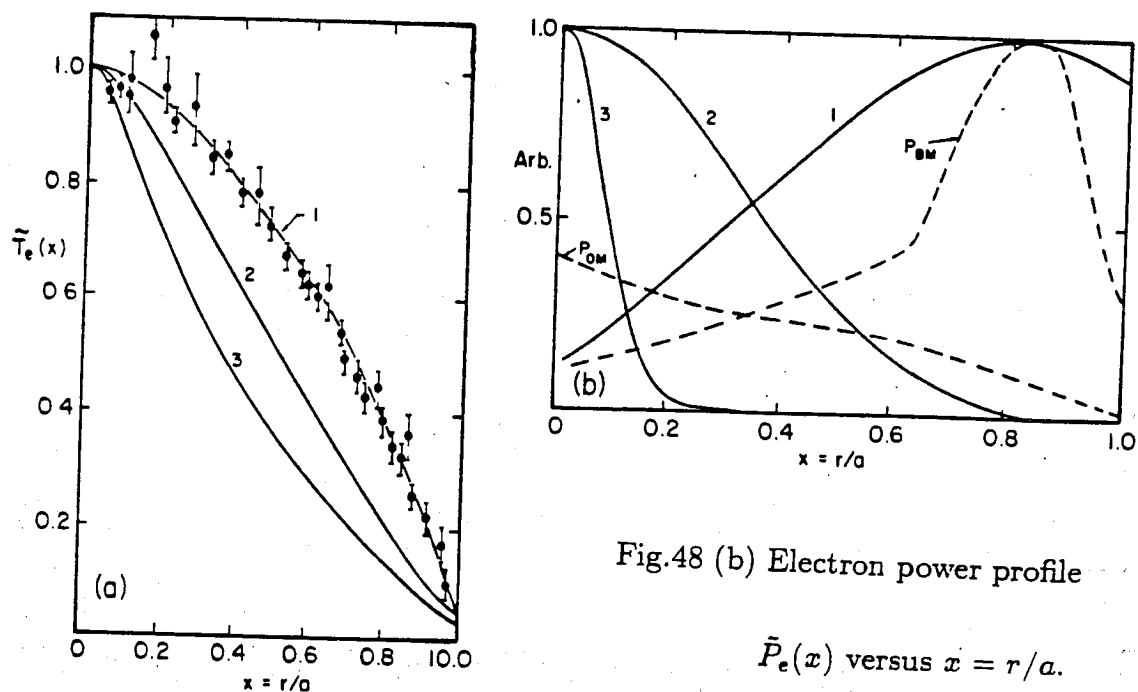


Fig.48 (b) Electron power profile

 $\tilde{P}_e(x)$ versus $x = r/a$.

Fig.48 (a) $\tilde{T}_e(x)$ versus $x = r/a$. Solid curves 1, 2, 3 in Fig.48 (a) are the electron temperature profiles corresponding to the electron power density profiles represented, respectively, by solid curves 1, 2, 3 in Fig.48 (b). The dots with error bars represent the experimental results in TFTR "edge heating"¹⁶¹ corresponding to power density profile given by dashed lines in Fig.48 (b).

Fig.48

p ; it ranges between 0.9 - 1.1 for the values b and p which characterize normal discharges. For some unusual discharges, e.g., those with power density highly concentrated in the center, $\tilde{F}(b, p)$ may be well above 1.4. However, the narrower temperature profile does not mean a substantial gain in electron stored energy.

Before presenting a detailed comparison of the theoretically predicted electron temperature $T_e(r)$ with experiments, we point out several limitations of the present approach:

(a) The present theory can only cope with the situations where the MHD activity is either absent or has a minor effect on the electron dynamics. For example, in some cases the sawtooth activity does construct a flat-top in the temperature profile within the inversion surface. In such cases, the present theory is valid only in the region outside the inversion surface, i.e., the "confinement region".

(b) Since the detailed knowledge of $\tilde{P}_e(x)$ is generally not available, Λ is taken to be a measure of $T_e(0)$ to be compared with the experiment (the parameter ξ is supposed to be machine independent).

$$\Lambda \equiv \left[\frac{eB\omega_{pe}(0)a^3\tilde{P}_e}{c^2n(0)} \right]^{1/2} = 2.44 \left[\frac{B_{[T]}(a/R)P_{e[MW]}}{\sqrt{n_{[14]}(0)}} \right]^{1/2} [\text{keV}] \quad (12.2.5)$$

where $B_{[T]}$ is the magnetic field B in Tesla, $n_{[14]}$ is the density in 10^{14} cm^{-3} , $P_{e[MW]}$ is the bulk electron power in MW, R is the major radius. For those experiments with sawtooth activity the Λ should be reinterpreted as the value of Eq.(12.2.5) multiplied by a factor. This factor is characterized by the ratio

of normalized temperature at the inversion surface to that at the center. To determine the ratio use is made of typical theoretical profile [for instance, the curve 2 in Fig.48.a] and the experimental value of the inversion surface.

(c) The present theory [Eq.(12.1.1), and thereafter] is not likely to be valid for discharges where the electron distribution function departs substantially from a Maxwellian, for example, in discharges dominated by lower hybrid current drive at low density.

Guided by the aforementioned consideration, we display in Fig. 49 a comparison between the theoretical predicted (characterized by Λ) and experimentally observed [$T_e(0)$] central electron temperature. The data is primarily collected from published literature. We have considered discharges ranging from 0.3 to 7 keV in temperature with a variety of heating schemes such as Ohmic (OH), ion cyclotron resonance (ICRH), electron cyclotron resonance (ECRH), and neutral injection (NI) heating. It is clear that most of the points ($\Lambda - T_e(0)$ plot) fall in a straight narrow band parallel to the $\Lambda = T_e(0)$ line. This allows us to estimate $\xi \sim 0.8$, although some points are located on the upper side of the narrow band. These latter points are known to correspond to the L-mode, and are believed to be plagued by strong MHD activity. However, even these data points are not far from our predictions. The principal message of the plot is strikingly obvious: all these machines with a large variation in parameters and heating schemes are characterized by a region (the confinement region) where electron dynamics is anomalous and dominant.

In addition to comparing the specific values of Λ and $T_e(0)$, we must also

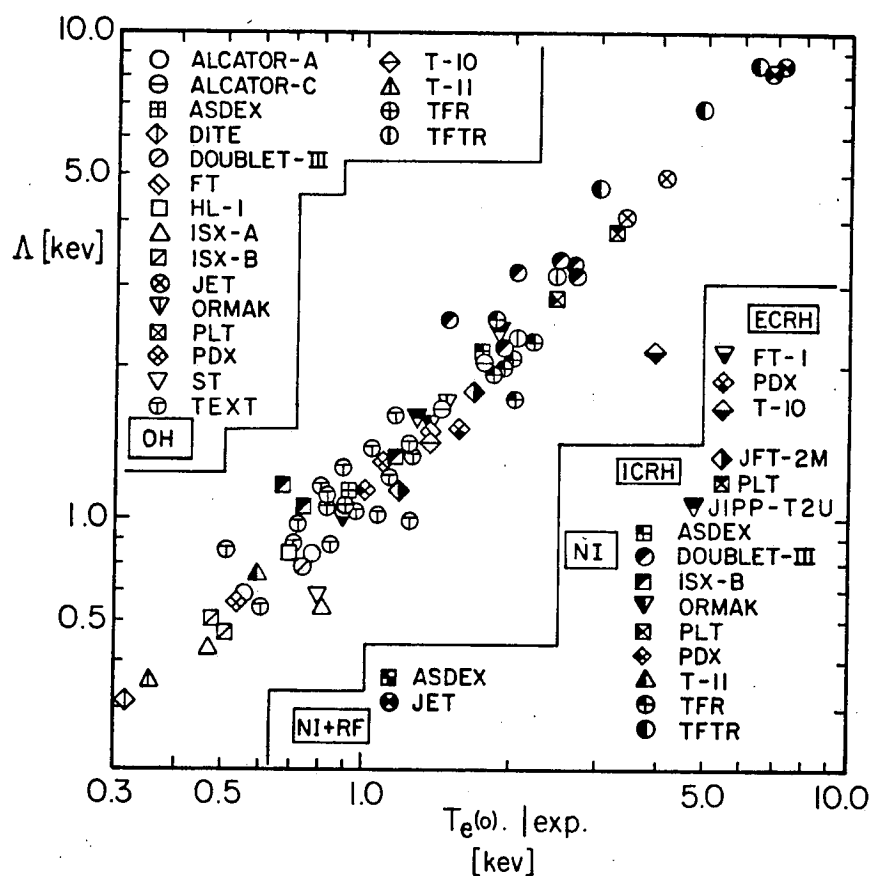


Fig.49 Λ versus $T_{e(0)}|_{exp.}$, Λ - the characteristic central electron temperature given by Eq.(12.2.5), and $T_{e(0)}|_{exp.}$ the experimental result.

compare the predicted and observed parametric dependence of the central electron temperature, in particular the scaling with the external magnetic field B , the density n , and the total electron power P_e . Before displaying our data, we would like to mention that several empirical and semi-empirical scaling of $T_e(0)$ have been suggested for tokamaks with Ohmic¹⁶³⁻¹⁶⁶ as well as neutral beam heating.¹⁶⁷ Most of these scalings are similar to the scaling contained in Λ . It indicates that the $T_e(0)$ scaling alone is not a strong criterion to prove or disprove a model, on which basis the corresponding scaling is inferred.

For ohmically heated tokamaks with Spitzer-Harm resistivity, the local electron energy confinement is derived to be

$$\tau_{E_e}(0) \sim Z_{eff}^{-2/7} n^{9/14} B^{1/7} a^{5/7} R^{4/7} q^{4/7}(a) \quad (12.2.6)$$

The predicted density dependence of $\tau_{E_e}(0) \sim n^{9/14}$ is compared with the Alcator A data¹⁶⁸ in Fig.50. The agreement is very good up to $n \sim 8 \times 10^{14} \text{ cm}^{-3}$ beyond which the energy loss through the ion channel probably accounts for the deviation.

Because of difficulties involved in a direct measurement of \bar{P}_e we show only one experiment on Doublet III with auxiliary heating¹⁴¹ to compare our $T_e(0) \sim P_e^{1/2}$ scaling. It is easy to see from Fig. 51 that the theoretical scaling is an excellent fit to the experimental data, where $P_{total} \sim P_e$ is assumed. From the temperature scaling, the electron energy confinement time is then inferred to be $\tau_{E_e} \sim P_e^{-1/2}$.

We have analyzed the anomalous electron transport on the model based on a model ($k_{\parallel} \sim 0$) electromagnetetic microturbulence driven by electron

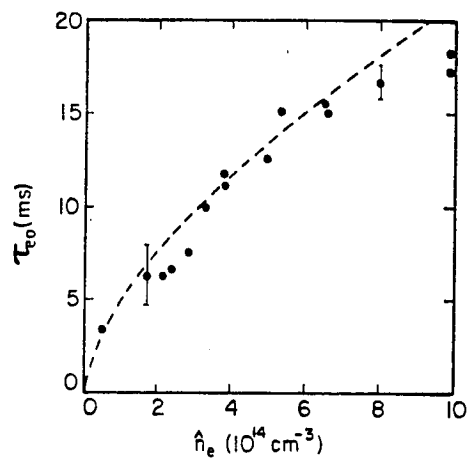


Fig.50 $\tau_{E_e}(0)$ versus \hat{n}_e . Dots represent the experimental results on Alcator - A¹⁶⁸. The dashed line represents $\hat{n}^{9/14}$ curve fitting to the data. ($\hat{n}_e = 6 \times 10^{14} \text{ cm}^{-3}$ is taken as reference point.)

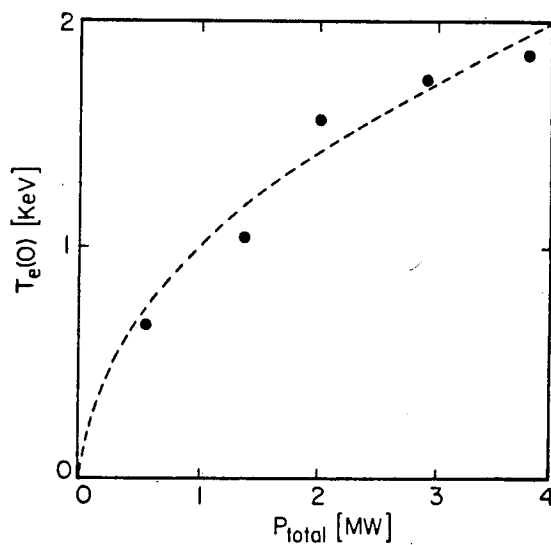


Fig.51 $T_e(0)$ versus P_{total} . Dots are experimental results on Doublet-III¹⁴¹. The dashed line is the theoretical curve $T_e(0) \sim P_{total}^{1/2}$ ($P_{total} = 3 \text{ MW}$ is taken as reference point).

temperature gradients. We find that the predictions of this simple theory are in good agreement with tokamak experiments.

XIII. η_e - Mode and the Induced Electron Transport

The electromagnetic wave is not the unique choice for fluctuations that have small effect on the ions. If the fluctuation wavelength is much smaller than the ion Larmor radius, the ion response to such a wave is essentially adiabatic, and the convective nonlinearity goes to zero. This finite Larmor radius effect suppresses the ion diffusive term in the transport equation by the factor $\Gamma_0(b) \ll 1$ [Eq.(10.3.10)].

In collisionless plasma, the η_e - mode is essentially an electrostatic wave with perpendicular wavelength so short ($k_\perp \rho_i \gg 1$) that the ions respond adiabatically. This mode is destabilized by the finite electron temperature gradient. Since the ion transport due to this mode is negligible, we examine its consequences for the electron transport.

In a shearless slab model the linear gyrokinetic equation⁷⁵ is solved for Maxwellian equilibrium distribution. The perturbed distribution is found to be (j is the species index)

$$\begin{aligned} \delta f_k(v_\parallel) = & \frac{q_j}{T_j} f_{0j}(v_\parallel) \delta \phi_k - \frac{q_j}{T_j} \frac{1}{\omega - k_\parallel v_\parallel} \left\{ \omega_{jn}^* \eta_j b_j \Gamma_1(b_j) \right. \\ & \left. - (\omega - \omega_{jn}^* [1 + \eta_j \left(\frac{m_j v_\parallel^2}{2T_j} - \frac{1}{2} - b_j \right)]) \Gamma_0(b_j) \right\} f_{0j}(v_\parallel) \left(\delta \phi_k - \frac{v_\parallel}{c} \delta A_k \right), \end{aligned} \quad (13.1)$$

where q_j, m_j, T_j are respectively the charge, mass and temperature, ω_{jn}^* is the diamagnetic frequency due to density gradients, $\eta_j \equiv (L_n/L_{T_j})$, $b_j \equiv (1/2)\rho_j^2 k_\perp^2$, ρ_j is the Larmor radius, $\Gamma_n(b_j) = I_n(b_j) \exp(-b_j)$ with I_n - the modified Bessel function of n th order, $f_{0j}(v_\parallel) \equiv (1/v_{th,j} \sqrt{\pi}) \exp(-v_\parallel^2/v_{th,j}^2)$,

with $v_{th,j}$ the thermal velocity, $T_j \equiv (1/2)m_j v_{th,j}^2$, and $k \equiv (\omega, k_{\parallel}, k_{\perp})$.

The perturbed density and current result from the appropriate v_{\parallel} moments:

$$\begin{aligned} \delta n_k = & -\frac{q_j n}{T_j} \left\{ 1 - \left(1 - \frac{\omega_{jn}^*}{\omega} \right) \Gamma_0(b_j) + \frac{\omega_{jT}^*}{\omega} b_j [\Gamma_1(b_j) - \Gamma_0(b_j)] \right\} \delta \phi_k \\ & + \frac{q_j n}{T_j} \sigma_j(k) \left(\delta \phi_k - \frac{\omega}{k_{\parallel} c} \delta A_k \right) \end{aligned} \quad (13.2)$$

and

$$\delta J_{\parallel,k} = -\frac{q_j^2 n}{T_j} \frac{\omega}{k_{\parallel}^2} \sigma_j(k) \left(\frac{\omega}{c} \delta A_k - k_{\parallel} \delta \phi_k \right) \quad (13.3)$$

with

$$\begin{aligned} \sigma_j(k) \equiv & \frac{\omega_{jn}^* - \omega}{\omega} \Gamma_0(b_j) [1 + \zeta_j Z(\zeta_j)] + \frac{\omega_{jT}^*}{\omega} \left\{ [1 + \zeta_j Z(\zeta_j)] b_j [\Gamma_1(b_j) - \Gamma_0(b_j)] \right. \\ & \left. + [\zeta_j + \zeta_j^2 Z(\zeta_j) - 1/2 Z(\zeta_j)] \zeta_j \Gamma_0(b_j) \right\}, \end{aligned} \quad (13.4)$$

where $\zeta_j \equiv \omega/k_{\parallel} v_{th,j}$ and Z - the dispersion function. For adiabatic ions, $\Gamma_n(b_i) \rightarrow 0$.

Substituting Eqs.(13.2) to (13.4) into the quasi-neutrality equation and Ampere's law yields the dispersion relation for the η_e - mode.

$$\tau + 1 - \left(1 - \frac{\omega_{en}^*}{\omega} \right) \Gamma_0(b_e) + \frac{\omega_{eT}^*}{\omega} b_e [\Gamma_1(b_e) - \Gamma_0(b_e)] = \frac{k_{\perp}^2 \sigma_e(k)}{k_{\perp}^2 + 2\zeta_e^2 \frac{\omega_{pe}^2}{c^2} \sigma_e(k)}, \quad (13.5)$$

where $\tau \equiv T_e/T_i$. The term proportional to $(\omega_{pe}/c)^2$ in the denominator of the last term of Eq.(13.5) arises from electromagnetic part of the perturbation. The quantity $2\zeta_e^2 \sigma_e(k) (\omega_{pe}^2/c^2 k_{\perp}^2)$ then measures the ratio of the electromagnetic to electrostatic component.

Marginal stability ($\text{Im}\omega = 0$) condition is determined by solving the following two equations,

$$\eta_e d_n \Gamma_0(b_e) \zeta_e^2 = (\eta_e/2 - 1) d_n \Gamma_0(b_e) - \eta_e d_n b_e [\Gamma_1(b_e) - \Gamma_0(b_e)] + \zeta_e \Gamma_0(b_e) \quad (13.6)$$

and

$$\tau + 1 - \Gamma_0(b_e) + \frac{d_n \Gamma_0(b_e)}{\zeta_e} + \frac{d_n}{\zeta_e} \eta_e b_e [\Gamma_1(b_e) - \Gamma_0(b_e)] = \frac{\frac{d_n \eta_e}{2 \zeta_e} \Gamma_0(b_e)}{1 + \Gamma_0(b_e) \frac{d_n \eta_e}{\hat{k}_\perp^2 \zeta_e}}, \quad (13.7)$$

where $\hat{k}_\perp^2 \equiv k_\perp^2 c^2 / \omega_{pe}^2$, $d_n \equiv \omega_{en}^* / |k_\parallel| v_e$.

The conductivity [defined by Eq.(13.4)] at the marginal stability is found to be

$$\sigma_e(k) = \frac{1}{2} \frac{\omega_{eT}^*}{\omega} \Gamma_0(b_e) \quad (13.8)$$

After some algebraic manipulations on the Eqs.(13.6) and (13.7), we obtain

$$\zeta_e = \frac{d_n \left(1 + \frac{\hat{\tau}}{\hat{k}_\perp^2}\right) [(\eta_e/2) \Gamma_0(b_e) - \hat{\Gamma}(b_e)]}{\hat{\tau} \left(1 + \frac{\Gamma_0(b_e)}{\hat{k}_\perp^2}\right) + X \Gamma_0(b_e) \hat{\Gamma}(b_e)}, \quad (13.9)$$

and a quadratic equation for $X \equiv d_n^2 \eta_e / \hat{k}_\perp^2$,

$$\begin{aligned} \Gamma_0^2(b_e) \hat{\Gamma}^2(b_e) X^2 + \left\{ \Gamma_0(b_e) \hat{\Gamma}(b_e) (2\hat{\tau} + \Gamma_0(b_e) + \Gamma_0(b_e) \frac{\hat{\tau}}{\hat{k}_\perp^2}) \right. \\ \left. - (1 - \frac{\hat{\tau}}{\hat{k}_\perp^2})^2 (\frac{\eta_e}{2} \Gamma_0(b_e) - \hat{\Gamma}(b_e)) \hat{k}_\perp^2 \Gamma_0(b_e) \right\} X \\ + \hat{\tau} [\hat{\tau} + \Gamma_0(b_e)] \left(1 + \frac{\Gamma_0(b_e)}{\hat{k}_\perp^2}\right) = 0, \end{aligned} \quad (13.10)$$

where

$$\hat{\tau} = \tau + 1 + \Gamma_0(b_e), \quad \hat{\Gamma}(b_e) \equiv \Gamma_0(b_e) + \eta_e b_e [\Gamma_1(b_e) - \Gamma_0(b_e)].$$

Only two positive roots of Eq.(13.10) are meaningful. The critical point occurs when the two positive roots merge. The necessary condition for instability turns out to be

$$\eta_e \geq [\eta_e]_{cr.} = \frac{K_a}{K_d} \quad (13.11)$$

with

$$K_a = \left(1 - \frac{\hat{\tau}}{\hat{k}_\perp^2}\right)^2 \hat{k}_\perp^2 + 2\hat{\tau} + \Gamma_0\left(1 + \frac{\hat{\tau}}{\hat{k}_\perp^2}\right) + 2\sqrt{\hat{\tau}(\hat{\tau} + \Gamma_0)\left(1 + \frac{\Gamma_0}{\hat{k}_\perp^2}\right)}$$

and

$$K_d = \left(1 - \frac{\hat{\tau}}{\hat{k}_\perp^2}\right)^2 \hat{k}_\perp^2 \left[\frac{1}{2} + b_e\left(1 - \frac{\Gamma_1}{\Gamma_0}\right)\right] + b_e\left(1 - \frac{\Gamma_1}{\Gamma_0}\right) \left[2\hat{\tau} + \Gamma_0\left(1 + \frac{\hat{\tau}}{\hat{k}_\perp^2}\right) + 2\sqrt{\hat{\tau}(\hat{\tau} + \Gamma_0)\left(1 + \frac{\Gamma_0}{\hat{k}_\perp^2}\right)}\right],$$

where the argument of $\Gamma_n(b_e)$ is suppressed.

In the electrostatic limit ($\hat{k}_\perp^2 \rightarrow \infty$), Eq.(13.11) reduces to

$$[\eta_e]_{cr.} = \frac{1}{\frac{1}{2} + b_e \left[1 - \frac{I_1(b_e)}{I_0(b_e)}\right]} \quad (13.12)$$

The critical $\eta_e([\eta_e]_{cr.})$, given by Eq.(13.11), is plotted versus b_e in Fig. 52 for given τ and \hat{k}_\perp^2 (or β_e). It shows that the electromagnetic part has a strong stabilizing effect on the mode at longer wavelength. For example, when $\tau = 1$, $\hat{k}_\perp^2 = 10.0$ and $\beta_e = 0.005$, the η_e - mode can not be destabilized unless

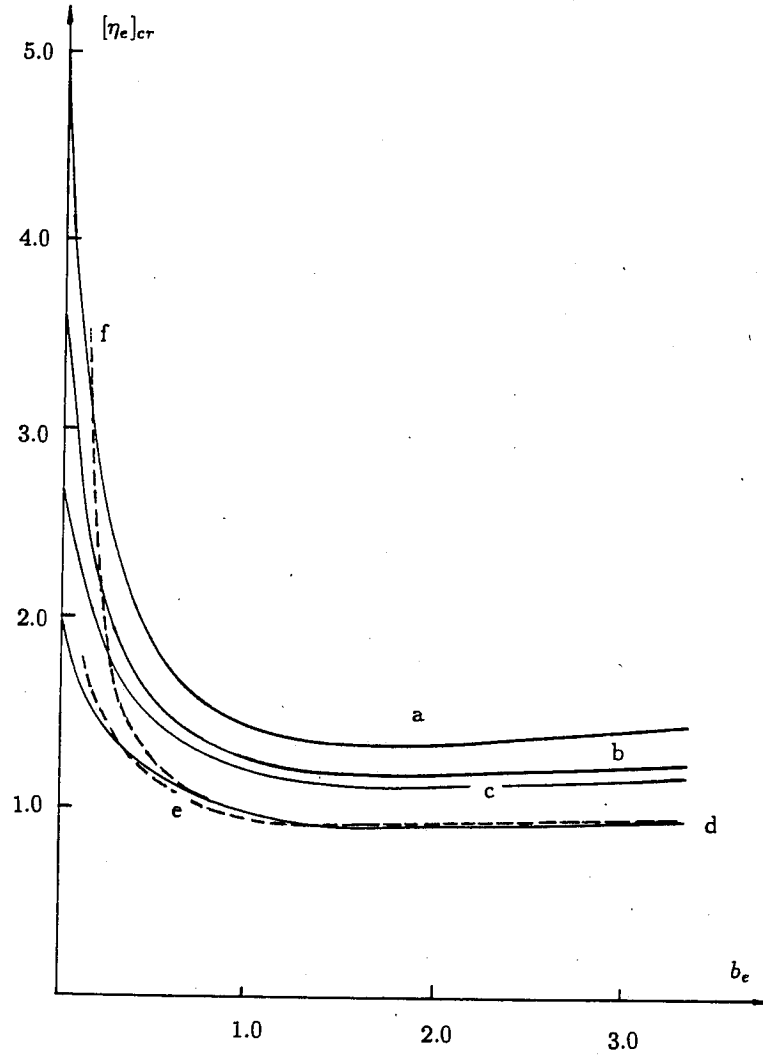


Fig.52 Minimum marginal stability of η_e mode for parameters $b_e = \rho_e^2 k_\perp^2 / 2 = (1/2)\beta_e (k_\perp c / \omega_{pe})^2$. Curve a: $\tau = 2.0, (k_\perp c / \omega_{pe})^2 = 10.0$; Curve b: $\tau = 1.0, (k_\perp c / \omega_{pe})^2 = 10.0$; Curve c: $\tau = 0.5, (k_\perp c / \omega_{pe})^2 = 10.0$; Curve d: $\tau = 1.0, (k_\perp c / \omega_{pe})^2 = 10^4$, Curve e: $\tau = 1.0, \beta_e = 1.0 \times 10^{-3}$, Curve f: $\tau = 1.0, \beta_e = 1.0 \times 10^{-2}$ respectively. Stable regions are below the corresponding curves.

$\eta_e > 3.4$ (Fig.52 curve b). However, when the electromagnetic part is ignored [Eq.(13.12)], the stability threshold is reduced to $\eta_e > 2.0$.

In Fig. 53 the threshold of η_e versus $|k_{\parallel}|v_e/\omega_{en}^*$ is shown for fixed τ, b_e and β_e . The two edges of $\eta_e - |k_{\parallel}|v_e/\omega_{en}^*$ curves in Fig. 53 are two positive roots of Eq.(13.10), while the minimum is determined by Eq.(13.11).

Substituting the solution of Eq.(13.10), X or $d_n(> 0)$, into Eq.(13.9) results in the frequency of the η_e - mode at marginal stability [Fig. 54]. We illustrate in Fig. 55 the threshold \hat{k}_{\perp}^2 versus $|k_{\parallel}|v_e/\omega_{en}^*$ for fixed η_e, τ , and β_e . It is found that the minimum $\hat{k}_{\perp}^2 \equiv k_{\perp}^2 c^2/\omega_{pe}^2$ for instability is quite sensitive to η_e . When $\eta_e < 2.0$, the mode can only be destabilized for $k_{\perp} c/\omega_{pe} \gg 1$.

In contrast with the η_i - mode of collisionless plasmas,¹¹⁹ there is enhancement of stability threshold for the η_e - mode at small $|k_{\parallel}|v_e/\omega_{en}^*$ [Fig. 53]. This is caused by the stabilizing effect of the electromagnetic part . The stabilizing effect of the electromagnetic part on the η_i - mode can be ignored, however.

The dispersion relation Eq.(13.5) is solved numerically for both the growth rate and the condition for marginal stability. The latter results are in agreement with analytical ones given by Eqs.(13.9) and (13.10). In Fig.56 the growth rate of Eq.(13.5) is compared with the corresponding results in a sheared slab model,¹⁵⁹ whereupon k_{\parallel} of the shearless slab model is identified as L_s^{-1} , the inverse shear length of the sheared slab model. The qualitative resemblance between the two implies the soundness for the results of the simple shearless model.

The phase space $(\omega - k_{\parallel}v_e)$ properties of the η_e mode are shown in Fig.

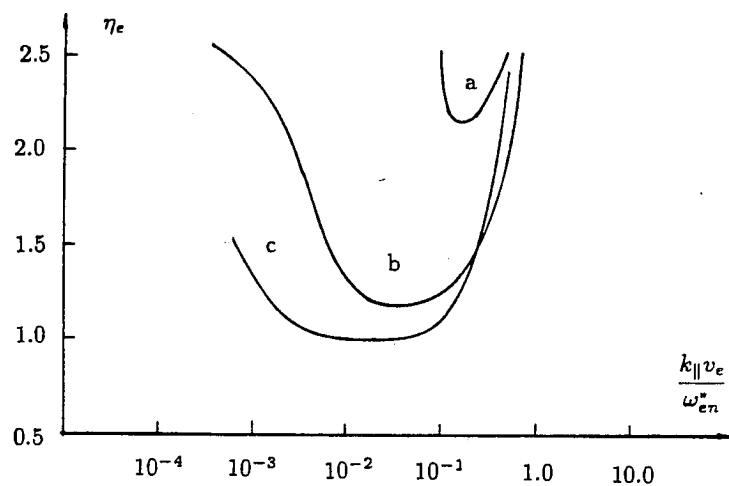


Fig.53 (a)

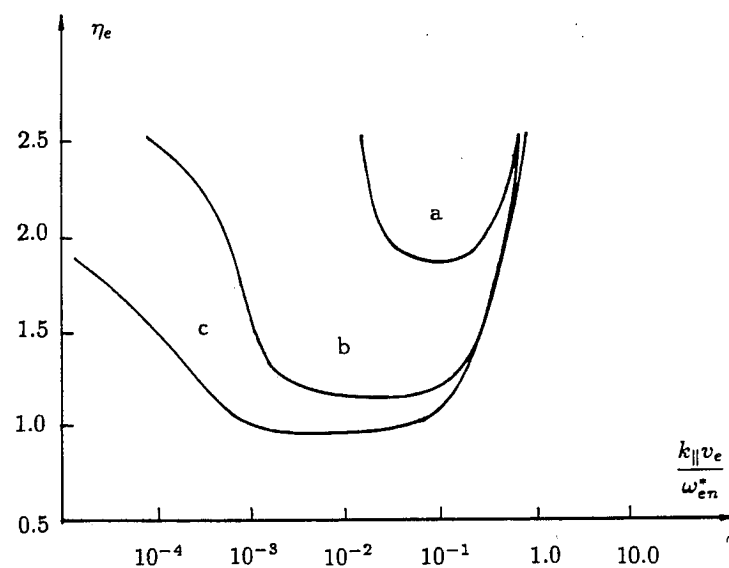


Fig.53 (b) Marginal stability for same parameters as Fig.53 (a)
except $\beta_e = 2.0 \times 10^{-3}$

Fig.53 Marginal stability of η_e - mode for $\tau = 1.0, \beta_e = 1.0 \times 10^{-3}$. $b_e = 0.1, 0.5, 1.0$ for curves a, b, c respectively. Stable regions are below corresponding curves.

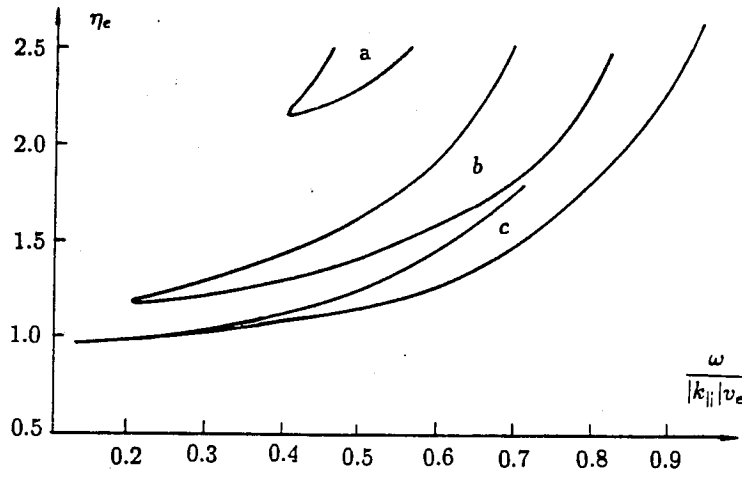


Fig.54 (a) Marginal stability of η_e - mode for same parameters as Fig.53 (a).

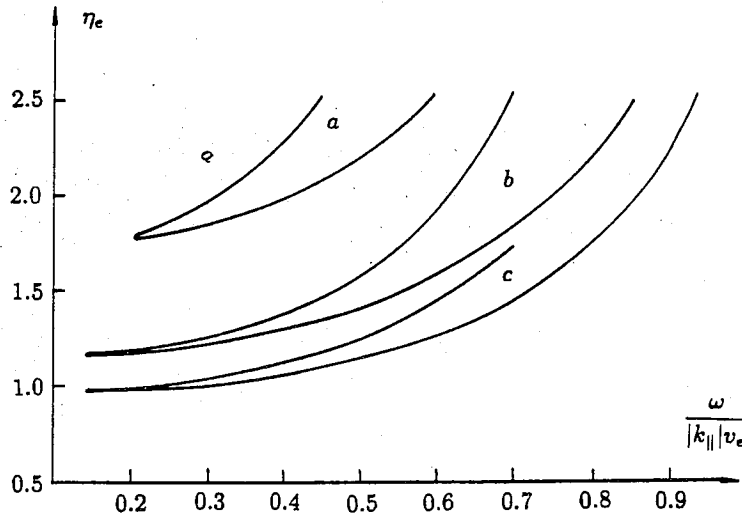


Fig.54 (b) Marginal stability of η_e - mode for same parameters as Fig.53 (b).

Fig.54 Marginal stability of η_e - mode for $\tau = 1.0, \beta_e = 2.0 \times 10^{-3}$. Curves a, b, c correspond to $\eta_e = 1.5, 2.0$ and 3.0 respectively. Stable regions are below corresponding curves.

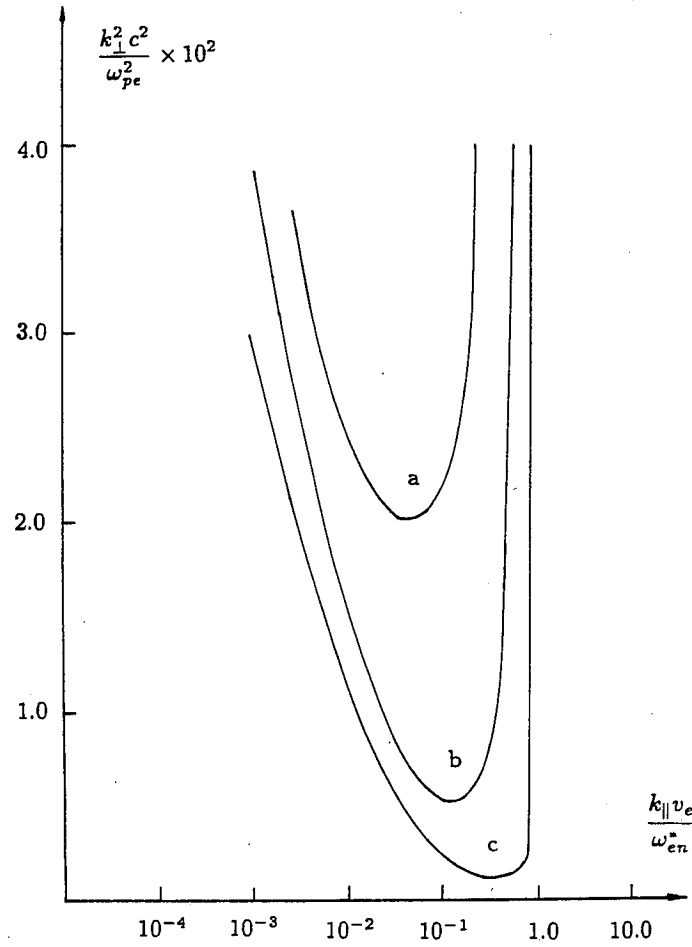


Fig.55 Marginal stability of η_e - mode for $\tau = 1.0, \beta_e = 2.0 \times 10^{-3}$. Curves a, b, c correspond to $\eta_e = 1.5, 2.0$ and 3.0 respectively. Stable regions are below corresponding curves.

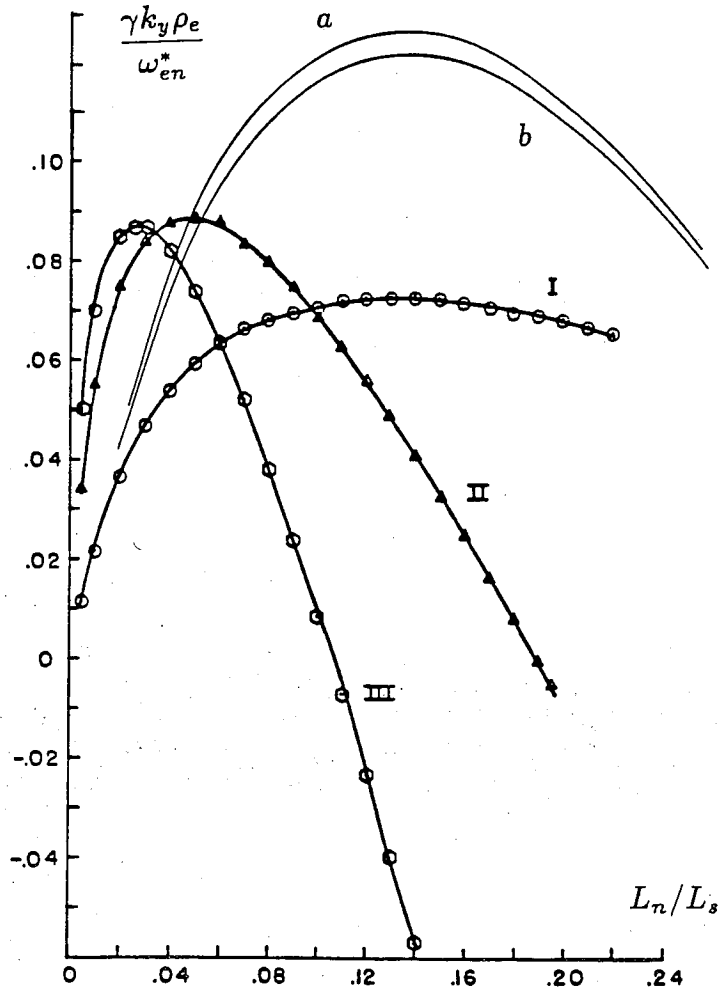


Fig.56 A comparison of growth rate in shearless slab model with those in sheared slab¹⁵⁹. k_{\parallel} in the shearless slab is identified as $1/L_s$. Curves I, II, III are results in Fig.10 of Ref.159. Curve a and b are results in shearless slab model for $\beta_e = 1 \times 10^{-5}, 2 \times 10^{-3}$ respectively, with other parameters same as Fig.10 in Ref.159.

57. The solid curve is the marginal stability for $\tau = 1.0$, $\beta = 2 \times 10^{-3}$, $\eta_e = 2.0$. The asterisk (*) on the curve is the minimum $(k_{\perp} c / \omega_{pe})^2 = 53.9$. The arrows indicate the direction of increasing $(k_{\perp} c / \omega_{pe})^2$, while the numbers by dots on the curve indicate the $(k_{\perp} c / \omega_{pe})^2$ - value. There are two lines encircled by the curve in the plot. The line *a* and *b* represent the locus of unstable modes with $(k_{\perp} c / \omega_{pe})^2 = 400.0$ and 300.0 respectively, whereupon the growth rates, γ / ω_{en}^* , at points (1), (2), (3) are 0.0657, 0.0771, 0.034 respectively (for line *a*) and 0.0516, 0.0656, 0.0291 respectively (for line *b*). The growth rates at point 2 are the maximum ones for given $(k_{\perp} c / \omega_{pe})^2$.

The electron transport coefficient due to the η_e - mode is estimated by two methods: the mixing length theory and the solution of the nonlinear dispersion relation.

The normalized growth rate $\hat{\gamma} \equiv \gamma / \omega_{en}^* \sqrt{b_e}$, maximized with respect to $k_{\parallel}, b_e(k_{\perp})$ are shown in Fig.58 as a function of η_e for fixed $\tau = 1.0$, $\beta_e = 2 \times 10^{-3} [\beta_e \equiv (\omega_{pe} \rho_e / c)^2]$. The electron transport coefficient implied by mixing length theory is thus found to be

$$D_{\perp} \sim \frac{\gamma}{k_{\perp}^2} \sim \frac{\hat{\gamma}}{\sqrt{2}} \frac{T_e c \rho_e}{e B L_n}. \quad (13.13)$$

A nonlinear dispersion relation is constructed and solved to estimate the electron transport due to η_e - mode also. In the construction of the nonlinear dispersion relation we replace the bare propagator of the Vlasov equation, $\omega - k_{\parallel} v_{\parallel}$, by the renormalized propagator, $\omega - k_{\parallel} v_{\parallel} + i\Gamma$, with $\Gamma \sim k_{\perp}^2 D_{\perp}$. The Γ is determined by the marginal stability of the nonlinear dispersion relation. We found that the transport coefficient given by this approach is quite close to the

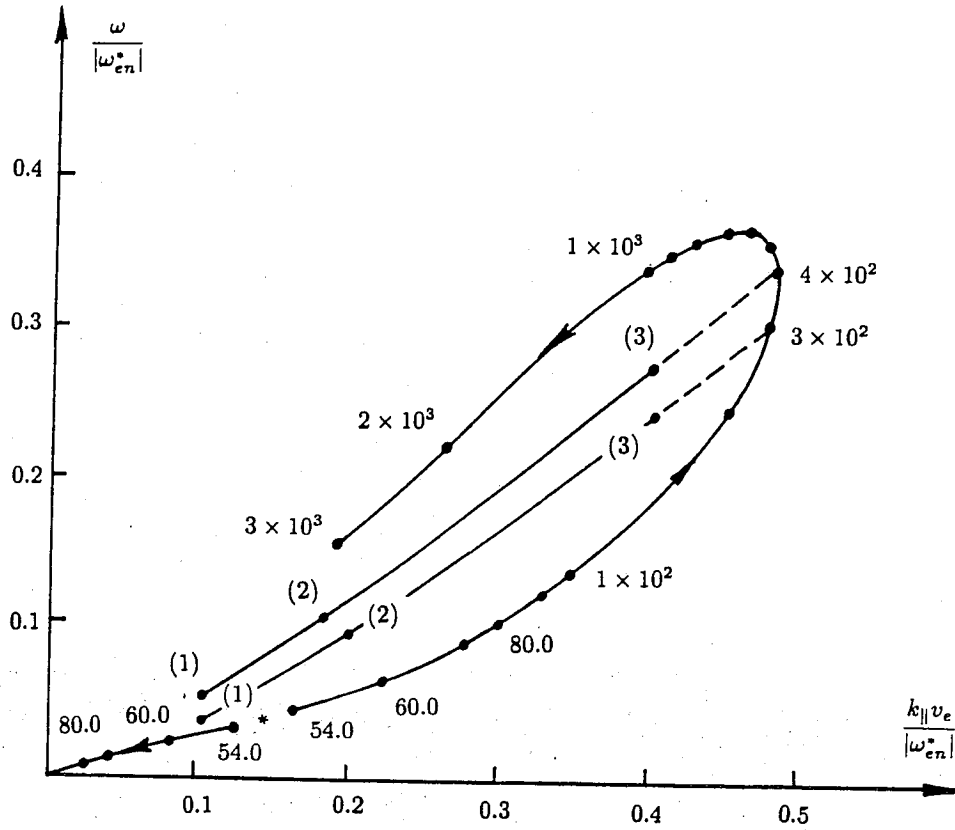


Fig.57 Phase space plot of η_e - mode for $\tau = 1.0, \beta_e = 2 \times 10^{-3}, \eta_e = 2.0$. Solid curve is the marginal stability, which encircles unstable region. The numbers by the dots on the curve denotes the value of $(k_{\perp} c / \omega_{pe})^2$. * is the minimum value of $(k_{\perp} c / \omega_{pe})^2 = 53.9$ on the curve. Lines a and b represent the locus of unstable modes with $(k_{\perp} c / \omega_{pe})^2 = 400.0, 300.0$ respectively, whereupon the growth rates γ / ω_{en}^* at point (1), (2), (3) are 0.0657, 0.0771, 0.034 respectively for line a; and 0.0516, 0.0656, 0.0291 respectively for line b.

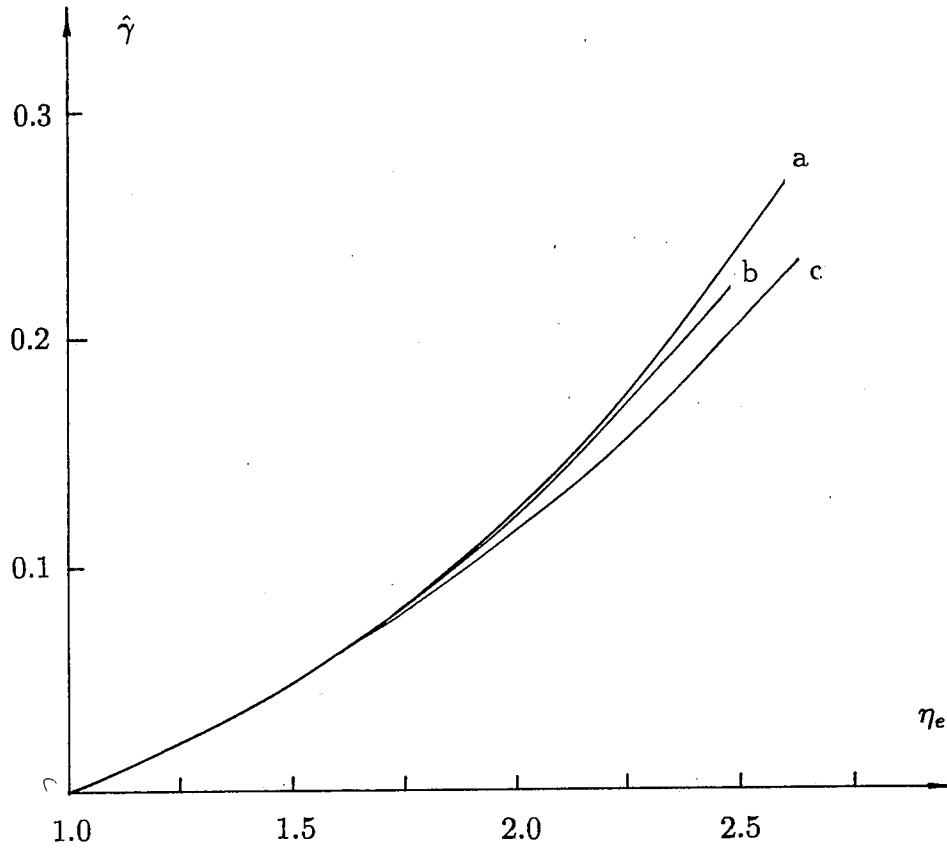


Fig.58 The transport coefficient due to η_e turbulence maximized with respect to k_{\perp} and k_{\parallel} for parameter $\tau = 1.0$. Curve a, b, c correspond to $\beta_e = 1 \times 10^{-3}, 2 \times 10^{-3}$ and 1×10^{-2} respectively.

result from the mixing length theory. Both the approaches indicate that the electron transport coefficient due to the η_e - mode turbulence is more than one order smaller than that typically observed in tokamak experiments. We also note that the fluctuation level of the η_e - mode can be approximated by the following estimate:

$$k_{\perp} \frac{c}{B} \delta\phi \sim \frac{\omega}{k_{\perp}}, \quad (13.14)$$

which combined with the "strong turbulence" type of diffusion $D_{\perp} \sim \omega/k_{\perp}^2$, and $k_{\perp}^{-1} \sim \rho_e$ (the step size of random walk) gives a result resembling to Eq.(13.13).

XIV. Electromagnetic Fluctuations Induced by η_e - Mode

Since the observed anomalous electron energy transport in tokamaks is not explainable as a direct consequence of the very short wavelength η_e - mode (as observed in XIII) one may attempt to examine if the η_e - mode plays an indirect role towards the understanding of the anomalous transport, particularly, through the agency of the electromagnetic mode (henceforth, to be called the A - mode) suggested in XII. In a sheared system like a tokamak, the A - mode suffers strong shear damping and can not naturally grow. In the presence of externally caused turbulence (for instance, by the naturally unstable η_e - mode), the effective dielectric properties of the plasma can undergo sufficient change that the A - mode could grow in this altered medium. The mechanism is similar to (though not identical with) the effect of classical collisions on the mode characteristics. In fact, Drake *et al.*¹⁴⁹ have shown that unrealistically high classical collision frequency can, in principle, destabilize a microtearing mode (obtained by retaining the electrostatic component associated with the A - mode as well). We shall investigate this mechanism in XIV.1.

The annihilation of η_e modes is another mechanism for generation of the A - mode. The amplitude of the forced A - mode obtained from the annihilation of known η_e modes is estimated in XIV.2. Simplifying assumptions needed to carry out the calculation will be discussed along with the results.

XIV.1 Nonlinear Destabilization of A - Mode by η_e - Mode

The existence of η_e turbulence modifies the Ampere's law through the addition of an induced nonlinear (in the amplitude of η_e mode) current whose strength can be measured by an effective turbulent collision frequency ν_t . Clearly ν_t must exceed some critical value (due to shear damping) before the η_e turbulence could drive the mode unstable. We shall presently calculate the threshold condition and examine if it can be satisfied for typical tokamak plasmas. Notice that the free energy for the eventual growth of the A - mode is still the expansion free energy (contained in the temperature gradients) which is first harnessed by the η_e mode, and then transferred to the A - mode.

In a collisionless plasma, the purely electromagnetic linear A - mode is described by the parallel component of the Ampere's law (in a sheared slab)

$$\frac{d^2}{dx^2} \delta\Psi - k^2 \delta\Psi = -\frac{4\pi}{c} \delta J_{\parallel}^{(l)} \equiv \frac{\sigma(x)}{x^2} \delta\Psi, \quad (14.1.1)$$

where $\delta J_{\parallel}^{(l)}$ is the linear current, $\delta\Psi = (\omega/c k') \delta A_{\parallel}$, is proportional to the perturbed vector potential, $k_{\parallel} = k' x \equiv (k_y/L_s)x$, L_s is the shear length, $k = (k_y c/\omega_{pe})$ is the normalized wave vector along y , x is the direction of inhomogeneity. In Eq.(14.1.1) all length are normalized to $\delta_e = c/\omega_{pe}$, the collisionless skin depth, and the normalized conductivity is given by

$$\begin{aligned} \sigma(x) = 2\zeta\zeta_0 \left\{ \left(1 - \frac{\zeta}{\zeta_0}\right) \left[1 + \frac{\zeta}{|x|} Z\left(\frac{\zeta}{|x|}\right)\right] \right. \\ \left. + \eta_e \frac{\zeta}{|x|} \left[\frac{\zeta}{|x|} + \left(\frac{\zeta}{|x|}\right)^2 Z\left(\frac{\zeta}{|x|}\right) - \frac{1}{2} Z\left(\frac{\zeta}{|x|}\right) \right] \right\}, \end{aligned} \quad (14.1.2)$$

where Z is the plasma dispersion function, $\zeta \equiv \omega/|k'| \delta_e v_e$, $\zeta_0 \equiv (\omega_{en}^*/|k'| \delta_e v_e)$, where ω_{en}^* is the electron diamagnetic drift frequency (due to density gradient

alone) and $\eta_e \equiv L_n/L_T$ is the ratio of the temperature to the density gradients. We shall see later that the mode described by Eq.(14.1.1) is shear damped.

It was pointed out earlier that the presence of the η_e turbulence will affect the dynamics of the A - mode. The principal effect is the addition of the turbulence induced nonlinear current to the r.h.s. of Eq.(14.1.1). The nonlinear current has two distinct terms, i.e., $\delta J^{(n)} = \delta J_1^{(n)} + \delta J_2^{(n)}$, where $\delta J_1^{(n)}$ comes from the modification of the wave-particle iteration due to the influence of short wavelength turbulence, and $\delta J_2^{(n)}$ is due to turbulence induced electron self-energy effects (or Compton scattering of electrons by the η_e waves). For the problem under consideration, the former is found to be always destabilizing while the latter becomes destabilizing for $\eta_e > 1$, which is typically the case in tokamaks.

General expressions for $\delta J^{(n)}$ can be quite complicated. Considerable simplification results by making a set of very reasonable (to be stated at the appropriate juncture) assumptions; some of these are:

(1). The η_e - mode is essentially electrostatic and will be represented by the electrostatic potential $\delta\phi$ alone, while the A - mode is primarily electromagnetic.

(2). The calculation for the nonlinear current is carried out in a shearless slab model using weak turbulence formalism.

(3). The parallel phase velocity of the A - mode is assumed to be faster than that for the η_e - mode, for which $v_{ph} \sim v_e$, the electron thermal velocity. The condition $\omega_A > (k_{\parallel} v_e)_A$ will eventually imply a bound on the strength of the magnetic shear.

Within the framework of the preceeding discussion, and making use of the scheme developed in X.1, we obtain

$$\delta J_1^{(n)} = \frac{e}{c} \sum_{k_1} \int dv_{\parallel} v_{\parallel}^2 G_k \hat{L}(k_1, k - k_1) G_{k-k_1} \hat{L}(k, -k_1) G_{-k_1} \cdot \hat{L}_0^{(2)}(k_1, k, -k_1) f_0(v_{\parallel}^2) \langle \delta \phi_{k_1} \delta \phi_{k_1}^* \rangle \delta A_k, \quad (14.1.3)$$

and

$$\delta J_2^{(n)} = \frac{e}{c} \sum_{k_1} \int dv_{\parallel} v_{\parallel}^2 G_k \hat{L}(k_1, k - k_1) G_{k-k_1} \hat{L}(-k_1, k) G_k \cdot \hat{L}_0^{(2)}(k_1, -k_1, k) f_0(v_{\parallel}^2) \langle \delta \phi_{k_1} \delta \phi_{k_1}^* \rangle \delta A_k, \quad (14.1.4)$$

where $\hat{L}(k_1, k_2)$, $\hat{L}_0^{(2)}(k_1, k_2, k_3)$, are defined by Eqs. (10.1.3) and (10.1.10) respectively.

Notice that we have used $k_1(k)$ to denote the wavevector associated with the η_e - mode (A - mode). The v_{\perp} integration in $\hat{L}_0^{(2)}$ is readily carried out by remembering that for the A -mode $k_{\perp} \rho_e \ll 1$ allowing us to replace the J_0 's (with the argument $k_{\perp} \rho_e$) by unity. We should, of course, keep the J_0 's associated with the η_e - mode because $k_{1,\perp} \rho_e \sim 1$. The nonlinear current takes the form

$$\delta J_1^{(n)} = -\frac{e^2}{cT_e} \left(\frac{c}{B} \right)^2 \sum_{k_1} [(\mathbf{k}_1 \times \mathbf{k}) \cdot \mathbf{b}]^2 \int dv_{\parallel} v_{\parallel}^2 G_k G_{k-k_1} G_{-k_1} \omega_1 \Gamma_0(b_e) f_0(v_{\parallel}^2) \delta I_{k_1} \delta A_k, \quad (14.1.5)$$

and

$$\delta J_2^{(n)} = -\frac{e^2}{cT_e} \left(\frac{c}{B} \right)^2 \sum_{k_1} [(\mathbf{k}_1 \times \mathbf{k}) \cdot \mathbf{b}]^2 \int dv_{\parallel} v_{\parallel}^2 G_k G_{k-k_1} G_k \left\{ (\omega - \omega_{en}^*) \Gamma_0(b_e) - \eta_e \omega_{en}^* \left(\frac{v_{\parallel}^2}{v_e^2} - \frac{1}{2} \right) \Gamma_0(b_e) + b_e [\Gamma_1(b_e) - \Gamma_0(b_e)] \right\} f_0^s(v_{\parallel}^2) \delta I_k \delta A_k, \quad (14.1.6)$$

where $\Gamma_n(b_e) = I_n(b_e) \exp(-b_e)$, $b_e = \rho_e^2 k_\perp^2 / 2$ and $\delta I_k = \langle \delta \phi_k \delta \phi_k^* \rangle$. Highly simplified forms of Eqs.(14.1.5) and (14.1.6) result assuming that the η_e spectrum has perpendicular reflection symmetry, i.e., δI_{k_1} is invariant under the transformation $\mathbf{k}_{1,\perp} \rightarrow -\mathbf{k}_{1,\perp}$. Making use of the symmetries and doing the v_\parallel integration, we can write the leading part of $\delta J^{(n)}$ in the following form

$$\frac{4\pi}{c} \delta J^{(n)} = \frac{4\pi}{c} (\delta J_1^{(n)} + \delta J_2^{(n)}) = i \delta_e^2 \cdot \frac{\nu_t}{\omega} \cdot \left[3 - \frac{\omega_{en}^*}{\omega} (1 - \eta_e \bar{\delta}) \right] \delta A_k, \quad (14.1.7)$$

where

$$\nu_t = 2\sqrt{\pi} \left(\frac{c}{B} \right)^2 \sum_{k_1} \frac{[\mathbf{k}_1 \times \mathbf{k} \cdot \mathbf{b}]^2}{k_{1,\parallel}^2 v_e^2} \delta I_{k_1} \Gamma_0(b_e) \frac{\omega_1^2}{|k_{1,\parallel}| v_e} \quad (14.1.8)$$

can be interpreted as an effective turbulent collision frequency, and $\bar{\delta} \sim 1$ for the regime of interest.

The A - mode equation (14.1.1) is now modified as

$$\left\{ \frac{d^2}{dx^2} - k^2 - \frac{\sigma}{x^2} + N \right\} \delta \Psi = 0, \quad (14.1.9)$$

where

$$N \equiv i \frac{\bar{\nu}_t}{\zeta} \left[3 + (\eta_e \bar{\delta} - 1) \frac{\zeta_0}{\zeta} \right]$$

with $\bar{\nu}_t \equiv \nu_t / |k'| \delta_e v_e$, and must be solved as an eigenvalue problem. We do this by setting up a variational principle.^{169,170} The appropriate variational functional for Eq.(14.1.9) is

$$S = \int dx \left(\frac{d}{dx} \delta \Psi \right)^2 - \int dx \left\{ k^2 + \frac{\sigma}{x^2} - N \right\} (\delta \Psi)^2, \quad (14.1.10)$$

which can be evaluated using the trial function

$$\delta \Psi = \exp(-\alpha x^2 / 2), \quad \text{Re } \alpha > 0, \quad (14.1.11)$$

where α is a variational parameter. The eigenvalue ζ and α are obtained by a simultaneous solution of the equation

$$\frac{\partial S}{\partial \alpha} = 0 \quad \text{and} \quad S = 0.$$

Inserting Eq.(14.1.11) into Eq.(14.1.10) and carrying out the x integration, we find¹⁷¹

$$\bar{S} = \sqrt{\frac{\alpha}{\pi}} S = -\frac{\alpha}{2} - k^2 + N + \sqrt{\frac{\alpha}{\pi}} 2\zeta \left[\left(\frac{\zeta_0}{\zeta} - 1 \right) \alpha \frac{\partial I}{\partial \alpha} - \frac{\eta_e}{\zeta} \left(\alpha^2 \frac{\partial^2 I}{\partial \alpha^2} + \frac{\alpha}{2} \frac{\partial I}{\partial \alpha} \right) \right] \quad (14.1.12)$$

with

$$I \equiv 2i\sqrt{\pi} \left[K_0(2\zeta\sqrt{\alpha}) + \frac{i\pi}{2} J_0(2i\zeta\sqrt{\alpha}) - \frac{\pi}{2} \mathbf{H}_0(2i\zeta\sqrt{\alpha}) \right], \quad (14.1.13)$$

where $(K_0)J_0$ is the (modified) Bessel function and \mathbf{H}_0 is a struve function. To make further analytical progress, we need to make simplifying assumptions. For the weak shear case we assume $|2\zeta\sqrt{\alpha}| > 1$, and expand the transcendental function to obtain an algebraic approximation for I ,

$$\sqrt{\frac{\alpha}{\pi}} I \sim -\frac{1}{\zeta} - \frac{1}{4\zeta^2\alpha}. \quad (14.1.14)$$

We must, of course, check the constraint imposed by the above assumption *a posteriori*, i.e., once we have evaluated α . Making use of Eqs. (14.1.12) and (14.1.14) we obtain by solving the variational problem $S = 0, \partial S/\partial \alpha = 0$

$$\alpha = \frac{i}{\zeta} \sqrt{\frac{3}{2} \left[(1 + 2\eta_e) \frac{\zeta_0}{\zeta} - 1 \right]}, \quad (14.1.15)$$

and the dispersion relation

$$(1 + \eta_e) \frac{\zeta_0}{\zeta} = \frac{\alpha}{2} + 1 + k^2 - N + \frac{3}{4\alpha\zeta^2} \left[1 - \frac{(1 + 2\eta_e)\zeta_0}{\zeta} \right], \quad (14.1.16)$$

which yields the mode frequency

$$\zeta \sim \frac{1 + \eta_e}{1 + k^2} \zeta_0 + \frac{i \bar{\nu}_t}{1 + k^2} \left[3 + \frac{\eta_e \bar{\delta} - 1}{1 + \eta_e} (1 + k^2) \right] - \frac{i}{1 + k^2} \sqrt{\frac{3}{2} \left[\frac{1 + 2\eta_e}{1 + \eta_e} (1 + k^2) - 1 \right]}, \quad (14.1.17)$$

The eigenvalue problem of Eq.(14.1.9) can also be solved by the WKB approximation, when the condition $|\zeta/x| > 1$ is assumed. For the absence of η_e turbulence, the eigenmode equation then reduces to the Weber equation:

$$\left\{ \frac{d^2}{dx^2} - k^2 - \left(1 - (1 + \eta_e) \frac{\zeta_0}{\zeta} + \frac{3}{2\zeta^2} \left[1 - (1 + 2\eta_e) \frac{\zeta_0}{\zeta} \right] x^2 \right) \right\} \delta\Psi(x) = 0, \quad (14.1.18)$$

For large x (but not too large to suffer Landau damping) we balance d^2/dx^2 and x^2 term to get

$$-k_x^2 + \frac{3}{2\zeta^2} \left[(1 + 2\eta_e) \frac{\zeta_0}{\zeta} - 1 \right] x^2 = 0$$

The WKB mode behavior is found to be

$$\delta\Psi(x) \sim \exp \left\{ \pm i \frac{x^2}{2} \sqrt{\frac{3}{2\zeta^2} \left[(1 + 2\eta_e) \frac{\zeta_0}{\zeta} - 1 \right]} \right\}$$

The sign in front of the argument of the exponential should be determined by the outgoing wave boundary condition:

$$\frac{\partial}{\partial k_x} \omega \text{Sgn}(x) > 0.$$

For the A - mode, of which the lowest order solution is

$$\zeta \sim \frac{1 + \eta_e}{1 + k^2} \zeta_0 \quad (14.1.18),$$

we must chose minus sign to fit the outgoing wave boundary condition. It yields a damping wave with the same damping rate as given by the last term of Eq.(14.1.17). The WKB mehtod can also be applied to the eigenvalue problem in the presence of η_e turbulence. For the A - mode [the lowest order solution is given by Eq.(14.1.18)], we obtain the same result as Eq.(14.1.17), given by the variational approach.

The threshold condition for growth

$$\bar{\nu}_t > \frac{\sqrt{\frac{3}{2} \left[\frac{1+2\eta_e}{1+\eta_e} (1+k^2) - 1 \right]}}{3 + \frac{\eta_e \bar{\delta} - 1}{1+\eta_e} (1+k^2)}, \quad (14.1.19)$$

and the requirement $|2\zeta\sqrt{\alpha}| > 1$

$$2\sqrt{\frac{\omega_{en}^* L_s}{k_y \delta_e v_e}} = 2\sqrt{\frac{\rho_e}{\delta_e} \frac{L_s}{L_n}} > 1 \quad (14.1.20)$$

define the parameter space for which this analysis is meaningful. For typical tokamak parameters, $(\rho_e/\delta_e)(L_s/L_n) \sim 1$, and Eq.(14.1.20) is expected to be marginally satisfied. The weaker the shear, the easier it is to satisfy the above condition.

To examine Eq.(14.1.19) we must estimate the magnitude $\bar{\nu}_t$. Use is made of Eq.(13.14) to give

$$\bar{\nu}_t \sim 2\sqrt{\pi}\Gamma_0(b_e) \left(\frac{k_{\perp}}{k_{1,\perp}} \right)^2 \left(\frac{\omega_1}{k_{1,\parallel} v_e} \right)^3 \frac{\omega_1}{|k'| \delta_e v_e}, \quad (14.1.21)$$

where subscript 1 is the denotation for the η_e - mode, while $k_{\perp} \sim 1/\delta_e$ is typical wave number of the A - mode. Estimating $(\omega_1/k_{1,\parallel} v_e) \sim O(1)$, $\omega_1 \sim 0.3\omega_{en}^*$ (

Fig.57) $k_{\perp}/k_{1,\perp} \sim \rho_e/\delta_e, 2\sqrt{\pi}\Gamma_0(b_e)$

$$\bar{\nu}_t \sim 0.3 \left(\frac{\rho_e}{\delta_e} \right)^2 \left(\frac{L_s}{L_n} \right), \quad (14.1.22)$$

typically one order smaller than that required for destabilization of the A - mode in tokamak discharges.

XIV.2 Electromagnetic Fluctuation Forced by η_e - Mode

The existence of η_e turbulence not only provides a nonlinear coherent current that modifies the dielectric properties of plasma (this effect has been evaluated in XIV.1 as a possible mechanism for destabilizing A - mode), but also provides a nonlinear incoherent current as an external sources for the A - wave. To the lowest order of perturbation theory this process is equivalent to the three wave interaction, or the annihilation of two η_e - waves to generate one A - wave. Since both the frequency and growth rate of the η_e - mode is higher than the mode frequency of the A - mode. the correlation broadening [cf. VIII.4] of the η_e - mode is sufficiently large to allow the annihilation process.

The wave equation describing the externally driven A - mode is given by

$$\left(\frac{d^2}{dx^2} - k_y^2 \right) \delta A_k(x) + \frac{4\pi}{c} \delta J_{\parallel,k}^{(l)}(x) = -\frac{4\pi}{c} \delta J_{\parallel,k}^{(in)}(x), \quad (14.2.1)$$

where $\delta J_{\parallel}^{(l)}$ is the linear current of the A - mode, $\delta J_{\parallel,k}^{(in)}$ is the nonlinear incoherent current due to two η_e - waves (specified as $\delta\phi_{k_1}$ and $\delta\phi_{k_2}$). In Eq.(14.2.1) we have ignored the contribution from the nonlinear coherent current (associated with η_e - mode) whose effects were investigated in XIV.1.

To solve this forced wave equation, we must calculate the incoherent current in terms of the nonlinear η_e - waves. A basic *ansatz* in doing this is that the η_e turbulence is stationary, i.e., the lifetime of η_e vortices is much longer than its growing time, the inverse of the growth rate of the mode. Use is made of gyro-kinetics [cf. X.1] to calculate the incoherent current $\delta J_{\parallel}^{(in)}$ in a sheared model. We have

$$\begin{aligned} \delta J_{\parallel,k}^{(in)}(x) = & i \frac{e^2}{T_e} \left(\frac{c}{B} \right) \int dv_{\parallel} v_{\parallel} G_k \sum_{k_1+k_2=k} \left\{ k_{1y} \frac{d}{dx} G_{k_2} \hat{L}_0(k_2) \delta\phi_{k_1}(x) \delta\phi_{k_2}(x) \right. \\ & \left. - k_y G_{k_2} \hat{L}_0(k_2) \delta\phi_{k_2}(x) \frac{d}{dx} \delta\phi_{k_1}(x) \right\} f_0(v_{\parallel}^2), \end{aligned} \quad (14.2.2)$$

where

$$\hat{L}_0(k) \equiv \left\{ \omega - \omega_{en}^* \left[1 + \eta_e \left(\frac{v_{\parallel}^2}{v_e^2} - \frac{1}{2} - b_e \right) \right] \right\} \Gamma_0(b_e) - \eta_e \omega_{en}^* b_e \Gamma_1(b_e) \quad (14.2.3)$$

and

$$G_k = \frac{1}{\omega - k_{\parallel} v_{\parallel}}, \quad G_{k_2} = \frac{1}{\omega_2 - k_{2,\parallel} v_{\parallel}} \quad (14.2.4)$$

with

$$k_{\parallel} = \frac{k_y}{L_s} (x - x_0), \quad k_{2,\parallel} = \frac{k_{2y}}{L_s} (x - x_2), \quad (14.2.5)$$

in which x_0 and x_2 are respectively the positions of rational surfaces defined by $q(x_0) = m/n, q(x_2) = m_2/n_2$, where q is the safety factor, and $m(m_2), n(n_2)$ are poloidal and longitudinal wave numbers respectively.

The integration over v_{\parallel} yields:

$$\int dv_{\parallel} v_{\parallel} G_k G_{k_2} \hat{L}_0(k_2) f_0(v_{\parallel}^2) = n \omega_{en}^*(2) \frac{Q(2)}{k_{2,\parallel} \omega - k_{\parallel} \omega_2} \quad (14.2.6)$$

with

$$Q(2) \equiv [\Gamma_0(b_e) + \eta_e b_e (\Gamma_1 - \Gamma_0)] \cdot [\zeta_2 Z(\zeta_2) - \zeta Z(\zeta)] + \eta_e \Gamma_0(b_e) [W_2(\zeta_2) - W_2(\zeta)], \quad (14.2.7)$$

where $\zeta \equiv \omega/|k_{\parallel}|v_e$, $\zeta_2 \equiv \omega_2/|k_{2,\parallel}|v_e$, Z - the plasma dispersion function and

$$W_2(\zeta) \equiv \zeta \{ \zeta [1 + \zeta Z(\zeta)] - Z(\zeta)/2 \}.$$

It is important to note that the two η_e - waves, $\delta\phi_{k_1}(x)$ and $\delta\phi_{k_2}(x)$, can provide an incoherent source as wide as the A - mode width in the x - direction, since the rational surfaces of the two modes are not necessarily at exactly the same position. We may model the η_e - mode structure by the Gaussian type:

$$\delta\phi_{k_i}(x) \sim \delta\hat{\phi}_{k_i}(x_i) \exp[-(x - x_i)^2/\sigma^2] \quad (14.2.8)$$

where x_i is the position of the rational surface associated with $\delta\phi_{k_i}(x)$, and σ measures the η_e - mode width [typically, the electron Larmor radius ρ_e]. Noting that the conservation law $k_1 + k_2 = k$ demands

$$x_1 = x_2 + \frac{k_y}{k_y - k_{2y}}(x_0 - x_2), \quad (14.2.9)$$

we then carry out the longitudinal wave number summation that is approximately replaced by an integration, and obtain

$$\delta\phi_{k_1}(x)\delta\phi_{k_2}(x) \rightarrow |\delta\hat{\phi}|^2 \exp\left\{-\frac{k_y^2}{2k_{2y}^2\sigma^2}(x - x_0)^2\right\}. \quad (14.2.10)$$

In this manipulation we have assumed that $\delta\hat{\phi}_{k_1}(x_1)$ and $\delta\hat{\phi}_{k_2}(x_2)$ are approximately in phase and weakly depend on the position of rational surface.

The results obtained in XIII allow us to estimate the important linear parameters of the mode:

$$\omega_1 \sim k_{1,\parallel} v_e, \quad \frac{c}{B} k_{1,\perp} \delta \phi_{k_1} \sim \frac{\omega_1}{k_{1,\perp}}$$

$$k_{1,\perp} \sim k_{2,\perp} \sim 1/\rho_e, \quad \omega_1 \sim 0.3 \omega_{en}^*(1)$$

For the electromagnetic wave (A - mode), the solution of the linear dispersion relation in a sheared slab is

$$\omega \sim \frac{1 + \eta_e}{1 + k_{\perp}^2 \delta_e^2} \omega_{en}^* - i k_{\parallel} v_e \frac{\sqrt{\frac{3}{2} \left[\frac{1 + 2\eta_e}{1 + \eta_e} (1 + k_{\perp}^2 \delta_e^2) - 1 \right]}}{1 + k_{\perp}^2 \delta_e^2}$$

with the consistency condition: $\omega > k_{\parallel} v_e$. The linear dispersion relation yields the estimate: $\omega \sim \omega_{en}^*, k_{\perp} \sim 1/\delta_e$ [cf. XIV.1]. Since the linear A - mode is a damped mode, with the damping rate $\gamma \sim \omega_{en}^*$, it is impossible to generate the A - mode resonantly by the external incoherent current.

Substituting the calculated nonlinear current $\delta J_{\parallel,k}^{(in)}$ into the Ampere's law and using the above estimates, we estimate the level of the magnetic fluctuations forced by the annihilation of two η_e - waves to be

$$\frac{\delta B}{B} \sim 0.3 \lambda \left(\frac{\omega_{pe}}{c k_{2,\perp}} \right)^2 \frac{\rho_e}{L_n} \left(\frac{\omega_{en}^*(k_2)}{\omega_{en}^*(k) + i \Gamma_k} \right). \quad (14.2.11)$$

The numerical factor λ on the r.h.s. of Eq.(14.2.11) is $O(1)$. However, the above estimate is flawed, since the perturbation theory used in the estimate breaks down, i.e., the " perturbation parameter " $(c/B) k_{2,\perp}^2 G_{k_2} \delta \phi_{k_2} \sim O(1)$, so that the contributions from higher orders is expected to be as important as

the contribution from the lowest order. In a sense, Eq.(14.2.11) is reasonable only for scaling, and not for the magnitude.

For $\lambda \sim 1.0, \Gamma_k < \omega_{en}^*$ makes Eq.(14.2.11) [$k_2 = \rho_e^{-1}, k = \delta_e^{-1}$]

$$\frac{\delta B}{B} \sim 0.3 \frac{\rho_e}{L_n} \frac{\rho_e}{\delta_e}. \quad (14.2.12)$$

For typical tokamak parameters Eq.(14.2.12) implies that the fluctuation of the forced mode lies in the weak turbulence regime ($\Gamma_k \ll \omega$). Substituting Eq.(14.2.12) into the Rechester-Rosenbluth formula [Eq.(12.1)] yields the transport coefficient

$$D_{\perp} \sim (0.3)^2 \frac{qR}{L_n} \frac{T_e c \rho_e}{e B L_n} \left(\frac{\rho_e}{\delta_e} \right)^2, \quad (14.2.13)$$

which is much smaller than the transport observed in tokamak experiments.

The above analysis is based on two fundamental assumptions concerning the nature of the η_e turbulence: the stationarity of the turbulence, and complete correlation between two closely located modes. Departures from these assumptions will lead to a reduction in the fluctuation level.

In summary, we have investigated two mechanisms for generating electromagnetic fluctuations by the presence of η_e turbulence. The calculations are carried out on the basis of perturbation theory and restricted to the lowest order in both the coherent and incoherent currents. These calculations have shown that neither the coherent, nor the incoherent current driven by η_e turbulence is sufficiently high to generate magnetic fluctuations required for the electron transport in tokamaks. However, we can not completely rule out the

role played by the η_e turbulence in the generation of electromagnetic fluctuations. One reason is the breaks down (at the saturation level of the the η_e turbulence) of the perturbation theory, and the other reason is that in the above calculation we did not take into account the entire inverted cascading process. This process may drive the original η_e - spectrum contineously down to longer wavelength regions, so that the ordering $k_{1,\perp} \sim k_{2,\perp} \sim \rho_e^{-1}$ may be greatly altered. However, the calculation for the inverted cascading process is much more complicated, and will be attempted later.

Appendix A Quadratic Forms

Here we compare different quadratic forms in MHD theory and the form derived from kinetic theory.

The quadratic form of the MHD energy principle is formulated from the ideal MHD equations [continuity equation, force balance, ideal Ohm's law and adiabatic evolution equation]. It yields the Bernstein - Frieman - Kruskal - Kulsrud form:¹⁷²

$$\delta W_p = \frac{1}{2} \int dr \left\{ \delta B^2 + \mathbf{J} \cdot \boldsymbol{\xi} \times \delta \mathbf{B} + (\nabla \cdot \boldsymbol{\xi})(\boldsymbol{\xi} \cdot \nabla P) + \gamma P (\nabla \cdot \boldsymbol{\xi})^2 \right\}, \quad (\text{A.1})$$

where $\boldsymbol{\xi}$ is defined by $\delta \mathbf{B} \equiv \nabla \times (\boldsymbol{\xi} \times \mathbf{B})$, \mathbf{J} - the plasma current, P - the plasma pressure. γ - the gas constant.

Making use the following equations

$$\delta B_{\parallel} = -\frac{1}{B} \left\{ \boldsymbol{\xi}_{\perp} \cdot \nabla (P + B^2) + B^2 \nabla \cdot \boldsymbol{\xi}_{\perp} \right\} \quad (\text{A.2})$$

$$\mathbf{J}_{\perp} \cdot \boldsymbol{\xi}_{\perp} \times \delta \mathbf{B} = \frac{1}{B^2} (\boldsymbol{\xi}_{\perp} \cdot \nabla P) \left\{ \boldsymbol{\xi}_{\perp} \cdot \nabla (P + B^2) + B^2 \nabla \cdot \boldsymbol{\xi}_{\perp} \right\} \quad (\text{A.3})$$

and equilibrium equation

$$\nabla_{\perp} \left(P + \frac{B^2}{2} \right) = B^2 \kappa, \quad (\text{A.4})$$

where κ is the curvature, we obtain the Furth - Killen - Rosenbluth - Coppi form:¹⁷³

$$\begin{aligned} \delta W_p = \frac{1}{2} \int dr \left\{ \delta B_{\perp}^2 - J_{\parallel} (\boldsymbol{\xi} \times \mathbf{b}) \cdot \delta \mathbf{B}_{\perp} - 2(\boldsymbol{\xi} \cdot \nabla P)(\boldsymbol{\xi} \cdot \boldsymbol{\kappa}) + \gamma P (\nabla \cdot \boldsymbol{\xi})^2 \right. \\ \left. + [\delta B_{\parallel} - \boldsymbol{\xi}_{\perp} \cdot \nabla P / B]^2 \right\} + \int_{\sigma} ds (\boldsymbol{\xi}_{\parallel} \mathbf{b}) (\boldsymbol{\xi} \cdot \nabla P). \end{aligned} \quad (\text{A.5})$$

The Johnson - Green form¹⁷⁴ can be obtained by minimizing Eq.(A.5):

$$\delta W_p = \frac{1}{2} \int dr \left\{ \delta B_\perp^2 - J_\parallel (\xi \times \mathbf{b}) \cdot \delta \mathbf{B}_\perp - 2(\xi \cdot \nabla P)(\xi \cdot \kappa) \right\} \quad (\text{A.6})$$

with

$$\nabla \cdot \xi = 0 \quad \text{and} \quad \nabla_\perp \cdot \xi_\perp = 0. \quad (\text{A.7})$$

Defining

$$\begin{aligned} \hat{Q}_L &\equiv \delta B_\parallel + \xi \cdot \nabla B - B \xi \cdot \kappa \\ &= -B \left[\nabla \cdot \xi - \xi \cdot \kappa + \mathbf{b} \cdot (\mathbf{b} \cdot \nabla) \xi \right] \end{aligned} \quad (\text{A.8})$$

and choosing $\mathbf{b} \cdot \xi = 0$, so that

$$\hat{Q}_L = -B[\nabla \cdot \xi - 2\xi \cdot \kappa], \quad (\text{A.9})$$

we can rewrite Eq.(A.5) as

$$\begin{aligned} \delta W_p &= \frac{1}{2} \int dr \left\{ \delta B_\perp^2 - J_\parallel (\xi \times \mathbf{b}) \cdot \delta \mathbf{B}_\perp - 2(\xi \cdot \nabla P)(\xi \cdot \kappa) \right. \\ &\quad \left. + |\hat{Q}_L|^2 + \gamma P(\nabla \cdot \xi)^2 \right\} \end{aligned} \quad (\text{A.10})$$

In the isotropic and low β approximation the Antonson - Lee form⁷⁶ (as a kinetic form with $\xi \cdot \mathbf{b} = 0$) is

$$\begin{aligned} \delta W_p &= \frac{1}{2} \int dr \left\{ \delta B_\perp^2 - J_\parallel (\xi \times \mathbf{b}) \cdot \delta \mathbf{B}_\perp - 2(\xi \cdot \nabla P)(\xi \cdot \kappa) + |\hat{Q}_L|^2 \right\} \\ &\quad + \frac{1}{2} \int dr d\Gamma \delta f_L \left\{ \mu(\hat{Q}_L^* + B \xi^* \cdot \kappa) + m v_\parallel^2 \xi^* \cdot \kappa \right\}. \end{aligned} \quad (\text{A.11})$$

The last term of Eq.(A.11) is named as δW_k , while the other terms are named as δW_{MHD} .

Appendix B Diagramatic Rules

Because of the importance of the diagrammatic scheme introduced in the developing the renormalized perturbation theory, a detailed account of the diagrammatic rules is given in this appendix.

In each diagram the *solid line* represents the propagator G_k , with k denoting the four - momentum of the particles carried by the propagator. The one exception to this representation is when the solid line is at the lowest part of the diagram which then represents the fluctuating distribution function $\delta f_{k'}$.

There is always an arrow to denote the direction of its k . The solid line deflects whenever it meets a *wiggly line* which represents wave $\delta\phi_{k_1}$. The redirection indicates that there is a vertex \hat{L} which is called *wave - particle interaction vertex* implying their interaction. At the vertex there must be conservation of momentum. When the wiggly line of momentum k_1 is an external line, of which one end connecting with the solid line of momentum k at the vertex, while the other end being free, the momentum connected with it is taken up by the solid line below the vertex has a momentum $k - k_1$. The vertex at the intersection between solid line and wiggly line is an operator, which generally does not commute with the propagator G . At the end of the lowest solid line it may be connected to a shaded bubble $\otimes \equiv \hat{L}_0(k)f_0$ or it may be open ended. In the latter case this lowest solid line means $\delta f_{k'}$. A hollow circle \bigcirc is introduced here to denote $i\Gamma_k$. The wiggly line which connects two vertices is called an internal line and it denotes $|\delta\phi_k|^2$. Sometimes several wiggly lines meet

at one point. The point is called *multiwave vertex*. There is no interaction at a multiwave vertex akin to the interaction \hat{L} at the wave - particle vertex. However, the multiwave vertex provides the conservation of four - momentum of waves $k_1 + k_2 + \dots + k_n = 0$, where k_1, k_2, \dots, k_n are the four - momentum of waves connected to the multiwave vertex. Both the internal line and the multiwave connecting wiggly lines imply a non - fluctuating closed structure for the correlation of corresponding waves.

A summation index with parenthesis, (k_i) , means $k_i \neq k$ (k is the coherent momentum) and the designated wiggly line by (k_i) is uncorrelated with other wiggly lines designated by momentum with parenthesis in the same diagram. A typical example of this diagrammatical rule can be seen from the last two terms of Eq.(8.1.25). They correspond the following analytical expressions respectively:

$$\sum_{k_1, k_2} G_k \hat{L}(k_1) |\delta\phi_{k_1}|^2 G_{k-k_1} \hat{L}(k_2) \delta\phi_{k_2} G_{k-k_1-k_2} \hat{L}(k-k_2) \delta\phi_{k-k_2} G_{-k_1} \hat{L}(-k_1) f_0,$$

and

$$\sum_{(k_1), (k_2), (k_3)} G_k \hat{L}(k_1) \delta\phi_{k_1} G_{k-k_1} \hat{L}(k_2) \delta\phi_{k_2} G_{k-k_1-k_2} \hat{L}(k_3) G_{k-k_1-k_2-k_3} \cdot \hat{L}(k_3) f_0 \delta\phi_{k-k_1-k_2-k_3}.$$

Appendix C Correlation Expansion

In the perturbation a systematic procedure, named correlation expansion, is adopted based on the definition of the correlation function to all orders.

The stochastic quantities for any stochastic process, $A, B, C \dots$ might be correlated with each other, so that we have

$$\langle A \rangle = \langle A \rangle \quad (C.1)$$

$$\langle AB \rangle = \langle A \rangle \langle B \rangle + \langle \langle AB \rangle \rangle \quad (C.2)$$

$$\begin{aligned} \langle ABC \rangle = & \langle A \rangle \langle B \rangle \langle C \rangle + \langle A \rangle \langle \langle BC \rangle \rangle + \langle B \rangle \langle \langle AC \rangle \rangle \\ & + \langle C \rangle \langle \langle AB \rangle \rangle + \langle \langle ABC \rangle \rangle, \end{aligned} \quad (C.3)$$

where $\langle \dots \rangle$ is the ensemble average, $\langle \langle AB \rangle \rangle, \langle \langle ABC \rangle \rangle \dots$ are called the correlation functions of stochastic quantities $A, B, C \dots$. They simplify the dependent probability of multiple stochastic quantities and defined as the difference of the ensemble average from the lower order ones. Having the definition of correlation functions in mind, we can expand the product of stochastic quantities $A, B, C \dots$ in terms of correlation functions. For example,

$$AB = (A)(B) + \langle \langle AB \rangle \rangle \quad (C.4)$$

The quantities in parenthesis are not correlated with each other. When the ensemble average is taken over them, the average is split into that acting on each single quantity, because the correlated part has been extracted from them, $\langle (A)(B) \rangle = \langle A \rangle \langle B \rangle$. We readily find the consistency of Eq.(C.4) with Eq.(C.2).

For three quantities we have

$$ABC = (A)(B)(C) + (A)\langle \langle BC \rangle \rangle + (B)\langle \langle AC \rangle \rangle + (C)\langle \langle AB \rangle \rangle + \langle \langle ABC \rangle \rangle \quad (C.5)$$

A quantity in parenthesis may be correlated with the quantities not in the parenthesis, however, no quantity in $\langle\langle\cdots\rangle\rangle$ could be correlated with quantities outside. In fact, the correlation expansion can be done only for part of the product. Thus we may write, for example,

$$ABC = (A)(B)C + \langle\langle AB \rangle\rangle C \quad (C.6)$$

Further expansion of Eq.(C.6), according to the above rule, reads

$$(A)(B)C = (A)(B)(C) + (B)\langle\langle AC \rangle\rangle + (A)\langle\langle BC \rangle\rangle + \langle\langle ABC \rangle\rangle. \quad (C.7)$$

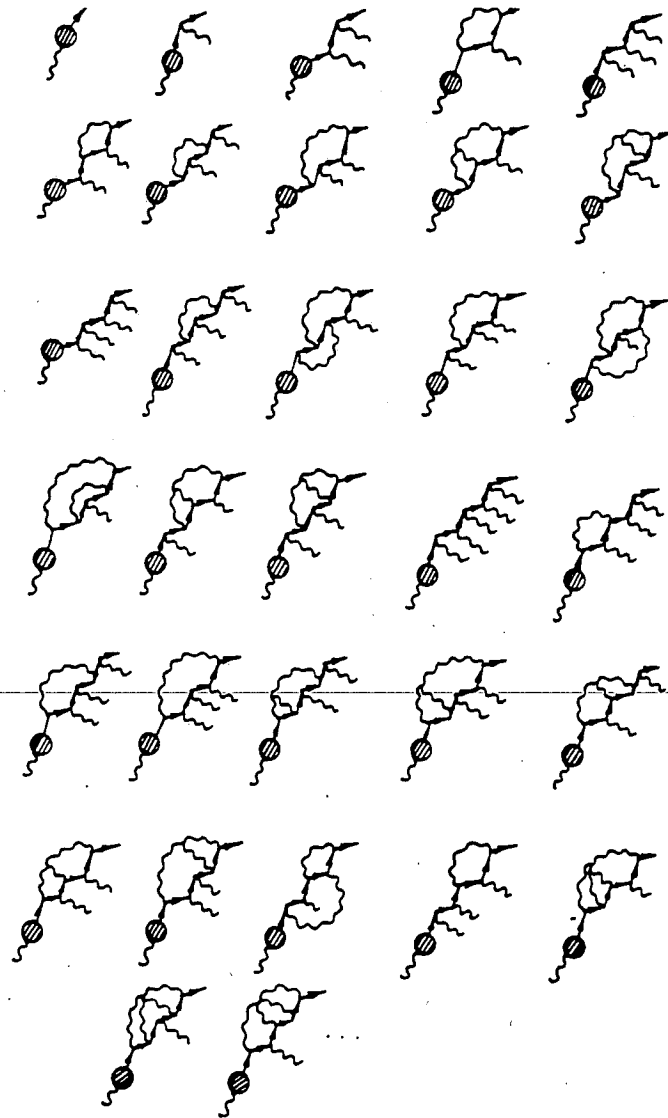
When combining Eq.(C.6) and Eq.(C.7), we readily see the consistency with the result of Eq.(C.5).

The correlation expansion is equivalent to the cluster expansion used in the BBGKY hierarchy¹⁷⁵ and functional for both the distribution function δf and the electric fields $\delta \mathbf{E}$ by virtue of their linear relationship given by the Poisson equation.

Appendix D Perturbative Expansion of δf_k

In this representation the wiggly lines above the shaded bubble are uncorrelated with each other, while the wiggly line connected to the shaded bubble may or may not be correlated with the other open wiggly lines in a given diagram as discussed in VIII.1.

$\delta f_k =$



Appendix E Construction Rule of $\delta f_k^{(c)}$ and $\delta \bar{f}_k$

We introduce some useful definitions first.

Definition E1. *Primitive Frame Diagram*

It consists of a solid line with n wave - particle vertices, each of which connects with an open wiggly line, a shaded bubble with a wiggly line connected to the lowest end of the solid line. The four - momentum conservation holds for lines. We illustrate the fourth order primitive frame diagram as the left diagram in Fig. 35.

Definition E2. *Fundamental Constructive Diagram*

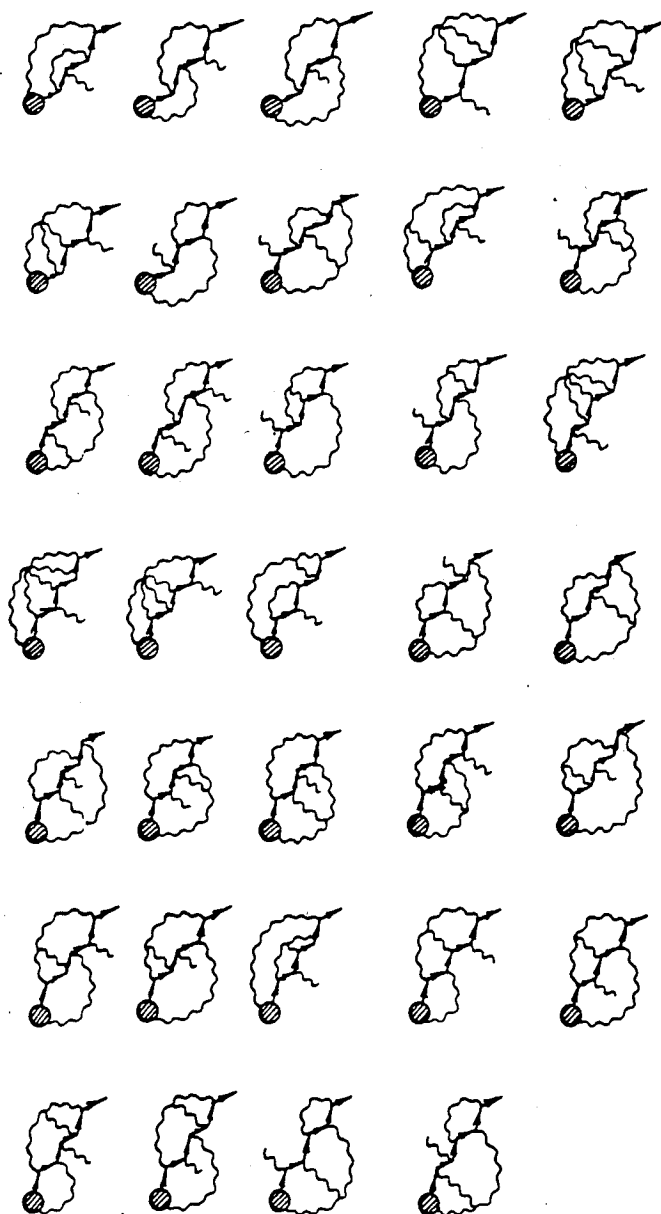
Starting with the given order primitive frame diagram, we combine the wiggly lines in all possible way to form internal line and/or closed structure containing multi - wave vertex with the exception that it will cause any type of self - energy sub - structure and zero - momentum propagator in the diagram. The set of the resultant diagrams is called the fundamental constructive diagram for the given order.

The construction rule of $\delta f_k^{(c)}$

All fundamental constructive diagrams with only single open wiggly line comprise the contribution to $\delta f_k^{(c)}$ for any given order. The diagrammatic expression of $\delta f_k^{(c)}$ to the fifth order order is illustrated as follows:

$$\delta f_k^{(c)} =$$

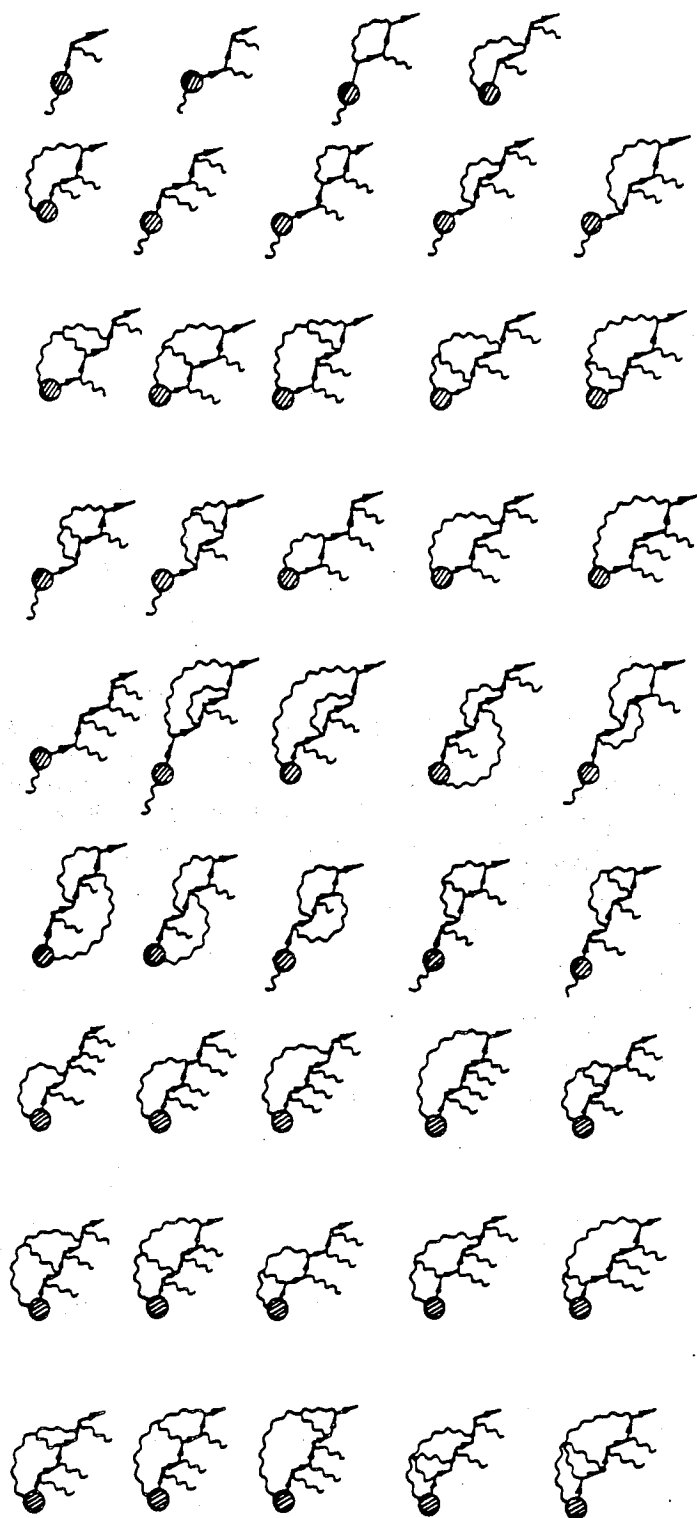


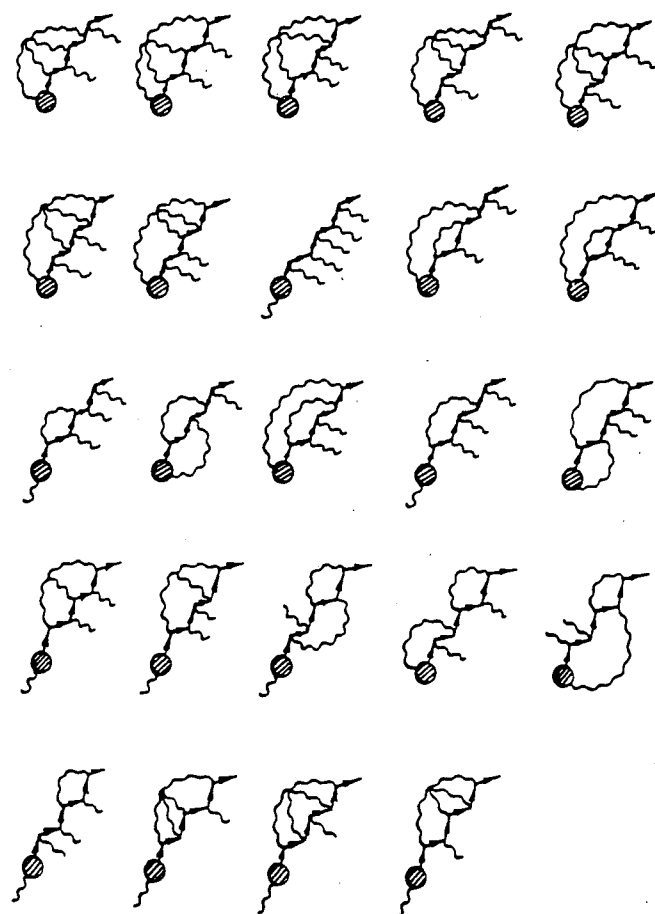


The construction rule of $\delta \tilde{f}_k$

All fundamental constructive diagrams with more than one open wiggly line comprise to $\delta \tilde{f}_k$ for any given order. The diagrammatic expression of $\delta \tilde{f}_k$ to the fifth order is illustrated as follows:

$$\delta \tilde{f}_k =$$





Appendix F Adjoint Diagrams in Fourth Order

The non - zero diagrams in fourth order are given below. They are cancelled with each other according to Lemma II, while the zero diagrams, to be zero by Lemma I, are not illustrated.

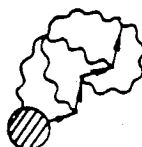
The sources composed the diagrams are given on the left of each diagram. They can be found in **Appendix D**.

A

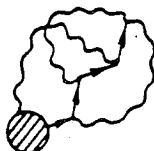
$$\langle \delta \phi_k^* G_k^{-1} A \delta \phi_k \rangle$$



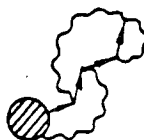
(F.1)



(F.2)



(F.3)

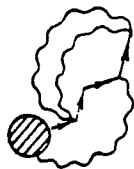


(F.4)

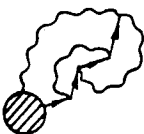
A



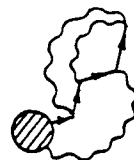
$$\langle \delta\phi_k^* G_k^{-1} A \delta\phi_k \rangle$$



(F.5)



(F.6)

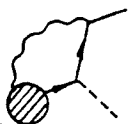
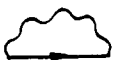


(F.7)

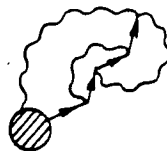
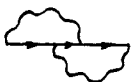
 $(-i\Gamma_k)$

A

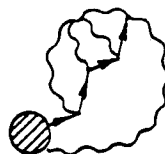
$$\langle \delta\phi_k^* (-i\Gamma_k) A \delta\phi_k \rangle$$



(F.8)



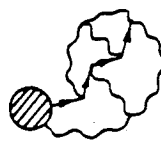
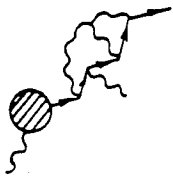
(F.9)



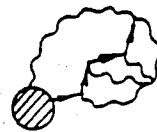
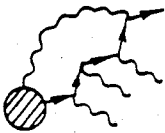
(F.10)

$\delta \tilde{f}_k$ $\langle \delta \phi_K^* G_k^{-1} \delta \tilde{f}_k \rangle$ 

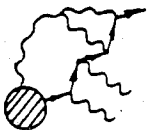
(F.11)



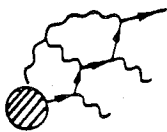
(F.12)



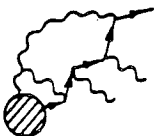
(F.13)



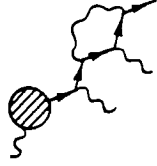
(F.14)



(F.15)



(F.16)

$\delta \tilde{f}_k$  $\langle \delta \phi_K^* G_k^{-1} \delta \tilde{f}_k \rangle$ 

(F.17)



(F.18)

 $(-i\Gamma_k)$  $\delta \tilde{f}_k$  $\langle \delta \phi_k^* (-i\Gamma_k) \delta \tilde{f}_k \rangle$ 

(F.19)



(F.20)

The adjoint pairs are: (4) + (8) = 0, (5) + (7) = 0, (6) + (9) = 0 [the pairs within the coherent part]; (13) + (16) = 0, (14) + (17) = 0, (18) + (20) = 0 [the pairs within the incoherent part]; (1) + (19) = 0, (2) + (11) = 0, (3) + (12) = 0, (10) + (15) = 0 [the pairs between the coherent and incoherent part].

REFERENCES

1. V. D. Shafranov, in Rev. of Plas. Phys., ed. by M. A. Leontovich (Consultants Bureau, New York), Vol. **II**, p.103.
2. B. B. Kadomtsev, in Rev. of Plas.Phys., ed. by M. A. Leontovich (Consultants Bureau, New York), Vol.**II**, p.153.
3. J. A. Wessen, Nucl. Fusion **18**, 87 (1978).
4. G. Bateman and D. J. Sigmar, Nucl. Fusion (1982).
5. H. P. Furth, Nucl. Fusion **15**, 487 (1975).
6. P. R. Bartsch, E. L. Cantrell, R. F. Gribble, K. A. Klare, K. A. Kutac, G. Miller, and R. E. Sieman, Phys. Fluids **21**, 2287 (1978).
7. G. Bateman, MHD instabilities (MIT, Cambridge, Mass.), 1978.
8. H. A. Bodin, and A. A. Newton, Nucl. Fusion **20**, 1255 (1980).
9. R. B. White, in Handbook of Plasma Physics, ed. by M.N.Rosenbluth, and R. Z. Sagdeev, (North-Holland Publishing Company,1983) Vol. **I**, p.611.
10. H. P. Furth, Phys. Fluids **28**, 1595 (1985).
11. J. P. Freidberg, Rev. Mod. Phys. **54**, 801 (1982).
12. R. F. Post, Ann. Rev. Energy, **1**, 213 (1976).
13. D. E. Baldwin, Rev. Mod. Phys. **49**, 317 (1977).
14. Ch. P. Ritz, R. D. Bengtson, S. J. Levinson, E. J. Powers, Phys. Fluids **27**, 2956 (1984).
15. C. M. Surko, R. E. Slusher, Science **221**, 817 (1983).
16. S. J. Zweben, R. W. Gould, Nucl. Fusion **25**,171 (1985).

17. P. C. Liewer, Nucl. Fusion **25**, 543 (1985).
18. B. B. Kadomtsev, O. P. Pogutse, Rev. of Plas. Phys., ed. by M. A. Leontovich (Consultants Bureau, New York), Vol. V, p.249.
19. A. A. Vlasov, Zh. Exp. Teor. Fiz. **8**, 291 (1938).
20. L. D. Landau, Zh. Exp. Teor. Fiz. **16**, 574 (1946).
21. D. B. Nelson and C. L. Hedrick, Nucl. Fusion **19**, 283 (1979).
22. M. N. Rosenbluth, and C. L. Longmire, Ann. Phys. (N.Y.) **1**, 120 (1957).
23. J. W. VanDam and Y. C. Lee, in Proc. EBT Ring Physics Workshop (ORNL, Oak Ridge, 1979) Conf-791228, P.471.
24. D. B. Nelson, Phys. Fluids **23**, 1850 (1980).
26. H. P. Furth, Phys. Fluids **8**, 2020 (1965).
27. H. L. Berk, R. N. Sudan, J. Plasma Phys. **6**, 113 (1971).
28. N. A. Krall, Phys. Fluids **9**, 820 (1966).
29. H. L. Berk, Phys. Fluids **19**, 1255 (1976).
30. R. R. Dominguez and H. L. Berk, Phys. Fluids **21**, 827 (1978).
31. A. M. El Nadi Phys. Fluids **25**, 2019 (1982).
32. H. L. Berk, J. W. VanDam, M. N. Rosenbluth, and D. A. Spong, Phys. Fluids **26**, 201 (1983).
33. D. P. Stotler, H. L. Berk, and M. G. Engquist, Phys. Fluids **29**, 1149 (1986).
34. M. N. Rosenbluth, Phys. Rev. Lett. **46**, 1525 (1981).
35. J. W. VanDam, M. N. Rosenbluth, and Y. C. Lee, Phys. Fluids **25**, 1349 (1982).

36. D. M. Kruskal and C. Oberman, *Phys. Fluids* **1**, 275 (1958).
37. D. E. Baldwin and H. L. Berk, *Phys. Fluids* **26**, 3695 (1983).
38. H. L. Berk and H. V. Wong, *Phys. Fluids* **28**, 1881 (1985).
39. H. L. Berk and T. B. Kaiser, *Phys. Fluids* **28**, 345 (1985).
40. H. L. Berk and Y. Z. Zhang, *Phys. Fluids* **30**, 1123, (1987).
41. Kang T. Tsang and X. S. Lee, *Phys. Rev. Lett.* **53**, 2094 (1984).
42. H. L. Berk, J. W. VanDam, and D. A. Spong, *Phys. Fluids* **26**, 606 (1983).
43. H. L. Berk, C. Z. Cheng, M. N. Rosenbluth, and J. W. VanDam, *Phys. Fluids* **26**, 2642 (1983).
44. T. M. Antonsen, Jr., Y. C. Lee, H. L. Berk, M. N. Rosenbluth, J. W. VanDam, *Phys. Fluids* **26**, 3580 (1983).
45. M. N. Rosenbluth, N. A. Krall, and N. Rostoker, *Nucl. Fusion Supp.*, Pt 1, 143 (1962).
47. H. L. Berk, H. V. Wong, and K. T. Tsang, *Phys. Fluids* **30**, 2681 (1987).
48. J. H. Hammer and H. L. Berk, *Phys. Fluids* **28**, 2450 (1985).
49. H. V. Wong, private communication.
50. N. C. Christofilis, R. J. Briggs, R. E. Hester, E. J. Lauer, P. B. Weiss, Lawrence Livermore Laboratory Report, UCRL-14282, 1965.
51. D. A. Phelps, A. C. Smith, D. M. Woodall, R. A. Meyer, and H. H. Fleischmann, *Phys. Fluids* **17**, 2226 (1974).
52. H. L. Berk, M. N. Rosenbluth, H. V. Wong, T. M. Antonsen, Jr., *Phys. Fluids* **27**, 2705 (1984).
53. D. A. Spong, H. L. Berk, and J. W. VanDam, *Phys. Fluids* **27**, 2292

- (1984).
54. M. N. Rosenbluth, S. T. Tsai, J. W. VanDam, M. G. Engquist, Phys. Rev. Lett. **51**, 1967 (1983).
 55. T. M. Antonsen, Jr. Y. C. Lee, in Proc. of Hot Electron Workshop (ORNL, Oak Ridge, 1981), p.191.
 56. R. B. White, L. Chen, F. Romanelli, and R. Hay, Phys. Fluids **28**, 278 (1985).
 57. K. McGuire, R. Goldstone, M. Bell, M. Bitter, K. Bol, K. Brau, D. Buchenauer, T. Crowley, S. Davis, F. Dylla, H. Eubank, H. Fishman, R. Fonck, B. Grek, R. Grimm, R. Hawryluk, H. Hsuan, R. Hulse, R. Izzo, R. Kaita, S. Kaye, H. Kugel, D. Johnson, J. Manickam, D. Manos, D. Mansfield, E. Mazzucato, R. McCann, D. McCune, D. Monticello, R. Motley, D. Mueller, K. Oasa, M. Okabayashi, K. Owens, W. Park, M. Reusch, R. Slusher, H. Takahashi, F. Tenney, P. Thomas, H. Towner, J. Valley, and R. White, Phys. Rev. Lett. **50**, 891 (1983).
 58. L. Chen, R. B. White, and M. N. Rosenbluth, Phys. Rev. Lett. **52**, 278 (1984).
 59. R. B. White, R. J. Goldston, K. McGuire, A. H. Boozer, D. A. Monticello, and W. Park, Phys. Fluids **26**, 2958 (1983).
 60. B. Coppi, Contribution presented at the Varenna Workshop on Plasma Transport (Varenna, Italy, July 1982), and at the PPPL Workshop on Bean-Shaped and High β -Tokamaks (Princeton, NJ, April 1983).
 61. B. Coppi, and F. Porcelli, Massachusetts Institute of Technology Report

- PTP-85/13 (1985).
62. J. W. Connor, R. J. Hastie, T. J. Martin, M. F. Turner, in *Heating in Toroidal Plasmas* (Commission of the European Communities, Brussel, 1982), Vol.I, p.65.
 63. G. Rewoldt and W. M. Tang, *Nucl. Fusion* **24**, 1573 (1984).
 64. D. A. Spong, D. J. Sigmar, W. A. Cooper, D. E. Hastings, and K. T. Tsang, *Phys. Fluids* **28**, 2494 (1985).
 65. D. P. Stotler and H. L. Berk, *Phys. Fluids* **30**, 1429 (1987).
 66. J. Weiland and L. Chen, *Phys. Fluids* **28**, 1359 (1985).
 67. D. A. Spong, D. J. Sigmar, W. A. Cooper, D. E. Hasting, and K. T. Tsang, *Phys. Fluids* **28**, 2494 (1985).
 68. M. N. Rosenbluth and N. Rostoker, *Phys. Fluids* **2**, 23 (1959).
 69. J. B. Taylor, and R. J. Hastie, *Phys. Fluids* **8**, 232 (1965).
 70. H. Grad, *Phys. Fluids* **9**, 225 (1966).
 71. R. Kursrud, in *Advanced Plasma Theory*, (Proc. of the Enrico Fermi International School of Physics), ed. by M. N. Rosenbluth (Academic, New York, 1964), pp.54-97.
 72. G. E. Guest and C. L. Hedrick, Oak Ridge National Laboratory Report No. ORNL-TM-3943, 1972.
 73. J. Andreoletti, *C. R. Acad. Sci. Paris* **256**, 1251 (1963).
 74. B. A. Trubnikov, *Phys. Fluids* **5**, 184 (1962).
 75. T. M. Antonsen, Jr. and B. G. Lane, and J. J. Ramos, *Phys. Fluids* **24**, 1465 (1981).

76. T. M. Antonsen, Jr. and Y. C. Lee, *Phys. Fluids* **25**, 132 (1982).
77. H. L. Berk and B. G. Lane, *Phys. Fluids* **29**, 1076 (1986).
78. H. L. Berk and B. G. Lane, *Phys. Fluids* **29**, 3749 (1986).
79. H. V. Wong, *Phys. Fluids* **25**, 1811 (1982).
80. Y. Ohsawa and J. M. Dawson, *Phys. Fluids* **27**, 1491 (1984), and Y. Ohsawa and J. W. VanDam, *Phys. Fluids* **30**, 3237 (1987).
81. G. F. Chew, M. L. Goldberger, and F. E. Low, *Proc. R. Soc. London Ser. A* **236**, 112 (1956).
82. T. Kamimura, private communication.
83. H. L. Berk, Y. Z. Zhang, and T. Kamimura, preprint (1987).
84. K. Appert, J. Vaclavik, and L. Villard, *Phys. Fluids* **27**, 1491 (1984).
85. D. L. Hillis, J. B. Wilgen, T. S. Bigelow, E. F. Jaeger, D. W. Swain, O. E. Hankins, and R. E. Juhala, *Phys. Fluids* **29**, 3796 (1986).
86. H. Ikegami, M. Hosokawa, H. Iguchi, T. Shoji, T. Kamimura, H. Sanuki, K. Takasugi, F. Tsuboi, T. Takeuchi, A. Komori, K. Kadota, J. Fujita, C. Honda, M. Yokoo, M. Maeda, K. Muraoka, T. Yuyama, T. Michishita, H. Kubo, and M. Fujiwara, in IAEA, 11th International Conference on Plasma Physics and Controlled Nuclear Fusion Research, Kyoto, Japan (1986), IAEA-CN-47/D-III-4.
87. B. H. Quon, R. A. Dandle, W. DiVergillo, G. E. Guest, L. L. Lao, N. H. Lazar, T. K. Samec, and R. F. Wuerker, *Phys. Fluids* **28**, 1503, (1985).
88. L. Hedrick, L. W. Owens, B. H. Quon, R. A. Dandl, *Phys. Fluids* **30**, 1860 (1987).

89. AMPC STAFF, " Determination of Electron Ring Properties in STM ",
Final Report, AMPC-26-027, DOE/ER/53230-1, Mar.1987.
90. Xing Chen, B. G. Lane, D. L. Smatlak, R. S. Post, S. A. Hokin, Mas-
sachusetts Institute of Technology Plasma Fusion Center Report, PFC/JA-
87-43, Oct. 1987, and Private Communication with Xing Chen.
91. T. H. Dupree, Phys. Fluids **9**, 1773 (1966).
92. W. Horton, Jr., Duk-In Choi, Phys. Rept. **49**, 275 (1979).
93. A. A. Galeev, Zh. Eksp. Teor. Fiz. **59**, 1361 (1969), (Soviet Phys. JETP
30, 737 (1970).
94. L. I. Rudakov, V. N. Tsytovich, Plas. Phys. **13**, 213 (1971).
95. T. H. Dupree, D. J. Tetrault, Phys. Fluids **21**, 425 (1978).
96. T. Boutros-Ghali, T.H. Dupree, Phys. Fluids **24**, 1839 (1981).
97. P. H. Diamond, M. N. Rosenbluth, Phys. Fluids **24**, 1641 (1981).
98. P. L. Similon, P. H. Diamond, Phys. Fluids **27**, 916 (1984).
99. B. B. Kadomtsev, Plasma Turbulence (Academic Press, Reading, Mass),
1965.
100. J. A. Krommes, Handbook of Plasma Physics, eds., M. N. Rosenbluth and
R. Z. Sagdeev, Vol.2: Basic Plasma Physics II, edited by A. A. Galeev and
Sudan (Elsevier, 1984).
101. P. C. Martin, E. D. Siggia, H. A. Rose, Phys. Rev. **8**, 423 (1973).
102. R. H. Kraichnan, Phys. Fluids **8**, 575, 2219 (1965).
103. S. A. Orszag, R. M. Kraichnan, Phys. Fluids **10**, 1720 (1967).
104. D. F. Dubois, M. Espedal, Plas. Phys. **20**, 1209 (1978).

105. J. A. Krommes, Phys. Fluids **23**, 736 (1980).
106. D. F. Dubois, Phys. Fluids **19**, 1764 (1976).
107. T. H. Dupree, Phys. Rev. Lett. **25**, 789 (1970).
108. T. H. Dupree, Phys. Fluids **15**, 334 (1972).
109. T. H. Dupree, Phys. Fluids **21**, 783 (1978).
110. D. J. Tetrault, Phys. Fluids **26**, 3247 (1983).
111. V. N. Tsytovich, *Theory of Turbulent Plasma*, Consultants Bureau, (New York, 1977).
112. Y. Z. Zhang, S. M. Mahajan, Phys. Rev. A **32**, 1759 (1985).
113. D. J. Korteweg and G. de Vries, Phil. Mag. **39**, 422 (1895).
114. J. Boussinesq, J. Math. Pure Appl., ser 2, **17**, 55 (1872).
115. L. D. Landau and E. M. Lifshitz, in Fluid Mechanics, Pergamon Press.
116. V. E. Zakharov and A. B. Shabat, Soviet Phys. JETP **34**, 62 (1972).
117. J. A. Krommes, R. G. Kleva, Phys. Fluids **22**, 2168 (1979).
118. D. Biskamp, Zeitschrift fur Naturforschung B **23a** Heft **9**, 1362 (1968).
119. T. Antonsen, Jr., B. Coppi, R. Englande, Nucl. Fusion **19**, 641 (1979).
120. E. A. Frieman, Liu Chen, Phys. Fluids **25**, 502 (1982).
121. L. A. Berry and ORMAK GROUP, in Plasma Physics and Controlled Nuclear Fusion Research (Proc. 5th Int. Conf. Tokyo, 1974), Vol.1, IAEA, Vienna (1975) 101.
122. L. A. Berry and ORMAK GROUP, in Plasma Physics and Controlled Nuclear Fusion Research (Proc. 6th Int. Conf. Berchtesgaden, 1976), Vol.1, IAEA, Vienna (1977) 49.

123. EQUIPE TFR, in Plasma Physics and Controlled Nuclear Fusion Research (Proc. 6th Int. Conf. Berchtesgaden, 1976), Vol. 1, IAEA, Vienna (1977) 35.
124. EQUIPE TFR, Nucl. Fusion **20**, 1227 (1980).
125. A.Gondhalekar and ALCATOR GROUP, in Plasma Physics and Controlled Nuclear Fusion Research (Proc. 7th Int. Conf. Innsbruck, 1978), Vol. 1, IAEA, Vienna (1979) 199.
126. W. Stodiek and PLT GROUP, in Plasma Physics and Controlled Nuclear Fusion Research (Proc. 8th Int. Conf. Brussels, 1980), Vol. 1, IAEA, Vienna (1981) 9.
127. H. Eubank and PLT GROUP, Phys. Rev. Lett. **43**, 279 (1979).
128. M. Murakami and ISX-A GROUP, Phys. Rev. Lett. **42**, 655 (1979).
129. B. Blackwell and ALCATOR-C GROUP in Plasma Physics and Controlled Nuclear Fusion Research (Proc. 9th Int. Conf. Baltimore, 1982), Vol. 2, IAEA, Vienna (1983) 27.
130. S. M. Wolfe et al., Nucl. Fusion **26**, 329 (1986).
131. F. L. Hinton and R. D. Hazeltine, Rev. Mod. Phys. **48**, 239 (1976).
132. M. Gaudreau et al., Phys. Rev. Lett. **39**, 1266 (1977).
133. F. Alladio et al., Nucl. Fusion **22**, 479 (1982).
134. C. S. Chang and F. L. Hinton, Phys. Fluids **25**, 1493 (1982).
135. F. De Marco, L. Pieroni, F. Santini, S. E. Segre, Nucl. Fusion **26**, 1193 (1986).
136. S. Ejima et al., Nucl. Fusion **22**, 1627 (1982).

137. W. W. Pfeiffer, et al., GA-A 16178 (1980).
138. EQUIPE TFR, in Plasma Physics and Controlled Nuclear Fusion Research (Proc. 7th Int. Conf. Innsbruck, 1978) Vol. **1**, IAEA, Vienna (1979) 135.
139. EQUIPE TFR, Nucl. Fusion **16**, 279 (1976).
140. M. Brusati, S. L. Davis, J. C. Hosea, J. D. Strachan, S. Suckewer, Nucl. Fusion **21**, 1079 (1981).
141. N. Ohyabu and DOUBLET-III GROUP, Nucl. Fusion **25**, 49 (1985).
142. R. H. Fowler et al., Oak Ridge National Lab., TN, Rep. ORNL-TM-6845 (1979).
143. J. D. Callen, R. J. Colchin, R. H. Fowler, D. G. McAlees, J. A. Rome, in Plasma Physics and Controlled Nuclear Fusion Research (Proc. 5th Int. Conf. Tokyo, 1974), Vol. **1**, IAEA, Vienna (1975) 645.
144. S. M. Kaye, R. J. Goldstone et al., Nucl. Fusion **24**, 1303 (1984).
145. R. Hawryluk, in Physics of Plasmas Close to Thermonuclear Conditions (Proc. Course Varenna, 1979), Vol. **1**, Commission of the European Communities, Brussels (1979) 19.
146. R. J. Goldstone et al., J. Comput. Phys. **43**, 61 (1981).
147. T. Ohkawa, Phys. Lett. **67A**, 35 (1978).
148. A. B. Rechester and M. N. Rosenbluth, Phys. Rev. Lett. **40**, 38 (1978).
149. J. F. Drake, N. T. Gladd, C. S. Liu, C. L. Chang, Phys. Rev. Lett. **44**, 994 (1980).
150. V. V. Parail, O. P. Pogutse, in Plasma Physics and Controlled Nuclear

Fusion Research (Proc. 8th Int. Conf., 1980), Vol.1, IAEA, Vienna (1981)

67.

151. V. G. Merezhkin, V. S. Mukhovatov, Sov. JETP Lett. **33**, 446 (1981).
152. G. Hasselberg, A. Rogister, Nucl. Fusion **23**, 1351 (1983).
153. B. Carreras, P. Diamond et al. Phys. Rev. Lett. **50**, 503 (1983).
154. J. W. Connor, J. B. Taylor, M. F. Turner, Nucl. Fusion **24**, 642 (1984).
155. B. B. Kadomtsev, O. P. Pogutse, Sov. JEPT Lett. **39**, 264 (1984).
156. T. Ohkawa, Comments on Plasma Physics and Controlled Fusion, **9**, 127 (1985).
157. P. N. Guzdar, C. S. Liu, J. Q. Dong, Y. C. Lee, Phys. Rev. Lett. **57**, 2818 (1986).
158. W. Horton, D. I. Choi, P. N. Yushmanov, V. V. Parail, Plas. Phys. Cont. Fusion **29**, 901 (1987).
159. Y. C. Lee, J. Q. Dong, P. N. Guzdar, C. S. Liu, Phys. Fluids **30**, 1331 (1987).
160. B. Coppi, Comments on Plasma Physics and Controlled Fusion, **5**, 261 (1980).
161. H. P. Furth, Plasma Physics Lab., Princeton University, Report PPPL-2263 (1985).
162. V. Erckmann and W VII-A TEAM, ECRH GROUP Plasma Physics and Controlled Fusion **28**, No. 9A, 1227 (1986).
163. EQUIPE TFR, Nucl. Fusion **20**, 1227 (1980).
164. W VII-A TEAM, Institut fur Plasmaphysik, Garching, Report IPP-2-241

(1978).

165. W. M. Tang, C. Z. Cheng, J. A. Krommes, W. W. Lee, C. R. Oberman, et al., in Plasma Physics and Controlled Nuclear Fusion Research (Proc. 10th Int. Conf. London, 1984), Vol.II, IAEA, Vienna (1985) 213.
166. G. Taylor, et al. Nucl. Fusion **20**, 339 (1980).
167. F. W. Perkins, in "heating in Toroidal Plasmas" (Proc. 4th Int. Symp. Rome, 1984), Vol.II, ISPP and ENEA (1984) 977.
168. A. Gondhalekar and ALCATOR Group, in Plasma Physics and Controlled Nuclear Fusion Research (Proc. 7th Int. Conf. Innsbruck, 1978), Vol.I, IAEA, Vienna (1979) 199.
169. R. D. Hazeltine, H. R. Strauss, Phys. Fluids **21**, 1007 (1978).
170. R. D. Hazeltine, D. W. Ross, Phys. Fluids **21**, 1140 (1978).
171. S. M. Mahajan, R. D. Hazeltine, H. R. Strauss, and D. W. Ross, Phys. Fluids **22**, 2147 (1979).
172. I. B. Bernstein, E. A. Freiman, M. D. Kruskal, R. M. Kulsrud, Proc. R. Soc. London Ser. **A244**, 17 (1958).
173. H. P. Furth, J. Killen, M. N. Rosenbluth, B. Coppi, in Plasma Physics and Controlled Nuclear Fusion Research (Proc. 1st Int. Conf. Culham, 1965), Vol.I, Vienna (1965) p.103.
174. J. L. Johnson, J. M. Greene, Plasma Physics **9**, 611 (1967).
175. D. C. Montgomery, D. A. Tidman, in Plasma Kinetic Theory, McGraw-Hill Book Company, New York, (1964).

VITA

Yang-zhong Zhang was born in Peking (Beijing), China on September 8th 1941, the son of Ming Tao Chang and Juan Chang Jiang. After completing his work at the 101st High School of Peking, he entered the Department of Technology Physics of The Peking University, Beijing, China. He received his Bachelor of Science degree in Physics from The Peking University in 1964. During the following years he worked as a research assistant, senior research fellow since 1979, in the Southwestern Institute of Physics, Leshan, Sichuan Province, China. In September 1982, he entered the graduate school of Boston College. In June 1983 he entered the graduate school of The University of Texas at Austin. Since that time he has been employed as a Research Assistant II and III in the Institute for Fusion Studies. He married Zhao Zhen from Beijing, China in 1976 and they have one son Wen-wei (William) Zhang born in 1977.

Permanent Address:

Southwestern Institute of Physics,
P.O.Box 15, Leshan, Sichuan, China.